Volume 73A

Number 3

May–June 1969

J. Res. Nat. Bur. Stand. (U.S.), A
CODEN: JNBAA 73A (3) 277–388 (1969)

Physics and Chemistry

U.S. DEPARTMENT
OF COMMERCE

SECTION A

JOURNAL OF RESEARCH

NATIONAL BUREAU OF STANDARDS

Journal of Research

of the

National Bureau of Standards

A. Physics and Chemistry

May-June • 1969

VOLUME • 73A

NUMBER • 3

Editor: C. W. Beckett

Associate Editor: D. D. Wagman

Publication dates:
Feb. 1, Apr. 1, June 1, Aug. 1, Oct. 1, Dec. 1, 1969

JOURNAL OF RESEARCH

The National Bureau of Standards Journal of Research reports research and development in the fields of activity shown at right. Also included from time to time are survey articles on topics closely related to the Bureau's scientific and technical program.

The Journal is published in three separate sections as follows:

A. Physics and Chemistry

Contains papers of interest primarily to scientists working in these fields. Issued six times a year. Annual subscription: domestic, $9.50; foreign, $11.75. Single copy, varies.

B. Mathematical Sciences

Presents studies and compilations designed mainly for the mathematician and the theoretical physicist. Issued quarterly. Annual subscription: domestic, $5.00; foreign, $6.25. Single copy, $1.25.

C. Engineering and Instrumentation

Reports research and development results of interest chiefly to the engineer and the applied scientist. Issued quarterly. Annual subscription: domestic, $5.00; foreign, $6.25. Single copy, $1.25.

The National Bureau of Standards[1] was established by an act of Congress March 3, 1901. Today, in addition to serving as the Nation's central measurement laboratory, the Bureau is a principal focal point in the Federal Government for assuring maximum application of the physical and engineering sciences to the advancement of technology in industry and commerce. To this end the Bureau conducts research and provides central national services in four broad program areas. These are: (1) basic measurements and standards, (2) materials measurements and standards, (3) technological measurements and standards, and (4) transfer of technology.

The Bureau comprises the Institute for Basic Standards, the Institute for Materials Research, the Institute for Applied Technology, the Center for Radiation Research, the Center for Computer Sciences and Technology, and the Office for Information Programs.

THE INSTITUTE FOR BASIC STANDARDS provides the central basis within the United States of a complete and consistent system of physical measurement; coordinates that system with measurement systems of other nations; and furnishes essential services leading to accurate and uniform physical measurements throughout the Nation's scientific community, industry, and commerce. The Institute consists of an Office of Measurement Services and the following technical divisions:

Applied Mathematics—Electricity—Metrology—Mechanics—Heat—Atomic and Molecular Physics—Radio Physics[2]—Radio Engineering[2]—Time and Frequency[2]—Astrophysics[2]—Cryogenics.[2]

THE INSTITUTE FOR MATERIALS RESEARCH conducts materials research leading to improved methods of measurement standards, and data on the properties of well-characterized materials needed by industry, commerce, educational institutions, and Government; develops, produces, and distributes standard reference materials; relates the physical and chemical properties of materials to their behavior and their interaction with their environments; and provides advisory and research services to other Government agencies. The Institute consists of an Office of Standard Reference Materials and the following divisions:

Analytical Chemistry—Polymers—Metallurgy—Inorganic Materials—Physical Chemistry.

THE INSTITUTE FOR APPLIED TECHNOLOGY provides technical services to promote the use of available technology and to facilitate technological innovation in industry and Government; cooperates with public and private organizations in the development of technological standards, and test methodologies; and provides advisory and research services for Federal, state, and local government agencies. The Institute consists of the following technical divisions and offices:

Engineering Standards—Weights and Measures—Invention and Innovation—Vehicle Systems Research—Product Evaluation—Building Research—Instrument Shops—Measurement Engineering—Electronic Technology—Technical Analysis.

THE CENTER FOR RADIATION RESEARCH engages in research, measurement, and application of radiation to the solution of Bureau mission problems and the problems of other agencies and institutions. The Center consists of the following divisions:

Reactor Radiation—Linac Radiation—Nuclear Radiation—Applied Radiation.

THE CENTER FOR COMPUTER SCIENCES AND TECHNOLOGY conducts research and provides technical services designed to aid Government agencies in the selection, acquisition, and effective use of automatic data processing equipment; and serves as the principal focus for the development of Federal standards for automatic data processing equipment, techniques, and computer languages. The Center consists of the following offices and divisions:

Information Processing Standards—Computer Information—Computer Services—Systems Development—Information Processing Technology.

THE OFFICE INFORMATION PROGRAMS promotes optimum dissemination and accessibility of scientific information generated within NBS and other agencies of the Federal government; promotes the development of the National Standard Reference Data System and a system of information analysis centers dealing with the broader aspects of the National Measurement System, and provides appropriate services to ensure that the NBS staff has optimum accessibility to the scientific information of the world. The Office consists of the following organizational units:

Office of Standard Reference Data—Clearinghouse for Federal Scientific and Technical Information[3]—Office of Technical Information and Publications—Library—Office of Public Information—Office of International Relations.

[1] Headquarters and Laboratories at Gaithersburg, Maryland, unless otherwise noted; mailing address Washington, D.C. 20234.
[2] Located at Boulder, Colorado 80302.
[3] Located at 5285 Port Royal Road, Springfield, Virginia 22151.

U.S. DEPARTMENT OF COMMERCE
Maurice H. Stans, Secretary
NATIONAL BUREAU OF STANDARDS
A. V. Astin, Director

Order all publications from the Superintendent of Documents
U.S. Government Printing Office, Washington, D.C. 20402.

Use of funds for printing this publication approved by the Director of the Bureau of the Budget (June 22, 1966).

JOURNAL OF RESEARCH of the National Bureau of Standards—A. Physics and Chemistry
Vol. 73A, No. 3, May–June 1969

New Even Levels and Classified Lines in the First Spectrum of Tungsten (W I)

C. H. Corliss

Institute for Basic Standards, National Bureau of Standards, Washington, D.C. 20234

(January 24, 1969)

Ten new even levels, which classify 161 previously unclassified lines, have been found in the first spectrum of tungsten. Nine of these fit levels in the $(5d+6s)^6$ mixture of configurations calculated theoretically by Shadmi and Caspi.

Key words: Atomic energy levels in W I; classified lines of W I; spectrum, W I; tungsten, first spectrum; W I.

Recently Laun and Corliss [1968] published an extensive list of levels and classified lines for the first spectrum of tungsten (W I). Prompted by these experimental data, Shadmi and Caspi [1968] published a theoretical interpretation of the low even levels arising from the $(5d+6s)^6$ mixture of configurations. Their work provided an interpretation for every level found experimentally below 40000 cm^{-1} and predicted values for numerous levels not yet found. It seemed worthwhile to search for some of these levels.

The search has been made with the Combo program for finding energy levels, which was developed by J. L. Tech in the National Bureau of Standards Spectroscopy Section. With this program, the wavenumbers of 1391 unclassified W I lines were used to search for new even levels in the energy region where levels were predicted to lie. Ten new levels with numbers of combinations significantly above the noise were found. (The noise level in this case was about 6 to 8 combinations for fortuitous levels.) The new levels, which have J-values 2, 3, 4, and 5 are marked with asterisks (*) in table 1.

The previously known levels with J-values from 1 through 5 are also listed in order to show the remarkable regularity in the relationship between the number of combinations (N) made by each level and the level value. According to Shadmi and Caspi, the three levels marked in parentheses seem of doubtful reality, in view of the relatively large differences between the observed and calculated values for these levels. However, the tabulations in table 1 show that the number of combinations made by these three levels in question is about the number to be expected. Furthermore, since that number is about five times above the noise level number, it is likely that the levels are indeed real.

TABLE 1. *Even levels in* W I.

Number of combinations	J	Observed level (cm^{-1})	Calculated level (cm^{-1})	Difference O–C (cm^{-1})
87	1	1670.29	1697	−27
103	1	13307.10	13405	−98
84	1	18082.83	18095	−12
78	1	20427.84	20407	21
58	1	23455.02	23541	−86
34	1	(27670.48)	28123	(−453)
24	1	28720.88	28877	−156
15	1	32378.40	32443	−65
128	2	3325.53	3382	−57
144	2	13777.71	13708	70
149	2	14976.18	15058	−82
131	2	18116.84	18240	−123
132	2	18280.48	18385	−105
130	2	19253.56	19283	−30
110	2	20983.02	21031	−48
77	2	23982.80	24028	−45
57	2	24789.66	24799	−9
61	2	26861.64	26844	18
44	2	(28204.20)	28576	(−372)
34	2	28898.96	28790	109
30	2	(30374.20)	29840	(534)
18	2	*31077.79	31037	41
107	3	2951.29	2833	118
145	3	4830.00	4836	−6
173	3	13348.56	13424	−76
173	3	15460.01	15405	55
154	3	17701.18	17736	−35
152	3	18974.51	18994	−20
154	3	19827.68	19759	69
114	3	23930.08	23870	60
85	3	24610.88	24741	−130
62	3	28291.88	28196	96
54	3	28347.60	28454	−106
26	3	*29430.50	29409	21
17	3	*32217.95	31996	222

TABLE 1. *Even levels in* W I. — Continued

Number of combinations	J	Observed level (cm^{-1})	Calculated level (cm^{-1})	Difference O–C (cm^{-1})	Number of combinations	J	Observed level (cm^{-1})	Calculated level (cm^{-1})	Difference O–C (cm^{-1})
13	3	*32826.63	32821	6	50	4	29853.66	29813	41
11	3	*33952.85	33675	278	31	4	32135.94	31902	234
10	3	*34465.83	34566	−100	17	4	*33569.53	33421	149
10	3	*37414.11	37143	271	26	4	34302.04	34159	143
					14	4	*35299.82	35219	81
133	4	6219.33	6105	114					
159	4	12161.96	12162	0	123	5	15069.93	15124	−54
144	4	16431.31	16567	−136	115	5	19535.01	19391	144
153	4	17107.01	17043	64	115	5	19826.04	20035	−209
138	4	19256.24	19275	−19	68	5	27849.80	27755	95
117	4	22476.68	22442	35	67	5	28233.44	28273	−40
99	4	22852.80	22826	27	49	5	31389.08	31256	133
81	4	27213.82	27114	100	20	5	*33201.61	.....	.....
48	4	29479.32	29453	26	28	5	33291.80	33352	−60

TABLE 2. — *Newly Classified Lines of* W I

Wavelength Å	Intensity	Wavenumber (cm^{-1})		Classification (levels in cm^{-1})	Wavelength Å	Intensity	Wavenumber (cm^{-1})		Classification (levels in cm^{-1})
		Observed	O–C				Observed	O–C	
3113.876	8	32105.01	0.01	29430_3–61535°_4	4736.036	3	21108.80	0.11	33201_5–54310°_5
3523.446	3	28373.19	0.03	29430_3–57803°_4	4809.642	3	20785.76	−0.05	32217_3–53003°_2
3578.011	2	27940.51	0.10	32217_3–60158°_4	4865.33	3	20547.85	0.02	33569_4–54117°_3
3580.40	2	27921.87	0.05	29430_3–57352°_3	5019.52	3	19916.67	−0.01	33201_5–53118°_4
3608.904	4	27701.34	0.06	29430_3–57131°_3	5023.423	2*b*	19901.19	0.05	37414_3–57315°_4
3625.059	2	27577.90	−0.04	31077_2–58655°_2	5044.908	4	19816.44	0.11	31077_2–50894°_3
3627.611	2	27558.50	0.04	32826_3–60385°_4	5094.173	6	19624.80	0.08	33569_4–53194°_5
3726.776	2	26825.22	0.07	29430_3–56255°_4	5107.78	5	19572.52	0.03	33201_5–52774°_5
3749.935	2	26659.55	−0.10	33569_4–60229°_5	5133.11	20	19475.94	0.00	32217_3–51693°_2
3918.195	2	25514.73	0.18	32217_3–57732°_3	5145.453	8	19429.22	0.05	32826_3—52255°_3
3931.44	2	25428.77	0.12	29430_3–54859°_2	5282.646	4*b*	18924.64	0.05	34465_3–53390°_3
3978.822	2	25125.96	0.03	29430_3–54556°_3	5295.252	6	18879.59	0.11	33201_5–52081°_5
4005.893	8	24956.17	0.00	34465_3–59422°_2	5295.252	6	18879.59	−0.10	34465_3–53345°_3
4012.704	1	24913.81	−0.06	32217_3–57131°_3	5310.37	4	18825.84	−0.13	33569_4–52395°_5
4048.854	5	24691.37	0.12	33952_3–58644°_3	5312.282	5	18819.07	0.11	35299_4–54118°_1
4062.26	1	24609.89	0.04	33569_4–58179°_5	5312.282	5	18819.07	−0.02	34465_3–53284°_2
4101.648	3	24373.57	0.07	35299_4–59673°_5	5345.887	3*b*	18700.77	0.04	33952_3–52653°_2
4116.718	3	24284.34	0.15	32217_3–56502°_4	5389.661	3	18548.88	0.08	35299_4–53848°_4
4158.954	2	24037.73	−0.01	32217_3–56255°_4	5392.78	4	18538.16	0.04	29430_3–47968°_4
4167.002	2*b*	23991.30	0.01	33569_4–57560°_5	5443.35	12	18365.94	0.02	31077_2–49443°_1
4240.913	3	23573.19	−0.03	29430_3–53003°_2	5469.932	2	18276.68	0.05	32217_3–50494°_2
4257.978	3	23478.72	0.08	31077_2–54556°_3	5471.50	3	18271.45	0.02	33201_5–51473°_4
4262.267	4	23455.09	0.09	29430_3–52885°_2	5479.229	10	18245.67	0.17	32826_3–51072°_3
4282.922	1	23341.98	0.10	31077_2–54419°_1	5495.256	3	18192.46	0.09	31077_2–49270°_2
4290.53	2	23300.59	0.10	33201_5–56502°_4	5526.644	2*b*	18089.14	0.02	33201_5–51290°_5
4314.424	2	23171.55	0.16	32217_3–55389°_3	5539.91	2	18045.82	0.12	35299_4–53345°_3
4352.11	2*b*	22970.90	−0.08	37414_3–60385°_4	5550.319	4	18011.98	−0.05	29430_3–47442°_2
4359.37	2	22932.65	0.08	33569_4–56502°_4	5563.97	4*b*	17967.79	0.00	32217_3–50185°_3
4364.40	3	22906.22	0.04	35299_4–58206°_3	5641.39	5	17721.21	0.01	33569_4–51290°_5
4381.862	5	22814.94	0.18	32217_3–55032°_2	5721.10	2	17474.31	0.03	35299_4–52774°_5
4509.30	4*b*	22170.17	0.15	29430_3–51600°_3	5726.43	2	17458.04	0.03	32826_3–50284°_4
4535.389	2	22042.64	0.10	29430_3–51473°_4	5803.04	3	17227.57	0.00	33201_5–50429°_6
4584.244	3	21807.74	0.03	31077_2–52885°_2	5848.81	2	17092.76	0.00	31077_2–48170°_3
4731.027	2	21131.15	−0.02	33952_3–55084°_2	5905.05	4	16929.97	−0.07	32217_3–49147°_4
4731.027	2	21131.15	0.08	34465_3–55596°_4	5931.13	2	16855.52	−0.14	37414_3–54269°_3

TABLE 2.—*Newly Classified Lines of* W I—Continued

Wavelength Å	Intensity	Wavenumber (cm^{-1}) Observed	O−C	Classification (levels in cm^{-1})	Wavelength Å	Intensity	Wavenumber (cm^{-1}) Observed	O−C	Classification (levels in cm^{-1})
5980.95	2	16715.12	0.01	33569_4–50284°_4	7245.88	1	13797.14	−0.02	29430_3–43227°_2
6053.17	2*b*	16515.70	0.05	31077_2–47593°_3	7318.95	1	13659.40	−0.02	31077_2–44737°_1
6082.89	3	16435.00	0.09	33201_5–49636°_4	7416.29	1	13480.12	−0.12	29430_3–42910°_3
6179.66	3	16177.64	−0.12	31077_2–47255°_1	7416.29	1	13480.12	0.11	37414_3–50894°_3
6181.39	2	16173.12	−0.10	35299_4–51473°_4	7473.90	1	13376.21	−0.05	35299_4–48676°_4
6243.10	2	16013.25	0.07	33952_3–49966°_3	7590.55	1	13170.65	−0.04	29430_3–42601°_3
6251.48	5	15991.79	0.03	29430_3–45422°_2	7641.04	3	13083.62	−0.02	29430_3–42514°_3
6253.63	6	15986.29	−0.02	33201_5–49187°_5	7678.57	6	13019.68	−0.06	29430_3–42450°_4
6269.28	4	15946.38	0.04	33201_5–49147°_4	7680.12	1	13017.05	−0.02	21448°_2–34465_3
6298.57	6	15872.23	−0.04	33201_5–49073°_5	7702.63	2*b*	12979.01	0.02	33952_3–46931°_4
6415.03	1	15584.08	0.04	29430_3–45014°_3	7704.00	1*b*	12976.70	0.00	34465_3–47442°_2
6417.36	4	15578.43	0.01	33569_4–49147°_4	7747.07	3	12904.56	−0.04	33201_5–46106°_6
6447.25	1	15506.20	−0.05	35299_4–50806°_5	7797.57	5	12820.98	−0.03	29430_3–42251°_3
6448.76	1	15502.57	−0.04	33569_4–49072°_3	7812.44	7	12796.58	−0.05	32217_3–45014°_3
6449.93	3	15499.76	−0.02	32826_3–48326°_3	7826.86	3	12773.00	−0.05	31077_2–43850°_3
6461.78	5	15471.34	−0.08	32217_3–47689°_4	7967.14	20	12548.10	−0.02	29430_3–41978°_2
6461.78	5	15471.34	−0.05	37414_3–52885°_2	7998.74	2	12498.53	0.04	33569_4–46068°_3
6464.43	4	15464.99	−0.06	33952_3–49417°_3	8039.04	1	12435.88	−0.04	32826_3–45262°_4
6515.44	3	15343.92	−0.01	32826_3–48170°_3	8061.78	2*b*	12400.80	0.01	31077_2–43478°_3
6602.37	1	15141.89	−0.10	32826_3–47968°_4	8076.41	2	12378.34	−0.03	32217_3–44596°_2
6612.24	2	15119.29	0.00	33952_3–49072°_3	8101.05	1	12340.68	0.06	34465_3–46806°_2
6652.98	1	15026.71	−0.12	31077_2–46104°_1	8125.47	10	12303.60	−0.03	29430_3–41734°_2
6669.22	2	14990.12	−0.11	31077_2–46068°_3	8137.38	8	12285.59	0.14	37414_3–49699°_2
6671.59	1	14984.79	−0.03	35299_4–50284°_4	8151.80	1	12263.86	0.02	29430_3–41694°_3
6726.42	4	14862.65	−0.06	32826_3–47689°_4	8161.04	1	12249.97	−0.07	33201_5–45451°_5
6770.04	8	14766.89	0.08	32826_3–47593°_3	8175.02	1	12229.02	−0.09	32217_3–44447°_3
6846.90	1	14601.12	0.10	33569_4–48170°_3	8181.34	1	12219.58	−0.03	33569_4–45789°_5
6846.90	1	14601.12	−0.05	37414_3–52015°_3	8251.89	1	12115.11	−0.06	33952_3–46068°_3
6852.84	2	14588.46	−0.08	32217_3–46806°_2	8283.50	2	12068.87	−0.06	29430_3–41499°_3
6862.07	5	14568.84	−0.01	33569_4–48138°_5	8289.01	1	12060.85	−0.09	33201_5–45262°_4
6900.54	12	14487.62	−0.10	33201_5–47689°_4	8390.39	10	11915.12	−0.04	33201_5–45116°_4
6971.64	15	14339.87	−0.08	33201_5–47541°_6	8428.10	1	11861.81	−0.11	34465_3–46327°_2
6992.96	10	14296.15	−0.06	31077_2–45374°_1	8470.08	4	11803.02	−0.07	32217_3–44021°_3
7031.56	2	14217.67	−0.03	33952_3–48170°_3	8495.70	8	11767.43	−0.07	32217_3–43985°_4
7033.14	2	14214.48	−0.04	35299_4–49514°_3	8619.49	2	11598.43	−0.04	33952_3–45551°_3
7043.94	4*b*	14192.69	0.02	37414_3–51606°_2	8651.92	1	11554.95	−0.03	35299_4–46854°_5
7060.86	5	14158.68	0.10	33201_5–47360°_4	8662.53	1	11540.80	−0.07	32826_3–44367°_2
7081.21	1	14117.99	−0.09	35299_4–49417°_3	8691.03	1*b*	11502.96	0.00	32217_3–43720°_4
7098.22	15	14084.15	−0.03	29430_3–43514°_2	8698.35	8	11493.28	−0.05	29430_3–40923°_3
7128.71	2	14023.92	0.01	33569_4–47593°_3	8791.89	1	11371.00	−0.04	33569_4–44940°_4
7132.89	1	14015.70	−0.07	33952_3–47968°_4	8947.10	1	11173.74	0.02	31077_2–42251°_3
7151.20	1	13979.81	−0.01	32826_3–46806°_2	9018.33	1	11085.48	−0.01	34465_3–45551°_3
7173.38	5*b*	13936.59	−0.17	31077_2–45014°_3	9270.69	1	10783.72	−0.08	33201_5–43985°_4
7218.22	6*b*	13850.01	−0.10	32217_3–46068°_3	9353.72	2	10688.00	−0.05	32826_3–43514°_2
7219.18	2	13848.17	0.04	35299_4–49147°_4	9928.10	5	10069.66	0.09	37414_3–47483°_3
					9968.85	2	10028.50	0.08	37414_3–47442°_2

The new level at 33201.61 ($J=5$) has no place in the $(5d+6s)^6$ theoretical scheme as given by Shadmi and Caspi. Since it makes 20 combinations (3 times above the noise level) it is probably real.

The lines classified by these new levels are listed in table 2. The line at 7098 Å was inadvertently omitted from table 3 of Laun and Corliss [1968].

References

Laun, Donald D. and Corliss, C. H. (1968), J. Res. NBS **72A** (Phys. and Chem.) No. 6, 609 (1968).

Shadmi, Y. and Caspi, E. (1968), J. Res. NBS **72A** (Phys. and Chem.) No. 6, 757 (1968).

(Paper 73A3–551)

JOURNAL OF RESEARCH of the National Bureau of Standards—A. Physics and Chemistry
Vol. 73A, No. 3, May–June 1969

The Heat of Combustion of Beryllium in Fluorine*

K. L. Churney and G. T. Armstrong

Institute for Materials Research, National Bureau of Standards, Washington, D.C. 20234

(February 11, 1969)

An experimental determination of the energies of combustion in fluorine of polytetrafluoroethylene film and powder and of mixtures of beryllium with polytetrafluoroethylene gives for reaction (1) $\Delta H^\circ_{25^\circ C} = -1022.22$ kJ mol^{-1} (-244.32 kcal mol^{-1}) with an overall precision of 0.96 kJ mol^{-1} (0.23 kcal mol^{-1}) at the 95 percent confidence limits. The total uncertainty is estimated not to exceed ± 3.2 kJ mol^{-1} (± 0.8 kcal mol^{-1}). The measurements on polytetrafluoroethylene give for reaction (2a) and reaction (2b) $\Delta H^\circ_{25^\circ C} = -10369.7$ and -10392.4 Jg^{-1}, respectively. Overall precisions expressed at the 95 percent confidence limits are 3.3 and 6.0 Jg^{-1}, respectively.

$$Be(c) + F_2(g) = BeF_2(\text{amorphous}) \quad (1)$$

$$C_2F_4(\text{polymer powder}) + 2F_2(g) = 2CF_4(g) \quad (2a)$$

$$C_2F_4(\text{polymer film}) + 2F_2(g) = 2CF_4(g) \quad (2b)$$

Be_2C and Be metal were observed in a small carbonaceous residue from the combustion of the beryllium-polytetrafluoroethylene mixtures. Methods of analysis for these substances were developed. Gases resulting from the solution of the solid residues in aqueous KOH were analyzed for H_2 and CH_4 by differential absorption in molecular sieves at low temperatures.

Key words: Analysis of methane-hydrogen mixtures; beryllium fluoride; beryllium metal; combustion calorimetry; fluorine; heat of formation; molecular-sieve gas analysis; polytetrafluoroethylene.

1. Introduction

No direct determination of the heat of formation of crystalline beryllium fluoride by combustion of beryllium in fluorine has been published, probably because of the difficulty of obtaining reasonably complete combustion and the difficulty of obtaining a crystalline beryllium fluoride product.

All the published determinations are indirect and involve the heats of formation of BeO(s) and HF(aq). A heat of formation of BeF_2(s) near -242 kcal mol^{-1} (see [1][1]) is obtained if one assumes ΔH°_f [BeO(s)] is -143.1 kcal mol^{-1} based on Cosgrove and Snyder's [2] study of the direct oxidation reaction. An examination by Parker [3] of other values [4, 5, 6, 7] for the heat of formation of BeO(s) suggests the above value may be too positive by approximately one or more kcal mol^{-1}. The uncertainty in the heat of formation of HF(aq), a few tenths of a kilocalorie per mole, introduces a smaller though still significant effect.

Direct combination of beryllium with fluorine was undertaken to obtain a value for the heat of formation of BeF_2(s) that is independent of the heats of formation of BeO(s) and HF(aq). Better than 99 percent conversion of beryllium to beryllium fluoride was obtained by the device of burning a mixture of beryllium and polytetrafluoroethylene (PTFE) in fluorine.

X-ray analysis of the solid combustion products showed that amorphous rather than crystalline BeF_2 had been formed. The products also contained unburned beryllium, appreciable quantities of Be_2C, and a residue containing carbon and fluorine. The magnitudes and the uncertainties of the energy corrections for the various constituents of the combustion products are relatively larger fractions of the energy liberated by formation of BeF_2 than would be indicated by the degree of completeness of combustion since 65 to 70 percent of the total energy was due to the combustion of PTFE.

Failure to correct for the formation of Be_2C and the carbonaceous residue would have led to errors of the order of 0.1 percent and 1 percent, respectively, in the heat of formation of BeF_2. Consequently, an accurate method for determining the amounts of Be_2C and the residue as well as unburned beryllium metal was required, and its development constituted an important part of the experimental work.

*This work was supported by the Air Force Office of Scientific Research under Order No. OAR ISSA 65–8 and the Advanced Research Projects Agency under Order No. 20–60.

[1] Figures in brackets indicate the literature references at the end of this paper.

2. Preliminary Combustion Experiments

Attempts by other workers to burn beryllium foil [8], powder [9], or rod [9] to completion in fluorine have been notably unsuccessful (in general, less than 50% of the sample has burned). Similar difficulties encountered with aluminum were overcome in this laboratory by burning a pelleted mixture of aluminum and polytetrafluoroethylene powders in 20 atm pressure of fluorine [10]. The applicability of this method to combustion of beryllium was tested using metal powders with two sizes of particles. The first was a powder of 12 μm or finer particle size (passing 200 mesh) and 98.9 percent purity, designated as type BB; and the second was a powder of 25 μm or finer particle size (passing 100 mesh) and 99.7 percent purity, designated as type NM.

Type NM metal powder in mixtures with ratios of the weight of polytetrafluroethylene to weight of beryllium ranging from 2 to 20 burned with approximately the same percentage combustion, 75 to 90 percent. Spattering of beryllium metal onto the combustion-bomb walls, formation of glassy (lump) BeF_2, and corrosion of the holder were minimal when 0.1 g of metal was mixed with 1.7 g of polymer. Combustions of type BB beryllium powder in pellets of the last mentioned composition were 99 to 100 percent complete.

Of several sample supports tested only nickel resisted corrosion. Stainless steel and Monel reacted with the beryllium in the pellet to varying degrees. Calcium fluoride disks tended to crack or melt.

Both type BB and NM beryllium powders were burned in the preliminary combustion experiments and some calorimetric measurements were made with each. Only measurements made with the finer powder, type BB, were used in the final experiments because the disadvantage of a lower sample purity in the case of the finer powder was largely offset by its higher completeness of conversion to BeF_2. On the basis of experience obtained in the preliminary combustions, some changes in procedure and apparatus were made and are mentioned in the following sections.

A method of determining unburned beryllium accurate to 30 μg or better was required. An analysis based upon the reaction of beryllium metal with concentrated KOH to give hydrogen fulfilled this requirement and is summarized in section 9.

3. Materials

Beryllium. The amounts and assumed states of the impurities of the two beryllium samples are given in table 1. The amounts of the major impurities given in the batch analyses supplied with the samples were checked and, in general, confirmed by a nuclear activation technique. Carbon was determined as CO_2 by the Analysis and Purification Section of the National Bureau of Standards. The uncertainties in the amounts of the impurities were found from check analyses where performed; the remainder are our estimates of the uncertainties in the suppliers' analyses. An effort to obtain a check on the assay of metal from measurements of the amount of hydrogen evolved on dissolving the powders in aqueous HF, done in conjuction with other work performed in this laboratory [11], was only suggestive of the general accuracy of the impurity analysis in table 1, because the quantitative technique for collection of hydrogen had not been fully worked out.

Polytetrafluoroethylene (PTFE). The powder was obtained as a commercial preparation designated as TFE Fluorocarbon Resin, "Teflon 7". It was composed of irregularly shaped particles with an average size of 35 μm. Polytetrafluoroethylene film, designated as FEP Fluorocarbon Resin film, of 0.0025 cm thickness, was used to enclose the beryllium-PTFE mixtures. Neither the film nor the powder was modified or specially treated before use.

Fluorine. Two commercial preparations of fluorine were used, one of which was purified specially for the bomb calorimetry work. Samples were periodically analyzed by absorbing the fluorine in mercury and observing the residual pressure of the unreacted gases [16]. The residual gas was analyzed in a mass spectrometer. Typical analyses appear in table 2. The estimated uncertainties in the amounts of individual impurities include the uncertainty in our measurement of the total mole percent as well as the uncertainties in the relative amounts of impurities that were estimated by the mass spectrometrist. In the case of the purified fluorine a variation was observed in oxygen content, which gave rise to differing total impurities. Data obtained during composition analyzis definitely suggests that the major portion of SiF_4 and its variability are due to the reaction of fluorine with the glass walls of the gas analysis bulbs. It may be that the oxygen arose in this or a related process.

4. Calorimetric Apparatus

Heat measurements were made with an isothermal-jacket, stirred-water calorimeter of the Dickinson design [17] as modified by Prosen and co-workers [18]. One small change was made. The jacket and calorimeter vessel stirrers were coupled by rubber O-rings and pulleys to individual motors mounted on an insulated bracket on the jacket wall to minimize heat transfer between the motors and calorimeter. The jacket-water temperature was held constant to ± 0.002 °C near a value of 31 °C. The connections for the electrical leads between the calorimeter vessel and jacket were designed to insure good thermal contact with the calorimeter jacket.

Timing and temperature-measuring equipment and procedures for making the heat measurements are adequately described elsewhere [19, 20].

The combustion reactions were carried out in a commercially available combustion bomb with an internal arrangement similar to that described elsewhere [10]. The only major difference in the bomb arrangement is the presence of a filter to prevent the loss of BeF_2

TABLE 1. *Impurities in beryllium samples*

Impurity [a]	Amount (weight %)	Estimated uncertainty	Assumed products	Assumed ΔH_{f298} (kcal mol^{-1})	Reference
		Sample BB			
Li	0.0001	0.00005	LiF(c)	−147.1	[See Sec. 8.2].
B	.00004	.00002	BF_3(g)	−271.75	[12].
Be_2C	[b].20	.025	([e])	([f])	
Be_3N_2	.0393	.0197	BeF_2(s), N_2(g)	([f])	
BeO	[c].7252	.0445	BeF_2(s), O_2(g)	([f])	
Mg	.01	.01	MgF_2(c)	−268.7	[13].
Al	[c].0436	.0004	AlF_3(c)	−359.5	[12].
Si	[c].00831	.00126	SiF_4(g)	−385.98	[12].
Ca	.005	.005	CaF_2(c)	−290.3	[14].
Mn	[c].0056	.0004	MnF_3(c)	−238	[14].
Fe	[c].0795	.0108	FeF_3(c)	−235	[14].
Cu	.005	.0025	CuF_2(c)	−126.9	[14].
Ag	.0005	.00025	AgF(c)	−48.5	[14].
Cd	.00007	.00004	CdF_2(c)	−167.4	[12].
Ni	.009	.004	NiF_2(c)	−159.5	[14].
Pb	.0005	.0005	PbF_2(c)	−158.7	[12].
Mo	.001	.0005	MoF_6(g)	−372.35	[15].
Co	.0004	.0002	CoF_3(c)	−187	[14].
Cr	.009	.004	CrF_3(c)	−350	[14].
	1.14212				
Be (metal)	98.85788	[g] ±0.057			
Be (atomic)	99.26838	[g] ±0.040			
		Sample NM			
Be_2C	[b] 0.125	0.0250	([e])	([f])	
Be_3N_2	.0008	.0004	BeF_2(s), N_2(g)	([f])	
BeO	[c].1302	.0169	BeF_2(s), O_2(g)	([f])	
Al	[d].0016	.0004	AlF_3(c)	−359.5	
Si	[d].0017	.0004	SiF_4(g)	−385.98	
Mn	.0008	.0004	MnF_3(c)	−238	
Fe	[d].0013	.0003	FeF_3(c)	−235	
Cu	.0008	.0004	CuF_2(c)	−126.9	
Ni	.0005	.0003	NiF_2(c)	−159.5	
Cr	.0001	.0001	CrF_3(c)	−350	
	0.2628				
Be (metal)	99.7372	[g] ±0.030			
Be (atomic)	99.8597	[g] ±0.011			

[a] C, N, O are assumed to be combined as Be_2C, Be_3N_2, BeO.
[b] Determined by converting carbon to CO_2.
[c] Determined by nuclear activation.
[d] Determined by supplier for this sample.
[e] Be_2C is formed.
[f] ΔH°_{f298}: Be_2C(s), −26; Be_3N_2(s), −140.6; BeO(s), −145 kcal mol^{-1} [3].
[g] Square root of the sum of the squares of the individual uncertainties.

TABLE 2. *Typical analyses of Fluorine*

Analysis number	1		4	
Batch	Regular fluorine (1)		Purified, fluorine (2)	
Impurity	Mole %	Uncertainty	Mole %	Uncertainty
N_2	0.103	0.005	0.057	0.004
O_2	1.50	.1	.42	.03
Ar	0.0028	.001	.0017	.0003
CO_2	.070	.004	.068	.005
CF_4	.027	.002	.0055	.005
SO_2F_2	.0054	.0009	.0018	.0003
SiF_4	.38	.05	.047	.007
C_2F_6	.0028	.0003	.0011	.0002
C_3F_8	.0012	.0004	.00037	.00006
C_4F_8 (unsaturated)	.0005	.0002	.00010	.00005
C_2F_4 or C_4F_8 (cyclic)	.0003	.00015	.00011	.00005
SF_6	.0010	.0003	.00009	.00003
Total	2.09	[a].08	.633	[a].05

[a] Total uncertainty is based only on the a priori estimate of the uncertainty of the measurement of total moles of impurity.

when fluorine is removed from the bomb. The filter element, a Monel fritted disk, is held by lead O-rings in a stainless steel holder that screws into the inside of one port of the bomb head. Beryllium-PTFE pellets were burned in a shallow nickel cup resting on a nickel base plate that fitted into the bottom of the stainless steel liner of the combustion bomb. Combustions of PTFE powder and film alone were carried out on a Monel holder similar to that described by Domalski and Armstrong [10] after removal of the base plate, the cup, and the filter from the bomb.

The standard initial calorimeter for the fluorine experiments consisted of the combustion bomb with the internal arrangment for a beryllium-PTFE combustion, 6 cm of 0.005-cm diam tungsten fuse wire connected between two aluminum electrodes, an electrical heater (see [10] for a description of the heating element), a platinum resistance thermometer, and the calorimeter vessel with a weighed quantity of water.

5. Fluorine Manifold

The manifold and accessory equipment for filling the combustion bomb with fluorine, emptying it, and obtaining samples of fluorine and volatile products of combustion are nearly identical to that described by Domalski and Armstrong [10]. Two differences are noteworthy:

1. In the preliminary fluorine combustions, the bomb was connected to the manifold by a line (1/4 in O.D., 0.035 in wall-thickness Monel tubing) containing a filter of fritted monel. Prior to the loading with fluorine the bomb was evacuated by a vacuum pump, via the manifold and this line containing the filter, until the pressure in the manifold was less than 10^{-2} mm Hg. Occasionally premature ignition occurred (two beryllium-PTFE pellets and one PTFE pellet burned prematurely). The subsequent discovery of severe corrosion of the monel fritted filter suggested the premature ignition was due to poor evacuation of the bomb. Accordingly, in the final combustion experiments, the filter was removed from the line and, in addition, a second vacuum system was connected to the other bomb port via a short 3/8 in O.D. copper line. A thermocouple gage was mounted on this line at its connection to the bomb to give a more accurate indication of the pressure inside the bomb. The bomb was evacuated by both vacuum pumps until the manifold pressure was less than 10^{-2} mm Hg and the bomb pressure was less than 10^{-3} mm Hg. No further trouble was encountered with premature ignition in the final series of fifteen combustion experiments.

2. A ballast tank was installed in the manifold to allow the reduction of the pressure of the entire gaseous contents of the bomb after combustion to 1 atm prior to sampling for mass spectrometer analysis.

6. Beryllium Manipulation

On the basis of consultation of the literature [21, 22, 23, 24] and the experience of others who handled beryllium [25, 8], special procedures and certain equipment arrangements were deemed necessary for the safe handling of beryllium.

All manipulations involving the transfer or fluorine-combustion of beryllium powder were carried out in a high-exhaust-velocity fume hood which was decontaminated regularly by washing with dilute hydrochloric acid and water. The fluorine manifold and the calorimeter were in the hood and were protected from contamination by enclosure of the former in a water-tight lucite box and the latter in a polyethylene bag with a removable top. The manifold valves were operated by extension rods passing through PTFE O-ring seals in the box. The calorimeter controls were mounted outside the hood. The Monel fritted-disk filter mounted on the lower side of the combustion bomb head under the fluorine port was to prevent the escape of BeF_2 into the manifold while fluorine and volatile combustion products were being removed.

All transfers of solid combustion products were carried out in a dry box, after which all working surfaces of the box, the combustion bomb, and contaminated equipment were washed with water. The atmosphere of the box and box entry chamber was filtered and dried prior to removal of any equipment.

7. Combustion Experiments

7.1. Calibration

The calorimeter was calibrated by burning benzoic acid (standard sample 39h) in high purity (99.996%) oxygen at 30 atm pressure. The internal bomb arrangement differed from that in the standard fluorine bomb, as given in section 4, as follows: (1) the absence of the filter, nickel pellet cup, and aluminum electrodes; (2) the use of a Monel, instead of a nickel, base plate; and (3) the presence of platinum electrodes, a platinum crucible, a 2-cm piece of chromel-C fuse wire (0.16-mm dia) supported over the sample by platinum wire, and 1 cm^3 of distilled water. The energy equivalent of the oxygen calorimeter, calculated using standard procedures [19, 20], was 14,621.0 J $°C^{-1}$ with a standard deviation of the mean for seven experiments of 1.1 J $°C^{-1}$. The energy equivalent of the standard fluorine calorimeter was 14,656.68 J $°C^{-1}$.

7.2. Pellet Preparation

The weights of pellets of PTFE formed by rapid compression of powder decreased appreciably with time (as much as 400 μg in 20 hr). Consequently, PTFE pellets were weighed after being stored in the balance case for 1 month, and pellets of both powder and film were formed by slow compression in the die pieces.

Beryllium-PTFE mixtures were prepared in PTFE bags to reduce losses during transferring and pelleting that occurred in earlier mixing techniques [10] where no bags were used. Since being developed for the present study, this pelleting technique has been further modified and applied successfully to the combustion of other substances in fluorine [26–29]. A bag was made out of PTFE film. The film was sealed by sandwiching a fold in the film layers between two strips of aluminum and gently heating the exposed crease near an open flame. For preparation of the pellets about 1.7 g of PTFE and 0.1 g of beryllium were transferred to the weighed bag. The materials were weighed after each addition. The bag contents were mixed by moving the enclosed bubble of air through the mixture. The bag was then punctured, placed in a pellet die piece, slowly compressed into a pellet, and stored in a desiccator.

Weight changes for a number of pellets prepared during this research are summarized in table 3. The method of pellet preparation in the final combustion experiments was different from that used in the preliminary experiments in the following ways:

1. Beryllium powder was added to the bag before the PTFE powder in final experiments. This reduces the possibility that any weight loss on sealing the bag (item (1), table 3) is due to loss of beryllium rather than PTFE. However, in all cases this weight loss was assumed to be loss of PTFE bag.
2. A larger puncture was made in the bag and pressure was applied more slowly to the die pieces in forming a pellet in final experiments (30 min rather than 2 min). This resulted in better agreement between the weight of the pellet just before it was burned and the weight of the sealed bag plus contents just prior to pelleting (item (3), table 3). The weights of all newly formed pellets except sample 6 of the preliminary combustions were greater than the weights before pelleting (item (2), table 3); however, the weights of the pellets approached a constant weight in the final experiments in a shorter period of time than in the preliminary experiments.
3. More closely fitting die pieces were used in the preparation of the pellets of final experiments. As a consequence, no PTFE was found on the die pieces and no correction was necessary for loss of PTFE.

7.3. Experimental Heat Measurements

Eight experiments summarized in table 4 were used to establish the energy of combustion of the PTFE

TABLE 3. *Weight changes (μg) in beryllium-PTFE pellet preparation*

Series	Preliminary combustions						Final combustions				
Sample No.*	1(1)	2	3	4	5(3)	6	1	2(4)	3(5)	4(6)	5(7)
(1) Wt. after minus wt. before sealing	−72	−18	−29	−246	−278	−88	−36	−39	−115	−15	−24
(2) Wt. after minus wt. before pelleting	201	198	125	282	23	259	151	207	218	168	215
(3) Wt. prior to combustion minus wt. before pelleting	51	46	−15	−23	−45	−19	−26	−14	22	2	−1
Elapsed time (days) between weighing before pelleting and before combustion	12	18	54	56	60	61	15	16	17	18	3

*Number in parentheses corresponds to expt. No. in tables 6 and 8.

powder. The combustion in each case was almost entirely complete. The residues recovered in no case amounted to more than 0.02 percent of the original mass. The energy of combustion of the PTFE film was determined separately in a series of three combustion experiments summarized in table 5. The degree of completeness of these combustions was comparable to that of the powder.

Four final combustions of beryllium-PTFE pellets were successfully completed and are listed in table 6. Three preliminary combustion experiments of beryllium-PTFE pellets are also listed in table 6 for sake of comparison and discussion in section 8.4.

7.4. Analysis of Combustion Products

After a PTFE combustion, the area of the sample holder that had been in contact with the pellet was covered with a thin black film. This minute residue was weighed by difference by wiping off the film and was assumed to be unburned PTFE. Correction for the effect of adsorption of water by the fluoride coated holder was made by determining the increase in mass of the holder as a function of time and extrapolation to the time the holder was first exposed to air. The corrected mass of residue is the second entry in table 4 and 5.

Samples of the volatile combustion products were analyzed with a mass spectrometer after absorption of the fluorine in mercury. Results of some typical analyses are presented in table 7 in terms of the differences in the amounts of impurity present after a combustion from those present prior to a combustion. The uncertainties include those of the fluorine analyses as well as the volatile combustion product analyses. The average changes in higher fluorocarbons listed at the bottom of table 7 were used in calculating item 8 of table 4, 5, and 6.

TABLE 4.[a] *Combustion of PTFE powder*

Experiment	1	2	3	4	5	6	7	8
m(pellet)....g	4.287787	4.297522	3.796061	4.349297	4.368609	2.926029	4.318171	2.860629
m(residue)....g	0	0.000600	0.000756	0.000361	0.000142	0.000233	0.000299	0.000364
1. m'(PTFE reacted)....g	4.287787	4.296922	3.795305	4.348936	4.368467	2.925796	4.317872	2.860265
2. $p_i(F_2)$....atm	18.58	18.57	20.26	20.18	20.40	20.25	20.62	20.09
3. E^i(cont)....J °C^{-1}	−19.96	−19.97	−19.83	−19.14	−18.93	−20.11	−19.08	−20.24
4. Δt_c....°C	3.04130	3.04877	2.69334	3.08567	3.09823	2.07538	3.06222	2.02860
5. ΔE_{IBP} [b]....J	−44,514.66	−44,623.96	−39,422.01	−45,166.62	−45,351.12	−30,376.44	−44,823.55	−29,691.48
6. ΔE(gas) [c]....J	18.68	18.72	17.26	20.07	20.48	13.13	19.70	12.57
7. $-n\Delta E°$(fuse)....J	17.71	18.75	18.49	18.64	17.49	21.87	20.74	20.93
8. $-n\Delta E$(Imp, gas)....J	1.99	1.99	1.99	1.99	1.99	1.99	1.99	1.99
9. $\Delta E°_c(t_h)/M$....J g^{-1}	−10,372.78	−10,375.91	−10,377.10	−10,376.31	−10,372.32	−10,369.64	−10,371.11	−10,368.34
10. $(31\text{-}t_h)\times\underline{\Delta C_p}$....J g^{-1}	−0.10	−0.10	−0.29	−0.10	−0.08	−0.11	−0.11	−0.11
11. $\Delta E°_c(31°)/M$....J g^{-1}	−10,372.88	−10,376.01	−10,377.39	−10,376.41	−10,372.40	−10,369.75	−10,371.22	−10,368.46

Mean $\Delta E°_c(31\ °C)/M = -10{,}373.07$ J g^{-1}; standard deviation of mean = 1.16 J g^{-1}
$\Delta C_p \times (25\text{–}31) = +3.41$ J g^{-1}
$\Delta E°_c(25\ °C)/M = -10{,}369.66$ J g^{-1}; standard deviation of mean = 1.16 J g^{-1}

[a] Symbols employed are explained in refs. [31, 32].
[b] $\Delta E_{IBP} = [E(\text{calor}) + E^i(\text{cont})] \times (-\Delta t_c)'$
[c] $\Delta E(\text{gas}) = \Delta E(\text{gas})\,[g_i{}^{(\text{gas})} + \Delta E^f(\text{gas})]^a_{pf(\text{gas})}$

TABLE 5.[a] *Combustion of PTFE film*

Experiment	1	2	3
m(pellet)....g	3.106874	3.097896	3.074705
m(residue)....g	0.000438	0.000837	0.000685
1. m'(PTFE reacted)....g	3.106391	3.097059	3.074020
2. $p^i(F_2)$....atm	20.22	20.26	19.59
3. E^i(cont)....J °C^{-1}	−19.98	−19.98	0.97
4. Δt_c....°C	2.20895	2.20266	2.18224
5. ΔE_{IBP}[a]....J	−32,331.74	−32,239.67	−31,986.51
6. ΔE(gas)[a]....J	13.92	13.84	12.48
7. $-n\Delta E°$(fuse)....J	22.63	20.74	22.63
8. $-n\Delta E°$(Imp, gas)....J	1.99	1.99	1.99
9. $\Delta E_c°(t_h)/M$....J g^{-1}	−10,395.73	−10,397.96	−10,393.36
10. $(31°-t_h)\times\Delta C_r$....J g^{-1}	−0.11	−0.11	−0.12
11. $\Delta E_c°(31\ °C)/M$....J g^{-1}	−10,395.84	−10,398.07	−10,393.48

Mean $\Delta E_c°(31\ °C)/M = -10{,}395.80$ J g^{-1}; standard deviation of mean 1.33 J g^{-1}
$\Delta C_r \times (25-31) = +3.41$ J g^{-1}
$\Delta E_c°(25\ °C)/M = -10{,}392.39$ J g^{-1}

[a] See footnotes to table 4.

TABLE 6.[a] *Combustion of beryllium-PTFE mixtures*

Number, type of Be	Preliminary combustions			Final combustions			
	1,NM	2,BB	3,NM	4,BB	5,BB	6,BB	7,BB
1a. m(PTFE powder), g	2.031374	2.159857	2.187286	1.983933	2.479838	2.005580	2.082622
1b. m(PTFE film), g	0.528567	0.494459	0.537886	0.462695	0.473074	0.436645	0.464008
1c. m(Be sample), g	.100614	.089802	.104813	.089153	.080249	.113741	.091545
1d. m(atomic Be in sample), g	.100473	.089145	.104666	.088501	.079662	.112909	.090875
1e. m(Be_2C formed), g	.005316	.000033	.006447	.000101	.000035	.000178	.000102
1f. m(Be in Be_2C, products), g	.003266	.000128	.003947	.000167	.000117	.000243	.000171
1g. n(beF_2 formed), mol × 10^3	8.72939	9.86097	9.19720	9.78562	8.80151	12.49062	10.05448
2. $p^i(F_2)$, atm	19.99	20.08	20.35	18.87	18.73	18.90	18.84
3. E^i(cont), J °C^{-1}	−85.06	8.92	−32.09	9.20	9.90	9.56	9.47
4. Δt_c, °C	2.42047	2.55480	2.55497	2.40858	2.69866	2.59427	2.49879
5. ΔE_{IBP}, J	−35,270.17	−37,467.67	−37,365.39	−35,323.95	−39,580.11	−38,048.19	−36,647.63
6. ΔE(gas), J	8.30	8.54	9.62	7.10	9.60	6.35	7.50
7. $-n\Delta E°$(Fuse), J	22.61	22.61	21.69	20.79	18.86	20.75	22.63
8. $-n\Delta E°$(Imp, gas), J	9.80	−12.37	−12.37	−12.37	−12.37	−12.37	−12.37
10. $(t_h - 31) \times \Delta C_v$, J g^{-1}	0.44	0.37	0.26	0.23	0.14	0.11	0.12
12. $-n\Delta E°$(PTFE powd.)[b], J	21,070.69	22,403.55	22,688.30	20,579.02	25,723.19	20,803.80	21,602.93
13. $-n\Delta E°$(PTFE film)[b], J	5,494.64	5,140.11	5,591.62	4,809.98	4,917.92	4,539.23	4,823.68
14. $-n\Delta E°$(Be_2C formed), J	−143.96	−0.89	−174.58	−2.74	−0.95	−4.82	−2.76
15. $-n\Delta E°$(residue), J	−62.85	−32.70	−141.64	−47.66	−40.88	−37.75	−32.93
16. $-n\Delta E°$(imp, solid), J	−2.96	−10.93	−3.08	−10.85	−9.77	−13.84	−11.14
17. $-n\Delta E°$(BeF_2), J	−8,873.90	−9,949.75	−9,385.83	−9,980.68	−8,974.51	−12,746.84	−10,250.09
18. $\Delta E°$(BeF_2), kJ mol^{-1}	−1,016.55	−1,009.00	−1,020.51	−1,019.93	−1,019.65	−1,020.51	−1,019.46
19. ΔnRT_h, kJ mol^{-1}	−2.52	−2.52	−2.52	−2.53	−2.53	−2.53	−2.53
20. $\Delta C_p° \times (25 - t_h)$, kJ mol^{-1}	+0.18	+0.18	+0.19	+0.19	+0.20	+0.20	+0.20
21. $\Delta H°_{25}$(BeF_2), kJ mol^{-1}	−1,018.89	−1,011.34	−1,022.84	−1,022.27	−1,021.98	−1,022.84	−1,021.79

Mean $\Delta H°_{25}$ (BeF_2)[c] = −1,022.22 kJ mol^{-1} (−244.32 kcal mol^{-1}): standard deviation of mean 0.23 kJ mol^{-1} (.05 kcal mol^{-1}).

[a] See footnotes to table 4.
[b] $\Delta E°$ for PTFE powder and PTFE bags were corrected to t_h for each experiment.
[c] Final combustions only.

TABLE 7. *Typical volatile product analysis and increase in constituents on combustion* [a]

Combustion ingredients	Be(NM) [b] PTFE, 0.0510 mol Fluorine (1), 0.287 mol		Be(NM) PTFE, 0.0492 mol Fluorine (2), 0.270 mol		PTFE, 0.0874 mol Fluorine (2), 0.276 mol	
Impurity	Increase	Uncertainty	Increase	Uncertainty	Increase	Uncertainty
	μ mol	*μ mol*	*μ mol*	*μ mol*	*μ mol*	*μ mol*
N_2	540	40	60	20	270	30
O_2	7400	400	170	70	1190	30
Ar	80	10	400	60	80	40
CO_2	−30	10	−3.0	10	160	10
SO_2F_2	5.0	6.0	7.0	3.4	−4.1	0.5
SF_6	−0.1	2.0	0.0	.....	−2.5	0.8
C_2F_4	−0.9	0.5	−0.3	0.15	.....	.....
C_2F_6	−4.0	3.0	12.3	5.4	2.6	2.2
C_3F_8	−3.4	1.0	−0.8	0.2	−0.5	0.2
C_4F_8	−1.9	0.5	3.4	1.0	−1.3	0.6
Average changes	Be-PTFE-Fluorine (1)		Be-PTFE-Fluorine (2)		PTFE-Fluorine (2)	
C_2F_4	−0.9	0.5	−0.3	0.15	0.0	0.2
C_2F_6	−4.0	3.0	12.5	5.4	2.6	1.7
C_3F_8	−3.4	1.0	−0.8	0.2	−0.5	0.2
C_4F_8	−1.9	0.5	3.0	1.0	−1.3	0.4

[a] See table 2 for appropriate typical fluorine analysis.
[b] Be(NM) is the type NM beryllium sample.

After combustion of a beryllium-PTFE mixture, the exterior of the bomb was dried in the dry box entry chamber by evacuation of the entry chamber. After disposal of volatile combustion products by use of the manifold, the bomb was filled with 1 atm pressure of helium and was opened in the dry box in which the atmosphere has been dehumidified until the dew point was −78 °C. The solid combustion products from the bomb were stored in vials or petri dishes in a desiccator.

The inner surfaces of the bomb were covered with a fine white hygroscopic powder after a beryllium-PTFE combustion. The larger part of this powder was confined to the nickel pellet cup, where it covered a small amount of mixture of black particles. Analysis of the beryllium content (measured as BeO) of a known weight of the white powder showed it to be correct for BeF_2; the x-ray pattern was similar to that observed by Warren and Hill [30] for vitreous BeF_2.

The contents of the pellet cup were analyzed by reaction with hot concentrated KOH, for the amount of unburned beryllium (as H_2 gas) and beryllium carbide (as CH_4 gas) by the procedure described in section 9. The black residue remaining in the KOH solution was filtered, washed, dried, and weighed. Its appearance suggested a mixture of unburned PTFE and fine black powder.

Residues from the beryllium-PTFE combustions were collected quantitatively in glass fritted-disk filters, weighed, and sent to the NBS Analysis and Purification Section for analysis of either carbon or fluorine content.

Table 8 is a summary of the combustion product analyses. Details of the determinations of beryllium and beryllium carbide are given in section 9. Precisions of the determinations of beryllium and beryllium carbide are the 95 percent confidence limits based on the standard deviation of the single measurements of the moles of gas cited in section 9.

TABLE 8. *Results of combustion-product analyses*

Expt. No.	Unburned beryllium	Precision	Be_2C in products	Precision	Weight of residue	Precision	Residue analysis	
							% C	% F
	mg	*mg*	*mg*	*mg*	*mg*	*mg*		
Preliminary combustions								
1.	18.536	0.037	5.442	0.125	1.683	0.04	54.7	.....
2.	0.148	.005	0.213	.015	1.706	.04	34.0	.....
3.	17.832	.034	6.578	.059	2.131	.04	87.8	.....
Final combustions								
4.	0.144	0.003	0.279	0.003	2.420	0.04	.....	.....
5.	.184	.006	.195	.016	2.011	.04	35.3	.....
6.	.098	.003	.405	.034	1.916	.04	.....	9.4
7.	.091	.003	.285	.011	1.670	.04	.....	5.4

8. Discussion and Results

8.1. Treatment of Combustion Data

The notation of tables 4, 5, and 6 and method of standard state corrections are explained in detail elsewhere [31, 32]. The numbered entries are: (1) the mass (weight in vacuum) of PTFE reacted (tables 4 and 5), or moles of beryllium fluoride (table 6, item 1g) formed; (2) the initial pressure of fluorine; (3) corrections to be added to the energy equivalent of the standard fluorine calorimeter for fluorine, combustion sample, and variations in internal bomb arrangement; (4) the observed increase in calorimeter temperature corrected for heat exchanged between the calorimeter and its surroundings and for stirring; (5) the energy equivalent of the actual calorimeter multiplied by the corrected temperature rise; (6) the net correction due to the hypothetical compression and decompression of bomb gases; (7) the correction for fuse energy; (8) the correction for the change in the amounts of higher gaseous fluorocarbons as estimated in table 3; (9) the energy of combustion of PTFE powder (table 4) or film (table 5) at the temperature, t_h, to which the isothermal bomb process is referred in each experiment; (10) the correction to be added to the energy of combustion at t_h of PTFE powder or film per unit mass to obtain the value at 31 °C (tables 4 and 5) or vice versa (table 6); (11) the standard state energy change at 31 °C per gram of PTFE film (table 4) or powder (table 5) for reaction (2); (12) and (13) corrections for the energy contributed by the PTFE powder and by the film assuming both are completely converted to CF_4; (14) the correction for the formation of Be_2C(s) according to reaction (4);

$$2Be(s) + CF_4(g) \rightarrow Be_2C(s) + 2F_2(g) \qquad (4)$$

(15) the correction for carbon, according to reaction (5a), and unburned PTFE, according to reaction (5b) in the combustion products;

$$CF_4(g) \rightarrow C(s) + F_2(g) \qquad (5a)$$

$$2CF_4(g) \rightarrow C_2F_4(\text{polymer film}) + 2F_2(g) \qquad (5b)$$

(16) the correction for the combustion of the impurities in the sample of beryllium excluding Be_2C; (17) the energy change associated with the formation of BeF_2(s), alone, at the temperature t_h; (18) the same energy change divided by the moles of BeF_2(s) formed; (19) the correction to obtain the enthalpy change per mole of BeF_2(s) at t_h; (20) the standard state enthalpy of formation of BeF_2(s) at 25 °C by reaction (1).

For item (1) of tables 4 and 5, the PTFE "residue" is treated as unburned PTFE. Items 1a-1c of table 6 list the contents of the beryllium-PTFE pellet. Item 1g of table 6 is computed from item 1d, table 6, minus the sum of item 1f, table 6, and the weight of unreacted beryllium in table 8. Thus, this gives the total number of moles of BeF_2(s) formed from BeO(s) and Be_3N_2(s) as well as Be(s). In item (5), the ignition energy was assumed to be zero (as in the calibration experiments). Items (9) and (10) are based on the mass of PTFE film and powder before the pellet was formed. The loss in weight occurring on sealing the bag was assumed to be loss of PTFE film. No correction was applied to the film weight for loss during pelleting unless film was found on the pellet die pieces. Item (14) is based on a value of $\Delta E°$(31 °C) of 27.08 J mg^{-1} of Be_2C(s) formed and item 1e. Item (15) assumes the residue consists of carbon and unburned PTFE film (pieces of film were observed in combustion residues). Experiments 1, 2, 3, and 5 are based on the analyses cited in table 8 while the remainder assume 34.6 percent carbon by weight (the average of experiments 2 and 5). $\Delta E°$(31 °C) for reaction (6b) was taken to be 77.19 J mg^{-1} of carbon. Item (16) is based on table 1. The corrections used were 2.22 J g^{-1} for sample NM and 58.35 J g^{-1} for sample BB. The temperature of the hypothetical isothermal process to which each of items (2) through (13) refers, t_h, is the final temperature the calorimeter would have had for each experiment if no heat had been exchanged with the surroundings and the stirring energy was zero.

8.2. Auxiliary Data

Buoyancy corrections for the masses of beryllium, PTFE powder, and PTFE film were calculated using densities of 1.84 [33], 2.15, and 2.21 g cm^{-3}, respectively. The densities of the PTFE film and powder were determined experimentally.

A heat of formation of WF_6(g) of −416 kcal mol^{-1} [34] was used to compute the fuse energy (22.61 J for 6 cm of wire).

Data for the net heat correction for the hypothetical compression and decompression of bomb gases are based on the parameters of the Lennard-Jones 6–12 potential function determined for fluorine by White, Hu, and Johnston [35] and for CF_4 by Douslin [36]. Second virial coefficients for the mixture of F_2(g) and CF_4(g) in the reaction products were calculated from those of the pure products. The values used for C_v (20 atm, 304.15 K) and $C_v°$ (298.15 K) for fluorine and C_v (298.15 K) for CF_4 were 5.54, 5.499 [37], and 12.607 [38] cal deg^{-1} mol^{-1}, respectively. Values of C_p in cal deg^{-1} g^{-1} for beryllium, PTFE, and BeF_2(c) were taken to be 0.436 [39], 0.280 [40], 0.264 [41], respectively.

The heats of formation used in the calculation of heat corrections for impurities in the beryllium samples, the formation of Be_2C, and the beryllium-PTFE residues are those given in table 1 and a heat of formation of −221 [12] kcal mol^{-1} for CF_4(g). While this value for CF_4 has been superseded [27], the change introduced in this correction is insignificant in comparison to other errors (see table 10).

For $\Delta H_f°$[LiF(c)], the heat of solution found by Stephenson, Hopkins, and Wulff [42] was combined with values for the heats of formation of Li^+(aq) [43] and F^-(aq) [12]. The heats of formation of C_2F_4(g), C_2F_6(g), C_3F_6(g), C_3F_8(g), and C_4F_8(g) used to calculate the heat correction for the change in higher fluorocarbon content of the gases in a fluorine combus-

TABLE 9. *Calorimetric results*

Quantity	Units	Value	Precision of measurements[a]	Overall precision	Uncertainty
(1) ΔH_c°(25 °C)/M, PTFE powder	J g^{-1}	−10,369.7	2.7	[b] 3.3	
(2) ΔH_c°(25 °C)/M, PTFE film	J g^{-1}	−10,392.4	5.7	[b] 6.0	
(3) ΔH_f°(25 °C), BeF_2(s, amorphous)[e]	k J mol^{-1}	−1,022.22	0.73	[c] 0.96	[d] ±3.2
ΔH_f°(25 °C), BeF_2(s, amorphous)	kcal mol^{-1}	−244.32	0.17	0.23	±0.8

[a] Based on 95 percent confidence limits, Students' t distribution.
[b] Includes effect of precision of 2.7 J $°C^{-1}$ of energy equivalent of calorimeter.
[c] Includes effect of (1) and (2) as well as b.
[d] See table 10.
[e] Results of final combustions.

tion were −155.5 [12], −310 [12], −259 [44], −409 [44], and −352[44] kcal mol^{-1}, respectively.

Atomic weights used in the calculations were taken from the 1961 Table of Atomic Weights based on $C^{12}=12$ [45]. The atomic weights of Be and F are 9.0122 and 18.9984, respectively. The unit of energy is the joule. One calorie is taken as 4.184 J.

8.3. Summary of Results and Estimates of Uncertainties

Table 9 is a summary of our results and our estimates of their uncertainties. Precisions, as used here, give the 95 percent confidence limits calculated from the Student t distribution. The column "precision of the measurements" was calculated from the standard deviations of the means of the measurements. The column "overall precision" includes the scatter due to the calibration experiments, item (1), and, in the case of the heat of formation of BeF_2(s), item (5), also includes the scatter due to the PTFE combustion, items (2) and (3), combined as the root mean squares using the usual propagation of error formulas. The enthalpy of combustion found for PTFE powder differs by only 0.003 percent from that reported by Domalski and Armstrong [27]. The overall uncertainty is the root mean square of the systematic error and overall precision.

Estimates of the systematic errors in the heat of formation of amorphous beryllium fluoride due to recognizable uncertainties are listed in table 10 for both types of beryllium samples. Unless otherwise indicated errors are of indeterminant sign. Where a sign is given, the error is to be added to the absolute value of the heat of formation of BeF_2(s). They arise respectively from (1) the initial weight of beryllium sample; (2) weight of unburned beryllium; (3) the difference in energy equivalent of the internal bomb arrangement in the calibration and fluorine experiments; (4) failure to collect all the unburned fuse; (5) the estimated change in higher fluorocarbons than CF_4 in the bomb during the combustion; (6a) the weight of PTFE in a beryllium-PTFE experiment; (6b) composition and weight of the residue in PTFE combustions used to determine ΔE° (PTFE); (7a) weight of the beryllium carbide in the products of combustion; (7b) the heat of formation of beryllium carbide; (7c) effect of assuming carbon is present in the elemental state rather than Be_2C in the initial beryllium sample; (8a) weight of carbon in the residue from beryllium-PTFE combustions; (8b) effect of computing the PTFE content of the beryllium-PTFE residues on the bases of fluorine content; (8c) energy of formation of CF_4(g) used in this calculation; (9) the correction for the effect of impurities in the initial beryllium sample; (10) reaction of beryllium with fluorine prior to carrying out the heat measurements; (11) corrosion of components of the combustion bomb.

The errors were calculated using 10.283×10^{-3} and 8.963×10^{-3} moles of BeF_2(s) formed for sample type BB and NM, respectively. $\Delta E^\circ(BeF_2)$, item 18 of table 6, was taken to be 1020 kJ mol^{-1} for both sample types.

Item (1) assumes an error of 0.02 mg in the weight of the initial sample of beryllium. This is probably

TABLE 10. *Systematic errors in* $\Delta H_f^\circ[BeF_2(s)]$

Samples	BB	NM
(1) Wt. of beryllium sample	0.021%[a]	0.025%[a]
(2) Wt. of unburned beryllium	.011	.15
(3) ΔE_{IBP}	.054	.054
(4) $-n\Delta E^\circ$(fuse)	−.015	−.022
(5) $-n\Delta E^\circ$(Imp, gas)	.036	.041
(6) $-n\Delta E^\circ$(PTFE powd., film)		
(a) Wt. PTFE	.005	.005
(b) ΔE°(31 °C)/M, PTFE	−.023	−.026
(7) $-n\Delta E^\circ$(Be_2C formed)		
(a) Wt. of Be_2C in products	.011	.045
(b) ΔE° (Be_2C formed)	−.003	.15
(c) Free carbon in beryllium	−.051	−.035
(8) $-n\Delta E^\circ$(residue)		
(a) Wt. of carbon	.083	.083
(b) PTFE on basis of F^-	+.097	
(c) $\Delta E^\circ[CF_4(g)]$	−.023	
(9) $-n\Delta E^\circ$(Imp, beryllium sample)	.033	.010
(10) Prereaction	+.10	
(11) Corrosion	−.10	−0.10
Total	±0.3%	

[a] Percentages without signs are of indeterminant sign. Those preceded by a sign are to be added to the absolute value of $\Delta H_f^\circ[BeF_2(s)]$.

valid only when the pellet was prepared in the manner described for the final combustions.

Item (2) assumes errors of 0.01 mg and 0.12 mg in the weight of the unburned beryllium for samples BB and NM, respectively. These are approximately three times the a priori precision of the determinations. In the case of sample BB, this corresponds to a 10 percent uncertainty in the average weight of unburned beryllium (0.129 mg). The error due to the assumption that hydrogen is produced only by unburned beryllium in the combustion products appears to be within these estimates. If, for example, all impurities other than BeO(s), Be_2C(s), and Be_3N_2(s) in sample type BB did not react with fluorine but reacted with KOH to give H_2(g), the resulting error would be -0.003 percent.

Item (3) is based on a 5 percent uncertainty in the heat capacity of components added to the combustion bomb for the beryllium-PTFE experiments. Item (4) assumes 0.5 mg loss in collection of unburned fuse in the beryllium-PTFE and PTFE experiments. Item (5) is based on the uncertainties given in table 7.

Item (6a) assumes an uncertainty in loss of PTFE film due to sealing equal to the average loss in the weight of pellets prepared for the final combustion in table 3. Item (6b) is computed on the basis that the maximum systematic error in $\Delta E°$(PTFE) is 0.01 percent due to assuming the residue in a PTFE combustion is PTFE. Domalski and Armstrong [27] have shown on the basis of residue analyses of PTFE combustions that this assumption is most probably true. The close similarity of our combustion arrangement to the one used in that work and the close agreement of our results (0.007%) on the same sample of PTFE supports our estimate of an error considerably less than that caused in $\Delta E°$(PTFE), of $+0.06$ percent for powder and 0.14 percent for film, and in $\Delta H_F°(BeF_2)$ of -0.18 percent, if the residues from the PTFE combustions were free carbon.

Item (7a) assumes an error of 0.1 mg and 0.03 mg in the weight of Be_2C in the products of combustion of samples NM and BB, respectively (see table 8). Item (7b) is based on a net uncertainty of 2 kcal mol^{-1} in the energy correction for reaction (4). Item (7c) considers the effect if carbon is present as free carbon in the initial beryllium sample.

Item (8a) assumes an uncertainty of 0.1 mg in carbon content in the residue. Item (8b) is the maximum correction one would obtain for the combustion experiments 6 and 7 if the fluoride and estimated average carbon contents of the residues are used. The error in sample NM is assumed to be the same. Item (8c) is the effect of altering the formation of CF_4(g) from -221 to the more accurate value of -223 kcal mol^{-1}[27]. Item (9) is based on the uncertainties in table 1 and is the net effect on the moles of BeF_2(s) produced, $-n\Delta E°$ (Be_2C formed), and $-n\Delta E°$ (Imp, solid).

Item (10) is based on the observed weight change in a beryllium-PTFE pellet exposed to fluorine during the preliminary combustion experiments (i.e. prior to the improvements in evacuation of the combustion bomb). The probability that poor evacuation during this experiment promoted prereaction suggests the estimate is an upper limit for the final combustion experiments. Additional evidence that substantially more prereaction was occurring during the preliminary combustions than the final combustion experiments comes from a comparison of the cooling constants of the calorimeter for the PTFE combustion experiments[2] and the beryllium-PTFE preliminary[3] and final combustion[4] experiments. Since one PTFE pellet as well as two beryllium-PTFE pellets ignited prematurely during the preliminary combustion experiments, it is impossible to assign the prereaction to beryllium alone during the preliminary combustions.

The basis for item (11) is the estimate of corrosion of the nickel cup in which the beryllium-PTFE pellet was burned. In a separate test, it was found that the weight change of a cup after prolonged boiling in concentrated KOH was negligible (< 0.02 mg). The weight increase of the cup upon exposure to fluorine was small (~ 0.08 mg). However, the average loss in the weight of the cups after the fluorine combustions and the reaction with concentrated KOH were carried out was 0.83 mg corresponding to a loss of 1.4×10^{-5} moles of nickel. While this is equivalent to the moles of hydrogen ascribed to unburned beryllium in the final experiments, there was no observable indication that any part of the cup during the KOH reaction was was giving off hydrogen. Since no pitting of the cups where the unburned beryllium had been located was observed, it seems probable the weight loss was due principally to NiF_2(s) formation during the fluorine combustion and its dislodgment during the rotation of the nickel cup during the KOH reaction. Thus the error estimate is probably an upper limit.

The errors of indeterminant sign were combined as the square root of the sum of the squares of the individual errors to give 0.11 percent for sample BB. The total error was computed as the extremes of the sum of the errors of determinant sign and the aforementioned averages. Since the error bounds are nearly symmetrical an uncertainty of ± 0.3 percent was taken for the systematic error and combined with the overall precision given in table 9 to yield the overall systematic error, also given in table 9.

8.4. Discussion of Results

The results of the preliminary beryllium-PTFE combustion experiments were assigned zero weight because of poor sample preparation and the possibility of appreciable amounts of "prereaction" of beryllium whenever the combustion bomb was poorly evacuated prior to filling with fluorine. The results were presented because the approximate agreement of those based on beryllium sample type NM, which has nearly 20 percent unreacted beryllium in the reaction products, with the final combustion experiments. We feel this lends additional confidence in the method for determining unreacted beryllium. Also, the large quantities of methane found in the gases evolved in

[2] 2.104 $min^{-1} \pm 0.003$ min^{-1} (std. dev. of mean for 11 experiments).
[3] 2.144 $min^{-1} \pm 0.007$ min^{-1} (std. dev. of mean for 5 experiments).
[4] 2.102 $min^{-1} \pm 0.001$ min^{-1} (std. dev. of mean for 4 experiments).

the combustion product reaction with KOH in experiments 1 and 3, undoubtedly due to Be_2C, support our assumption that the small amount of methane found in the KOH analyses of experiments 4 through 7 also originates from Be_2C.

The relatively large quantity of "PTFE residue" in the beryllium-PTFE combustion products plus the problems of determining its composition constitute a serious drawback in our experiments. As noted in section 8.1, we assumed the residue consisted solely of carbon and PTFE and computed the results using the observed carbon contents for experiments 1 and 3 and the average of the percentage carbon contents of experiments 2 and 5 for the remainder. The higher carbon contents of the residues in experiments 1 and 3 (54 and 89%, respectively) as compared to the other experiments (~ 35%) are consistent with the presence of the much greater amount of unreacted beryllium and the formation of beryllium carbide and are unequivocal evidence that free carbon (or a fluorocarbon polymer having higher carbon content than PTFE) is present. The expectation that the carbon content of the residues of remaining experiments is relatively constant (we assume $34.6 \pm 5\%$, item 8a of table 10) is compatible with the idea that the unreacted beryllium and amounts of Be_2C are small. However, the fluoride contents of the residues of experiments 6 and 7 are in gross disagreement with the assumption of presence of only carbon and PTFE in these residues; about 0.9 mg of other materials must be present to obtain mass balance if we assume all the fluorine is present as unburned PTFE. Even if we assume the fluoride contents are systematically low as expected [46], it is most unlikely they are low by a factor of 5. If we had assumed that the carbon content of the residues of experiments 2 and 4–7 (all from combustion of sample type BB) was 34.6 percent, and that 1.09 mg of residue weight is due to materials other than carbon and unburned PTFE, we would have obtained a result of -1023.21 kJ mol^{-1} (244.55 kcal mol^{-1}) with a standard deviation of the mean of 0.15 kJ mol^{-1} (0.03 kcal mol^{-1}). This value is 0.10 percent more negative than that adopted and is the basis for calculating item 8b of table 10. The assumption that the carbon contents of the residues of experiments 2 and 5 are low by 100 percent or more and the fluorine contents are correct appears to be most improbable. Thus, a preliminary value, obtained for the final series of combustions, before PTFE residue analyses were completed, of -1030.5 kJ mol^{-1} (-246.28 kcal mol^{-1}), based on the assumption the residues were 88 percent carbon and 12 percent fluorine by weight as had been obtained by analysis of sample 3, has been discarded. The higher value of the standard deviation of the mean for this result, 1.9 kJ mol^{-1} (0.22 kcal mol^{-1}), is compatible with this decision. An earlier preliminary value [11] of -242.89 kcal mol^{-1}, based on an erroneous assumption that the residues were entirely PTFE, has also been discarded.

Our value of -244.3 ± 0.8 kcal mol^{-1} for the heat of formation of amorphous BeF_2 obtained by direct combination of the elements indicates the heat of formation of BeO(s), found by Cosgrove and Snyder [2] is too positive by one or two kilocalories. In view of the forthcoming publication by Parker [47] of a critical evaluation of thermodynamic data for beryllium compounds,[5] we will not attempt a review or assessment of our value in comparison to other values in the literature here. Suffice it to say that our value is in good agreement with preliminary "best" value of the heat of formation BeF_2(glass), -244.2 kcal mol^{-1} selected by Parker [3]. This assumes, of course, that the heat of formation of amorphous and glassy BeF_2(s) are identical. Using a value of -1.12 kcal [48] for the enthalpy of transition of the glassy form of BeF_2(s) to the quartz form of BeF_2(s), our results yield a value of -245.44 k mol^{-1} for the heat of formation of the quartz form of BeF_2(s).

9. Gas Analysis of Solid Combustion Products

The reaction chamber for reaction of the products of the combustion of a beryllium-PTFE pellet in fluorine with 25 cm^3 of 50 weight-percent KOH is shown in figure 1. The nickel cup containing the combustion products was placed in the chamber in a dry atmosphere to prevent reaction of unburned beryllium with moisture. After evacuation of the chamber to less than 10^{-3} mm Hg, the degassed KOH was admitted to the chamber. The reaction was carried out at room temperature for 1 hr and then the chamber was placed in an oil bath where temperature was slowly raised and held at 80 to 100 °C for 10 to 12 hr. Kel-F grease was used on all ground glass joints. "Bumping" of the KOH was minimized by rotation of the nickel cup with a magnetic stirrer. The reaction chamber was found to leak consistently less than 2×10^{-8} moles of air during this procedure.

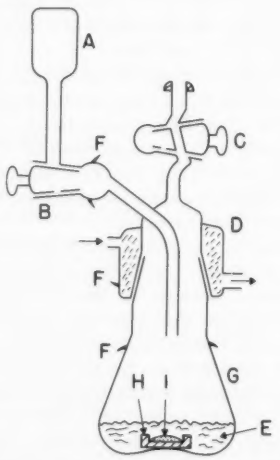

FIGURE 1. *Reaction chamber for analyzing combustion residues.*

A, bulb, 50-cm^3, containing degassed base; B, stopcock to admit degassed base into reaction chamber; C, stopcock to gas analysis system; D, water-cooled ground glass joint; E, base (conc. KOH); F, "wings" to secure spring clamps; G, reaction-chamber flask; H, 1¼ in diam nickel pellet cup from combustion bomb; I, solid combustion products.

[5] In association with the revision of NBS circular 500. (NBS Tech. Note 270 Series [12]).

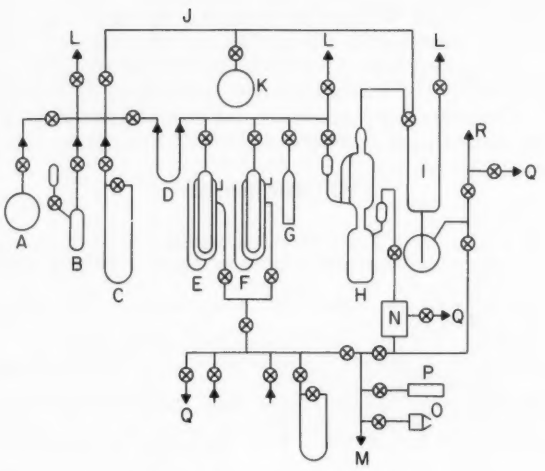

FIGURE 2. *Gas analysis system.*

A, sample bulb; B, reaction chamber; C, mercury manometer; D, U-tube cold trap at −78 °C; E, sieve separator; F, sieve pump; G, thermocouple gage; H, Toepler pump; I, gas burettes; J, recycle line; K, storage bulb; L, connections to vacuum pump (1); M, connection to vacuum pump (2); N, solenoid valves to control Toepler pump; O, connection to reaction chamber head for degassing base; P, thermocouple gage; Q, vent to air; R, connection to air pressure; ▲ arrow head showing direction of gas flow. ⊕ Stopcock.

After completion of KOH reaction, the evolved gases were removed from the chamber by adsorption on 30 g of type 5A molecular sieve held near −215 °C in a sieve separator, E of figure 2, or a sieve pump, F of figure 2, when the amount of gas was 10^{-5} moles (from sample type BB) or 10^{-3} moles (from sample type NM), respectively. An enlarged sketch of the sieve separator (the sieve pump is identical) is shown in figure 3. Gas collected using the sieve separator was released by warming the separator to room temperature and measuring the total moles of gas in the gas burete, I of figure 2. Part of the gas was then analyzed mass spectrometrically and the remainder by the sieve separator. Aliquots of the gas collected by use of the sieve pump were released from the sieve pump by progressive warming, separated by the sieve separator, and measured with the gas burette. A check of possible contamination of the gas fractions was carried out by mass spectrometric methods. The sieve separation procedure consisted of warming the separator to −190 °C or lower to release hydrogen, −180 to −170 °C to release N_2 and O_2 from air, if present, and −130 °C to room temperature to release methane and small amounts of other gases. The purity of the fractions was maximized by slowly warming the separator and maintaining the "separation temperature" for 1 hr.

Measurements of burete temperature, volume, and pressure had overall uncertainties of 0.1 °C, 0.03 cm³, and 0.02 mm of Hg, respectively. Experience showed that the precisions for a single measurement of the quantity of gas in the burete were 1, 0.15, and 0.10 percent for 2×10^{-5}, 2×10^{-4}, and 1.1×10^{-3} moles of gas, respectively.

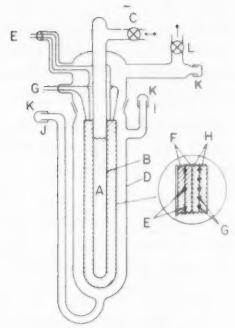

FIGURE 3. *Sieve separator*

A, type 5A molecular sieve; B, sieve well; C, stopcock to gas analysis system; D, jacket; E, thermocouples; F, aluminum foil; G, heater wire; H, asbestos tape; I, liquid nitrogen entry port; J, flushing port; K, removable rubber caps; L, stopcock to rough vacuum for pumping on liquid nitrogen. The inset shows an enlarged detail of the heater element, M.

Table 11 is a comparison of the molecular-sieve-separation and mass-spectrometer analysis of about 2×10^{-5} moles of gas liberated by the reaction of KOH with the solid combustion products. Experiment numbers correspond to those in table 7 of the combustion experiments. Mass spectrometer values of N_2, O_2, Ar, and CH_4 were added to give the value of CH_4 since the "methane fraction" of the sieve analysis would be expected to contain all these components. The largest uncertainties of the mass spectrometer analyses (esti-

TABLE 11. *Comparison of analysis by mass spectrometer and by molecular sieve absorption*

[In percent]

Ingredient	Mass spectrometer	Sieve	Difference
Experiment 2			
H_2	67.0 ± [c] 3	63.4 ± 1.5	−3.6
CH_4 [a]	30.8 ± 3	36.6 ± 2.5	+5.8
Other [b]	2.2 ± 5	0.0 ± 2.9	−2.2
Experiment 5			
H_2	74.2 ± 3	64.3 ± 1.8	−9.9
CH_4 [a]	23.0 ± 3	26.1 ± 2.1	+3.1
Other [b]	2.8 ± 5	9.6 ± 2.7	+6.8
Experiment 6			
H_2	46.1 ± 3	40.4 ± 1.1	−5.7
CH_4 [a]	50.7 ± 3	55.5 ± 2.3	+4.8
Other [b]	3.2 ± 5	4.1 ± 2.5	+0.9
Experiment 7			
H_2	50.5 ± 3	45.7 ± 1.3	−4.8
CH_4 [a]	46.8 ± 3	48.2 ± 1.5	+1.4
Other [b]	2.7 ± 5	6.1 ± 1.9	+3.4

[a] Includes 5.0 to 7.6 percent N_2, O_2 and Ar observed in the mass spectrometer.
[b] In the mass spectrometer this was observed as H_2O, acetone, propene, propane, and other hydrocarbons.
[c] Uncertainty estimated by mass spectrometer analyst.

mated by the analyst) are those for hydrogen and methane. The uncertainties of the sieve analyses are the estimated 95 percent confidence limits assuming the standard deviation of a single measurement of the quantity of gas to be 1 percent. Although it is apparent there may be some discrepancies between the two analyses, the agreement is well within the requirements for our problem (see sec. 9.1). Neither the origin of the small quantities of hydrocarbons, present in all the combustion product analyses, or the N_2 or O_2 is known with certainty.

The fraction listed as "other" in table 11 was the portion observed in the mass spectrometer as H_2O vapor and organic substances more complex than methane. For the molecular sieve analysis it was all material not recovered in either the H_2 or CH_4 fraction.

Table 8 contains a summary of the combustion product analyses based on the molecular sieve gas separations. Methane, for experiments 2, 5, 6, and 7 was calculated from the moles of gas in the "methane fraction" given by the sieve analyses adjusted for small amounts of other gases in this fraction given by the mass spectrometer analyses. Since no mass spectrometer analysis was made for experiment 4, the percent of methane in the sieve analysis "methane fraction" was estimated from the results of the above experiments. Methane and hydrogen for experiments 1 and 3 where the total moles of gas was large (i.e., 2×10^{-3}), were calculated using the results of the sieve analysis and corrections for the relatively small amounts of impurities (air, methane in the hydrogen fraction of the sieve analysis from 0.2 to 0.4%) given by the mass spectrometer analyses.

Table 12 lists two of the test runs made to check the accuracy and precision of the sieve separator.

TABLE 12. *Tests of molecular sieve separator*

Ingredient	Initial composition moles × 10^4 [a]	Analyzed composition moles × 10^4
[a] Sample 1, separation temperature, −144 °C		
H_2	3.367 ± [b] 0.004	3.354 ± [b] 0.004
CH_4	2.031 .003	2.049 .003
Total	5.398 .005	5.403 .005
[b] Sample 2, separation temperature, −130 °C		
H_2	1.474 ± 0.002	1.478 ± 0.002
CH_4	> 2.0	> 2.0
Total		

[a] The initial composition was determined by prepurification of the gas samples with the sieve separator and measurement of the quantity of each by a gas burette. Purity was checked by mass spectra.

[b] Uncertainties are estimated 95 percent confidence limits, Students' t distribution (based on actual observations).

The authors express their indebtedness to the NBS Analysis and Purification Section of the Analytical Chemistry Division for the numerous analyses that form an integral part of this work. In particular, we wish to thank William D. Dorko for the mass spectra, Rolf A. Paulsen for the analysis of the carbon-PTFE residues, and Mrs. E. June Maienthal for the analysis of BeF_2(s). The authors express their thanks to Eugene S. Domalski for the advice and instruction given to one of us (K.L.C.) in fluorine bomb calorimetry.

10. References

[1] Kolesov, V. P., Popov, M. M., and Skuratov, S. M., Zh. Neorg. Khim **4,** 1233–6 (1959) (J. Inorg. Chem. (USSR) **4,** 557–8 (1959)).

[2] Cosgrove, L. A., Snyder, P. E., J. Am. Chem. Soc. **75,** 3102–3 (1953).

[3] Parker, V. B., Informal communication, January 1967.

[4] Roth, W. A., Boerger, E., and Siemonsen, H., Z. anorg. u. allgem. Chem. **239,** 321–326 (1938).

[5] Neuman, B., Kroeger, C., and Kunz, H., Z. anorg. u. allgem. Chem. **218,** 379–401 (1934).

[6] Moose, J. E., and Parr, S. W., J. Am. Chem. Soc. **46,** 2656–61 (1924).

[7] Mielenz, W., and von Wartenberg, H., Z. anorg. u. allgem. Chem. **116,** 267–8 (1921), W. Mielenz, Dissertation, Berlin, 1914.

[8] Simmons, J., Atlantic Research Corp., private communication, 1962.

[9] Gross, P., Fulmer Research Institute, private communication, November 1960.

[10] Domalski, E. S., and Armstrong, G. T., J. Res. NBS **69A** (Phys. and Chem.), No. 2, 137–147 (1965).

[11] Armstrong, G. T., Coyle, C. F., American Chemical Society, Western Regional Meeting, Los Angeles, California, November 18–20, 1965 (Gmelin Reference No. AED-Conf. 65–358–1, Nuclear Science Abstracts **20,** No. 42369).

[12] Wagman, D. D., Evans, W. H., Parker, V. B., Halow, I., Bailey, S. M., Schumm, R. H., Selected values of Chemical Thermodynamic Properties Tables for the first Thirty-four Elements in the Standard Order of Arrangement, NBS Technical Note 270–3, January 1968, Supt. of Document, U.S. Govt. Printing Office, Washington, D.C. 20402.

[13] Wise, S. S., and Margrave, J. L., J. Phys. Chem. **67,** 815–821, 1963.

[14] Armstrong, G. T., and Krieger, L. A., Heats of Formation of Inorganic Fluorine Compounds—A Survey, Chapter 2. Progress in Internatl. Research on Thermodynamic and Transport Prop., J. F. Masi and D. H. Tsai, Eds. (Academic Press, New York, 1962).

[15] Settle, J. L., Feder, H. M., and Hubbard, W. N., J. Phys. Chem. **65,** 1337–40 (1961).

[16] Armstrong, G. T., and Jessup, R. S., J. Res. NBS **64A** (Phys. and Chem.), No. 1, 49–59 (1960).

[17] Dickinson, H. C., Bull. BS **11,** 189–257 (1914).

[18] Prosen, E. J., Johnson, W. H., and Pergiel, F. Y., J. Res. NBS **62,** 43–7 (1959) RP2927.

[19] Coops, J., Jessup, R. S., and Van Nes, K., Chapter 3, Experimental Thermochemistry, F. D. Rossini, Editor (Interscience Publishers, Inc., New York, 1956).

[20] Jessup, R. S., Precise Measurement of Heat of combustion in a bomb calorimeter, NBS Monograph No. 7, February 26, 1960.

[21] Darwin, G. E., and Buddery, J. H., Beryllium (Academic Press, Inc., New York 1960).

[22] White, D. W., Jr., and Burke, J. E., The Metal Beryllium (American Society for Metals, Cleveland, 1955).

[23] Breslin, A. J., and Harris, W. B., Health Protection in Beryllium Facilities; Summary of Ten Years Experience (Health and Safety Laboratory, U.S.A.E.C., New York Operations Office, May 1, 1958).

[24] Tepper, L. B., Hardy, H. L., and Chamberlin, R. I., Toxicity of Beryllium Compounds (Elsevier Publishing Co., Amsterdam, New York, 1960).

[25] Mears, T. W., Johnson, W. H., and Gilliland, W. A., NBS private communications, 1962.

[26] Domalski, E. S., and Armstrong, G. T., J. Res. NBS **71A** (Phys. and Chem.), No. 2, 105–118 (1967).

[27] Domalski, E. S., and Armstrong, G. T., J. Res. NBS **71A** (Phys. and Chem.) No. 3, 195–202 (1967).
[28] Domalski, E. S., and Armstrong, G. T., J. Res. NBS **71A** (Phys. and Chem.) No. 4, 307–315 (1967).
[29] Domalski, E. S., and Armstrong, G. T., J. Res. NBS **72A** (Phys. and Chem.) No. 2, 133–139 (1968).
[30] Warren, B. E., and Hill, C. F., Z. Krist. **89,** 31 (1935).
[31] Hubbard, W. N., Scott, D. W., and Waddington, G., Chapter 5, Experimental Thermochemistry, F. D. Rossini, Editor (Interscience Publishers, Inc., New York, 1956).
[32] Hubbard, W. N., Chapter 5, Vol. II, Experimental Thermochemistry, H. A. Skinner, Editor (Interscience Publishers, Inc., New York, 1962).
[33] Handbook of Chemistry and Physics, 44th edition (Chemical Rubber Publishing Company, Cleveland, Ohio, 1962).
[34] Meyers, O. E., and Brady, A. P., J. Phys. Chem. **64,** 591 (1960).
[35] White, D., Hu, J. H., and Johnston, H. L., J. Phys. Chem. **21,** 1149 (1953).
[36] Douslin, D. R., Paper 11, Progress in International Research on Thermodynamic and Transport Properties, J. F. Masi and D. H. Tsai, Editors (Academic Press, New York, 1962).
[37] Evans, W. H., Hilsenrath, J., and Woolley, H. W., private communication, July 1960.
[38] Dow Chemical Company, JANAF Thermochemical Tables. PB168370 (Clearinghouse for Federal Scientific and Technical Information, Springfield, Virginia, 1965).
[39] Furukawa, G. T., Reilly, M. L., Henning, J. M., Douglas, T. B., Victor, A. C., and Beaudoin, A. R., Informal communication, July 1959.
[40] Good, W. D., Scott, D. W., and Waddington, G., J. Phys. Chem. **60,** 1080 (1956).
[41] Furukawa, G. T., and Reilly, M. L., informal communication, January 1964.
[42] Stephenson, C. C., Hopkinson, H. P., Jr., and Wulff, C. A., J. Phys. Chem. **68,** 1427–29 (1964).
[43] Rossini, F. D., Wagman, D. D., Evans, W. H., Levine, S., and Jaffe, I., NBS Circular 500, February 1952.
[44] Patrick, C. R., The Thermochemistry of Organic Fluorine Compounds, Vol. **2,** M. Stacey, J. C. Tatlow, A. G. Sharpe, Editors, (Butterworths, Washington, 1961).
[45] Cameron, A. E., and Wichers, E., J. Am. Chem. Soc. **84,** 4175 (1962).
[46] Paulson, R. A., NBS, private communication.
[47] Parker, V. B., NBS, private communication (to be published in J. Research NBS).
[48] Taylor, A. R., Gardner, T. E., U.S. Bureau of Mines Rept. Invest. **6664** (1965).

(Paper 73A3–552)

JOURNAL OF RESEARCH of the National Bureau of Standards—A. Physics and Chemistry
Vol. 73A, No. 3, May–June 1969

Deuterium Isotope Effect on the Dissociation of Weak Acids in Water and Deuterium Oxide

R. A. Robinson,[1] Maya Paabo, and Roger G. Bates

Institute for Materials Research, National Bureau of Standards, Washington, D.C. 20234

(November 14, 1968)

The dissociation constants of *o*-nitroanilinium ion, *m*-nitroanilinium ion, and 4-chloro-2,6-dinitrophenol in deuterium oxide at 25 °C have been determined by a spectrophotometric method, and an emf method has been used to obtain $(pK_1 + pK_2)/2$ for citric acid in deuterium oxide. In addition, data for the dissociation constants of other weak acids in ordinary and heavy water have been critically examined with a view to clarifying the relationship between the deuterium isotope effect and the intrinsic strength of the acid. The difference ΔpK between the pK value in deuterium oxide and that in water varies linearly with pK above $pK = 7$. Two stronger inorganic acids (sulfuric and phosphoric) also appear to lie on an extension of this same line. On the contrary, a considerable group of organic acids with pK less than 7 have values of ΔpK that are more or less constant near $\Delta pK = 0.55$. It appears, therefore, that the isotope effect is more complex than has heretofore been assumed.

Key words: Acidic dissociation; acidity; deuterium isotope effect; dissociation constants; heavy water; isotope effect; pK values.

1. Introduction

Shortly after the discovery of heavy water by Urey, Brickwedde, and Murphy [1][2] in 1932, it was shown by Lewis and Schutz [2] that acids are weaker in deuterium oxide than they are in ordinary water as solvent. For example, the dissociation constant of chloroacetic acid was found to be 2.7 times greater in ordinary water than in heavy water. From this study and the work of LaMer and his colleagues [3, 4, 5] and of Martin and Butler [6], it appears that the difference in pK value, $\Delta pK = pK$ (in D_2O) $- pK$ (in H_2O), increases approximately linearly with an increase in pK (in H_2O). This relation has been ascribed [7] to a difference in zero-point energy between the isotopes in the acid molecules or perhaps [8] to a difference in zero-point energy between the hydrogen-bonded molecules and the solvent. Thus, $\Delta pK = 0.43$ for chloroacetic acid, 0.50 for benzoic acid [5], and 0.56 for *p*-nitrophenol [6]. Figure 1 is a plot of these pK differences for 11 acids from measurements made prior to 1940.

Curry and Hugus [9] have found $\Delta pK = 0.60$ for the second stage of dissociation of carbonic acid, giving a point not far from the straight line drawn in figure 1. This is true also for the data for 2,2,2-trifluoroethanol and 2-chloroethanol [10]. McDougall and Long [11] have determined the pK differences for 13 acids—iodic, oxalic (both stages of dissociation), γ-resorcylic, phosphoric (first stage), chloroacetic, salicylic, *m*-nitrobenzoic, and glycolic acids and for 2,4- and 2,6-dinitrophenol and *o*- and *p*-nitrophenol. A plot of their data gives points not far from the straight line in figure 1.

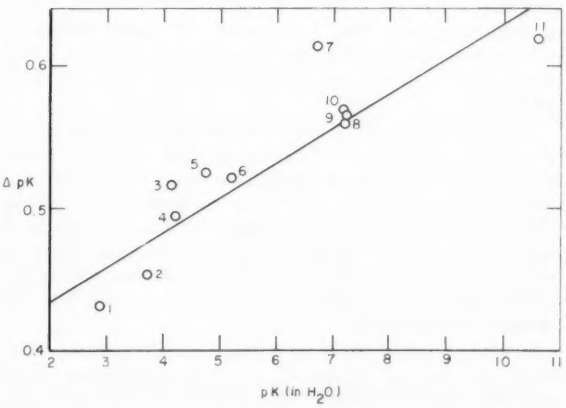

FIGURE 1. *Deuterium isotope effects* (ΔpK) *for weak acids obtained prior to 1940, plotted as a function of the* pK *of the acid in* H_2O.

1. Chloroacetic acid
2. 2,6-Dinitrophenol
3. 2,4-Dinitrophenol
4. Benzoic acid
5. Acetic acid
6. 2,5-Dinitrophenol
7. 3,5-Dinitrophenol
8. Dihydrogen phosphate ion
9. *p*-Nitrophenol
10. *o*-Nitrophenol
11. Hydroquinone.

[1] Present address: Department of Chemistry, State University of New York at Binghamton, Binghamton, New York 13901.
[2] Figures in brackets indicate the literature references at the end of this paper.

Other results, however, do not always support this relationship. For phosphoric acid, $pK_1 = 2.148$ (in H_2O), McDougall and Long found $\Delta pK = 0.234$, in contrast to the value of $\Delta pK = 0.438$ predicted from figure 1. For salicylic acid, with $pK = 2.996$ (in H_2O), $\Delta pK = 0.75$, whereas $\Delta pK = 0.46$ would be consistent with the plot in figure 1; this discrepancy may well be due to the abnormal amount of hydrogen bonding in salicylic acid. Although, more recently, Glasoe [12] has found $\Delta pK = 0.56$ for salicylic acid, this is still higher than one would expect from figure 1.

Furthermore, the isotope effect found by McDougall and Long [11] for *o*-nitrophenol ($\Delta pK = 0.75$) seems high: Martin and Butler [6] gave $\Delta pK = 0.57$ and Glasoe [12] gave $\Delta pK = 0.60$. On the contrary, the value for *p*-nitrophenol $\Delta pK = 0.48$, seems somewhat low: Martin and Butler found $\Delta pK = 0.56$ and Glasoe $\Delta pK = 0.58$. The value ($\Delta pK = 0.70$) for 2,4-dinitrophenol is higher than that of Martin and Butler ($\Delta pK = 0.52$) and of Glasoe ($\Delta pK = 0.56$); Bell and Kuhn [13] found $\Delta pK = 0.52$.

The apparent effect of an unusual amount of hydrogen bonding is also noted [14] in maleic acid. It was found that $\Delta pK = 0.625$ for the first stage in the dissociation of maleic acid. As the pK value in ordinary water is 1.921, one might expect, from figure 1, that ΔpK would be about 0.43. On the contrary, for the second stage in the dissociation of maleic acid ΔpK was found to be 0.379; with $pK_2 = 6.225$ in ordinary water, one might expect $\Delta pK = 0.54$.

This abnormal hydrogen bonding is often associated with an unusually high value of the ratio of K_1/K_2 in ordinary water. For maleic acid, this ratio is 2×10^4. But a high value of this ratio does not always mean an abnormal value of ΔpK. Thus, Glasoe [15] found for diethylmalonic acid ($pK_1 = 2.21$, $pK_2 = 7.33$ in ordinary water, $K_1/K_2 = 1.32 \times 10^5$) that $\Delta pK = 0.49$ for the first stage of dissociation and $\Delta pK = 0.41$ for the second stage. Further anomalies are found in highly alkylated succinic acids [16]; thus, a difference of $\Delta pK = 0.90$ is indicated for the first stage of dissociation of tetraethylsuccinic acid, the pK value in ordinary water being 3.39. This is almost the highest value of ΔpK yet found.

Bell and Kuhn [13] have studied the isotope effect on the dissociation of 13 acids. The pK values of these acids in ordinary water ranged from 2.50 to 5.20 and their values of ΔpK, with one exception, lie within 0.05 of the straight line in figure 1. The exception is bromoacetic acid. Their conclusion is that there is little to support a linear relation for the carboxylic acids, although a better case can be made for the phenols and alcohols.

In recent years, we have made a number of measurements of the pK values of acids in deuterium oxide solution, and it seems worthwhile to examine the relation of our results to other work. While we do not claim to have a complete solution to the problem, we have come to the very tentative conclusion that the linear relation may be valid for acids with pK greater than about 7, but that ΔpK is more or less constant at about 0.55 for stronger acids. Two notable exceptions, namely the first acid group of phosphoric acid and the second of sulfuric acid, will be discussed later in this paper.

2. Experimental Procedures

A commercial preparation of *o*-nitroaniline was recrystallized twice from methanol. *m*-Nitroaniline and 4-chloro-2,6-dinitrophenol were purified as described before [17]. A solution of deuterium chloride obtained commercially was standardized by gravimetric determination of chloride (weighing as silver chloride). The dissociation constants of the phenol and the two anilines were measured by a spectrophotometric method already described [18].

The potassium dihydrogen citrate was a portion of the same sample used in other work [19]. Emf measurements were made with cells containing potassium dideuteriocitrate and potassium chloride, using deuterium gas electrodes and silver-silver chloride electrodes; the cells were those used in the earlier work [19]. The dideuteriocitrate was formed in solution by exchange between potassium dihydrogen citrate and the deuterium oxide solvent.

TABLE 1. *The dissociation constant of o-nitroanilinium ion in deuterium oxide solution at 25 °C*

Conc. of *o*-Nitroaniline: 1.74×10^{-4} *M*, 1 cm cell, 418 nm, $D_1 = 0$, $D_2 = 0.776$.

Conc. of DCl[a]	D	$\log \frac{D_2 - D}{D - D_1}$	$-\log m_{D^+}$	pK'
0	.....	.....	.....	[b] 0.305
0.1552	0.580	−0.471	0.809	.338
.2983	.455	−.151	.525	.374
.4010	.398	−.022	.397	.375
.4536	.366	+.049	.343	.392
.5352	.321	+.151	.271	.422
.6447	.280	+.248	.191	.439

[a] In moles per kilogram of solvent.
[b] Extrapolated by means of the equation $pK' = 0.305 + 0.204\ m_{DCl}$.

TABLE 2. *The dissociation constant of m-nitroanilinium ion in deuterium oxide solution at 25 °C*

Conc. of *m*-Nitroaniline: 3.98×10^{-4} *M* (3.61×10^{-4} mol/kg), 1 cm cell, 360 nm, $D_1 = 0.038$, $D_2 = 0.568$.

Conc. of DCl[a]	D	$\log \frac{D_2 - D}{D - D_1}$	$-\log m_{D^+}$	pK
0.000801	0.362	−0.197	3.180	2.983
.000984	.334	−.102	3.083	2.981
.001460	.272	+.102	2.900	3.002
.001784	.244	+.197	2.806	3.003
.002081	.225	+.263	2.733	2.996
Average pK				2.993

[a] In moles per kilogram of solvent.

TABLE 3. *The dissociation constant of 4-chloro-2,6-dinitrophenol in deuterium oxide solution at 25 °C*

Conc. of 4-Chloro-2,6-dinitrophenol: 8.06×10^{-5} *M* (7.30×10^{-5} mol/kg), 1 cm cell, 447 nm, $D_1 = 0.002$, $D_2 = 0.583$.

Conc. of DCl [a]	D	$\log \frac{D_2 - D}{D - D_1}$	$-\log m_{D+}$	$-2 \log \gamma$ [b]	pK
0.0002153	0.341	−0.146	3.589	0.017	3.460
.0002587	.317	−.073	3.525	.018	3.470
.0002807	.311	−.055	3.495	.019	3.459
.0004352	.248	+.134	3.331	.023	3.488
.0004617	.239	+.162	3.308	.023	3.493
.0005448	.217	+.231	3.243	.025	3.499
.0008741	.160	+.428	3.049	.031	3.508
Average pK					3.482

[a] In moles per kilogram of solvent.
[b] Calculated by means of the equation

$$-2 \log \gamma = \frac{1.0826\, I^{1/2}}{1 + 1.5\, I^{1/2}}.$$

3. Results

3.1. Results of Present Work

The spectrophotometric data for the two anilines and the phenol are given in tables 1, 2, and 3. The notation is the same as that used previously [18]. For the case of the anilines, the pK values quoted are those corresponding to the acidic dissociation of the anilinium ion,

$$BH^+ \leftrightharpoons H^+ + B.$$

All values are expressed on the *molality* scale. The results are collected in table 4 and compared with the pK values found previously in ordinary water as solvent.

The pK values of *o*-nitroaniline and *m*-nitroaniline given by Högfeldt and Bigeleisen [21] are not in good agreement with the present data. Nevertheless, the differences of pK ($\Delta pK = 0.61$ for *o*-nitroaniline and 0.56 for *m*-nitroaniline) are in moderate agreement with those found in the present work. These pK differences give points lying considerably above the straight line in figure 1.

Bell and Kuhn [13] give pK (in H_2O) = 2.96, $\Delta pK = 0.49$, for 4-chloro-2,6-dinitrophenol, so that pK (in D_2O) = 3.45. However, Bell and Kuhn based all their data for deuterium oxide solutions on $pK = 5.28$ for acetic acid. We now know [22] that $pK = 5.313$ for acetic acid in deuterium oxide (molal scale) or $pK = 5.270$ (molar scale), so it is evident that their values all relate to the molar scale. Their value for 4-chloro-2,6-dinitrophenol on the molal scale is, therefore, 3.49, in agreement with the value found in the present work.

TABLE 4. *Dissociation constants in aqueous and deuterium oxide solutions at 25 °C determined by the spectrophotometric method*

	pK (in H_2O)	pK (in D_2O)	ΔpK
o-Nitroanilinium ion	−0.263 [20]	0.305	0.568
m-Nitroanilinium ion	2.460 [17]	2.993	.533
4-Chloro-2,6-dinitrophenol	2.969 [17]	3.482	.513

Table 5 gives values of the emf of the cell

$$Pt;D_2(g, 1\ atm), KD_2Cit\ (m), KCl(m = 0.01), AgCl; Ag$$

at 25 °C for four molalities of the citrate salt. The emf of this cell, E, is related to the $p(a_D\gamma_{Cl})$ ($\equiv -\log m_{D+} \cdot \gamma_{D+} \cdot \gamma_{Cl-}$) value of the buffer solution by the equation

$$\frac{E - E^\circ}{k} + \log m_{KCl} = p(a_D\gamma_{Cl}) \qquad (1)$$

where $m_{KCl} = 0.01$ mol kg^{-1}, $k = (RT \ln 10)/F$, and E°, the standard potential of the silver-silver chloride electrode, is taken to be 0.21266 V at 25 °C [23].

With the aid of the following convention [24],

$$-\log \gamma_{Cl-} = \frac{A\sqrt{I}}{1 + 1.5\sqrt{I}} \qquad (2)$$

values of $\log \gamma_{Cl-}$ can be calculated and are given in the fourth row of table 5. As will be shown in the appendix at the end of this paper, $p(a_D\gamma_{Cl}) - \log \gamma_{Cl-}$ (values of which are given in the fifth row) is a first approximation to $(pK_1 + pK_2)/2$. A good value of this quantity is obtained by extrapolation to $I = 0$, whereupon $(pK_1 + pK_2)/2$ is found to be 4.483. A more detailed analysis, taking into account the effect of overlapping stages of dissociation, is also given in the appendix and leads to values of $(pK_1 + pK_2)/2 = 4.468$, $\Delta pK = 0.523$.

TABLE 5. *Emf measurements of cells containing potassium dideuteriocitrate at 25 °C*

$Pt;D_2$, KD_2Cit (m), $KCl(m = 0.01)$, AgCl; Ag

m	0.02	0.06	0.08	0.10
E(V)	0.59167	0.58975	0.58913	0.58863
$p(a_D\gamma_{Cl})$	4.406_7	4.374_3	4.363_8	4.355_4
$-\log \gamma_{Cl-}$	0.0744	0.1025	0.1120	0.1199
$p(a_D\gamma_{Cl}) - \log \gamma_{Cl-}$	4.481	4.477	4.476	4.475
$(pK_1 + pK_2)/2$	4.468	4.467	4.470	4.469

3.2. Results Derived From Earlier Work at NBS

Some additional values of ΔpK can be derived from emf measurements of cells without transference. These are summarized in table 6. All of the pK values are on the molal scale.

In addition, the pK values of a few acids in deuterium oxide can be derived from emf measurements which

TABLE 6. *Dissociation constants from emf measurements in aqueous and deuterium oxide solutions at 25 °C*

	pK (in H_2O)	pK (in D_2O)	ΔpK
Acetic acid	4.756 [25]	5.313 [22]	0.557
Deuterioacetic acid	4.771 [26]	5.325 [27]	.554
Phosphoric acid (second step).	7.201 [28]	7.780 [29]	.579
Self-dissociation of solvent	13.997 [30]	14.955 [31]	.958

were made for a different purpose [32]. For example, the emf of the cell

Pt; D_2, $NaDCO_3$ (0.025 *m*), Na_2CO_3 (0.025 *m*),

NaCl (0.025 *m*), AgCl; Ag

was found to be 0.94815 V at 25 °C and, therefore, $-\log (a_{D^+}\gamma_{Cl^-})$, designated $p(a_D\gamma_{Cl})$, is 10.831. The dissociation constant is given by the expression

$$pK = p(a_D\gamma_{Cl}) - \log \frac{m_{CO_3^{--}}}{m_{DCO_3^-}} - \log \frac{\gamma_{CO_3^{--}}}{\gamma_{DCO_3^-}} \qquad (3)$$

where this pK refers to the second stage of dissociation of carbonic acid in deuterium oxide. For this acid in ordinary water, Harned and Scholes [33] found that the equation

$$-\log \frac{\gamma_{CO_3^{--}}}{\gamma_{HCO_3^-}\gamma_{Cl^-}} = \frac{2AI^{1/2}}{1+1.414\,I^{1/2}} \qquad (4)$$

gave a good representation of the activity coefficient term in eq (3). Thus, for a cell in which all three solutes were present at a concentration of 0.02620 *m*, $-\log (a_H^+\cdot\gamma_{Cl^-})$ [designated $p(a_H\gamma_{Cl})$] = 10.096, $2AI^{1/2}/(1+1.414\,I^{1/2}) = 0.245$, and the apparent pK value is 10.340; this requires only a small correction of −0.011, an allowance for the inadequacy of eq (4) and the necessity of a small, additional term linear in I, to give the true value, $pK = 10.329$. Assuming that eq (4), together with this small correction, is valid for solutions in deuterium oxide, and making the appropriate changes in the numerical value of the A parameter in eq (4) to allow for the different dielectric constant and density of heavy water, we calculate $-\log \gamma_{CO_3^{--}}/(\gamma_{DCO_3^-}\gamma_{Cl^-}) = 0.250$ and $pK = 11.070$ in deuterium oxide; $\Delta pK = 0.741$.

The pK for the second dissociation of deuteriocarbonic acid in heavy water has recently been determined carefully in this laboratory [34]. The value obtained (11.076 at 25 °C) lends confidence to the procedure described above, which provided a value of $pK = 11.070$ from a single measurement of $p(a_D\gamma_{Cl})$.

Similarly, the emf of the cell

Pt; D_2, $Na_2B_4O_7$ (0.05 *m*), NaCl (0.05 *m*), AgCl; Ag

is 0.87378 V at 25 °C and, hence, $p(a_D\gamma_{Cl}) = 9.875$. The pK value of boric acid in deuterium oxide is given by the equation

$$pK = p(a_D\gamma_{Cl}) - \log \frac{m_{BO_2^-}}{m_{DBO_2}} - \log \frac{\gamma_{BO_2^-}}{\gamma_{DBO_2}\cdot\gamma_{Cl^-}}. \qquad (5)$$

In their investigation of this acid in ordinary water, Manov, DeLollis, and Acree [35] found that the corresponding equation for aqueous solutions could be written

$$pK = p(a_H\gamma_{Cl}) - \log \frac{m_{BO_2^-}}{m_{HBO_2}} - \beta I \qquad (6)$$

with $\beta = 0.07$ mol^{-1} kg. Assuming that the same value of β can be used for deuterium oxide solutions, the pK value of boric acid in deuterium oxide is found to be 9.864, from which $\Delta pK = 0.630$.

For phosphoric acid, a solution containing D_3PO_4 ($m_1 = 0.06544$), KD_2PO_4 ($m_2 = 0.01579$), KCl ($m_3 = 0.06544$), $I = 0.1$, it was found [32] that $p(a_D\gamma_{Cl}) = 2.107$. The equation for the first dissociation constant is

$$pK_1 = pa_D - \log \frac{m_{D_2PO_4^-}}{m_{D_3PO_4}} - \log \frac{\gamma_{D_2PO_4^-}}{\gamma_{D_3PO_4}}$$

$$= pa_D - \log \frac{m_2 + m_{D^+}}{m_1 - m_{D^+}} - \log \frac{\gamma_{D_2PO_4^-}}{\gamma_{D_3PO_4}}. \qquad (7)$$

In calculating pa_D from $p(a_D\gamma_{Cl})$, Covington, Paabo, Robinson, and Bates [32] calculated the activity coefficient of the chloride ion by means of the Bates-Guggenheim convention [24], eq (2). If we assume that $-\log \gamma_{D^+} = -\log \gamma_{Cl^-} = 0.114$, then $-\log m_{D^+} = 1.879$, $m_{D^+} = 0.01321$, and also assume that $-\log \gamma_{D_2PO_4^-}/\gamma_{D_3PO_4} = 0.114$, then, by eq (7), $pK_1 = 2.362$. The result is, however, very sensitive to the assumption made about the activity coefficient terms; if we assume the validity of the limiting Debye-Hückel equation,

$$-\log \gamma = A\,I^{1/2} \qquad (8)$$

then $-\log \gamma = 0.171$, $pa_D = 1.936$, $-\log m_{D^+} = 1.765$, $m_{D^+} = 0.01718$, and $pK_1 = 2.273$. On the contrary, if we assume the equation,

$$-\log \gamma = \frac{AI^{1/2}}{1+7BI^{1/2}} \qquad (9)$$

then $-\log \gamma = 0.100$, $pa_D = 2.007$, $-\log m_{D^+} = 1.907$, $m_{D^+} = 0.01239$, and $pK_1 = 2.382$. As $pK_1 = 2.148$ in ordinary water [36], $\Delta pK = 0.214$, 0.125, or 0.234, depending on which of these assumptions about the activity coefficient terms is chosen.

Alternatively, pK_1 can be expressed in terms of $p(a_D\gamma_{Cl})$ as follows:

$$pK_1 \approx p(a_D\gamma_{Cl}) - \log \frac{m_2 + m_{D^+}}{m_1 - m_{D^+}} \qquad (10)$$

with the plausible assumption that $\gamma_{D_2PO_4^-}/(\gamma_{D_3PO_4}\gamma_{Cl^-})$

is close to unity in these dilute buffer solutions. Unfortunately, this procedure does not remove the major source of uncertainty, namely the estimation of m_{D^+} needed to calculate the concentration term in eq (7). The same value of pK_1 is obtained from the two equations when log γ and m_{D^+} are estimated in the same way.

Data are available for succinate buffer solutions, but the evaluation of the dissociation constants is complicated by the correction which has to be made for the deuterium ion concentration and the overlapping of the dissociation constants. Detailed consideration is reserved for the appendix at the end of this paper where it is shown that $\Delta pK = 0.546$ for the first stage of dissociation of succinic acid and $\Delta pK = 0.533$ for the second stage.

4. Discussion

4.1. Isotope Effects Calculated From Data Obtained at NBS

Figure 2 is a plot of ΔpK against pK (in H_2O) for all the systems we have studied. The figure suggests an approximately linear variation of ΔpK with pK for values of pK greater than about 7. For stronger acids, with a single exception, ΔpK seems to be approximately constant at about 0.55, or even to pass through a flat minimum and then to increase slowly with decreasing pK value.

The single exception we have found relates to the first stage of dissociation of phosphoric acid. Another exception (the second stage of sulfuric acid) will be discussed in the next section. The point shown in figure 2 for phosphoric acid is at $\Delta pK = 0.214$. It was derived on the assumption of the Bates-Guggenheim convention not only for the activity coefficient of the chloride ion but also for the other ions taking part in the dissociation equilibrium. We have seen that the value of ΔpK for acids as strong as phosphoric (K_1) and sulfuric (K_2) is very sensitive to the assumption made about the value of this activity coefficient, but no reasonable assumption can raise ΔpK to a value consistent with the upper curve of figure 2.

4.2. Isotope Effects Calculated From Data Obtained in Other Laboratories

The pK value for 3,5-dinitrophenol in ordinary water has been found [37] to be 6.692 at 25 °C. Martin and Butler [6] found that ΔpK for this phenol, when plotted on a graph such as that shown in figure 1, gives a point lying above the straight line shown in this figure. This value has been confirmed recently [38] when $pK = 7.305$ and $\Delta pK = 0.613$ were derived from spectrophotometric measurements in deuterium oxide buffer solutions containing potassium dideuteriophosphate and disodium deuteriophosphate, the $p(a_D\gamma_{Cl})$ values of which are known [29]. The point corresponding to this ΔpK value is plotted in figure 2. It can be seen that it lies about 0.03 above the curve drawn in the figure; it departs even further from the straight line drawn in this figure.

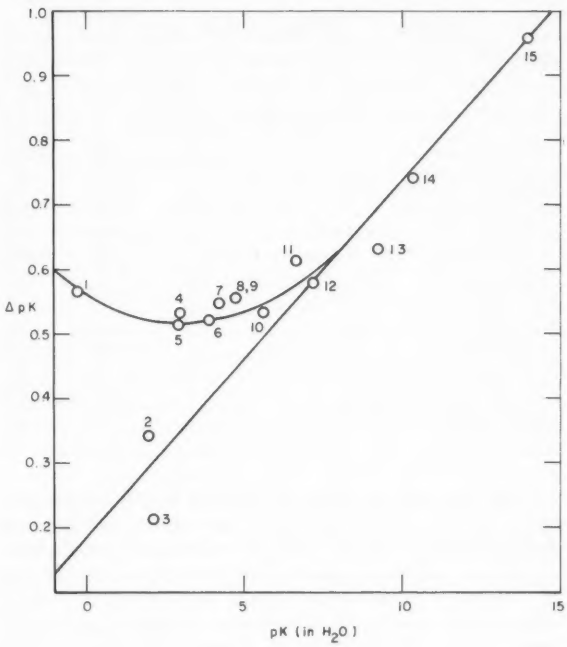

FIGURE 2. *Deuterium isotope effects* (ΔpK) *for weak acids at 25 °C, critically evaluated.*

1. *o*-Nitroanilinium ion
2. Bisulfate ion
3. Phosphoric acid (first step)
4. *m*-Nitroanilinium ion
5. 4-Chloro-2,6-dinitrophenol
6. Citric acid [$(pK_1 + pK_2)/2$]
7. Succinic acid (first step)
8. Acetic acid
9. Deuterioacetic acid
10. Hydrogen succinate ion
11. 3,5-Dinitrophenol
12. Dihydrogen phosphate ion
13. Boric acid
14. Bicarbonate ion
15. Self-dissociation of solvent.

Lietzke and Stoughton [39] have studied the second stage of dissociation of deuteriosulfuric acid and derived a value of $pK_2 = 2.326$ at 25 °C from measurements of the solubility of silver sulfate in deuteriosulfuric acid. Spectrophotometric measurements [40] have given $pK_2 = 1.983$ for the second stage of dissociation of sulfuric acid in ordinary water, and hence $\Delta pK = 0.343$. This value gives a point which is included in figure 2 and which undoubtedly belongs to the lower curve.

We now have measurements on 15 acids (only 14 points are shown in figure 2, because those for acetic acid and deuterioacetic acid are almost coincident). All of these determinations depend on sound thermodynamic theory. A well-established solubility method was utilized for one acid, and highly accurate emf measurements of cells *without* liquid junction gave results for 10 other acids; the data for four acids were obtained by spectrophotometric measurements. For three of these the acidity of the medium was determined by the addition of known amounts of deuterium chloride, while the fourth depended on $p(a_D\gamma_{Cl})$ values calculated from the emf of cells without liquid junction. The results are collected in table 7.

TABLE 7. *Values of* ΔpK *at 25 °C*

Acid	pK (in H_2O)	ΔpK
o-Nitroanilinium ion	−0.263	0.568
Sulfuric acid (second step)	1.983	.343
Phosphoric acid (first step)	2.148	.214
m-Nitroanilinium ion	2.993	.533
4-Chloro-2,6-dinitrophenol	2.969	.513
Citric acid $[(pK_1+pK_2)/2]$	3.945	.523
Succinic acid (first step)	4.207	.546
Acetic acid	4.756	.557
Deuterioacetic acid	4.771	.554
Succinic acid (second step)	5.638	.533
3,5-Dinitrophenol	6.692	.613
Phosphoric acid (second step)	7.201	.579
Boric acid	9.234	.630
Carbonic acid (second step)	10.329	.741
Self-dissociation of solvent	13.997	.958

From the results given in table 7 and illustrated in figure 2, it therefore seems evident that there are two distinct isotope effects. The only common factor which appears to separate the two effects seems to be that all "organic" acids give points on the upper curve, whereas the two acids which give points on the lower curve are "inorganic" or "mineral" acids. This unexpected conclusion must be regarded as a tentative one, since we have only two examples of the latter category, and we must await further work to confirm or deny its validity.

As both curves merge into one at pK values greater than about 7, it is the behavior of acids of lower pK which is of most interest. Nevertheless, some recent measurements of acids of high pK are of interest. Wehry and Rogers [41] have studied phenol and a number of substituted phenols in both ordinary water and in heavy water. For phenol itself ($pK=10.00$ in H_2O), they find $\Delta pK=0.62$ on the molarity scale, and therefore $\Delta pK=0.66$ on the molality scale. This is consistent with the curve in figure 2. Similarly, they find $\Delta pK=0.59$, again on the molality scale, for the 4-phenolsulphonate ion with pK (in H_2O)$=8.97$, which is also consistent with the curve in figure 2. Furthermore, Wehry and Rogers give data for *p*-nitrophenol, *o*-bromophenol, *m*-methoxyphenol, 2-naphthol, and 4-hydroxyphenyltrimethylammonium chloride, all of which are consistent with this curve. Of more interest for our present purpose are their findings for two acids of lower pK value. For 2,4-dinitrophenol [pK (in H_2O)$=4.06$], ΔpK (molality scale)$=0.53$; and for 2,5-dinitrophenol [pK (in H_2O)$=5.19$], ΔpK (molality scale)$=0.55$. Both these values of ΔpK clearly lie on the upper curve and not on the lower curve of figure 2.

Pentz and Thornton [42] find $\Delta pK=0.57$, 0.62, and 0.54 for 2,4-dinitrophenol, *o*-nitrophenol, and the imidazolinium ion, respectively, all based on the molality scale. Their value for *o*-nitrophenol certainly does not fall on the lower curve of figure 2 and seems somewhat higher than one would expect for the upper curve. However, Martin and Butler [6] found $\Delta pK=0.61$ and Glasoe [12] $\Delta pK=0.64$, both values converted to the molality scale; there are thus three values for *o*-nitrophenol which suggest that the ΔpK value for this phenol is about 0.05 higher than the point read for the upper curve of figure 2.

We have already mentioned that Bell and Kuhn [13] obtained a value of $\Delta pK=0.49$ on the molarity scale (0.53 on the molality scale) for 4-chloro-2,6-dinitrophenol, which compares well with our value of 0.513 (table 4). Neither value falls on the lower curve of figure 2. It is very useful to have this confirmation of the ΔpK value for an acid of this charge type with such a low pK value, because it disposes of the argument that the part of the upper curve for $pK<3$ is peculiar to acids of the anilinium ion type. We now have a substituted phenol whose ΔpK value lies on the same curve. Bell and Kuhn obtained data for 12 other acids. Their ΔpK value for 2,4-dinitrophenol, pK (in H_2O)$=4.07$, is 0.56 (molality scale). In agreement with the findings of Pentz and Thornton [42] ($\Delta pK=0.57$) and of Wehry and Rogers [41] ($\Delta pK=0.53$), this gives a point on the upper curve of figure 2.

For 2,5-dinitrophenol, pK (in H_2O)$=5.20$, Bell and Kuhn give $\Delta pK=0.57$ (molality scale), in agreement with $\Delta pK=0.55$ given by Wehry and Rogers and consistent with the upper curve of figure 2. Bell and Kuhn give $\Delta pK=0.53$ (molality scale) for 2,6-dinitrophenol, pK (in H_2O)$=3.73$; this gives a useful point in figure 2 because it relates to an acid of comparatively low pK, and the point lies exactly on the upper curve. They also found ΔpK values for 9 substituted acetic acids; the values of pK (in H_2O) ranged from 2.50 to 5.03 and ΔpK from 0.45 to 0.58.

Högfeldt and Bigeleisen [21] measured ΔpK for 8 acids of the anilinium ion charge type with pK (in H_2O) ranging from −1.05 (4-chloro-2-nitroanilinium ion) to 2.76 (the protonated form of aminoazobenzene), and ΔpK (presumably on the molarity scale) ranged from 0.61 for the *o*-nitroanilinium ion to 0.50 for the 2,6-dichloroanilinium ion. Again, these ΔpK values do not fall on the lower curve of figure 2.

Benzoic acid is important because it is the archetype of many organic acids. Rule and La Mer [5] found K (in H_2O)/K (in D_2O)$=3.13$ for this acid. They found pK (in D_2O)$=7.749$ for the second stage of dissociation of phosphoric acid; a value of $pK=7.780$ on the molality scale has been measured recently [29], and it would seem therefore that Rule and La Mer were using either the "aquamolality" or the molarity scale. The correction to the molality scale is the same in either case, and hence Rule and La Mer's result for benzoic acid corresponds to $\Delta pK=0.54$ on the molality scale, again consistent with the upper but not the lower curve of figure 2.

4.3. Influence of Temperature on the Isotope Effect

Most of the measurements referred to have been made at 25 °C. It is known [30, 43] however, that the dissociation constants of many acids increase with an increase in temperature, pass through a maximum, and then decrease in value at higher temperatures. The pK

value of an acid can often [30] be represented by the equation

$$pK = \frac{A_1}{T} - A_2 + A_3 T \tag{11}$$

in which event the temperature corresponding to the maximum value of K (or minimum value of pK) is

$$T_{max} = (A_1/A_3)^{1/2} \tag{12}$$

and the pK value at this temperature is given by the equation

$$pK_{min} = 2(A_1 A_3)^{1/2} - A_2 \tag{13}$$

It might well be argued that a comparison between pK values in ordinary water and in deuterium oxide should be made, not at the same temperature, but at the temperature of minimum pK value in each solvent. There are, unfortunately, few measurements over a temperature range by means of which this suggestion can be verified. Nevertheless, from measurements of the dissociation constants of acetic acid [22, 25] and deuterioacetic acid [26, 27] and that of the second stage of phosphoric acid [28, 29] in ordinary water and in deuterium oxide, as well as the "self-dissociation" constants of these two solvents [30, 31], we can derive the data in table 8.

TABLE 8. *Values of* pK *in ordinary water and in heavy water at the temperature of the minimum* pK *value*

	Water		Deuterium oxide		
	t_{min}	pK_{min}	t_{min}	pK_{min}	ΔpK_{min}
Acetic acid	22.4	4.756	32.0	5.310	0.554
Deuterioacetic acid	22.9	4.771	32.4	5.323	0.552
Phosphoric acid (2nd step)	42.7	7.180	47.7	7.744	0.564
"Self-dissociation" constant	239	11.382	221	12.356	0.974

The temperature of maximum K value (or minimum pK value) is expressed in degrees Celsius. All pK values are on the molality scale.

The ΔpK_{min} value for the "self-dissociation" of the solvent obviously is not the same as those of the other three dissociation processes. It should be remembered, however, that the value for the "self-dissociation" of ordinary water at 239 °C ($pK_{min} = 11.382$) was obtained by means of an equation fitted to experimental data covering the temperature range 0 to 60 °C, the pK value at 60 °C being 13.017. Similarly, the value for deuterium oxide ($pK_{min} = 12.356$ at 221 °C) was obtained by an extrapolation of experimental data covering the temperature range 5 to 50 °C, the pK value at 50 °C being 14.182.

Extrapolation to temperatures so far from the experimental range cannot give more than a qualitative value of t_{min} and pK_{min}, and more has never been claimed. The value of ΔpK_{min} in table 8, therefore, contributes little to any quantitative theory that may be developed using the temperature of minimum pK value as a criterion of comparison.

Clarke and Glew [44] have suggested recently that eq (11), which expresses the variation of pK with temperature, be expanded by the addition of an A_4 ln T term and even A_5T^2, A_6T^3 terms on the right side. We find that the addition of an A_4ln T term in eq (11) leads, in some cases, to almost the same values of t_{min} and pK_{min} as those recorded in table 8. Thus, for acetic acid in deuterium oxide, $t_{min} = 32.6$ °C, $pK_{min} = 5.309$; for deuterioacetic acid in deuterium oxide, $t_{min} = 32.3$, $pK_{min} = 5.323$; for the second step in the dissociation of phosphoric acid in deuterium oxide, $t_{min} = 49.1$ °C, $pK_{min} = 7.743$. In these three cases, t_{min} lies within the temperature range over which pK values were measured. But for the self-dissociation of water, where t_{min} is considerably above the highest temperature (60 °C) at which measurements were made, the addition of an A_4 ln T term to eq (11) leads to a value of $t_{min} = 327$ °C and $pK_{min} = 10.982$. Moreover, a similar procedure with the self-dissociation constant of deuterium oxide leads to the conclusion that there is no minimum in the pK versus T curve. Hence, a valid treatment along these lines can be made only when experimental measurements at high temperatures are available.

The values of ΔpK_{min} given in table 8 for acetic acid and deuterioacetic acid are almost identical. This not surprising; it would have been most unexpected to find any significant difference. However, the values of ΔpK_{min} for acetic acid and for the second stage of dissociation of phosphoric acid differ by only 0.010, despite the fact that for acetic acid pK_{min} (in H_2O) = 4.756 and for phosphoric acid pK_{min} (in H_2O) is higher by 2.424.

Although these results suggest that ΔpK at t_{min} may be independent of the strength of the acid, confirmation of this simple rule must await the availability of deuterium isotope effects for many more acids over a temperature range.

5. Appendix

5.1. Dissociation Constants of Citric Acid at 25 °C

We have measured the emf at 25 °C of the cell

$$Pt;D_2, KD_2Cit\ (m), KCl\ (m = 0.01), AgCl;Ag$$

where Cit = citrate, using cells with four different values of the citrate molality (m). These values of m, together with the emf of the cell, are given in table 5, along with the values of $p(a_D\gamma_{Cl})$ calculated with the aid of the standard potential of the silver-silver chloride electrode in deuterium oxide at 25 °C, namely 0.21266V [23].

For the dissociation processes

$$D_3Cit = D^+ + D_2Cit^-$$

and

$$D_2Cit^- = D^+ + DCit^{--}$$

the following mass-law expressions can be written:

$$K_1 = a_{D^+} \frac{m_{D_2Cit^-}}{m_{D_3Cit}} \frac{\gamma_1}{\gamma_0} \tag{14}$$

and

$$K_2 = a_{D^+} \frac{m_{DCit^{--}}}{m_{D_2Cit^-}} \frac{\gamma_2}{\gamma_1} \tag{15}$$

where the subscripts to γ denote the charge of the citrate species. The condition for mass balance is $m = m_{D_3Cit} + m_{D_2Cit^-} + m_{DCit^{--}}$, and the condition for electrical neutrality is

$$m + m_{D^+} = m_{D_2Cit^-} + 2m_{DCit^{--}} + m_{OD^-}.$$

Hence, if m_{D^+} and m_{OD^-} are negligible compared with m,

$$m_{D_3Cit} = m_{DCit^{--}} \tag{16}$$

Thus

$$K_1K_2 = (a_{D^+})^2 \frac{\gamma_2}{\gamma_0} \tag{17}$$

or

$$(pK_1 + pK_2)/2 = pa_D - 1/2 \log \frac{\gamma_2}{\gamma_0}. \tag{18}$$

Making the reasonable assumption that $\gamma_0 \approx 1$ and that $\log \gamma_2 = 4 \log \gamma_{Cl^-}$, where $\log \gamma_{Cl^-}$ is given by eq (2), the convention proposed by Bates and Guggenheim [24], eq (18) can be written

$$(pK_1 + pK_2)/2 = p(a_D\gamma_{Cl}) - \log \gamma_{Cl^-} \tag{19}$$

Values of $\log \gamma_{Cl^-}$, calculated with the aid of eq (2), are given in table 5, together with values of $p(a_D\gamma_{Cl}) - \log \gamma_{Cl^-}$. If eq (19) were exact, the quantities on each side of the equation would be constant, independent of the total ionic strength. Table 5 shows that this is not strictly true, the value of $p(a_D\gamma_{Cl}) - \log \gamma_{Cl^-}$ increasing slowly as the concentration of potassium dideuteriocitrate in the cell solution decreases. This is undoubtedly due to minor imperfections in the assumptions we have made. These can be allowed for by rewriting eq (19) as follows:

$$(pK_1 + pK_2)/2 = p(a_D\gamma_{Cl}) - \log \gamma_{Cl^-} + \beta I = \alpha + \beta I. \tag{20}$$

Using the method of least squares, we find $\alpha = 4.483$, $\beta = -0.0747$ kg mol^{-1}. Hence $(pK_1 + pK_2)/2 = 4.483$. As the corresponding quantity for ordinary water as solvent is 3.945 [45], it follows that $\Delta pK = 0.538$.

Equation (18), however, is also not exact. A detailed examination of the problem requires a consideration of the effect of the third dissociation constant of citric acid [46, 47]. Let us consider the case of a tribasic acid at an initial concentration m, to which strong alkali is added in amount xm. Solution of the equations for electrical neutrality and mass balance yields the equation

$$S K_1K_2K_3 + R a_{D^+}K_1K_2 + Q a_{D^+}^2K_1 = P a_{D^+}^3 \tag{21}$$

where, for solutions sufficiently acidic that m_{OD^-} can be neglected, $P = (xm + m_{D^+})/\gamma_0$, $Q = [(1-x)m - m_{D^+}]/\gamma_1$, $R = [(2-x)m - m_{D^+}]/\gamma_2$, and $S = [(3-x)m - m_{D^+}]/\gamma_3$, where again the subscript to γ indicates the charge on the particular citrate species. The case with which we are now concerned is that in which sufficient alkali has been added to citric acid to complete the first stage of neutralization: $x = 1$. Then

$$K_1K_2 = \frac{m + m_{D^+}}{m - m_{D^+}} \frac{\gamma_2}{\gamma_0} a_{D^+}^2 + \frac{m_{D^+}}{m - m_{D^+}} \frac{\gamma_2}{\gamma_1} K_1a_{D^+} - \frac{2m - m_{D^+}}{m - m_{D^+}} \frac{\gamma_2}{\gamma_3} \frac{K_1K_2K_3}{a_{D^+}}. \tag{22}$$

The second and third terms on the right of eq (22) are small compared with the first term; consequently, only approximate values of K_1, K_2, and K_3 are needed. These were obtained from the known values in water, together with ΔpK values read from figure 2. The values used were $pK_1 = 3.67$, $pK_2 = 5.30$, and $pK_3 = 6.97$. Hence, K_1K_2 could be calculated, and the quantity $(pK_1 + pK_2)/2$ is given in the last row of table 5. There is no systematic trend with change in concentration m, and we take the mean, 4.468, as the best value of $(pK_1 + pK_2)/2$. Thus $\Delta pK = 0.523$.

5.2. First Dissociation Constant of Succinic Acid in Deuterium Oxide at 25 °C

We follow the method of Pinching and Bates [48]. Consider a solution of D_2S $(3m)$ + NaDS (m) + NaCl (m'), where S represents succinate. The first dissociation constant is given by the expression

$$K_1 = \frac{a_{D^+} m_{DS^-} \gamma_{DS^-}}{m_{D_2S} \gamma_{D_2S}} \tag{23}$$

and the second dissociation constant by

$$K_2 = \frac{a_{D^+} m_{S^{--}} \gamma_{S^{--}}}{m_{DS^-} \gamma_{DS^-}} \tag{24}$$

From eq (24),

$$m_{DS^-} = \frac{a_{D^+}}{K_2} \cdot m_{S^{--}} \cdot \frac{\gamma_{S^{--}}}{\gamma_{DS^-}}. \tag{25}$$

By the condition of electrical neutrality,

$$m + m_{D^+} = m_{DS^-} + 2m_{S^{--}} \tag{26}$$

and by the condition of mass balance,

$$m_{D_2S} + m_{DS^-} + m_{S^{--}} = 4m. \tag{27}$$

From (26) and (27) it follows that

$$m_{D_2S} = 3m - m_{D^+} + m_{S^{--}} \tag{28}$$

and from (25) and (26),

$$m_{S^{--}}\left(2 + \frac{a_{D^+}}{K_2} \cdot \frac{\gamma_{S^{--}}}{\gamma_{DS^-}}\right) = m + m_{D^+}. \tag{29}$$

For a solution of (0.03689 m D_2S + 0.01230 m NaDS + 0.08609 m NaCl) in deuterium oxide at 25 °C (ref. 32, table 1, solution No. 4a), it has been found that $p(a_D\gamma_{Cl}) = 4.253$ and, by the Bates-Guggenheim convention [24], $-\log \gamma_{Cl^-} = 0.114$; hence, $pa_D = 4.139$. Assuming that $\log \gamma_{D^+} = \log \gamma_{Cl^-}$, we have $-\log m_{D^+} = 4.025$, $m_{D^+} = 9.44 \times 10^{-5}$. The value of pK_2 is taken to be 6.209 (see the next section of the appendix). It is further assumed that $\log (\gamma_{S^{--}}/\gamma_{DS^-})$ in eq (25) is equal to 3 $\log \gamma_{Cl^-}$; it thus has the value −0.342. Then by eq (29), $m_{S^{--}} = 0.00023$ and, by eq (28), $m_{D_2S} = 0.03703$, and, finally, by eq (27), $m_{DS^-} = 0.1193$. Substitution of these values in eq (23), along with the approximation $\log (\gamma_{DS^-}/\gamma_{D_2S}) = \log \gamma_{Cl^-} = -0.114$, gives $pK_1 = 4.745$.

It is appropriate now to examine the assumptions we have made about the activity coefficient terms. Following the procedure of Pinching and Bates [48] for succinic acid in aqueous solution, we can write

$$-\log m_{D^+} = p(a_D\gamma_{Cl}) + 2 \log \gamma \tag{30}$$

where

$$-\log \gamma = \frac{AI^{1/2}}{1 + 7BI^{1/2}} \tag{31}$$

and A and B are the appropriate Debye-Hückel constants for deuterium oxide solutions ($A = 0.5413$ $kg^{1/2}$ $mol^{-1/2}$, $B = 0.3467 \times 10^8$ $kg^{1/2}$ $mol^{-1/2}$ cm^{-1} at 25 °C). Substitution of these values in eq (31) for the solution considered above, with $I = 0.09839$, gives $-\log \gamma = 0.097$, $m_{D^+} = 8.73 \times 10^{-5}$. If it is assumed with Pinching and Bates that the activity coefficients in eqs (23) and (25) can be calculated in the same way, we find $m_{S^{--}} = 0.00021$, $m_{D_2S} = 0.03701$, $m_{DS^-} = 0.01197$, and $pK_1 = 4.743$.

Applying the first approach to a solution containing 0.03689 m D_2S + 0.01230 m NaDS + 0.01500 m NaCl (see ref. 32, table 1, solution No. 4b) for which $I = 0.02730$, we find $pK_1 = 4.751$. Since we now have $pK_1 = 4.751$ at $I = 0.02730$ and $pK_1 = 4.745$ at $I = 0.09839$, the value of pK_1 at infinite dilution must be close to 4.753. In ordinary water, $pK_1 = 4.207$ and, therefore, $\Delta pK = 0.546$.

5.3. Second Dissociation Constant of Succinic Acid in Deuterium Oxide at 25 °C

The calculation follows the method of Pinching and Bates [49]. Consider a solution of NaDS (m) + Na_2S (m) + NaCl (m'). From eq (23)

$$m_{DS^-} = \frac{K_1}{a_{D^+}} \cdot m_{D_2S} \cdot \frac{\gamma_{D_2S}}{\gamma_{DS^-}}. \tag{32}$$

By the condition of electrical neutrality,

$$3m + m_{D^+} = m_{DS^-} + 2m_{S^{--}} \tag{33}$$

and by the condition of mass balance,

$$m_{D_2S} + m_{DS^-} + m_{S^{--}} = 2m. \tag{34}$$

From eq (33) and (34), it follows that

$$m_{DS^-} = m - m_{D^+} - 2m_{D_2S}. \tag{35}$$

Combining eq (35) with eq (32) gives

$$m_{D_2S}\left(2 + \frac{K_1}{a_{D^+}} \cdot \frac{\gamma_{D_2S}}{\gamma_{DS^-}}\right) = m - m_{D^+}. \tag{36}$$

For a solution of 0.02007 m NaDS + 0.02007 m Na_2S + 0.02007 m NaCl in deuterium oxide at 25 °C (ref. 32, table 1, solution No. 6), $p(a_D\gamma_{Cl})$ has been found to be 6.043, and, again by the Bates-Guggenheim convention [24], $-\log \gamma_{Cl^-} = 0.114$, $pa_D = 5.929$. If $\log \gamma_{D^+}$ is again taken equal to $\log \gamma_{Cl^-}$, we have $-\log m_{D^+} = 5.815$, $m_{D^+} = 1.53 \times 10^{-6}$, and the deuterium ion correction is negligible. Putting $pK_1 = 4.753$ (see appendix 5.2 above), eq (36) gives $m_{D_2S} = 0.00093$ and, by eq (35), $m_{DS^-} = 0.01821$. Finally, by eq (34), $m_{S^{--}} = 0.02100$ and, hence, by eq (24), $pK_2 = 6.205$. Pinching and Bates used eq (31) to express all the activity coefficients and, if we follow this procedure, we find $pK_2 = 6.171$. This is probably the better value, especially if a comparison with the pK_2 value in ordinary water (5.638 at 25 °C) is to be made; hence, $\Delta pK = 0.533$.

6. References

[1] Urey, H. C., Brickwedde, F. G., and Murphy, G. M., Phys. Rev. **39,** 864 (1932).
[2] Lewis, G. N., and Schutz, P. W., J. Amer. Chem. Soc. **56,** 1913 (1934).
[3] Korman, S., and La Mer, V. K., J. Amer. Chem. Soc. **58,** 1396 (1936).
[4] La Mer, V. K., and Chittum, J. P., J. Amer. Chem. Soc. **58,** 1642 (1936).
[5] Rule, C. K., and La Mer, V. K., J. Amer. Chem. Soc. **60,** 1974 (1938).
[6] Martin, D. C., and Butler, J. A. V., J. Chem. Soc. (London), 1366 (1939).
[7] Bell, R. P., The proton in chemistry, ch. 11 (Cornell University Press, Ithaca, N.Y., 1959).
[8] Bunton, C. A., and Shiner, V. J., J. Amer. Chem. Soc. **83,** 42 (1961).
[9] Curry, J., and Hugus, Z. Z., J. Amer. Chem. Soc. **66,** 653 (1944).
[10] Ballinger, P., and Long, F. A., J. Amer. Chem. Soc. **81,** 2347 (1959).
[11] McDougall, A. O., and Long, F. A., J. Amer. Chem. Soc. **84,** 429 (1962).
[12] Glasoe, P. K., J. Phys. Chem. **69,** 4416 (1965).
[13] Bell, R. P., and Kuhn, A. T., Trans. Faraday Soc. **59,** 1789 (1963).
[14] Dahlgren, G., and Long, F. A., J. Amer. Chem. Soc. **82,** 1303 (1960).
[15] Glasoe, P. K., and Hutchison, J. R., J. Phys. Chem. **68,** 1562 (1964).
[16] Glasoe, P. K., and Eberson, L., J. Phys. Chem. **68,** 1560 (1964).

[17] Sager, E. E., Robinson, R. A., and Bates, R. G., J. Res. NBS **68A** (Phys. and Chem.), No. 3, 305 (1964).
[18] Robinson, R. A., J. Res. NBS **68A** (Phys. and Chem.), No. 2, 159 (1964).
[19] Paabo, M., and Bates, R. G., Anal. Chem. **41,** 283 (1969).
[20] Biggs, A. I., and Robinson, R. A., J. Chem. Soc. (London), 388 (1961).
[21] Högfeldt, E., and Bigeleisen, J., J. Amer. Chem. Soc. **82,** 15 (1960).
[22] Gary, R., Bates, R. G., and Robinson, R. A., J. Phys. Chem. **69,** 2750 (1965).
[23] Gary, R., Bates, R. G., and Robinson, R. A., J. Phys. Chem. **68,** 1186 (1964).
[24] Bates, R. G., and Guggenheim, E. A., Pure Appl. Chem. **1,** 163 (1960).
[25] Harned, H. S., and Ehlers, R. W., J. Amer. Chem. Soc. **55,** 652 (1933).
[26] Paabo, M., Bates, R. G., and Robinson, R. A., J. Phys. Chem **70,** 540 (1966).
[27] Paabo, M., Bates, R. G., and Robinson, R. A., J. Phys. Chem. **70,** 2073 (1966).
[28] Bates, R. G., and Acree, S. F., J. Res. NBS **30,** 129 (1943).
[29] Gary, R., Bates, R. G., and Robinson, R. A., J. Phys. Chem. **68,** 3806 (1964).
[30] Harned, H. S., and Robinson, R. A., Trans. Faraday Soc. **36,** 973 (1940).
[31] Covington, A. K., Robinson, R. A., and Bates, R. G., J. Phys. Chem. **70,** 3820 (1966).
[32] Covington, A. K., Paabo, M., Robinson, R. A., and Bates, R. G., Anal. Chem. **40,** 700 (1968).
[33] Harned, H. S., and Scholes, S. R., Jr., J. Amer. Chem. So **63,** 1706 (1941).
[34] Paabo, M., and Bates, R. G., J. Phys. Chem. (in press).
[35] Manov, G. G., DeLollis, N. J., and Acree, S. F., J. Res. NB **33,** 287 (1944).
[36] Bates, R. G., J. Res. NBS **47,** 127 (1951).
[37] Robinson, R. A., Davis, M. M., Paabo, M., and Bower, V. E J. Res. NBS **64A** (Phys. and Chem.), No. 4, 347 (1960).
[38] Robinson, R. A., J. Chem. Eng. Data **14,** 247 (1969).
[39] Lietzke, M. H., and Stoughton, R. W., J. Phys. Chem. **6** 652 (1963).
[40] Klotz, I. M., Singleterry, C. R., Theses, University of Chicag 1940.
[41] Wehry, E. L., and Rogers, L. B., J. Amer. Chem. Soc. **8** 351 (1966).
[42] Pentz, L., and Thornton, E. R., J. Amer. Chem. Soc. **8** 6931 (1967).
[43] Harned, H. S., and Embree, N. D., J. Amer. Chem. Soc. **5** 1050 (1934).
[44] Clarke, E. C. W., and Glew, D. N., Trans. Faraday Soc. **6** 539 (1966).
[45] Bates, R. G., and Pinching, G. D., J. Amer. Chem. Soc. **7** 1274 (1949).
[46] Bates, R. G., J. Amer. Chem. Soc. **70,** 1579 (1948).
[47] Robinson, R. A., and Stokes, R. H., Electrolyte solution p. 347, revised edition (Butterworths, London, 1968).
[48] Pinching, G. D., and Bates, R. G., J. Res. NBS **45,** 444 (195
[49] Pinching, G. D., and Bates, R. G., J. Res. NBS **45,** 322 (195

(Paper 73A3–55

JOURNAL OF RESEARCH of the National Bureau of Standards—A. Physics and Chemistry
Vol. 73A, No. 3, May–June 1969

Vortex Motions in Ideal Bose Superfluid*

Martin J. Cooper

Institute for Basic Standards, National Bureau of Standards, Washington, D.C. 20234

(February 11, 1969)

A general nonlinear field equation is derived for the macroscopic order parameter of an ideal coherent Bose gas. It is shown that this noninteracting system can support stable quantized vortex-like motions within the superfluid phase. It is suggested that this coherent phase of the ideal Bose gas describes the dominant physical features of real superfluid liquid helium.

Key words: Coherent Bose gas; superfluid; vortices.

1. Introduction

The presence of quantized vortex motions in the superfluid phase of liquid helium was first postulated by Onsager [1] [1] and Feynman [2] and has since been confirmed by numerous experiments [3]. The microscopic theory of such macroscopic motions was developed independently by Gross [4] and Pitaevskii [5], who assumed the fluid to be a dilute gas of weakly repulsive Bose particles. They were able to show that a self-consistent equation-of-motion for the macroscopic order parameter of the Boson field contains a nonlinear contribution arising from the interactions between the particles. Stable vortex motions with quantized circulation appear as special solutions of the nonlinear field equation.

In this paper we suggest that vortex motions of the superfluid phase are due to the Bose statistics and are not dependent upon any interactions (either attractive or repulsive) between the particles. We shall demonstrate this by showing that quantized vorticles are stable configurations of the macroscopic order parameter within the ordered phase of a noninteracting free Bose gas.

It is generally remarked that the ideal Bose gas is an overly simple system which describes unphysical situations due to its oversensitivity to boundary conditions. If, for example, the gas is contained in a rigid box of large but finite dimensions, it is found that the particles will condense into a ground state with a highly nonuniform density profile [4]. Such an unreal distribution is usually removed by introducing repulsive interactions between the particles so that they smear themselves out more uniformly over the entire volume. Since we wish to exhibit certain properties as explicit characteristics of the Bose statistics in the absence of any interactions and independent of boundary conditions, we choose instead to think of the ideal Bose system within the framework of the Grand Canonical formalism. This permits us to consider an ensemble of N noninteracting Bosons contained in a volume $V(=L^3)$ at an equilibrium temperature $T(=1/\beta)$ in the thermodynamic limit of $N\to\infty$, $V\to\infty$ with a fixed number density N/V.

2. Field Equation

The appropriate description for the ideal gas of Boson particles is given in terms of the creation and annihilation operators of the quantized Bose field, $\psi^+(r)$, $\psi(r)$ with $[\psi(r), \psi^+(r')]=\delta(r-r')$. The presence of an ordered or condensed phase is characterized by the existence of a spontaneous macroscopic expectation value for the single operator $\psi(r)$ [6]. This author together with Green [7] have considered the condensation of such a system as a model second-order phase transition by removing the phase symmetry of the Fock states through a linear coupling of the field operators to a fictitious external source $S(r)$. Making use of the coherent state representation and following standard thermodynamic arguments, it was shown that the number density is of a simple analytic form. In the limit of a vanishing *uniform* source $S(r)=S\to 0$ (after the thermodynamic limit of N, $V\to\infty$, N/V finite) the number density separates into two branches at a critical value of the temperature, T_c. Below this temperature, the total density is composed of two uniform coexisting parts,

$$n=\eta T^{3/2}+\Psi^2 \tag{1}$$

*Not subject to copyright—contribution of the National Bureau of Standards.
[1] Figures in brackets indicate the literature references at the end of this paper.

where the constant $\eta=(2\pi\hbar/m)^{3/2}\zeta(\frac{3}{2})=(2\pi)^{3/2}$ 2.612 $\cdots$ in units of $\hbar=m=1$. The first term is just the number density for the normal component of the fluid. The quantity Ψ corresponds to a spontaneous thermal expectation value which is of finite magnitude below T_c and vanishes identically for all temperatures above it. In general, Ψ represents a complex order parameter for the coherent phase with both an amplitude and phase $\Psi=|\Psi(r)|\exp(i\phi(r))$. Within the framework of the two fluid model, $|\Psi|^2$ is associated with the number density of the ordered or superfluid phase, while the spatial gradient of the phase is interpreted as the superfluid velocity $v_s=\nabla\phi(r)$.

The thermodynamic potential describing the coherent phase as a function of the superfluid density $|\Psi|^2$ and temperature T in the vicinity of the transition as $(T-T_c)/T_c=t<0$ becomes small is given by

$$F(\Psi^2, T)=[\Psi^2(1+\tfrac{3}{2}t/\Psi^2)]^3 \tag{2}$$

Taking the actual superfluid to be locally a coherent Bose gas, [7, 8] this result provides the functional form of the thermodynamic potential density expressed in terms of the reduced temperature t and the magnitude of local macroscopic order parameter $\Psi(r)$. It is like a phenomenological Landau expansion for the free-energy carried to third order in Ψ^2. If the superfluid is spatially nonuniform or in motion relative to the normal component ($v_n=0$) then there is an additional contribution $\hbar^2|\nabla\Psi|^2/2m$ [9].

[Remark—We wish to note here the similarity between the thermodynamic potential for the coherent superfluid phase of the ideal Bose fluid given in eq (2) and certain recently proposed forms for the potential of superfluid helium. Several persons [10–12] have suggested variations of the conventional Landau theory of phase-transitions based on the expansion of $F(\Psi^2, T)$. Noting that the superfluid density varies like $(1-T/T_\lambda)^{2/3}$, Mamaladze[10] made ad hoc modifications in the temperature dependence of the lowest order expansion coefficients. Amit[11] proposed a more consistent formulation by including terms to order Ψ^6 and has been able to describe certain features of superfluid helium films. Miller and Luban[12] pointed out a further consequence of such a term would be the existence of two critical superfluid velocities.]

For stable configurations, the total potential function[9] $\mathcal{F}(\Psi^2, T)=\int dr[-\frac{1}{2}|\nabla\Psi|^2+F(\Psi^2, T)]$ must be a minimum with respect to Ψ (also, its conjugate Ψ^*). The variational procedure leads to a field equation for the magnitude of the local order parameter $\Psi(r)$ which describes the superfluid behavior of the coherent ideal Bose gas,

$$\nabla^2|\Psi(r)|+(\Psi^2+\tfrac{3}{2}t)^2|\Psi(r)|=0. \tag{3}$$

This result is like the equation obtained by Gross[4] and Pitaevskii[5] to describe the superfluid properties of an interacting Bose gas. Taking a finite fraction of the particles to be in a single quantum state, they showed that the condensate wave function ψ behaves like an effective hydrodynamic variable which obeys a nonlinear equation

$$\nabla^2\psi(r)+(1-2V\psi^2)\psi=0. \tag{4}$$

The theory is restricted by the requirement that the product of the condensate density and the effective potential, $|\psi|^2V$ remain small. A basic potential dependent dimension $\lambda=(2|\psi|^2V)^{-1/2}$ is used to characterize the length scale. The nonlinear contribution to the equation is directly proportional to the interaction potential. Thus, in the absence of such interactions, the *G–P* equation describes a simple free-field whose characteristic length becomes infinite.

The field describing the hydrodynamics of the superfluid phase of the coherent Bose gas is given by eq (3). There, despite the lack of any direct potential, the equation contains terms to order $|\Psi|^5$ and is therefore of a more nonlinear nature than that described by the *G–P* result.

3. Special Solutions

We shall consider solutions of the field equation for Ψ in two cases of particular physical interest, namely, the behavior of the superfluid near a wall and the possibility of vortex-like configurations. It is convenient to obtain a normalized field equation by introducing a reduced variable for the magnitude of the order parameter

$$\psi=\left(\frac{2}{3}|t|\right)^{1/2}|\Psi(r)|$$

and a new distance scale $\xi=\left(\frac{27}{2}\right)^{1/2}|t|r$

$$\nabla^2\psi+(1-\psi^2)^2\psi=0. \tag{5}$$

Consider first the problem of the Bose gas in a semi-infinite domain bounded by rigid wall (x-y plane). In this one dimensional geometry, the superfluid density vanishes at the wall ($\psi^2=0$, $z=0$) and has a uniform value (normalized $\psi^2=1$) far from it. With these boundary conditions, the solution of eq. (5) is given by

$$\psi(z)=z/(3+z^2)^{1/2}. \tag{6}$$

This implies that the superfluid density ψ^2 rises from zero to over half of its uniform value less than two distance units from the wall (3/4 of its uniform value by three distance units). It appears therefore that the coherent superfluid phase of the ideal Bose gas is strongly "self-healing" and not overly sensitive boundary conditions.

The occurrence of a natural length scale parameter as a general consequence of the nonlinear equation for the interacting Bose gas has already been noted. In the same one dimensional geometry, the *G–P* equation has the solution $\psi=(2V)^{-1/2}\tanh(z/2)$.

Here, the corresponding healing behavior of the superfluid density depends inversely on the strength of potential. Thus, as the interactions between the particles becomes small, the healing scale becomes increasingly large. As the potential vanishes, the characteristic length scale λ diverges, typifying the over response of the noninteracting Bose gas within the usual treatment.

The nonlinear nature of the field equation for the order parameter ψ suggests that vortex-like motions may be stable configurations within the ideal Bose superfluid [13]. This can be demonstrated by noting that the field equation (eq (5)) permits cylindrically symmetric solutions of the form $\psi(r, \theta, z)=R(r) \exp(i\nu\theta)$, where ν is an integer. The radial function $R(r)$, which is normalized by requiring that $2\pi \int dr r|R(r)|^2 =$ superfluid density per unit height along the z axis, satisfies the differential equation

$$\left(\frac{1}{r}\frac{d}{dr} r \frac{d}{dr} - \frac{\nu^2}{r^2}\right) R + (1-R^2)^2 R = 0. \tag{7}$$

While an explicit solution of this equation has not in general been possible, the asymptotic properties of the radial function can be determined [14]. Near the axis as $r \to 0$, the centrifugal force term dominates so that $R(r)$ must vanish like $r^{+|\nu|}$. Within this region the higher powers of R are negligible and the radial behavior may be approximated by the Bessel function of order $|\nu|$, $R(r) \sim J_{|\nu|}(r)$, (to within a constant multiplicative factor). At very large distances from the axis, the superfluid density approaches its uniform value, $\psi^2(r \to \infty)=1$, with the radial function of the asymptotic form $R(r) \simeq -|\nu|/r$. When $\nu=0$, only the simple solution of an everywhere uniform $R(r)=1$ is possible.

These cylindrical solutions for the quantum-mechanical order parameter ψ describe a field with a macroscopic axial component of angular momentum L_z,

$$L_z \equiv \frac{\hbar}{2i} \int dr \left[\psi^* \frac{\partial \psi}{\partial \theta} - \frac{\partial \psi^*}{\partial \psi} \psi\right] = \nu \int dr |R(r)|^2. \tag{8}$$

Thus, the total angular momentum is proportional to the superfluid density, $\psi^*\psi$. The flow field of the superfluid about the z axis has a tangential component of angular velocity v_θ,

$$v_\theta \equiv \frac{\hbar}{2i}\left[\psi^* \frac{1}{r}\frac{\partial \psi}{\partial \theta} - \frac{1}{r}\frac{\partial \psi^*}{\partial \theta}\psi\right] \Big/ \psi^*\psi \tag{9}$$

which falls off like $|\nu|/r$. Such a solenoidal flow pattern is characteristic of a "classical vortex line" found in the hydrodynamic theory of incompressible fluids. The vortex filament has a vorticity $\Omega_z \equiv (\text{curl } v)_z$ which is zero everywhere (except on the axis where the superfluid density vanishes such that the strength $(\Omega_z|\psi|^2=0,\ r=0)$. The circulation of the vortex flow

$$\Gamma = \oint d\theta r v_\theta = \hbar|\nu| > 0 \tag{10}$$

is quantized in units of $\hbar$.

One may estimate the effective size of the vortex core by setting the two asymptotic forms of $R(r)$ equal at a common value $r=\rho$ [11]. Requiring also continuity of the radial derivatives,

$$AJ_{|\nu|}(r) \simeq 1 - \nu/r$$

$$AJ'_{|\nu|}(r) \simeq \nu/r^2 \qquad (r=\rho) \tag{11}$$

we find a core dimension $\rho=(1+|\nu|)/|\nu|$.

Gross [4] and Pitaevskii [5] found similar vortex-like solutions to be stable configurations in the superfluid phase of the interacting Bose gas. In that system, the vortices owe their existence to the presence of the nonlinear term in the G–P field equation arising from the repulsive interactions between the particles. There the asymptotic solutions of the G–P radial equation are given by

$$R(r \approx 0) \simeq J_{|\nu|}(r)$$

$$R(r \gg 0) \simeq 1 - |\nu|^2/2r^2.$$

While these limiting forms for the radial behavior are independent of the interactions, the order parameter itself depends upon the strength of the potential through the normalization $\psi = (2V)^{1/2} R(r) \exp(i|\nu|\theta)$. Thus in the absence of any interactions between particles, such vortex lines vanish as possible solutions to the G–P field equation.

In general it is not possible to obtain explicit solutions to the field equation for the order parameter of either the ideal Bose system (eq (3)) or the interacting gas (G–P equation) [15]. Both are highly nonlinear equations and can be solved only for certain very special situations. In the limit of a low superfluid density to a first approximation, they are both nonlinear to the same order ψ^3, and will describe a somewhat similar type of physical behavior. It is, however, important to recognize the very essential difference in the physical origin of the nonlinearity. In the G–P equation, the nonlinear term arises from the direct repulsive interactions between the particles which are superimposed upon the Bose statistics. Without these interactions, the super-fluid order parameter satisfies a linear equation characteristic of a free noninteracting quantum field. Quite a different behavior was found for the superfluid phase of the ideal coherent Bose gas. In that description, since all terms in the field equation are due to the particle statistics, the nonlinear nature of the order parameter is a direct consequence of the Bose statistics. While any real gas must certainly have strong short-ranged repulsive interactions between particles, this nonlinear behavior suggests that the coherent phase of the ideal Bose gas might well describe the dominant physical features of superfluid liquid helium.

4. References

[1] Onsager, L., Nuovo Cimento, **S. 6,** 249 (1949).

[2] Feynman, R., Progress in Low Temperature Physics (North-Holland Publ. Co., Amsterdam, 1955) I, p. 17.

[3] Vinen, W., Proc. Roy. Soc. (London) **A260,** 218 (1961), Rayfield, G. W., and Reif, F., Phys. Rev. Letters **11,** 305 (1963). Also, review article by Andronikoshville, E., and Mamaladze, Y., Rev. Mod. Phys. **38,** 567 (1966).

[4] Gross, E. P., Nuovo Cimento **20,** 454 (1961); J. Math. Phys. **4,** 195 (1963).

[5] Pitaevskii, L. P., Sov. Phys. J.E.T.P. **40,** 646 (1961).

[6] An excellent discussion of the macroscopic mean-value of a quantum-field operator as the appropriate thermodynamic order parameter for quantum fluids is given by Anderson, P., Rev. Mod. Phys. **38,** 298 (1966).

[7] Cooper, M. J., and Green, M. S., Phys. Rev. **176,** 302 (1968).

[8] The use of the coherent state representation to describe ideal Bose condensation and its further application to the theory of superfluids has been discussed by a number of persons. [Casher, A., and Revzan, M., Amer. J. Phys. **35,** 1154 (1968); Cummins, F. W., and Johnston, J. R., Phys. **151,** 105 (1966); Langer, J. S., Phys. Rev. **167,** 183 (1968).] Particularly relevant is the work of Langer in which a free-energy functional like that described here is obtained by the expansion of an exponential form containing a slowly varying $\psi(r)$.

[9] The complete expression for $F(\psi^2,T)$ appropriate to a non-uniform system is given in eq (34) of ref. 7.

[10] Mamaladze, Y. G., Sov. Phys. J.E.T.P. **25,** 479 (1967).

[11] Amit, D., Phys. Letters **26A,** 448 and 466 (1968).

[12] Luban, M., and Miller, S., Phys. Letters **27A,** 501 (1968).

[13] The development in this section follows the argument presented by Gross in describing vortices in the interacting Bose condensate.

[14] The radial equation obtained from the G–P equation for the interacting Bose gas is given by

$$r^2R'' + rR' - \nu^2R + r^2(1-2VR^2)R = 0.$$

Explicit solution of this equation has not been possible over the entire range for r. The original work of Ginsburg, V., and Pitaevskii, L., contains a numerical solution, see Sov. Phys. J.E.T.P. **7,** 858 (1958).

[15] Some special solutions of the G–P equation appropriate to the description of physical problems are given by Wu, T. T., J. Math. Phys. **2,** 105 (1961). See also references 4, 5.

(Paper 73A3–554)

JOURNAL OF RESEARCH of the National Bureau of Standards—A. Physics and Chemistry
Vol. 73A, No. 3, May–June 1969

Franck-Condon Factors for the Ionization of H_2O and D_2O

R. Botter*

Centre d'Etudes Nucleaires, Saclay, France

and

H. M. Rosenstock

Institute for Materials Research, National Bureau of Standards, Washington, D.C. 20234

(February 11, 1969)

Franck-Condon factors have been calculated for vertical transitions of H_2O and D_2O involving both bond length and angle changes. It is shown that even in the harmonic oscillator approximation different Franck-Condon factors are obtained for positive and negative angle changes. The results are used to obtain the geometry of the ion ground state. Satisfactory agreement is obtained for the isotope effect on the vibrational transition probabilities. The effects of anharmonicity are discussed semi-quantitatively.

Key words: D_2O; Franck-Condon principle; geometry; H_2O; ion; photoionization; photoelectron spectroscopy.

1. Introduction

In recent years there has been growing interest in the quantitative formulation and application of the Franck-Condon principle to a variety of vertical transition processes in polyatomic molecules, including electronic absorption spectra, photoionization and photoelectron spectroscopy [1–11].[1] One of the major objectives of these studies has been to determine the structure of excited and ionized molecules from experimentally determined vibrational transition probabilities. In one case, the $C(^1B_1)$ Rydberg state of water, the results obtained by this method were in rather good accord with the geometry obtained by rotational analysis [4]. All these studies have in common the assumption of constant electronic transition moment, thus reducing the problem to an evaluation of vibrational overlap integrals, and a further simplification of using harmonic oscillator wave functions [12]. Three distinct approaches to the problem have been employed. First, consideration of only one progression of a totally symmetric vibration [1], second, consideration of all totally symmetric vibrations combined with a simplified normal coordinate transformation and an iterative procedure [2] and last, use of the method of generating functions [13] extended to n dimensions with consideration of all normal modes and including the possibility of symmetry as well as geometry differences between the initial and final states [9].

One application of the last method was an approximate determination of the water molecule-ion geometry from experimental Franck-Condon factors (hereafter called FCF) obtained from the staircase structure observed near threshold in the photoionization yield curve [11, 14]. The calculations reported in that study were based on a simplified normal coordinate transformation and, in addition, the extent and accuracy of the experimental data were limited to an unknown degree by interference from autoionization near threshold [11, 15]. Recently the FCF for both H_2O and D_2O ions have been determined by Brundle and Turner [16] with much greater accuracy and completeness by means of photoelectron spectroscopy. We report here new and more complete calculations based on their work, along with some new results concerning sign ambiguities in geometry determination, rough considerations concerning anharmonicity effects, and a comparison of the ion geometry with that of the $C(^1B_1)$ Rydberg state.

2. Method

The generating function method has already been described in detail elsewhere [9–10]. The basic problem in the polyatomic case is the determination of the transformation relating the normal coordinates

*Present address: Centre d'Etudes Nucleaires, Saclay, France.

[1] Figures in brackets indicate the literature references at the end of this paper.

of the initial and final states. As first pointed out by Duschinsky [17], this is in the most general case a linear matrix transformation relating initial and final state normal coordinate vectors $\mathbf{Q}$ and $\mathbf{Q}'$. It has the form

$$\mathbf{Q}' = J\mathbf{Q} + \mathbf{K}$$

where J is a matrix and $\mathbf{K}$ a vector. From symmetry considerations it follows that $\mathbf{K}$ has nonvanishing components only for totally symmetric modes. As a result, only totally symmetric vibrations are strongly excited in the vertical transition [18–19]. In the diatomic case there is an analogous transformation in which J incorporates the effect of frequency changes and $\mathbf{K}$ the effect of bond length change.

In the diatomic case, in the harmonic oscillator approximation, one obtains the same FCF for bond length changes of equal magnitude but opposite sign. This follows directly from the symmetry properties of the harmonic oscillator wave functions and the fact that the FCF is the square of the vibrational overlap integral. Consequently, one cannot directly determine the sign of the bond length change by working backwards from observed vibrational intensities. This ambiguity, of course, disappears when anharmonicity is taken into account. In the polyatomic case, on the other hand, this ambiguity disappears in the harmonic approximation if there is more than one totally symmetric mode and if the transformation relating the initial and final state totally symmetric modes involves a rotation in normal coordinate space, i.e., if the J matrix has off-diagonal elements. An illustration is given below.

The detailed form of the normal coordinate transformation given above is conveniently found starting with internal symmetry coordinates S and S' for the two states. With the choice of a force field, such as a simple valence force field, the normal coordinates are obtained by solving the vibrational eigenvalue problem from which one obtains matrices L and L' relating the respective normal coordinates to the internal symmetry coordinates

$$\mathbf{S} = L\mathbf{Q} \text{ and } \mathbf{S}' = L'\mathbf{Q}'.$$

The most general transformation relating the internal symmetry coordinates of the two states is again of the form

$$\mathbf{S}' = Z\mathbf{S} + \mathbf{R}$$

from which it follows that

$$J = L'^{-1}ZL \text{ and } \mathbf{K} = L'^{-1}\mathbf{R}$$

Using conventional stretching and bending internal symmetry coordinates, the relation between these coordinates for two states of bond angles 2β and $2\beta'$ and bond length r and r', respectively, is readily written down. (It is often convenient to work this out via cartesian displacement coordinates.)

$$S_1' = \cos(\beta-\beta')\cdot S_1 - \frac{r}{\sqrt{2}} \sin(\beta-\beta')\cdot S_2 + \sqrt{2}\,(r\cos(\beta-\beta') - r')$$

$$S_2' = \frac{\sqrt{2}}{r'}\sin(\beta-\beta')\cdot S_1 + \frac{r}{r'}\cos(\beta-\beta')\cdot S_2 + \frac{2r}{r'}\sin(\beta-\beta')$$

$$S_3' = \frac{\sin\beta'}{\sin\beta}\cdot S_3$$

where the subscripts 1, 2, and 3 refer (throughout) to the symmetric stretching, symmetric bending and antisymmetric stretching coordinate. It is seen from this transformation that the off-diagonal elements of the Z matrix will have different sign depending on the sign of the bond angle change. Further, inspection of the L' matrix elements also shows an unsymmetric behavior with respect to positive or negative bond angle differences compared to the other state. Consequently, a bond angle difference between the initial and final state will lead to somewhat different FCF depending on the sign of the difference. The L and L' matrices depend, of course, on the normal coordinates which, in turn depend on the assumed force field. However, these remarks are qualitatively correct.

A second effect of the mixing to stretching and bending normal modes in the transformation is that the FCF of the stretching mode is somewhat dependent on the angle change and, conversely, the FCF of the bending mode is dependent also on the bond length change.

3. Results and Discussion

3.1. Ambiguity of Sign

In order to illustrate the unsymmetric behavior with respect to geometry changes as discussed above, calculations were carried out for an idealized case. FCF were calculated for a transition of the water molecule in which the upper state had geometry but not frequency changes with respect to the lower state. For the initial state parameters, the geometry and the totally symmetric mode frequencies of the ground state water molecule were used. A simple valence force field was used to determine the antisymmetric stretching frequency and the normal modes. In table 1 are shown the FCF calculated at various geometries corresponding to all combinations of up to two increments of ± 0.0400 Å and ± 5.00 deg geometry change with respect to the initial state. The sum of the FCF for any given geometry may not equal unity because of contributions from higher overtone and combination transitions which are not tabulated. It is seen that when there is only a bond length change the sign ambiguity is still present, i.e., one obtains exactly the same transition probabilities. However, when angle changes occur one obtains numerically different values depending on the sign of both the angle and bond length change. Further, the dependence of stretching excita-

TABLE 1. *Franck-Condon Factors for Positive and Negative Geometry Changes in* H_2O [a]

$\frac{2\beta}{r}$	94.52°	99.52°	104.52°	109.52°	114.52°
			P (000–000)		
0.8772Å	0.37639	0.47072	0.51071	0.48097	0.39331
.9172	.62016	.78023	.84537	.78929	.63530
.9572	.73212	.92512	1.00000	.92530	.73326
.9972	.61925	.78468	0.84537	.77494	.60477
1.0372	.37529	.47610	.51071	.46364	.35643
			P (100–000)		
0.8772	0.23236	0.30657	0.34243	0.32415	0.26006
.9172	.08916	.12400	.14170	.13347	.10363
.9572	.00055	.00009	.00000	.00000	.00002
.9972	.11662	.13713	.14170	.12914	.10398
1.0372	.26512	.32515	.34243	.31019	.24196
			P (010–000)		
0.8772	0.14774	0.05205	0.00075	0.03155	0.11911
.9172	.21706	.07276	.00031	.05627	.19417
.9572	.22690	.07161	.00000	.07146	.22618
.9972	.16861	.04947	.00031	.06463	.18826
1.0372	.08897	.02387	.00075	.04163	.11197
			P (110–000)		
0.8772	0.07781	0.02928	0.00050	0.01758	0.06590
.9172	.02162	.00824	.00005	.00649	.02177
.9572	.00204	.00043	.00000	.00032	.00124
.9972	.04317	.01205	.00005	.01454	.04392
1.0372	.07493	.01982	.00050	.03237	.08909

[a] Ground state $r = 0.9572$Å $2\beta = 104.52°$, G. Herzberg, Electronic Spectra of Polyatomic Molecules (D. Van Nostrand, New York, 1966).

ν_1 – Symmetric stretching mode.
ν_2 – Symmetric bending mode.
ν_3 – Antisymmetric stretching mode.

tion on angle change and vice versa is clearly demonstrated by inspecting rows and columns. The results of including frequency differences as well as geometry differences are not very much different. For upper state frequencies corresponding to the Rydberg state of the ion (see table 3) there is a slight distortion of the FCF surfaces.

From a practical standpoint, this asymmetry effect is too small to be of use in this range of geometry variation. However, for still larger angle changes the effect will be quite pronounced. An extreme case of this type is the pyramidal planar-transition of NH_3 [20].

3.2. Franck-Condon Factors for Ionization

In table 2a are shown the experimental FCF for H_2O and D_2O determined by Brundle and Turner [16] by photoelectron spectroscopy. In table 2b are listed the FCF relative to the zero-zero transition computed

TABLE 2a. *Experimental Franck-Condon Factors for the ionization of* H_2O *and* D_2O *from photoelectron spectroscopy* [a]

Transition	H_2O	D_2O
000–000	0.757 ± [c] 0.005	0.702 ± 0.005
100–000	.143 ± .005	.148 ± .005
200–000	.018 ± .002	.025 ± .002
300–000	[b] < .008	.....
010–000	.069 ± .005	.087 ± 0.005
110–000	.013 ± .002	.034 ± .002
210–000	> .002	.004 ± .002

[a] Turner and Brundle, ref. [16].
[b] Detection limit; not observed.
[c] Throughout this paper indicated numerical error limits represent subjective estimates, by the authors cited or by the present writers, of probable limits of error.

from the photoelectron spectroscopy data along with other ratios obtained from photoionization experiments by Dibeler [11] and Brehm [15] and, for comparison, the results for the Rydberg C and D states determined spectroscopically by Bell [4]. It is seen that the photoionization data are in only moderate agreement with the photoelectron results. Both photoionization experiments show clear indication of autoionization structure just above the (100–000) step, and it is probable that there is interference from autoionization near threshold as well. In table 3 are listed the frequencies for the ground state, ion state, and the C and D Rydberg states determined by various workers. There is a very close correspondence between the ion frequencies and those of the Rydberg C state for both isotopic species. This, of course, leads to the expectation of very similar geometries for both states.

The FCF were calculated for both molecules as a function of both bond distance and angle, using the Rydberg C state frequencies for the upper state. Calculations were carried out for both a simple valence force field and for one with a potential interaction constant between the stretching and bending coordinate. The two gave essentially identical results. The ground state geometry is given in table 4. In figures 1 and 2 are shown the results in the region of interest corresponding to an increase in both angle and length. The curves may be visualized as cuts through the Franck-Condon surfaces at three different values of the bond length, and the tenfold difference in ordinate scale for both 000 and 100 should be kept in mind. Also shown are the experimental points for all transitions measured by Brundle and Turner [16]. The measure of agreement is whether all points lie on the same vertical line. It is clear that the agreement is only moderately good, with some deviation for 110 and 210. Noteworthy is the fact that the results for both ions lie at almost exactly the same geometry, that the significant deviations from ideal are in the same direction for the same transitions and, most important, that there is a major discrepancy in both cases for the 200–000 transition, with the experimental values several times as large as the calculated values. Also, inspection of the cuts at 0.99 and 1.01 A shows that the disagreement cannot be resolved

TABLE 2b. *Ratio of experimental Franck-Condon factors by different methods relative to the 000–000 transition*

		Photo-electron spectros-copy [16]	Photoionization [a]		Rydberg C State [4]	Rydberg D State [4]
			ref. 11	ref. 15		
H_2O	100–000	0.189		0.20 ± 0.03		
H_2O	010–000	.091	0.18 ± 0.03	$.14 \pm .03$		
D_2O	100–000	.222		$.18 \pm .03$	0.6 ± 0.2	0.60 ± 0.15
D_2O	010–000	.124		$.14 \pm .03$	$.2 \pm .1$	$.45 \pm .15$

[a] The values given are estimated from the published curves. Both sets of photoionization values are subject to error due to autoionization.

TABLE 3. *Frequencies for various states of* H_2O *and* D_2O, in cm^{-1}

	Ground State [a]	C Rydberg State		D Rydberg State ref. 4	Ion Ground State	
		ref. 4	ref. 22		P. I. ref. 15	P.E.S. ref. 16
$H_2O\nu_1$	3652	3179	3170	3268	3190 ± 50	3200 ± 50
$H_2O\nu_2$	1595	1407	[b] (1422)	1636	1420 ± 50	1380 ± 50
$H_2O\nu_3$	3756	(3238)	(3224)			
$D_2O\nu_1$	2666	2338	(2290)	2381	2280 ± 50	2310 ± 50
$D_2O\nu_2$	1179	1041	1038	1223	1050 ± 50	980 ± 50
$D_2O\nu_3$	2784	(2427)	(2365)	(2483)		

[a] G. Herzberg, Infrared and Raman Spectra, New York (1945).
In the FCF calculations a value of $\nu_1 = 3699$ was used. This has no effect on the results.
[b] All quantities in brackets have been calculated from simple valence force fields.

TABLE 4. *Geometry of various water states*

	Ground state [19]	C State rotational analysis [22]	C State FCF [4]	D State FCF [4]	Ion FCF [a]	Ion SCF calc. [23]
r	0.9512Å	1.013	1.022 ± 0.01	1.024 ± 0.01	0.995 ± 0.005	
2β	104.52°	106.7	109.7 ± 1.8	113.0 ± 1.8	[b] < 109	119

[a] This work.
[b] The value 110° is obtained for a harmonic oscillator calculation. The consideration of anharmonicity would decrease this value by perhaps several degrees, see text.

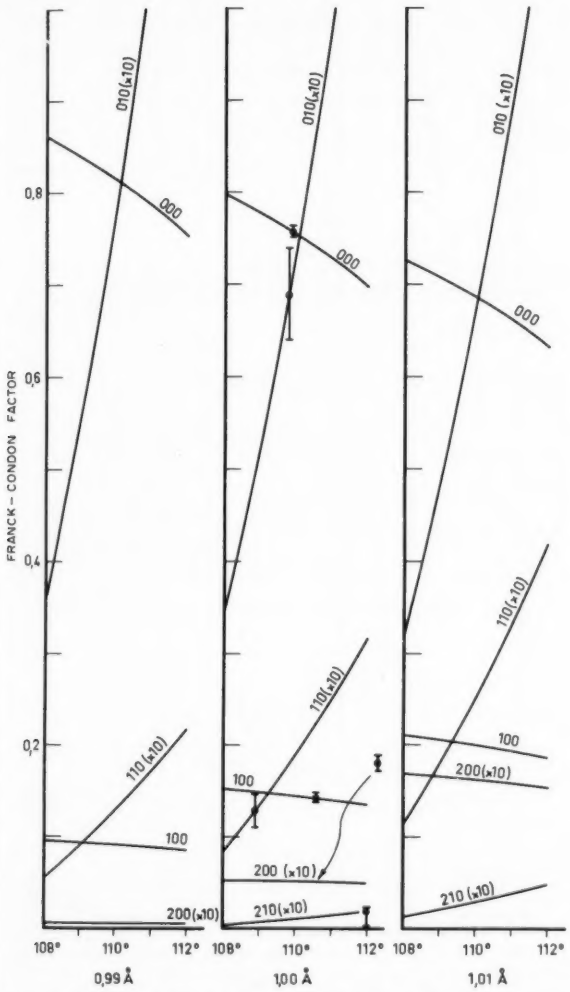

FIGURE 1. *Franck Condon factors for H_2O as a function of bond angle at three bond distances for the ion state.*
Experimental points with error bars are the photoelectron spectroscopy results of Brundle and Turner [16].

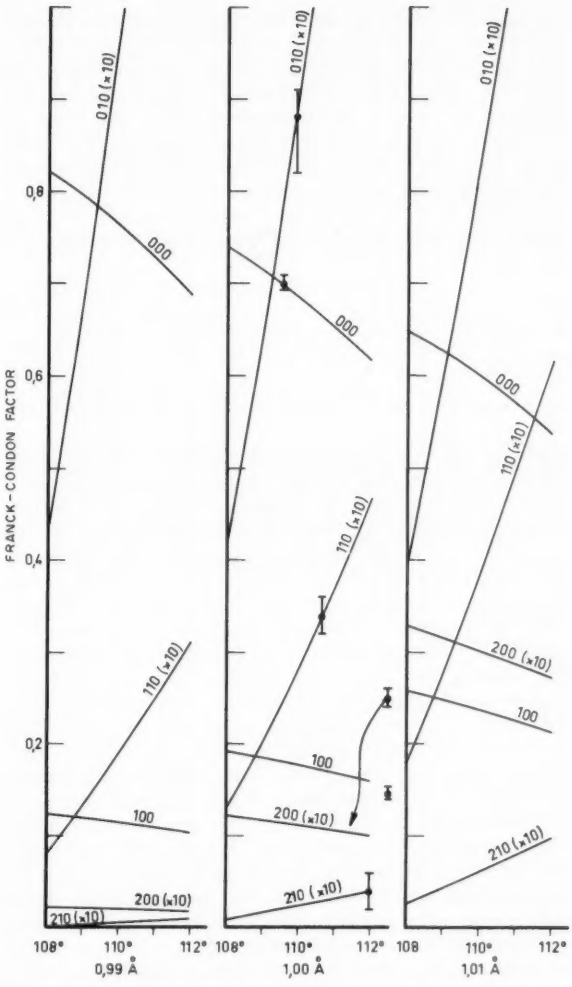

FIGURE 2. *Franck-Condon factors for D_2O as a function of bond angle at three bond distances for the ion state.*
Experimental points with error bars are the photoelectron spectroscopy results of Brundle and Turner [16].

by a slight geometry change. Thus, at first sight one has established a geometry estimate of 1.00 Å and 110 deg. with astoundingly good precision. The large deviations are due to anharmonicity, and the precision is a little deceptive.

3.3. Anharmonicity Effects

Before considering anharmonicity, one other factor has to be considered. In the H_2O and D_2O molecules and ions the frequencies of the antisymmetric stretching mode are quite close to the symmetric stretching frequencies. For the ions this is based purely on simple valence force field calculations which, as seen from table 3 give reasonably good results for the C Rydberg state. Comparing the values with those of the molecule ground state one has a decrease of about 500 and 300 cm^{-1} for the H_2O and D_2O ions, respectively. This is sufficient to produce a small excitation of the even overtones of the antisymmetric stretching modes, and it is very probable that the results of Brundle and Turner for the 200–000 transition include contributions from 002–000 as well. The calculated transition probability is about 0.001 for both H_2O and D_2O. Another possible interference is the (120–100) transition which would lie only several hundred wave numbers away from the (200–000) transition. The FCF for this transition depends on the geometry but, in this range has a value of about 0.003 to 0.004 for H_2O and 0.001 for D_2O. Thus the difference between the calculated and measured FCF is quite real, although the experimental value might be somewhat lower than stated.

There is no direct indication of the magnitude of

the anharmonicity in the water ions. Again, the results of Bell on the Rydberg C state are suggestive since they show first differences in both the stretching and bending progression [4]. However, they are far too fragmentary for a determination of anharmonicity. In view of this we have carried out only the very simplest one dimensional perturbed harmonic oscillator calculation corresponding to a cubic term in the potential for both the symmetric stretching and bending mode. For this model perturbation theory yields for the wave function

$$\psi_n = \psi_n^\circ + \frac{\sqrt{X_e}}{3\sqrt{30}} \{ -[n(n-1)(n-2)]^{1/2}\psi_{n-3}^\circ - 9n^{3/2}\psi_{n-1}^\circ + 9(n+1)^{3/2}\psi_{n+1}^\circ + [(n+3)(n+2)(n+1)]^{1/2}\psi_{n+3}^\circ \}$$

where x_e is the anharmonicity constant and n is the vibrational quantum number. In the absence of better information we note the remark of Bates [21] that in many diatomic molecules x_e has values of the order of magnitude 10^{-2}. Using the perturbed wave functions for the stretching normal mode it is a straightforward matter to recalculate the FCF using the overlap integrals previously calculated for that geometry. The results are shown in figure 3. The dashed lines show the anharmonic FCF as a function of $x_e^{1/2}$. They are shown for a geometry of 1.00 Å and 110 deg. The 000–000 transition probability decreases somewhat and both the 100–000 and 200–000 transition probabilities increase. The great slope difference between the latter two is again due to the tenfold difference in ordinate scale. It is interesting to note that a reasonable value of the anharmonicity parameter accounts for the intensity discrepancy in 200–000. At a slightly lower value of $r = 0.995$ Å one can bring all three transitions into accord with a value of x_e of about 0.008–0.009. The dependence of the FCF on the anharmonicity coefficient at that geometry is very similar to that shown for 1.00 Å. Further, with this value of anharmonicity one can calculate the effect on 300–000 as well, although at this transition the first order perturbed wave function is of doubtful utility. In any even the FCF calculated with the perturbed wave function did not exceed the upperbound determined experimentally.

It is evident that a similar situation holds for the bending vibration as well. A similar parametrized calculation indicates that for an anharmonicity of 0.01 the same FCF is obtained at 109 deg instead of 110, and for an anharmonicity of 0.04 at 108 deg. There is little question that the bending mode is anharmonic, and these results indicate that the accuracy as well as the precision of the bending angle estimate is somewhat lower than appears from the FCF curves and the small probable error of the experimental FCF.

3.4. Geometry of Water States

In table 4 are given the geometries of the various states determined spectroscopically [22] and by spec-

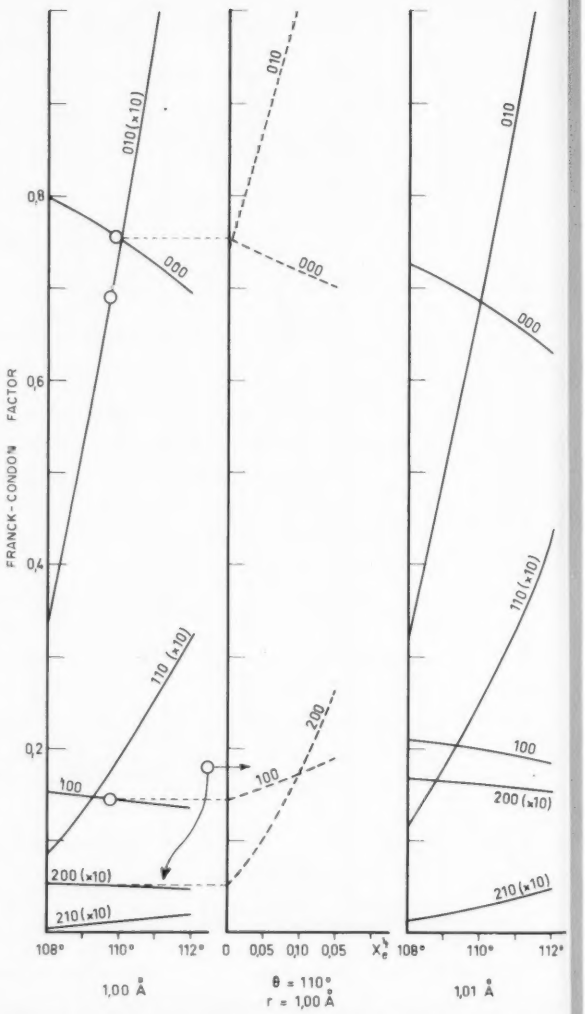

FIGURE 3. *Dependence of Franck-Condon factors for* H_2O *on the anharmonicity parameter* $x_e^{1/2}$, *for an upper state geometry of 1.00 Å and 110°.*

Left-hand and right-hand graphs give the dependence on geometry for comparison.

troscopic FC and photoelectron spectroscopic FC methods and the results of a SCF calculation by Krauss [23]. On the basis of the crude discussion of anharmonicity effects, one can suggest that at least part of the angle discrepancy between the FCF results of Bell and the rotational analysis of Johns is due to anharmonicity. In the harmonic approximation we obtained the same results as Bell. Further, in comparing the bond length of the C state and the ion state we note that the bond length of the ion is smaller. In addition, the ambiguity of geometry change determination which is still effectively present in the harmonic approximation is in fact removed by the anharmonicity assumptions required to account for the abnormally high 200–000 FCF. The analogous anharmonicity calculations for a *decrease* of bond

length of equivalent magnitude *below* the neutral molecule value would have led to an opposite effect on the "corrected" transition probability. Lastly, the bond angle estimate for the ion is of only moderate value. It may in fact be equal to, or even lower than that of the C state. The answer to that question will depend on improved knowledge of anharmonicity.

We thank D. W. Turner and C. R. Brundle for sending their results prior to publication and for helpful correspondence.

4. References

[1] Craig, D. P., J. Chem. Soc. **1950,** 2146.
[2] Coon, J. B., de Wames, R. E., and Loyd, C. M., J. Mol. Spectry. **8,** 285 (1962).
[3] Anno, T., and Sado, J. Chem. Phys. **32,** 1611 (1960).
[4] Bell, S., J. Mol. Spectry. **16,** 205 (1965).
[5] Humphries, C. M., Walsh, A. D., and Warsop, P. A., Trans. Faraday Soc. **63,** 513 (1967).
[6] Walsh, A. D., and Warsop, P. A., Trans. Faraday Soc. **63,** 524 (1967).
[7] Turner, D. W., and May, D. P., J. Chem. Phys. **46,** 1156 (1967).
[8] Villarejo, D., Stockbauer, R., and Inghram, M. G., J. Chem. Phys. **48,** 3342 (1968).
[9] Sharp, T. E., and Rosenstock, H. M., J. Chem. Phys. **41,** 3453 (1964). See also corrections in ref. 10.
[10] Botter R., Dibeler, V. H., Walker, J. A., and Rosenstock, H. M., J. Chem. Phys. **44,** 1271 (1966).
[11] Dibeler, V. H., Walker, J. A., and Rosenstock, H. M., J. Res. NBS **70A** (Phys. and Chem.) No. 6, 459 (1966).
[12] Two exceptions are: a one dimensional Rydberg-Klein-Reese calculation on carbon dioxide by Petropoulos, B., and Botter, R., C. R. Acad. Sci., in press, and calculations with a double minimum potential for chlorine dioxide by Coon, J. B., Cesari, F. A., and Loyd, C. M., Disc. Faraday Soc. **35,** 118 (1963).
[13] Hutchinson, E., Phys. Rev. **36,** 410 (1930).
[14] Botter, R., and Rosenstock, H. M., Adv. Mass Spectry. **4,** 579 (1968).
[15] Brehm, B., Z. Naturf. **21a,** 196 (1966).
[16] Brundle, C. R., and Turner, D. W., Proc. Roy. Soc. **A307,** 27 (1968).
[17] Duschinsky, F., Acta, Physicochem. URSS **7,** 551 (1937); see also ref. 2.
[18] Herzberg, G., and Teller, E., Z. Physik. Chem. **B21,** 410 (1933).
[19] Herzberg, G., Electronic Spectra of Polyatomic Molecules (D. Van Nostrand Co., Inc., Princeton, (1966)).
[20] Botter, R., and Rosenstock, H. M., in preparation.
[21] Bates, D. R., Mon. Not. Roy. Astron. Soc. **112,** 615 (1952).
[22] Johns, J. W. C., Can. J. Phys. **41,** 209 (1963).
[23] Krauss, M., J. Res. NBS **68A** (Phys. and Chem.) No. 6, 635 (1964).

(Paper 73A3-555)

JOURNAL OF RESEARCH of the National Bureau of Standards—A. Physics and Chemistry
Vol. 73A, No. 3, May–June 1969

Topological Features of Hot Carrier Induced Anisotropic Breakdown on Silicon Diode Surfaces

George G. Harman

Institute for Applied Technology, National Bureau of Standards, Washington, D.C. 20234

(February 11, 1969)

Both Gunn and Morozov have reported breakdown paths (tracking) on the surface of germanium under hot carrier conditions. Many silicon and gallium arsenide device failures appear to have been caused by similar breakdown tracks extending between contacts or across junctions. In the present work on silicon, extremely anisotropic tracking has been observed on the surface of long, thin, forward biased, n^+-p-p^+, silicon diodes. The tracks propagate only in ⟨100⟩ crystallographic directions, independent of the applied field orientation, the temperature, or the crystal growth direction. For example, on a sample with a {100} surface plane, having the field oriented along a ⟨110⟩ direction, the tracks propagate along ⟨100⟩ directions which are 45° away from the applied field. Tracks on {100} -plane, disk shaped diodes, propagate radially from the center (positive biased) ohmic contact region, and mark off the ⟨100⟩ directions within 2°. Tracking requires both high current densities ($\sim 5\times10^3$ A/cm²) and high fields (~ 15 kV/cm), and occurs most readily on the p-region of 10 Ω cm, n^+-p-p^+, ⟨100⟩ oriented diodes. Diodes with n^+-n-p^+ structures having n-regions ~ 1 Ω cm, and n^+-n-n^+ structures of ~ 1 Ω cm will also track, but require much higher fields and the ⟨100⟩ tracking orientation is not clearly defined. Tracking does not occur on diodes having the field oriented along a ⟨111⟩ direction.

Two basic types of tracks are observed. The first resembles a series of tiny explosion craters (~ 10 μ m diam). The second appears to be continuous in nature, even though it is extended by each applied pulse. These tracks may be several micrometers wide and deep.

It is also shown that hot-minority-carrier sample explosions are anisotropic and not, as generally assumed, caused by thermal breakdown. Typically a {110} ⟨111⟩ oriented n^+-p-p^+ sample requires 4 to 6 times more impulse energy to explode than a {100} ⟨100⟩ oriented sample.

Key words: Anisotropy; crystallographic orientation; hot carriers; semiconductor breakdown; silicon diodes.

1. Introduction

In early hot carrier experiments Gunn [1][1] observed "visible tracks" on the surface of his n-type germanium structures, when the fields were ~ 10kV/cm. No crystallographic orientation of his samples was reported and presumably the tracks were in the general direction of the applied field, originating at and extending from the electrodes. He found it necessary to shorten the pulse length to ~ 10^{-9} s in order to apply high fields without damage to his samples.

Morozov [2] observed oriented breakdown on germanium surfaces, extending from point contacts. He applied long (10–1000 μs), high current (up to 30 A peak) pulses by discharging a capacitor through the point contacts. Tracks were observed only when the point was positive, regardless of the carrier type. There was some evidence of molten material in the tracks. No absolute orientation preference was observed. However, at high power levels the breakdown generally followed the crystal growth direction, which was a ⟨111⟩.

Considering this history plus the fact that, commercial semiconductor devices often operate with fields as high or higher than the above hot carrier structures, it was decided to investigate the occurrence of the tracking phenomena on silicon, characterize it, and if possible relate it to various device breakdowns. Some preliminary results of this work have been recently reported [3, 4].

In the following work we will describe some of the high field, high current transport properties, including conductivity modulation, of long thin forward biased n^+-p-p^+ silicon diode structures. The hot carrier excitation produces surface breakdown tracks that propagate along ⟨100⟩ crystallographic directions, regardless of the field orientation. The general morphology of the two basic types of tracks will be described in detail. The average applied (and local) field and current density thresholds necessary to produce tracking will be given, and the effects of differing bulk carrier type and concentrations discussed. At very high impulse power levels all of the samples will explode. However, the power level for explosions is strongly dependent on the crystallographic orientation of the applied field. Various mechanisms that might result in such effects are discussed.

[1] Figures in brackets indicate the literature references at the end of this paper.

lographic orientation of the applied field. Various mechanisms that might result in such effects are discussed.

2. Apparatus and Sample Preparation

High voltage pulses were generated with a hydrogen thyratron delay-line system operating into 25 Ω impedance, similar to that described in reference 4. Pulse lengths could be varied from 0.06 to 3.0 μs. A 0.4 μs pulse length was used for most of the measurements reported here. The system could deliver up to 8 kV directly or could be stepped up to 25 kV through a specially designed pulse transformer. High voltage diode stacks were used as reverse polarity clippers both in the generator and on the transformer output, in order to protect the reverse characteristics of the junctions. The system was generally terminated within 2 cm of the sample using several 2 W carbon resistors in series, immersed in the same insulating liquid as the sample, either liquid nitrogen or a fluorocarbon. The current was measured either with a precision current transformer or across a 2 Ω load in series with the sample.

The long thin *p-n* junction samples present a nonlinear "inductive" load with an equivalent inductance of 30 to 50 μH. The current through the sample rises as a sawtooth from zero to, at times, greater than 40 A peak. This caused matching problems not encountered in the usual hot majority-carrier studies. Even with 25 Ω source impedance it was difficult to maintain a good square voltage waveshape at all times, so the reported pulse voltages and currents were measured at the same point in time, at the current peak on the *end* of the pulse. A very low repetition rate (typically 4 pps or less) was used, to assure that the sample temperature returned to the ambient value between pulses.

In order to determine the field distribution along the samples, a pulse probe apparatus was developed. This consisted of a tuned, high voltage oscilloscope probe with an internal impedance of 10^7 Ω. A coarse phosphor-bronze point contact (~7 μm diam tip) was attached to the end of the probe. This was then mounted on a micromanipulator platform and lowered onto the sample, using a microscope for alinement. The probe gave accurate voltage pulse shapes regardless of whether it was forward or reverse biased (through its 10^7 Ω internal impedance). In the reverse direction such a coarse point results in low breakdown voltages and high leakage currents, so that no effective barrier is observed. Since the sample impedances were typically less than 10^3 Ω, no probe induced perturbation of the internal field was anticipated. A comparative test with a 10^8 Ω probe yielded identical results.

The samples discussed in this paper were 1, 7, 10, and 100 Ω cm silicon of both *n* and *p* type, cut in different orientations from a small number of low oxygen content, float zone crystals having a ⟨111⟩ growth direction. For verification, samples obtained from different sources and having different growth techniques and directions were also used. Most of the samples were taken from silices cut with various orientations in {100} and {110} planes, but a few were prepared from {111} plane slices [5]. Figure 1 shows the two sample configurations used in this work with the typical dimensions and orientations. The dimensions were varied somewhat for specific experiments. The rectangular (linear) samples (fig. 1a) were variously prepared by an ultrasonic cutting process, or by milling (with a wide diamond wheel) a 0.25 cm wide, 0.01 cm deep indentation in the silicon slice at the desired orientation angle, then diamond sawing each sample out. Twenty to thirty samples, having various orientations could be obtained from one slice. This assured a minimum variation of material parameters from sample to sample so that the various comparisons would be meaningful. The disk samples (fig. 1b) were made by a two-step ultrasonic cutting process.

During processing all masking and etching was done individually by hand but the diffusions were made in as large numbers as practical to minimize sample to sample variations. The samples were etched, at least 50 μm on all sawed or abraded surfaces, to minimize work-damage-induced surface defects. Thus, the final surfaces were not mirror finishes but had the slight "orange peel" configuration that is typical of heavily etched silicon.

Ohmic contacts on the *p*-type samples were either alloyed aluminum or diffused boron, over-evaporated with aluminum. No significant electrical differences

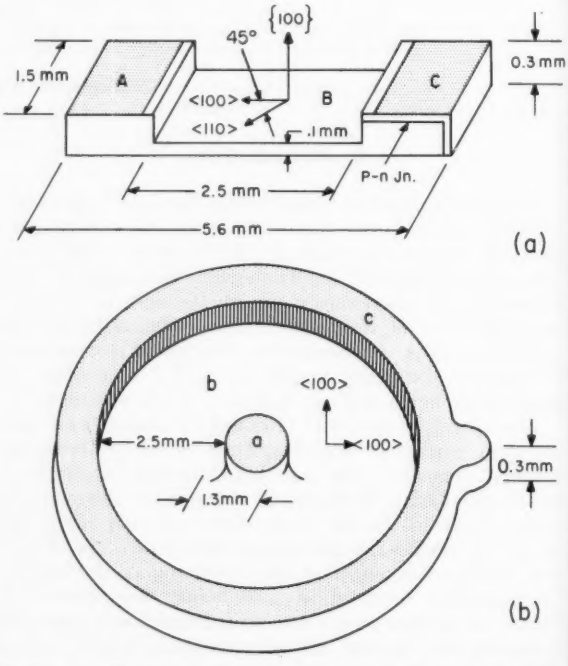

FIGURE 1. *Typical sample configurations with the most usual orientations indicated.*

Regions B and b are the same thickness. The surface plane orientations are ± 1/2 degree, directions are within 2 deg. A, a, are ohmic electrodes; B, b, high field region; C, c, *p-n* junction region.

3. Experimental Observations

3.1. Transport

The current and voltage characteristics of typical forward biased ⟨100⟩ oriented linear diodes are given in figure 2 for both 77 and 300 K sample temperatures (curves A and B). Current and voltage tracking thresholds are indicated at the top and a typical current wave shape (E), due to injection, is at the bottom. The lower curves (C and D) are for samples with noninjecting, ohmic contacts, at 300 K. These curves, and comparable ones taken at 77 K, show the typical current saturation expected of hot majority carriers. Comparison of curves C and D with B, demonstrates the very large conductivity modulation due to minority carrier injection. It is greater than a factor of ten. With the accompanying carrier velocity saturation, it is clear that this increased current density represents increased carrier density. The slopes (S) of various curves are indicated. The slopes of curves A and B increase up to about 2 with increasing pulse width. However, thermal effects become significant for pulse lengths $\sim 1\ \mu s$ and the slope actually decreases in the high peak power region. Very short pulse lengths ($< 0.1\ \mu s$) do not result in appreciable injection, so that such curves, and tracking characteristics, resemble those of ohmic contacted samples, to be described below. In curve B, the current wave shape of the 1.15 slope portion approximately follows the applied voltage squarewave pulse, indicating that few, if any, injected carriers are able to traverse the entire length of the sample before they recombine. The change of slope to 1.75 is accompanied by the sawtooth current wave shape (E) and is due to minority carrier transport through to the ohmic contact. This latter fact has been verified by infrared (1.1 μ) photographs of recombination radiation at the ohmic contact, and by studying the voltage wave shape along the sample, using a probe.

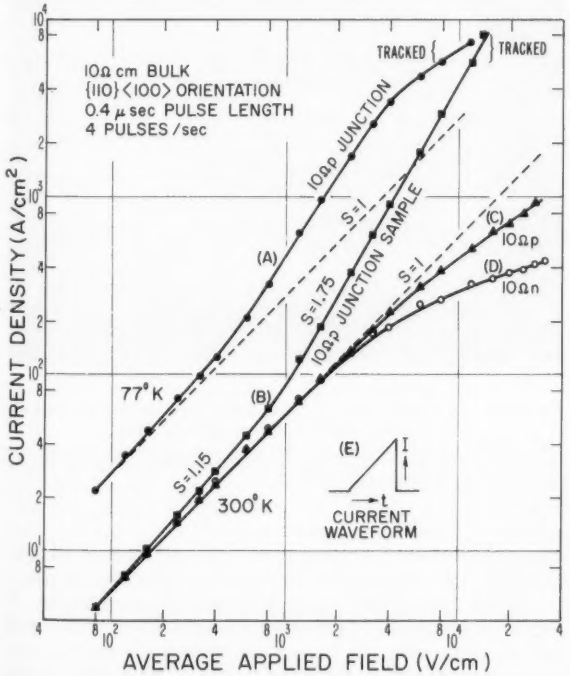

FIGURE 2. *The J—E characteristics of typical 10 Ωcm n⁺-p-p⁺, forward biased, ⟨100⟩ oriented linear diodes are given for 77 (curve A) and 300 K (curve B) sample temperatures.*

Tracking current and voltage thresholds are indicated at the top. The lower curves are for samples with noninjecting, ohmic contacts; (C)10Ωcm p^+-p-p^+, at 300 K, (D)10 Ωcm n^+-n-n^+ at 300 K, and (E) is the current wave shape in the $S = 1.75$ region of curve B, resulting from heavy injection.

The high current-density short pulse-conduction is not in equilibrium. However, it appears to be a case of double injection when the data is modified for the saturating velocities of the carriers, taking into account the effects of diffusion at the ends, by the method of Mayer, Baron and Marsh [6].

3.2. Anisotropic Tracking

When the voltage and current are increased through a forward biased long thin $n^+ - p - p^+$ diode, the first evidence of anything unusual is that short, weak pulses of avalanche radiation are emitted [4]. This is a form of prebreakdown light and can be detected with a photomultiplier. The intensity of these light pulses increases with current until at some point (~ 3 to 10 times threshold current, depending on orientation) there will appear very intense, fractional microsecond bursts of light that are visible with the dark accommodated eye and can saturate a photomultiplier. These occur simultaneously with the peak of the current pulse (fig. 2E) and are the first evidence that tracks have started. *At this time there is no indication on the current envelope itself.* After an extended period of pulsing, the current envelope may become erratic at the peak (the top 5% of the total current). By the time this is seen, several tracks would have started or a tiny chip may have been blown from the sample.

On n^+-p-p^+ silicon structures, the tracks are always oriented in a ⟨100⟩ crystallographic direction. Thus for samples having applied fields along the ⟨100⟩ direction the tracks will be parallel to the field. They originate in the high field region (B of fig. 1a), near the positively biased ohmic (noninjecting) contact end of the sample and propagate toward the negatively biased junction, progressing at a rate of from 1 to 10 μm per pulse, depending on the applied power level. The tracks will reach a maximum length for any given power level, and continued pulsing will only widen and deepen them. Relatively large surface imperfections produce only microscopic deviations in the direction of propagation of the track.

Figure 3 shows a sample with the field oriented in a ⟨110⟩ direction, having a {100} surface plane. The breakdown tracks are clearly at 45° from the direction of the applied field and thus are in a ⟨100⟩ direction. Figure 4 shows a section of a silicon web sample (growth direction in the $[2\bar{1}\bar{1}]$) where the field is also in a ⟨110⟩ direction, but the surface plane is a {111}. No ⟨100⟩ direction exists on this surface but the projection of a ⟨100⟩ lies at an angle of 30° from the ⟨110⟩

FIGURE 3a. *A 10Ωcm, p-type {100} ⟨110⟩ oriented, linear junction sample, showing breakdown tracks at 45° from the applied field direction and thus in the ⟨100⟩ direction.*

Breakdowns initiated and propagated on the back side (away from electrodes). The tracking threshold was 26 kV/cm, 22×10^3 A/cm², 0.5 μs pulse length, at 300 K.

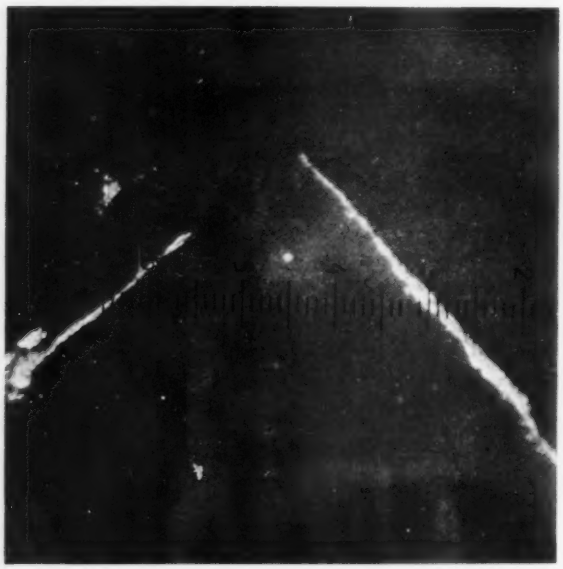

FIGURE 3b. *A larger magnification of the same sample emphasizing the 45° tracks.*

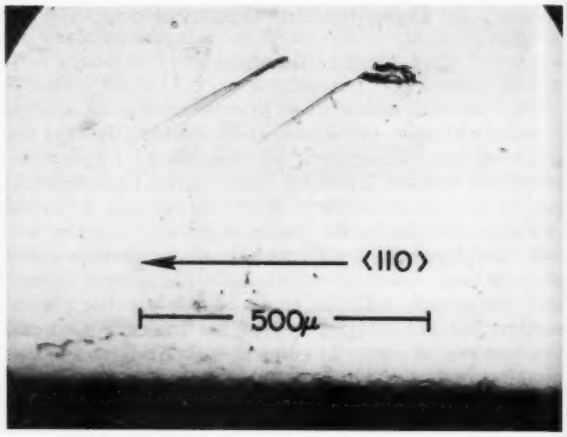

FIGURE 4. *A portion of a 7 Ωcm p-type {111} ⟨110⟩ oriented linear junction sample (made from silicon web) showing the breakdown tracks at 30°* from the applied field direction.

The tracks started in the high field region (B of fig. 1a), far away from the electrodes. The tracking threshold was 25 kV/cm- 8.5×10^3 A/cm², 0.25 μs pulse length, at 77 K.

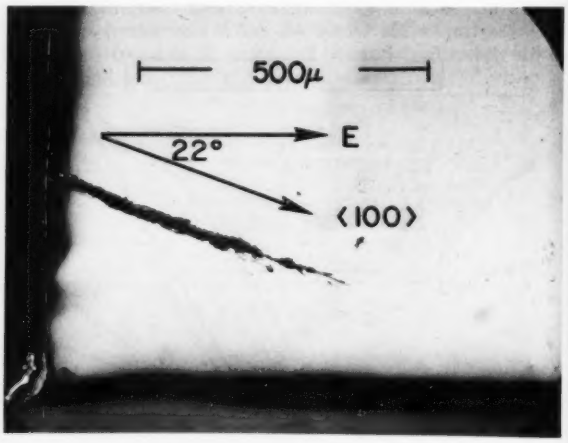

FIGURE 5. *A portion of a 10 Ωcm, {100} junction sample with the field oriented 22° from the ⟨100⟩ direction.*

The track originates on the thin, high field region in the shadow of the raised ohmic electrode and is at 22° from the applied field direction. The tracking threshold was 20 kV/cm, 4×10^3 A/cm², 0.4 μs pulse length, at 300 K.

and this is the angle the track made with respect to the applied field. Thus in the preceding two figures we have seen two different tracking directions with the field in the same direction, but with crystals having different surface planes. Returning to the {100} surface plane, but this time with the field applied 22° away from a ⟨100⟩ direction, we find in figure 5 that the track appears at an angle of 22° from the applied field direction.

The ⟨100⟩ track direction has now been established for linear samples. However, the ultimate proof of the orientational preference is given by a disk type sample (fig. 1b) where the field is equal in all directions on the ⟨100⟩ surface plane of the sample. In figure 6 it can be seen that the tracks clearly mark off a ⟨100⟩ axis. An even more definitive case is presented by the disk diode of figure 7. Here the alloyed aluminum making the center (ohmic) electrode was allowed to extend down the edge of the central mesa and slightly onto the flat region, in a ⟨110⟩ direction. This distorted the field and the track initiated in a ⟨110⟩ direction, but it quickly changed to a ⟨100⟩.

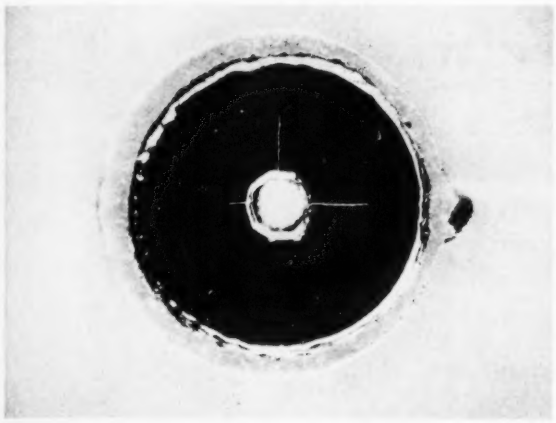

FIGURE 6. *A 10 Ωcm, p-type, {100} plane, disk sample with the p-n junction on the outer rim and the ohmic contact in the center.*

The tracks originate in the high field region at the base of the raised ohmic contact, and propagate in ⟨100⟩ directions only. The applied power to produce tracking was 1500 V, 6.5 A, 0.25 μs pulse length, at 77 K.

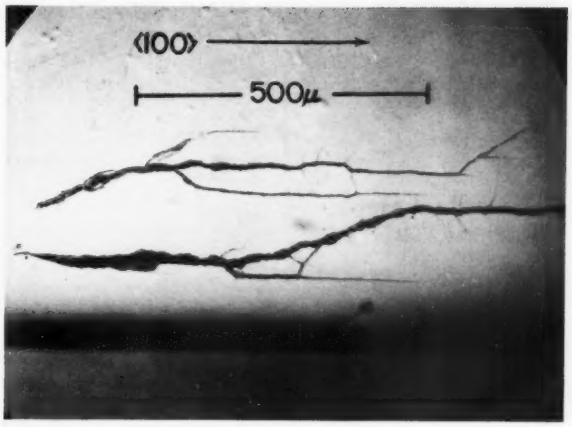

FIGURE 8. *Unoriented tracking on a 1 Ωcm p-type {100} ⟨100⟩ linear sample, having diffused boron, ohmic contacts.*

The tracks started in the high field region B, far away from the electrodes. The tracking threshold was 30 kV/cm, 12.5×10^3 A/cm², 0.4 μs pulse length, at 300 K.

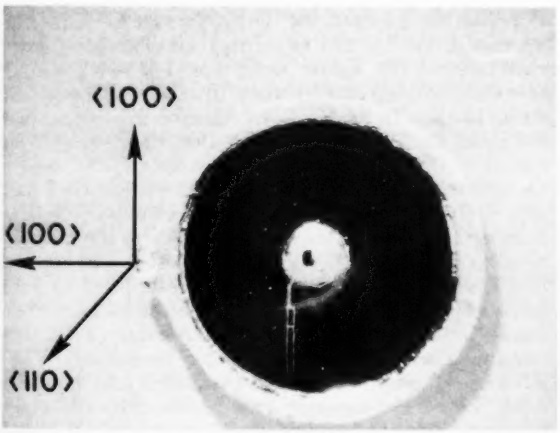

FIGURE 7. *A 10 Ωcm, p-type, {100} plane, disk sample with the junction on the rim and the ohmic contact in the center.*

The alloyed aluminum contacting the center electrode extended over the edge in a ⟨110⟩ direction. **The indicated orientations are all in the plane of the sample.**

Another interesting point is the development of the second major track with a cross coupling. Except for the initial breakdown, all tracks are nonradial but are nevertheless in ⟨100⟩ directions, including the cross linkage, which appears to have propagated against the field!

In contrast to the ⟨100⟩ orientation observed on *p*-type bulk when minority carriers are present, tracking occurs in strongly branched, random directions in their absence, as seen in figure 8. Such tracks are primarily influenced by the orientation of the applied field rather than the crystal structure. In addition the tracking threshold energy is much higher, very near thermal breakdown. Figure 8 is a picture of a ⟨100⟩ oriented 1 Ω cm *p*-type ohmic-contacted sample. Similar unoriented results are obtained from 1 Ω cm *n*-type ohmic specimens. No tracking (either oriented or as in fig. 8) is observed on 10 Ω cm *n*- or *p*-type ohmic contacted samples, presumably because the necessary high current density cannot be obtained (see fig. 2 curves C and D).

3.3. Morphology of the Tracks

There are two basic types of tracks. The first we shall call the *explosion* type and the second *continuous*. The first and most common type appears to propagate by a series of tiny explosions each one of which blows out a small crater ~ 10 μm deep and of similar diameter. Such a track is clearly shown in figure 9. The track initiated near the top of the picture in the shadow of the positively biased ohmic electrode. Numerous individual craters can be seen. These gradually merge, towards the bottom, into a more continuous path, but maintain approximately the same depth. This picture is an enlargement of the top track on the disk shown in figure 6. It should be noted that after extensive pulsing, such tracks generally widen and deepen. They lose the appearance of discrete explosion craters. The walls become more or less continuous and look highly eroded. Figures 3 and 5 are examples of such eroded tracks. Widths and depths of ~ 50 μm have occasionally been observed.

The second basic type of track appears to be continuous rather than a series of discrete explosions. These continuous tracks are clearly shown in figure 10. On a microscopic basis they look like finely ruled lines. Occasionally ones are seen that twist and turn around surface imperfections, but it is difficult to distinguish any discontinuities. However, they do extend slowly across the sample with each succeeding current pulse. They are generally 5 to 10 μm wide and of similar

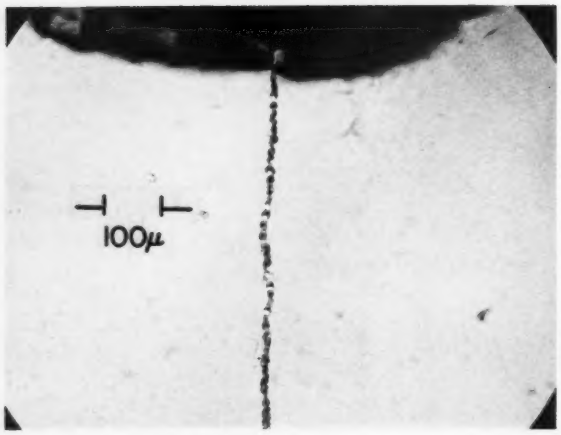

FIGURE 9. *An enlargement of a portion of a track shown in figure 6 revealing the explosion craters.*
Individual craters are ~10 μm in diameter.

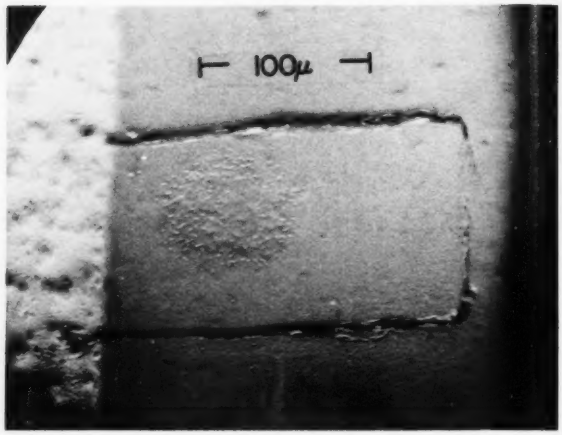

FIGURE 11. *Enlargement of the ohmic electrode area [region A of fig. 1(a)] of a 10 Ωcm p-type {100} ⟨100⟩ junction sample showing tracks that turn in on themselves.*
The white material on the left side of the picture is the alloyed aluminum electrode. (It was evaporated about 5° off perpendicular.)

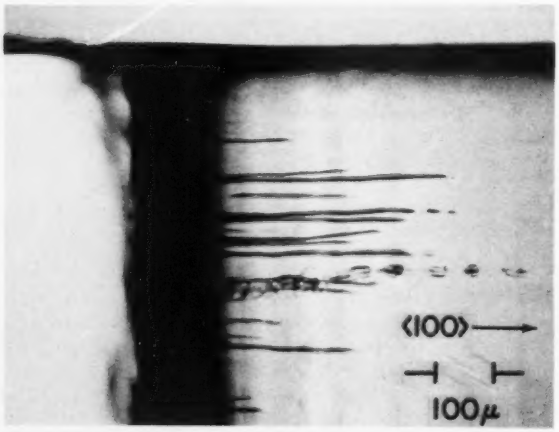

FIGURE 10. *"Continuous" tracks on a 10 Ωcm p-type {110} ⟨100⟩ oriented linear junction sample.*
Tracks started in the high field region, near the raised ohmic electrode (left side of figure). An "explosion" type track is in the middle of the group. The tracking threshold was 14 kV/cm, 7.5×10^3 A/cm², 0.4 μs pulse length, at 300 K.

depth. Continued pulsing extends the length, increases the number of individual tracks, but does not appreciably increase their depth. Both types of tracks can occur together, and one of the explosion type appears near the center of figure 10. Note how the two types of tracks snake around one another. They do not merge but go their own individual ways.

There are many unusual configurations that tracks may take. Outstanding among these are parallel tracks that turn in toward themselves and propagate perpendicular to both the field and the current! Figure 11 is an example of these. It is a greatly enlarged portion of a {100} ⟨100⟩ sample, showing only the raised ohmic electrode region (region A of fig. 1a). These tracks originate at the alloyed aluminum ohmic contact, and progress towards the edge of region B ignoring the large surface imperfection between them. At the edge, instead of moving downward toward the higher field region B (which would be in a ⟨100⟩ direction), they turn at right angles to the field (also in a ⟨100⟩ direction) and join together.

Tracks occasionally start in the thick, electroded, region A (fig. 1a) when alloyed aluminum is used as the ohmic contact. They are only rarely observed there with diffused boron ohmic contacts. The alloyed aluminum apparently creates defects that favor the initiation of tracks. This is so very prominent that whenever alloyed aluminum ohmic contacts are applied to a flat (planar) ⟨100⟩ sample, without raised or bulbous ends, tracks *will always* originate at the edge of the aluminum, and with very low energy thresholds. There have been cases in which the aluminum and the underlying Si-Al alloy material were removed by etching, to facilitate some additional processing step. However, later when the structure was subjected to hot carrier pulses, tracking originated from that same region, indicating that the defects had propagated far into the material. Also, electron microprobe measurements showed that electromigration of aluminum from planar contacts occurs in the tracks. In one case traces of aluminum extended 200 μm from the edge of the contact.

3.4. Tracking Threshold Energies and Conditions

Table 1 compares the averaged tracking thresholds of a number of linear samples having the dimensions of figure 1a. The orientations and contact characteristics are indicated. In order to present a meaningful comparison, the values given are all for 0.4 μs pulse length at 300 K and with samples immersed in a fluorocarbon heat exchange liquid. However, other samples have been observed to track with pulse lengths as short as 0.1 μs. Long pulse lengths (> 1 μs) can also produce tracking, but heating generally be-

TABLE 1. *Minimum applied impulse to produce tracking on linear samples at 300 K, immersed in a fluorocarbon electrically insulating, heat exchange liquid*

All pulse lengths were 0.4 μs. (Jn) indicates a junction sample, (ohmic) indicates noninjecting contacts, and (planar) indicates flat sample. Sample dimensions are those of figure 1a (except Planar).

No. of samples in average	Resistivity Ω cm	Bulk carrier type and contact	Surface plane and field orientation	Peak current density A/cm²	Field strength kV/cm	Impulse energy density[b] J/cm³
5	100	P(Jn)	{100} ⟨100⟩	2×10^3	[a]60	24, Nontrack[c]
10	10	P(Jn)	{100} and {110}, ⟨100⟩	6×10^3	15	18
5	10	P(Jn)	{100} ⟨110⟩	22×10^3	19	85
5	10	P(Jn) (planar)	{100} ⟨100⟩	3.5×10^3	6.5	3.5
5	10	P(Jn)	{110} ⟨111⟩	25×10^3	[a]32	160, Nontrack[c]
4	1	P(Jn)	{100} ⟨100⟩	50×10^3	16	160, Nontrack[c]
2 (3 more nontrack)	1	P(ohmic)	{100} ⟨100⟩	13×10^3	[a]32	165
3 (3 more nontrack)	1	N(ohmic)	{100} ⟨100⟩	7×10^3	[a]32	85

[a] Maximum field available for this particular test.
[b] Calculated on the basis of square current wave shape for ohmic samples and triangular shape (figure 2E) for junction (minority carrier injection) samples.
[c] These samples did not track at the indicated high voltage and current density. They exploded at a slightly higher impulse energy density. They are included in this table to compare the largest number of sample orientations and resistivities.

comes severe before the minimum-voltage tracking-threshold is reached. Samples have also been tracked at 77 K (energy thresholds slightly lower, see fig. 2), and in air at 300 K (thresholds approximately the same as in liquid but heating was evident).

Samples having different resistivities, orientations, carrier types, and nature of their contacts (ohmic or injecting), display different tracking thresholds. Certain orientations and resistivities will not track, but are thermally destroyed when the power is raised to sufficiently high levels. Maximum nondestructive data on some of these (indicated as nontrack) are included in table 1 for comparison purposes, to show the enormous power such samples can absorb without tracking.

From the data of table 1 it is apparent that the minimum *bulk* tracking threshold (not originating at planar contacts) is for samples with *applied* fields ~15 kV/cm oriented in a ⟨100⟩ direction, and having current densities ~6000A/cm². From the 100 and 1 Ω cm linear junction-sample data, it is apparent that tracking does not occur unless both the current density and the field (or their ⟨100⟩ components) approximately meet these conditions at the same time. Thus, appropriately longer 1 Ω cm junction samples (where the same field will produce less current density, due to minority carrier decay) or shorter 100 Ω cm ones can be made to track. This length effect has been tentatively verified on several samples. However, in order to avoid ambiguity, all data presented in this paper are for samples having the dimensions of fig. 1. *P*-type disk samples of 1, 10 and 100 Ω cm resistivity (with the ohmic contact in the center and junction on the perimeter) will all track, because the correct combination of E and J will always occur at some point as the field is increased. Likewise, ⟨100⟩ oriented planar junction samples (the same dimensions as figure 1a except that region B has the same thickness as A and C) will always track. The current density and field strength in the immediate vicinity of the electrode edge will meet the necessary conditions as the field is increased. In fact, the primary consideration for tracking in planar structures is the current density per unit length of forward edge of the contact. The appropriate local field is created by the current. A critical value of approximately 30 A/cm will produce tracking from alloyed-aluminum *planar* ohmic contacts on ⟨100⟩ oriented, 10 Ω cm *p*-type junction samples, with the dimensions of figure 1a.

Tracking has not been observed on 10 Ω cm *n-type* linear junction diodes. The large current densities (~5000A/cm²) that are necessary for tracking are difficult to obtain, except with disks. Graphs of linear diode I–V characteristics resemble the usual *n*-type hot carrier saturation, even though significant injection is present near the junction, as indicated from probe measurements. Presumably the lifetime of the injected holes is too short to permit them to traverse the entire length of the sample, thus limiting the current. Details of this will be investigated at a later date. As the pulse power is increased the samples thermally explode. However, examination of the resulting fragments of ⟨100⟩ oriented linear samples frequently reveal small tracks in the ⟨100⟩ direction (parallel to the field). These occur in the process of the explosion. *N*-type disks (fig. 1b) track diffusely, but with a general ⟨100⟩ orientation. In these cases the *n*-type tracking threshold energy was similar to that for comparable *p*-type disk specimens.

A number of 100 Ω cm *p*-type linear samples, with the dimensions of figure 1a were studied but none has been observed to track. As with the 10 Ω cm *n*-type samples, the maximum attainable current density is too low. Eventually, of course, as the power is increased the sample will thermally explode.

Table 1 presented data in terms of the average applied fields. This gives meaningful comparisons for samples with identical (fig. 1a) configurations but can

be misleading for variations such as planar electrodes, shorter samples, etc. Therefore, pulse probe measurements were made. For junction samples with figure 1a dimensions, and with a typical ⟨100⟩ oriented tracking field of 15 kV/cm applied, a peak field of 1.5 times the average applied field was observed. This peak was approximately 0.5 mm (in region B, fig. 1a) from the raised ohmic contact region A.

The situation was quite different for planar contacted samples. The field peaked to ~ 3 times the average applied field at the edge of the ohmic contact. Thus the *local* threshold field necessary to produce tracking on ⟨100⟩ oriented samples was similar for both electrode configurations.

Once a track has started, its surface becomes more conductive, and the local field in its vicinity is reduced about 20 percent, as measured with respect to the ohmic contact. The field reduction extends about 50 μm in all directions from the track. This was revealed by actually probing in and along growing tracks. Also, once started, a typical track that has reached an equilibrium length will increase that length by ~ 35 μm per kV increase in local field.

The thermal impulse heating of samples having the dimension of figure 1a was determined under hot carrier conditions with the specimens immersed in the fluorocarbon heat exchange liquid. The negative temperature characteristics of ohmic contacted samples were used by observing the current decrease from leading to trailing edge of the pulse. This was measured over a wide power range and at many different ambient temperatures. The graph of sample temperature versus applied power yielded a slope of 1, as anticipated if it is assumed that all heat loss from the sample to the liquid is by way of simple conduction. From this it was established that the pulse temperature rise of the planar samples (table 1) was only 4 K, and that of the 10 Ω cm {100} ⟨100⟩ *p*-type junction samples ~ 20 K. The temperature rise of 1 Ω cm *p*-type ohmic samples was so large (~ 200 K) that some thermally generated minority carriers were present and may have contributed to tracking, though not enough to straighten out the tracks (fig. 8). Tracking on ohmic samples occurs at energies only slightly below thermal breakdown.

3.5. Anisotropic Explosions

As shown above, the power required to produce tracking is anisotropic with crystallographic orientation. Since tracking represents a partial destruction of the sample, it is reasonable to assume that catastrophic destruction (exploding samples) is a related phenomenon and is also anisotropic. Figure 9 demonstrated that one mode of tracking is propagated by a series of tiny explosions. Such tracking was studied near its threshold power level. One can readily visualize a situation in which a single higher powered pulse is applied, and a large portion of the sample disintegrates as one macroscopic track. A few selected ⟨100⟩, and ⟨111⟩ junction and ohmic samples have been intentionally destroyed in one pulse. Microscopic observation of the many small pieces of the ⟨100⟩ junction samples indicated that part of the surface must have erupted in the manner of an exploding wire (macroscopic track). Ohmic contacted samples and ⟨111⟩ junction samples typically explode into several large pieces with no evidence of disintegration.

Partial explosions are apt to occur while slowly increasing the power level above the tracking threshold. A usual result of this is the blasting off of a chip from the edge of the sample. Typically this occurs in region B about 0.5 mm from the raised ohmic contact. This is the region of maximum local field as indicated by probing. A photograph of a partial explosion is given in figure 12. This {100} ⟨100⟩ oriented junction sample developed a deep track and then blasted off the chip. The edges of the hole clearly show {110} cleavage planes, attesting to the internal force of the tracking phenomenon. This track and hole are the only damage on an otherwise perfect sample, showing how localized such effects can be.

The first impression one might have is that samples simply disintegrate from thermal impulse. This undoubtedly has a contributory effect at high power levels. Therefore, it was necessary to separate the thermal impulse contribution from the macroscopic tracking effect. This was done by exploding ⟨111⟩ oriented samples. Such samples do not track, except occasionally in the actual process of exploding. Thus, the impulse required to explode these can be used as an upper or thermal breakdown limit. Table 2 compares the energy required to explode both tracking and nontracking samples. It includes the approximate temperature of the samples at the explosion energy. The relatively large energy difference required to explode ⟨111⟩ junction versus ohmic samples is not understood. However, the ⟨111⟩ junction sample results appear to be more relevant in defining a thermal breakdown limit for anisotropic tracking and explosions on other junction samples.

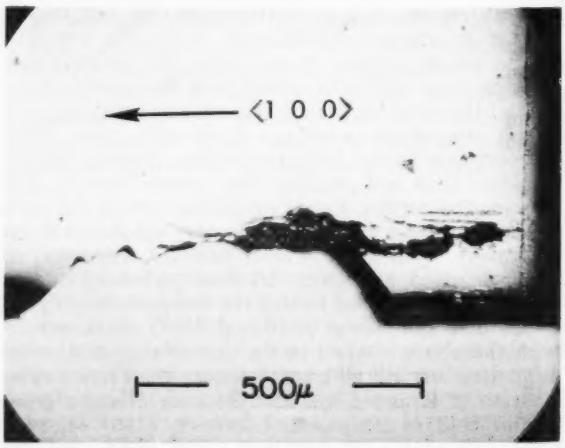

FIGURE 12. *A section of a 10 Ω cm p-type {100} ⟨100⟩ junction linear sample with a piece exploded out of its side.*

TABLE 2. *Applied power impulse required to explode silicon linear samples that are immersed in a fluorocarbon heat exchange liquid, at 300 K, 0.4 or 0.25 μs pulse length, 2 pulses per second*

Sample dimensions are those of figure 1a.

No. of samples in average	Resistivity Ω cm	Surface plane and field orientation	Bulk carrier type and contact	Approximate temp. rise [a] preceeding explosion TK	Impulse energy Density [b] J/cm³
4	10	{100} ⟨100⟩	P(Jn)	50	40
4	10	{100} ⟨110⟩	P(Jn)	140	120
6	10	{110} ⟨111⟩	P(Jn)	290	240
4	1	{110} ⟨111⟩	N(ohmic)	210	175

[a] These temperatures are considered approximate. The highest temperature rise (290 K) is a linear extrapolation from lower temperature data, assuming all heat loss is by conduction. Heat loss by radiation, which may be significant, will lower this temperature somewhat.
[b] See footnote b, Table 1.

The anisotropic explosion results are clearly in agreement with those of table 1 for tracking. It is evident from table 2 that ⟨110⟩ and ⟨111⟩ linear samples require significantly more energy to explode than do the ⟨100⟩ linear samples, and the differences are *far too great* to be attributed to heating effects.

4. Discussion

From the experimental evidence of table 1 it is clear that both high fields and high current densities are required to initiate tracking. It is assumed that each individual track starts on a defect, as a result of its crystallographic weakness or its perturbation of the local electric field. Once started, the local field is modified somewhat by the first crater (as indicated by probe measurements). Subsequent craters can then form without requiring a defect in the material.

However, there is no apparent reason why the track should propagate in the ⟨100⟩ direction when the field is applied in a different direction. The ⟨100⟩ direction is not known to have excessive defects propagating along it. Nor is it the weakest mechanical direction. Cleavage in silicon occurs along {110} planes and Poissons ratio has a sharp minimum there [7]. Oswald [8] has studied the fracture patterns for silicon when samples were subjected to massive electrical energy impulses. He exposed his specimens to 40 ns, 2.2 MeV electron beam pulses and found that fracture occurs along ⟨111⟩ directions. The energy was considered to be thermal in nature, and the samples were shown to crack by brittle fracture. There is no evidence that the tracks are related to the present crystal growth direction (⟨111⟩ or [2$\bar{1}\bar{1}$]), as Morozov [2] suggested for germanium. With mechanical and thermal properties ruled out as the source of anisotropic tracking, we will examine the various electronic properties of the material in an effort to understand the phenomena.

Anisotropy in the high voltage breakdown of insulator crystals has been known for years [9, 10, 11]. Depending on the particular crystal, the field strength, and the orientation, preferential paths have been observed along ⟨100⟩, ⟨110⟩, and ⟨111⟩ crystallographic directions. Generally each of the three paths can be obtained on a single material at different temperatures [12] or with overvoltage. Breakdown voltages for these effects on typical insulators, such as alkali halides, are $\sim 10^6$ V/cm. In general, oriented breakdowns of insulators are only observed when a crystal is placed between a point and a plane contact and immersed in a liquid insulating medium. Such an electrode arrangement does not remotely resemble the situation in the present work. Also, the high current density necessary for silicon tracking is clearly not a requirement for insulator tracking. In addition, no change in tracking orientation has presently been observed at different temperatures or with overvoltage.

During the present experiments the samples were immersed in liquid nitrogen (breakdown $\sim 10^6$ V/cm) or a fluorocarbon insulating liquid (breakdown $\sim 2 \times 10^5$ V/cm). Since the dielectric strength of silicon is very high, $\sim 5 \times 10^5$ V/cm (from reverse bias junction data), ordinary high voltage arcing within the silicon sample or in the surrounding media is not possible with the present applied or local fields. In addition, several samples were further insulated with 8000 A of grown silicon oxide over the entire surface. This film raised the threshold somewhat but the samples still tracked. Therefore, considering all of these facts, it appears that there is no connection between semiconductor tracking and the well-known tracking in insulators.

Warm and hot majority carrier conduction anisotropy in n-type silicon and germanium has been known for many years [13–18]. The presently accepted theory of conduction anisotropy in n-type silicon attributes the anisotropy primarily to the scattering of electrons from hot valleys (major axis of the energy ellipsoid perpendicular to the field) into cold valleys (major axis parallel to the field). This takes place with the spontaneous emission or absorption of high energy intervalley phonons. The effect is typically observed in silicon as a relative decrease in conductivity when the field is oriented in a ⟨100⟩ direction compared to the conductivity along ⟨111⟩ or ⟨110⟩ directions. This conductivity *difference* is maximum for applied fields in the order of several hundred volts per centimeter and decreases as the field is further increased. The difference also decreases as the carrier concentration increases, and all but vanishes when carrier densities and fields approach those required for the present tracking.

We have established that both high fields and high current (carrier) densities are necessary to produce the observed tracking phenomenon. Since ⟨111⟩ junction samples do not track (all valleys are equivalent), it appears that an intervalley exchange of minority carrier electrons is necessary for oriented tracking. However, majority carrier holes are also necessary for *low tracking thresholds* as seen from the 1 Ωcm *n*-type ohmic data of table 1. A further complication exists because the electrons are hot and the holes are merely warm. In addition, the field strength is not uniform along the sample, as determined by probe measurements. The carrier density is very high so that intercarrier scattering as well as lattice and intervalley scattering should be considered. Thus, the theoretical situation for hot carrier induced anisotropic tracking is much more difficult than majority carrier conduction anisotropy.

If the accepted conduction anisotropy theory for *n*-type silicon were applicable to the present work it would imply that the current, and thus the total energy, was *lowest* in the ⟨100⟩ direction of tracking. This does not present any obvious mechanism for tracking. One might then assume that there was a very high current (perhaps filamentary) flowing along the ⟨100⟩ track direction. Examination of figures 3, 7, and especially the converging tracks of figure 11 show that tracks can propagate in ⟨100⟩ directions in which high current cannot uniquely flow. The actual driving force for tracking must derive its energy from the high field and high current density. But, the force must also be independent of their direction in order to explain figures 3, 7, and 11. It should also manifest itself at the surface.

One theory that might conceivably be applicable to anisotropic tracking was given by Rashba [19]. He states that since the ellipsoids of a many valley semiconductor are inclined at different angles to the surface, an electric field parallel to the surface plane will scatter more electrons toward that surface than are scattered back. At low temperatures this can significantly increase the carrier concentration within ~10 μm of the surface and in an anisotropic manner. The theory is not completely developed. It is only solved in the case of a weak, constant electric field, for a four valley semiconductor, and would be exceedingly difficult to adapt to a two carrier, hot carrier situation. Its primary merit is that it proposes an increased concentration of carriers in the surface region of the sample, where tracking is observed.

Kornreich, Callen, and Gundjian [20] have recently reported the theory of "current striction." Not enough information has yet been published to evaluate it under the present two carrier, hot carrier situation. However, it is a new mechanism of electrostriction in a many valley semiconductor which should yield oriented characteristics. The effect on silicon is about 100 times larger than could be expected from conventional electrostriction mechanisms and is larger still for germanium. "The current striction effect lowers the energy of those valleys with major axes (which are along ⟨100⟩) parallel to the field, and thereby concentrates electrons into such valleys. This effect appears to be at least qualitatively similar to the tracking effect" [21]. In addition it would result in ⟨111⟩ oriented forces in germanium, as observed by Morozov. The current striction authors also indicated that they were extending their work to *p*-type material and such work, combined with their original paper, could yield a quantitative insight into why *p*-type bulk, with minority carriers present, produces by far the lowest thresholds for anisotropic tracking.

The obvious merit of the "striction" mechanism is that in silicon it produces oriented forces along ⟨100⟩ directions that need not be parallel to the applied field. The forces should be minimum with the field in a ⟨111⟩ direction, and would not produce tracking. Since the surface is normally considered the weakest portion of a sample, any large internal force will manifest itself there, and cause breakdown at the weakest point, which is a defect. Propagation would follow the direction of the force, the ⟨100⟩. Anisotropic explosions (macroscopic tracks) would be an expected consequence of such a "striction" mechanism.

Note added in the proof: Since this paper was submitted, a new mechanism, "Electronic Volume Effect in Semiconductors", has been described [W. B. Gauster, Bull. Am. Phys. Soc. **14**, 312 (1969)]. This mechanism is a *two carrier* effect, related to photo striction, and may be applicable to the present tracking phenomena.

5. Conclusions

The present paper has described the topological features of ⟨100⟩ oriented anisotropic tracking on silicon. The available evidence from tables 1 and 2 indicates that low threshold energy anisotropic tracking, and sample explosions are a two-carrier, hot-carrier phenomena. There is no obvious mechanical or electronic reason why tracks should propagate preferentially along ⟨100⟩ directions. The present hot carrier anisotropy theory fails to suggest an answer to this tracking. It appears that the explanation of both anisotropic tracking and explosions awaits further development of a two carrier "current striction" mechanism.

Some breakdowns in Gunn and avalanche devices [22, 23] strongly resemble tracks; similar situations have been observed in our laboratory. The structure of high-current-density planar devices makes them obvious targets for failures due to tracking, and narrow electrode spacings or other probable breakdown paths should be designed along ⟨111⟩ or ⟨110⟩ directions to avoid failure. Some additional protection can be obtained by covering surfaces with silicon dioxide. Also alloyed contacts should be avoided when possible. Another device failure mechanism, second breakdown, [24] should be reinvestigated for a possible orientation dependance. Examination of failures in certain high current, high voltage, *p-n-p-n* devices [25] and similar n^+-*p diodes* [26] has yielded oriented breakdown patterns in the vicinity of the junction,

or on its surface, that look similar to those of germanium [2]. Under any conditions the possibility of an orientation dependance of device *breakdown* should be considered, even though normal performance of the device may have been shown to be independent of crystallographic orientation.

The author is indebted to M. Bullis, E. Farabaugh, and J. Scales for valuable discussions. K. Leedy made the hot-carrier sample-temperature measurements. Phosphorous and boron diffusions were done in the facilities of Harry Diamond Laboratories of the Army Materiel Command.

6. References

[1] Gunn, J. B., J. Electronics **2,** 87 (1956).
[2] Morozov, A. I., Fizika Tverdogo Tela **2,** 620 (1960).
[3] Harman, G. G., Bull. Am. Phys. Soc. **13,** 406 (1968).
[4] Harman, G. G., Appl. Phys. Lett. **9,** 207 (1966).
[5] The general crystallographic orientation shorthand to be used is as follows: {111} indicates the surface plane of the slice or sample, ⟨110⟩ indicates the direction of the longest dimension of a rectangular sample and thus is the orientation of the applied field. A combination of these, {100} ⟨100⟩, completely describes the crystallography of rectangular samples. Only the surface plane is indicated for disk samples except where a tracking direction is discussed.
[6] Mayer, J. W., Baron, R., and Marsh, O. J., Phys. Rev. **137,** A286 (1965).
[7] Wortman, J. J., and Evans, R. A., J. Appl. Phys. **36,** 153 (1965).
[8] Oswald, R. B., Bull. Am. Phys. Soc. **11,** 363 (1966); IEE Trans. Nuclear Sci. **NS-13,** 63 (1966).
[9] Inge, L., and Walther, A., Z. Phys. **64,** 830 (1930).
[10] von Hippel, A., Z. Phys. **67,** 707 (1931); **68,** 309 (1931); **75,** 145 (1932).
[11] Offenbacker, E. L., and Callen, H. B., Phys. Rev. **90,** 401 (1953).
[12] Davisson, J. W., Phys. Rev. **70,** 685 (1946).
[13] Shibuya, M., Phys. Rev. **99,** 1189 (1955).
[14] Sasaki, W., Shibuya, M., Mizuguchi, K., and Hatoyama, G. M., J. Phys. Chem. Solids **8,** 250 (1959).
[15] Jørgensen, M. H., Meyer, N. I., and Schmidt-Tiedemann, K. J., Proc. 7th Intl. Conf. on Semiconductors, Paris 1964, page 457.
[16] Kastner, P., Roth, E.-P., and Seeger, K., Zeit. fur Physik **187,** 359 (1965).
[17] Gibbs, W. E. K., J. Phys. Chem. Solids **25,** 247 (1964).
[18] For a recent review see, B. R. Nag, Solid State Elect. **10,** 385 (1967).
[19] Rashba, E. I., J. Exptl. Theoret. Phys. (USSR) **48,** 1427 (1965).
[20] Kornreich, P., Callen, H. B., and Gundjian, A., Phys. Rev. **161,** 815 (1967).
[21] Callen, H. B., private communication.
[22] Jeppsson, B., and Marklund, I., Elect. Lett. **3,** 213 (1967).
[23] Schenck, J. F., and Midford, T. A., IEEE Trans. Elect. Devices **ED-14,** 619 (1967).
[24] Schafft, H. A., Proc. IEEE **55,** 1272 (1967).
[25] Localized Defects and Hot Spots in High Voltage *pnpn* Inverter Switches. General Electric Co. contract NO bsr-87648, Mod. Nr. 9, AD 489, 530; 810, 820; 804, 491 (released by the Clearinghouse for Federal Scientific and Technical Information, Springfield, Va. 22151).
[26] Thomson, I., and Wilkinson, E. L. G., Proc. Symposium on Test Methods and Measurements of Semiconductor Devices Page 101, Budapest, April 25, 1967.

(Paper 73A3–556)

JOURNAL OF RESEARCH of the National Bureau of Standards—A. Physics and Chemistry
Vol. 73A, No. 3, May–June 1969

The Third Spectrum of Praseodymium (Pr III) in the Vacuum Ultraviolet

Jack Sugar

Institute for Basic Standards, National Bureau of Standards, Washington, D.C. 20234

(February 13, 1969)

Measurements of the spectrum of doubly ionized praseodymium from 821 to 2103 Å are given. One hundred fifty-three energy levels deduced from these wavelengths and an earlier line-list of longer wavelengths are presented. These levels are identified with the configurations $4f^26s$, $4f^27s$, $4f^28s$, $4f^26p$, $4f^26d$, $4f^25f$, $5d^24f$, and $4f5d6s$ and are given term designations. Radial energy integrals belonging to these configurations are parametrically deduced from the known levels.

A value of 21.625 eV (174420 cm^{-1}) for the ionization energy of Pr III, with an estimated uncertainty of 0.016 eV (130 cm^{-1}), is derived from the $4f^2ns$ series ($n=6, 7, 8$).

Key words: Energy levels; interaction parameters; praseodymium; third spectrum; vacuum ultraviolet; wavelengths.

1. Introduction

The analysis of Pr III in the wavelength range from 2025 to 10716 Å [1,2][1] revealed nearly completely the energy level structure of the four low-lying configurations $4f^3$, $4f^25d$, $4f^26s$, and $4f^26p$, and some levels of $5d^24f$ and $4f^26d$. I have extended the observations to shorter wavelengths and measured 2948 lines in the range from 821 to 2103 Å. These new data have led to a considerable increase in the number of known levels of the $5d^24f$ configuration and to the discovery of levels belonging to the $4f5d6s$, $4f^25f$, and $4f^28s$ configurations. In addition, a reexamination of the old line-list yielded more levels of the configurations $4f^26s$, $4f^26d$, and $4f^27s$. In all, 153 energy levels of Pr III have been newly established.

The configurations to which they belong were treated theoretically for the purpose of determining parametrically the radial energy integrals and of calculating the level positions and eigenvectors. These calculations helped to confirm the experimental results and to locate unknown levels, as well as to provide an interpretation of the configurations in the most appropriate coupling schemes.

Of particular interest are the mutually interacting odd configurations $4f^26p$, $5d^24f$, and $4f5d6s$, which were treated as one complex. Many levels are strongly perturbed and were found to contain large percentages of terms of several configurations. In the $5d^24f$ configuration the addition of an "effective" two-body configuration interaction parameter for nonequivalent electrons decreased the rms error of the calculation by 25 percent.

The ionization energy of Pr III was calculated in ref. 2 by means of tentatively identified $4f^26d$ levels to form a $4f^2(^3H)nd$ ($n=5, 6$) series. The new analysis provides the $4f^2(^3H)ns$ series ($n=6, 7, 8$) with which to determine a more reliable value.

Three levels given in reference 2 which were found to be poorly substantiated and have now been discarded are listed below:

Rejected levels	J	Config.	New levels
45848.37 cm^{-1}	$2\frac{1}{2}$	$4f^26s$	45807.16 cm^{-1}
68676.55 cm^{-1}	$2\frac{1}{2}$	$4f^26p$	
79378.43 cm^{-1}	$2\frac{1}{2}$	$4f^26p$	79366.69 cm^{-1}

2. Observations

For the most part, the procedure outlined in reference 2 for obtaining the spectrum Pr III has been followed. The sliding spark was operated at peak currents of 50 and 500 A to enhance the third and fourth spectra selectively. I departed from the earlier method of producing the second spectrum by means of an arc. Instead a 6 A sliding spark was used which gave a more clear-cut distinction between second and third spectra when compared with the 50 A spark, as well as sharper lines. This technique has already been used in the classification of Ce III [3].

The new extension of the observations of Pr III to shorter wavelengths was made with a 10.3 m Eagle vacuum spectrograph, utilizing a grating of 1200

[1] Figures in brackets indicate the literature references at the end of this paper.

grooves/mm blazed at 1200 Å. The first order of diffraction was photographed, giving a reciprocal dispersion of 0.78 Å/mm. One half to 2 hr exposures were required to record the spectrum of the spark, operating at a repetition rate of 15 sparks per second. Calibration spectra of C, N. O, Ar, Si, Ge, and Cu [4, 5, 6, 7, 8] were obtained from pulsed rf-excited electrodeless lamps and hollow cathode discharges.

Two to five measurements of the lines in the 50 A spark were made, the number depending on the recurrence of a line on progressively weaker exposures. From the variation of wavelengths obtained with different exposures the accuracy of the final values is estimated to be ± 0.004 Å. Systematic shifts between the various sets of measurements were removed by standardizing on wavelengths of internal impurities of C, N, O, and Si.

The new measurements overlap the previous list [1] in the region from 2000 to 2103 Å and considerably augment it, thus indicating that stronger exposures may be needed beyond this overlap. Lines of intensity designated as 1 in the old list are usually assigned 200 in the new list, and the other common lines are correspondingly stronger.

A complete tabulation of the newly observed lines appears in table X. The wavelengths given in the first column are the values in vacuum. Following this are the visually estimated intensities with the following descriptive notations:

cl = measurement affected by a close neighboring line,
bl = a blend of two or more lines,
h = hazy,
w = wide.

Under "classification" appear the two energy levels from which the line originates, followed by a subscript *J*-value, and where appropriate a superscript degree mark representing odd parity. Double classifications of lines are given without repeating the wavelength.

In table I, newly classified lines from the longer wavelength list of reference 1 are given. Among these are lines having hfs, for which the following additional notations in the intensity column appear:

**r* = strongest component of flag pattern shaded to red,
**v* = strongest component of flag pattern shaded to violet,

TABLE I. *Newly classified lines of* Pr III, $\lambda > 2103Å$

λ_{air} Å	Intensity	σ (cm^{-1})	Classification	λ_{air} Å	Intensity	σ (cm^{-1})	Classification
4650.609	9* *v*	21496.54	$13887^{\circ}_{7/2} - 35384_{5/2}$	3011.282	20* *v*	33198.77	$50227_{5/2} - 83426^{\circ}_{5/2}$
4334.697	9*w*	23063.18	$11761^{\circ}_{9/2} - 34825_{7/2}$	3006.469	60* *r*	33251.92	$38726_{7/2} - 71978^{\circ}_{7/2}$
3607.068	4* *r*	27715.46	$52026_{3/2} - 79742^{\circ}_{1/2}$	3004.002	10* *r*	33279.22	$52026_{3/2} - 85306^{\circ}_{5/2}$
3577.336	8* *v*	27945.80	$33659_{5/2} - 61605^{\circ}_{7/2}$	3002.106	2	33300.24	$38694_{5/2} - 71994^{\circ}_{5/2}$
3567.897	1*bl*	28019.71	$50869_{1/2} - 78889^{\circ}_{3/2}$	2982.236	9* *r*	33522.11	$45844_{3/2} - 79366^{\circ}_{5/2}$
3565.845	9* *v*	28035.78	$50658_{13/2} - 78694^{\circ}_{11/2}$	2980.583	5* *r*	33540.70	$50869_{1/2} - 84409^{\circ}_{3/2}$
3564.405	30* *r*	28047.13	$50647_{11/2} - 78694^{\circ}_{11/2}$	2978.907	9* *v*	33559.57	$45807_{5/2} - 79366^{\circ}_{5/2}$
3510.532	20* *v*	28477.56	$50658_{13/2} - 79136^{\circ}_{13/2}$	2976.347	40* *v*	33588.43	$45807_{5/2} - 79395^{\circ}_{7/2}$
3509.142	3* *r*	28488.86	$50647_{11/2} - 79136^{\circ}_{13/2}$	2963.032	2	33739.36	$36642_{13/2} - 70381^{\circ}_{13/2}$
3462.700	1* *r*	28870.93	$52026_{3/2} - 80897^{\circ}_{3/2}$				
3462.432	1* *r*	28873.16	$50869_{1/2} - 79742^{\circ}_{1/2}$	2940.896	7* *v*	33993.30	$51312_{5/2} - 85306^{\circ}_{5/2}$
3412.607	7* *r*	29294.71	$50869_{1/2} - 80164^{\circ}_{3/2}$	2933.827	1	34075.21	$37919_{7/2} - 71994^{\circ}_{5/2}$
3402.969	50* *r*	29377.68	$52026_{3/2} - 81404^{\circ}_{5/2}$	2930.192	50* *v*	34117.48	$35291_{9/2} - 69408^{\circ}_{11/2}$
3379.131	50* *v*	29584.91	$51312_{5/2} - 80897^{\circ}_{3/2}$	2924.661	2* *v*	34181.99	$50227_{3/2} - 84409^{\circ}_{3/2}$
3377.141	100* *v*	29602.34	$45807_{5/2} - 75409^{\circ}_{3/2}$	2910.612	70* *v*	34346.98	$28885_{9/2} - 63232^{\circ}_{7/2}$
3367.350	200* *v*	29688.42	$35291_{9/2} - 64979^{\circ}_{7/2}$	2890.842	2	34581.86	$39024_{9/2} - 73606^{\circ}_{9/2}$
3359.973	3* *v*	29753.59	$45807_{5/2} - 75560^{\circ}_{5/2}$	2885.001	6* *r*	34651.87	$38726_{7/2} - 73378^{\circ}_{7/2}$
3358.083	30* *r*	29770.34	$45844_{3/2} - 75614^{\circ}_{5/2}$	2876.229	1	34757.55	$69138^{\circ}_{9/2} - 103895_{7/2}$
3353.866	50* *v*	29807.77	$45807_{5/2} - 75614^{\circ}_{5/2}$	2857.700	4	34982.90	$37011_{5/2} - 71994^{\circ}_{5/2}$
3322.203	6* *v*	30091.85	$51312_{5/2} - 81404^{\circ}_{5/2}$	2851.486	6* *r*	35059.13	$33466_{11/2} - 68525^{\circ}_{11/2}$
3161.330	7* *r*	31623.10	$50869_{1/2} - 82492^{\circ}_{3/2}$	2838.461	7* *r*	35220.00	$35801_{7/2} - 71021^{\circ}_{9/2}$
3147.878	9* *v*	31758.23	$35291_{9/2} - 67049^{\circ}_{9/2}$	2827.668	3	35354.43	$36640_{7/2} - 71994^{\circ}_{5/2}$
3122.646	7* *v*	32014.84	$45807_{5/2} - 77821^{\circ}_{5/2}$	2819.342	2	35458.83	$37919_{7/2} - 73378^{\circ}_{7/2}$
3108.884	7* *r*	32156.56	$50869_{1/2} - 83025^{\circ}_{3/2}$	2812.509	9* *v*	35544.98	$32760_{13/2} - 68305^{\circ}_{15/2}$
3098.474	3* *v*	32264.59	$50227_{3/2} - 82492^{\circ}_{3/2}$	2803.090	3	35664.41	$48745_{5/2} - 84409^{\circ}_{3/2}$
3087.175	1* *r*	32382.56	$52026_{3/2} - 84409^{\circ}_{3/2}$	2797.924	1*bl*	35730.25	$65935^{\circ}_{7/2} - 101665_{5/2}$
3061.277	9* *v*	32656.61	$45807_{5/2} - 78463^{\circ}_{7/2}$	2784.154	1	35906.96	$39732_{11/2} - 75640^{\circ}_{11/2}$
3039.680	7	32888.63	$45805_{9/2} - 78694^{\circ}_{11/2}$	2776.318	4	36008.30	$48401_{3/2} - 84409^{\circ}_{3/2}$
3036.913	8	32918.59	$44903_{5/2} - 77822^{\circ}_{5/2}$	2774.708	4	36029.19	$39732_{11/2} - 75762^{\circ}_{9/2}$
3018.701	20* *v*	33117.19	$51312_{5/2} - 84430^{\circ}_{7/2}$	2766.880	3	36131.12	$35863_{3/2} - 71994^{\circ}_{5/2}$

TABLE I. *Newly classified lines of* Pr III, $\lambda > 2103\text{Å}$ – Continued

λ_{air} Å	Intensity	σ (cm^{-1})	Classification	λ_{air} Å	Intensity	σ (cm^{-1})	Classification
2741.262	1	36468.76	$^{6}6148_{13/2}$–$10261\,7_{11/2}$	2564.509	4	38982.14	$^{6}5922_{11/2}$–$10490\,4_{11/2}$
2734.368	8	36560.70	$4874\,5_{5/2}$ – $^{8}5306_{5/2}$	2563.474	6	38997.87	$3664\,2_{13/2}$– $^{7}5640_{11/2}$
2732.952	1	36579.64	$^{6}8987_{7/2}$ –$10556\,6_{9/2}$	2561.773	6	39023.77	$^{6}3593_{9/2}$ –$10261\,7_{11/2}$
2720.409	1	36748.29	$^{6}6735_{13/2}$–$10348\,4_{15/2}$	2559.865	1	39052.85	$^{6}8801_{7/2}$ –$10785\,4_{9/2}$
2712.384	2	36857.01	$3513\,7_{3/2}$ – $7199\,4_{5/2}$	2559.277	2	39061.82	$^{6}3768_{7/2}$ –$10283\,0_{9/2}$
2707.422	2	36924.56	$^{6}8525_{11/2}$–$10545\,0_{11/2}$	2558.675	5	39071.01	$^{6}1717_{5/2}$ –$10078\,8_{7/2}$
2706.611	5	36935.62	$3667\,0_{11/2}$– $^{7}3606_{9/2}$	2558.537	4	39073.12	$^{6}1357_{9/2}$ –$10043\,0_{9/2}$
2704.403	1	36965.78	$3664\,0_{7/2}$ – $^{7}3606_{9/2}$	2557.323	3	39091.67	$3667\,0_{11/2}$– $^{7}5762_{9/2}$
2699.300	5* r	37035.65	$3872\,6_{7/2}$ – $^{7}5762_{9/2}$	2556.813	4	39099.46	$^{6}4235_{9/2}$ –$10333\,5_{9/2}$
2687.981	6* v	37191.60	$3844\,8_{9/2}$ – $^{7}5640_{11/2}$	2555.353	7	39121.80	$^{6}2553_{11/2}$–$10168\,0_{13/2}$
2687.506	1	37198.17	$^{6}3232_{7/2}$ –$10043\,0_{9/2}$	2554.979	1	39127.53	$3869\,4_{5/2}$ – $^{7}7822_{5/2}$
2686.455	3	37212.73	$^{6}3576_{5/2}$ –$10078\,8_{7/2}$	2549.531	1	39211.13	$^{6}7870_{9/2}$ –$10708\,1_{9/2}$
2673.055	5	37399.26	$^{6}5909_{5/2}$ –$10330\,8_{7/2}$	2545.790	9	39268.75	$^{6}4215_{13/2}$–$10348\,4_{15/2}$
2666.218	2	37495.16	$^{6}3576_{5/2}$ –$10107\,1_{5/2}$	2543.644	1	39301.88	$^{6}6148_{13/2}$–$10545\,0_{11/2}$
2663.415	3	37534.62	$^{6}5295_{7/2}$ –$10283\,0_{9/2}$	2541.080	8	39341.53	$^{6}1605_{7/2}$ –$10094\,7_{9/2}$
2650.675	1	37715.01	$^{6}3232_{7/2}$ –$10094\,7_{9/2}$	2540.311	7	39353.44	$^{6}1717_{5/2}$ –$10107\,1_{5/2}$
2647.019	1	37767.10	$^{6}8978_{5/2}$ –$10674\,5_{5/2}$	2539.759	5	39361.99	$^{6}8492_{7/2}$ –$10785\,4_{9/2}$
2640.290	4	37863.35	$^{6}8801_{7/2}$ –$10666\,5_{7/2}$	2537.099	2	39403.26	$3973\,2_{11/2}$– $^{7}9136_{13/2}$
2634.707	5	37943.58	$^{6}9138_{9/2}$ –$10708\,1_{9/2}$	2536.648	7	39410.26	$3972\,5_{15/2}$– $^{7}9136_{13/2}$
2629.918	1	38012.66	$^{6}5295_{7/2}$ –$10330\,8_{7/2}$	2534.759	9	39439.63	$^{6}2240_{11/2}$–$10168\,0_{13/2}$
2626.210	2	38066.33	$^{6}2558_{11/2}$–$10062\,5_{11/2}$	2531.925	7	39483.77	$^{6}6148_{13/2}$–$10563\,2_{13/2}$
2626.016	1	38069.14	$^{6}8676_{5/2}$ –$10674\,5_{5/2}$	2530.464	9	39506.57	$4490\,3_{5/2}$ – $^{8}4409_{3/2}$
2624.624	1	38089.33	$^{6}3576_{5/2}$ –$10166\,5_{5/2}$	2529.726	4	39518.09	$^{6}3816_{11/2}$–$10333\,5_{9/2}$
2622.448	5	38120.94	$^{6}8544_{9/2}$ –$10666\,5_{7/2}$	2529.430	2	39522.72	$^{6}8331_{7/2}$ –$10785\,4_{9/2}$
2619.706	3	38160.83	$^{6}9138_{9/2}$ –$10729\,9_{7/2}$	2529.110	9	39527.72	$^{6}5922_{11/2}$–$10545\,0_{11/2}$
2619.162	1	38168.76	$^{6}6735_{13/2}$–$10490\,4_{11/2}$	2528.330	2	39539.91	$^{6}3768_{7/2}$ –$10330\,8_{7/2}$
2618.891	2	38172.71	$^{6}8492_{7/2}$ –$10666\,5_{7/2}$	2526.636	1	39566.42	$^{6}3768_{7/2}$ –$10333\,5_{9/2}$
2617.740	3	38189.49	$^{6}2240_{11/2}$–$10043\,0_{9/2}$	2525.123	8	39590.12	$^{6}1357_{9/2}$ –$10094\,7_{9/2}$
2616.047	1	38214.21	$^{6}3232_{7/2}$ –$10144\,6_{7/2}$	2521.677	1	39644.22	$^{6}5922_{11/2}$–$10556\,6_{9/2}$
2613.377	3	38253.24	$^{6}2535_{9/2}$ –$10078\,8_{7/2}$ $^{6}8492_{7/2}$ –$10674\,5_{5/2}$	2521.021	7	39654.54	$^{6}4150_{11/2}$–$10380\,5_{13/2}$
				2520.662	2	39660.18	$^{6}4235_{9/2}$ –$10389\,5_{7/2}$
2611.527	1	38280.34	$^{6}8801_{7/2}$ –$10708\,1_{9/2}$	2517.515	8	39709.76	$^{6}5922_{11/2}$–$10563\,2_{13/2}$
2610.351	8	38297.59	$^{6}6301_{15/2}$–$10459\,8_{13/2}$	2516.337	1	39728.35	$^{6}1717_{5/2}$ –$10144\,6_{7/2}$
2606.515	5	38353.95	$3502\,4_{7/2}$ – $^{7}3378_{7/2}$	2515.487	7	39741.77	$^{6}3593_{9/2}$ –$10333\,5_{9/2}$
2604.457	3	38384.25	$^{6}2240_{11/2}$–$10062\,5_{11/2}$	2509.243	7	39840.66	$^{6}1605_{7/2}$ –$10144\,6_{7/2}$
2603.320	2	38401.01	$^{6}7049_{9/2}$ –$10545\,0_{11/2}$	2505.358	1	39902.44	$3791\,9_{7/2}$ – $^{7}7822_{5/2}$
2603.263	1	38401.86	$^{6}4215_{13/2}$–$10261\,7_{11/2}$	2503.391	5	39933.78	$3582\,8_{9/2}$ – $^{7}5762_{9/2}$
2602.446	2	38413.91	$^{6}8331_{7/2}$ –$10674\,5_{5/2}$	2502.526	5	39947.59	$^{6}1717_{5/2}$ –$10166\,5_{5/2}$
2602.224	1	38417.19	$3719\,7_{3/2}$ – $^{7}5614_{5/2}$	2499.968	10	39988.46	$^{6}3816_{11/2}$–$10380\,5_{13/2}$
2599.960	1	38450.64	$^{6}6148_{13/2}$–$10459\,8_{13/2}$	2499.686	6	39992.97	$3870\,1_{13/2}$– $^{7}8694_{11/2}$
2595.448	1	38517.48	$^{6}7049_{9/2}$ –$10556\,6_{9/2}$	2498.297	1	40015.20	$^{6}8544_{9/2}$ –$10855\,9_{11/2}$
2592.832	5	38556.34	$^{6}8525_{11/2}$–$10708\,1_{9/2}$	2497.143	2	40033.69	$^{6}8525_{11/2}$–$10855\,9_{11/2}$
2592.424	2	38562.40	$^{6}2062_{9/2}$ –$10062\,5_{11/2}$	2495.584	2	40058.70	$^{6}7240_{7/2}$ –$10729\,9_{7/2}$
2590.248	3	38594.80	$^{6}4235_{9/2}$ –$10283\,0_{9/2}$	2495.508	10	40059.92	$^{6}1605_{7/2}$ –$10166\,5_{5/2}$
2589.900	4	38599.98	$^{6}5295_{7/2}$ –$10389\,5_{7/2}$	2493.685	6	40089.20	$^{6}1357_{9/2}$ –$10144\,6_{7/2}$
2584.766	3	38676.65	$^{6}5922_{11/2}$–$10459\,8_{13/2}$	2491.326	6	40127.16	$^{6}3768_{7/2}$ –$10389\,5_{7/2}$
2582.712	1	38707.40	$^{6}8374_{9/2}$ –$10708\,1_{9/2}$	2487.750	6	40184.84	$^{6}8374_{9/2}$ –$10855\,9_{11/2}$
2577.866	2	38780.16	$^{6}7965_{3/2}$ –$10674\,5_{5/2}$	2482.577	1	40268.57	$^{6}0520_{7/2}$ –$10078\,8_{7/2}$
2576.922	3	38794.37	$^{6}7870_{9/2}$ –$10666\,5_{7/2}$	2480.487	9	40302.49	$^{6}3593_{9/2}$ –$10389\,5_{7/2}$
2576.109	1	38806.61	$^{6}8492_{7/2}$ –$10729\,9_{7/2}$	2475.946	1	40376.40	$^{6}2240_{11/2}$–$10261\,7_{11/2}$
2574.917	7	38824.58	$^{6}1605_{7/2}$ –$10043\,0_{9/2}$	2474.320	1	40402.94	$4490\,3_{5/2}$ – $^{8}5306_{5/2}$
2572.074	1	38867.49	$^{6}8987_{7/2}$ –$10785\,4_{9/2}$	2472.376	5	40434.70	$3870\,1_{13/2}$– $^{7}9136_{13/2}$
2570.170	4	38896.28	$^{6}6735_{13/2}$–$10563\,2_{13/2}$	2469.796	1	40476.94	$3513\,7_{3/2}$ – $^{7}5614_{5/2}$
2565.796	1	38962.58	$3665\,2_{5/2}$ – $^{7}5614_{5/2}$	2465.272	2	40551.21	$^{6}0520_{7/2}$ –$10107\,1_{5/2}$
2565.346	1	38969.42	$3667\,0_{11/2}$– $^{7}5640_{11/2}$	2462.895	10	40590.35	$3502\,4_{7/2}$ – $^{7}5614_{5/2}$

TABLE I. *Newly classified lines of* Pr III, $\lambda > 2103$Å—Continued

λ_{air} Å	Intensity	σ (cm^{-1})	Classification	λ_{air} Å	Intensity	σ (cm^{-1})	Classification
2460.719	10	40626.24	$44679\ ^{7}_{2} - 85306\ ^{5}_{2}$	2320.906	2	43073.39	$62558\ ^{11}_{2} - 105632\ ^{13}_{2}$
2451.381	2	40780.98	$60166\ ^{9}_{2} - 100947\ ^{9}_{2}$	2317.199	9	43142.29	$60166\ ^{9}_{2} - 103308\ ^{7}_{2}$
2449.908	4	40805.50	$62678\ ^{13}_{2} - 103484\ ^{15}_{2}$	2315.774	2	43168.84	$60166\ ^{9}_{2} - 103335\ ^{9}_{2}$
2449.636	1	40810.03	$37011\ ^{3}_{2} - 77822\ ^{5}_{2}$	2310.248	3	43272.09	$58174\ ^{9}_{2} - 101446\ ^{7}_{2}$
2442.697	1	40925.95	$60520\ ^{7}_{2} - 101446\ ^{7}_{2}$	2309.386	1	43288.24	$58158\ ^{7}_{2} - 101446\ ^{7}_{2}$
2432.678	7	41094.49	$34520\ ^{5}_{2} - 75614\ ^{5}_{2}$	2308.670	5	43301.66	$34520\ ^{5}_{2} - 77822\ ^{5}_{2}$
2431.260	8	41118.46	$29263\ ^{13}_{2} - 70381\ ^{13}_{2}$	2307.384	6	43325.79	$62240\ ^{11}_{2} - 105566\ ^{9}_{2}$
2423.700	3	41246.71	$62558\ ^{11}_{2} - 103805\ ^{13}_{2}$	2307.277	2	43327.80	$40098\ ^{5}_{2} - 83426\ ^{5}_{2}$
2422.883	6	41260.61	$60419\ ^{11}_{2} - 101680\ ^{13}_{2}$	2304.201	6	43385.64	$60419\ ^{11}_{2} - 103805\ ^{13}_{2}$
2416.527	1	41369.13	$65295\ ^{7}_{2} - 106665\ ^{7}_{2}$	2303.121	7	43405.98	$41023\ ^{7}_{2} - 84430\ ^{7}_{2}$
2384.757	5	41920.21	$62678\ ^{13}_{2} - 104598\ ^{13}_{2}$	2296.541	2	43530.34	$63768\ ^{7}_{2} - 107299\ ^{7}_{2}$
2382.979	3	41951.49	$61357\ ^{9}_{2} - 103308\ ^{7}_{2}$	2295.856	4	43543.32	$29835\ ^{9}_{2} - 73378\ ^{7}_{2}$
2382.588	6	41958.37	$35863\ ^{3}_{2} - 77822\ ^{5}_{2}$	2287.502	2	43702.33	$64857\ ^{9}_{2} - 108559\ ^{11}_{2}$
2380.051	4	42003.09	$65295\ ^{7}_{2} - 107299\ ^{7}_{2}$	2261.530	6	44204.17	$40205\ ^{3}_{2} - 84409\ ^{3}_{2}$
2378.867	6	42024.00	$36670\ ^{11}_{2} - 78694\ ^{11}_{2}$	2257.546	4	44282.17	$41023\ ^{7}_{2} - 85306\ ^{5}_{2}$
2369.081	10	42197.57	$60419\ ^{11}_{2} - 102617\ ^{11}_{2}$	2257.342	5*w*	44286.18	$26095\ ^{11}_{2} - 70381\ ^{13}_{2}$
2367.497	3	42225.80	$62678\ ^{13}_{2} - 104904\ ^{11}_{2}$	2251.445	8	44402.16	$25979\ ^{15}_{2} - 70381\ ^{13}_{2}$
2365.796	8	42256.16	$58174\ ^{9}_{2} - 100430\ ^{9}_{2}$	2243.485	1*w*	44559.69	$39870\ ^{9}_{2} - 84430\ ^{7}_{2}$
2360.786	5	42345.83	$62558\ ^{11}_{2} - 104904\ ^{11}_{2}$	2238.560	6	44657.71	$28720\ ^{9}_{2} - 73378\ ^{7}_{2}$
2357.627	3	42402.56	$41023\ ^{7}_{2} - 83426\ ^{5}_{2}$	2227.201	3	44885.45	$28720\ ^{9}_{2} - 73606\ ^{9}_{2}$
2357.176	3	42410.67	$60419\ ^{11}_{2} - 102830\ ^{9}_{2}$	2211.332	1	45207.52	$40098\ ^{5}_{2} - 85306\ ^{5}_{2}$
2354.942	6	42450.90	$58174\ ^{9}_{2} - 100625\ ^{11}_{2}$	2208.939	6	45256.49	$30505\ ^{11}_{2} - 75762\ ^{9}_{2}$
2354.128	2	42465.58	$36670\ ^{11}_{2} - 79136\ ^{13}_{2}$	2201.678	7*w*	45405.73	$39024\ ^{9}_{2} - 84430\ ^{7}_{2}$
2353.942	6	42450.90	$60166\ ^{9}_{2} - 102617\ ^{11}_{2}$	2196.775	7	45507.06	$37919\ ^{7}_{2} - 83426\ ^{5}_{2}$
2345.001	4	42630.85	$58158\ ^{7}_{2} - 100788\ ^{7}_{2}$	2176.676	3	45927.22	$29835\ ^{9}_{2} - 75762\ ^{9}_{2}$
2337.295	2	42771.39	$62678\ ^{13}_{2} - 105450\ ^{11}_{2}$	2162.611	2	46225.88	$27380\ ^{11}_{2} - 73606\ ^{9}_{2}$
2335.873	6	42797.43	$35024\ ^{7}_{2} - 77822\ ^{5}_{2}$	2155.562	5	46377.03	$29263\ ^{13}_{2} - 75640\ ^{11}_{2}$
2332.129	1	42866.12	$35828\ ^{9}_{2} - 78694\ ^{11}_{2}$	2148.203	1	46535.89	$23442\ ^{11}_{2} - 69978\ ^{11}_{2}$
2330.393	6	42898.06	$64401\ ^{5}_{2} - 107299\ ^{7}_{2}$	2135.942	2	46802.99	$23175\ ^{13}_{2} - 69978\ ^{11}_{2}$
2329.568	7	42913.25	$58158\ ^{7}_{2} - 101071\ ^{5}_{2}$				
2329.456	2	42915.31	$60419\ ^{11}_{2} - 103335\ ^{9}_{2}$				
2325.016	2	42997.26	$64857\ ^{9}_{2} - 107854\ ^{9}_{2}$				
2324.807	1	43001.12	$27380\ ^{11}_{2} - 70381\ ^{13}_{2}$				
2324.438	7	43007.95	$62558\ ^{11}_{2} - 105566\ ^{9}_{2}$				
2321.717	5	43058.35	$28936\ ^{3}_{2} - 71994\ ^{5}_{2}$				

3. New Energy Levels

The techniques for using electronic computers in the search for energy levels are now well-known. The method [9] by which the line-list is added to (or subtracted from) the known levels to obtain statistically significant numbers of repeating sums (or differences) was used here. The selection of real levels is based on the probability of the occurrence of a chain of repeating sums of a particular length and tolerance as well as the line intensity distribution in the chain. This method yields many energy levels, but there always remain a certain number which make few combinations (particularly levels of high J-value) and which must be sought by intensity criteria alone according to the appropriate selection rules, and predicted positions.

Most of the observed lines of Pr III with moderate to strong intensity in the vacuum ultraviolet range are due to transitions to the $4f^2 5d$ configuration. The highest density of lines occurs between 1000 and 1200 Å, the main region of the $4f^2 5d$—$4f^2 5f$ transition array. This is analogous to Ce III where the same region contained the $4f5d$—$4f5f$ array [3]. In both cases, the array is well isolated and easily accessible, so that a thorough description of it can be obtained. With these lines 74 levels of the $4f^2 5f$ configuration were found.

Designations in LS-coupling were assigned to these levels on the basis of relative line intensities. Although final designations are given in the $J_1 l$ scheme in

table II, the experimentally derived *LS* names were important in relating the theoretical calculation of this configuration to the observed levels. The calculated *LS* composition, while showing less purity than J_1l, gave single designations for many levels exceeding 50 percent. The largest *LS* component for each level has been included in table VI.

A second region of high line-density appears from the beginning of table X to about 1800 Å. This is the short wavelength end of the $4f^25d$—$(4f^26p + 5d^24f)$ transition array, which extends to about 2700 Å. Many of these lines were classified with the previously known levels. The tail of this array reaches to much shorter wavelengths due to the high-lying levels of $5d^24f$.

An extension of the high-level structure of even parity was made by using the longer wavelength line-list of reference 1. By combining these lines with the $4f^26p$ levels, more levels in the region of the previously identified $4f^26d$ group were found. Calculations of the structure of the configurations $4f^26d$ and $4f^27s$ provided the means to distinguish the latter configuration from among these levels.

Several low levels of the $4f^28s$ configuration were found by adding the vacuum ultraviolet lines to the $4f^26p$ levels. They were identified by their predicted location (compared with Ce III, $4f8s$), by their strong combinations with particular core terms of $4f^26p$, and by reasonable fitted values of the parameters $G^3(fs)$, $\zeta(4f)$ and $E^3(f^2)$.

A detailed investigation of the hfs of the $4f^26s$ configuration has been carried out by J. Reader and J. Sugar [10]. A by-product of this work was the discovery of the pair of levels based on the $4f^2(^3P_2)$ parent and the replacement of the level $\langle 4f^2(^1D_2), 6s, 5/2\rangle$.

The newly derived energy levels of Pr III are given in table II. Their designations result from calculations of the configurations in the purest coupling schemes, with radial parameters obtained by least squares fitting of linear energy formulas to the observed energy levels [11]. The results of these calculations are given in the sections which follow.

Designations of levels of the $4f^25f$, $5d^24f$, and $4f5d6s$ configurations in the *LS*-coupling scheme were made on the basis of relative strengths of the combinations with the $4f^25d$ terms. Later calculations of energy levels in this coupling scheme substantiated these assignments where the purity of the eigenvectors indicated a major *LS* component for a level. The successful correlation of observed and calculated energy levels was largely due to these experimental *LS* assignments.

The $4f^26d$, $4f^27s$, and $4f^28s$ levels were designated in J_1j-coupling according to the intensities of combinations with levels of $4f^26p$. In these transition arrays the selection rules $\Delta L_1 = 0$, $\Delta S_1 = 0$, and $\Delta J_1 = 0$ on parent levels are strongly obeyed. The J_1j-coupling designations given in table II for these configurations and for $4f^26s$ and $4f^26p$ contain the $4f^2$ core level and the *j*-value of the outer electron.

TABLE II. *New energy levels of* Pr III

Configuration	Designation	*J*	Energy/hc (cm^{-1})
$4f^26s$	$(^1D_2)1/2$	$2\frac{1}{2}$	[a]45807.1
	$(^3P_1)1/2$	$0\frac{1}{2}$	50869.3
	$(^3P_2)1/2$	$2\frac{1}{2}$	51312.8
	$(^3P_2)1/2$	$1\frac{1}{2}$	52026.9
$5d^24f$	$(^3F)^2I^\circ$	$5\frac{1}{2}$	68238.12
	$(^3F)^4I^\circ$	$7\frac{1}{2}$	68305.1
	$(^1D)^2H^\circ$	$5\frac{1}{2}$	69408.51
	$(^3P)^4G^\circ$	$2\frac{1}{2}$	69681.6
	$(^3F)^4G^\circ$	$5\frac{1}{2}$	69978.08
	$(^3F)^2I^\circ$	$6\frac{1}{2}$	70381.48
	$(^3P)^4G^\circ$	$4\frac{1}{2}$	71021.1
	$(^3P)^4G^\circ$	$3\frac{1}{2}$	71385.6
	$(^3P)^2D^\circ$	$1\frac{1}{2}$	71501.0
	$(^1D)^2D^\circ$	$2\frac{1}{2}$	71994.81
	$(^1G)^2H^\circ$	$4\frac{1}{2}$	73029.9
	$(^1G)^2G^\circ$	$3\frac{1}{2}$	73378.42
	$(^1D)^2G^\circ$	$4\frac{1}{2}$	73606.17
	$(^3P)^4G^\circ$	$5\frac{1}{2}$	73609.1
	$(^3P)^4D^\circ$	$2\frac{1}{2}$	74105.2
	$(^3P)^4F^\circ$	$1\frac{1}{2}$	74463.7
	$(^3P)^4F^\circ$	$3\frac{1}{2}$	75294.0
$4f^26p$	$(^1D_2)1/2^\circ$	$2\frac{1}{2}$	75614.81
$5d^24f$	$(^3F)^2H^\circ$	$5\frac{1}{2}$	75640.00
	$(^1G)^2G^\circ$	$4\frac{1}{2}$	75762.23
	$(^3F)^2D^\circ$	$1\frac{1}{2}$	76892.4
	$(^1G)^2F^\circ$	$2\frac{1}{2}$	77822.00
	$(^1G)^2F^\circ$	$3\frac{1}{2}$	78463.6
	$(^1G)^2I^\circ$	$5\frac{1}{2}$	78694.57
	$(^1G)^2I^\circ$	$6\frac{1}{2}$	79136.23
$4f^26p$	$(^1D_2)3/2^\circ$	$2\frac{1}{2}$	79366.65
$5d^24f$	$(^1G)^2D^\circ$	$1\frac{1}{2}$	82492.4
$4f^26p$	$(^3P_1)3/2^\circ$	$2\frac{1}{2}$	83426.55
	$(^3P_1)3/2^\circ$	$1\frac{1}{2}$	84409.93
	$(^3P_2)3/2^\circ$	$3\frac{1}{2}$	84430.98
	$(^3P_2)3/2^\circ$	$2\frac{1}{2}$	85306.10
$4f5d6s$	$(^3G)^4G^\circ$	$3\frac{1}{2}$	87511.6
	$(^3G)^4G^\circ$	$4\frac{1}{2}$	88220.2
	$(^3F)^4F^\circ$	$4\frac{1}{2}$	88948.6
	$(^3G)^4G^\circ$	$5\frac{1}{2}$	90119.8
	$(^3H)^2H^\circ$	$4\frac{1}{2}$	90629.2
	$(^3G)^2G^\circ$	$3\frac{1}{2}$	92441.7
$5d^24f$	$(^1S)^2F^\circ$	$2\frac{1}{2}$	92554.8
$4f5d6s$	$(^3H)^2H^\circ$	$5\frac{1}{2}$	93296.5
$5d^24f$	$(^1S)^2F^\circ$	$3\frac{1}{2}$	93967.4
$4f5d6s$	$(^3G)^2G^\circ$	$4\frac{1}{2}$	95147.9
	$(^1F)^2F^\circ$	$3\frac{1}{2}$	96830.5
$4f^26d$	$(^3H_4)3/2$	$4\frac{1}{2}$	100430.29
	$(^3H_4)3/2$	$5\frac{1}{2}$	100625.04
	$(^3H_4)3/2$	$3\frac{1}{2}$	100788.95
	$(^3H_4)5/2$	$4\frac{1}{2}$	100947.18
	$(^3H_4)3/2$	$2\frac{1}{2}$	101071.43
	$(^3H_4)5/2$	$3\frac{1}{2}$	101446.27
	$(^3H_4)5/2$	$2\frac{1}{2}$	101665.58
	$(^3H_4)5/2$	$6\frac{1}{2}$	101680.38
	$(^3H_5)3/2$	$5\frac{1}{2}$	102617.24
	$(^3H_5)3/2$	$4\frac{1}{2}$	102830.43
	$(^3H_5)3/2$	$3\frac{1}{2}$	103308.53
	$(^3H_5)5/2$	$4\frac{1}{2}$	103335.06
	$(^3H_5)5/2$	$7\frac{1}{2}$	103484.19
	$(^3H_5)5/2$	$6\frac{1}{2}$	103805.38
	$(^3H_5)5/2$	$3\frac{1}{2}$	103895.83

TABLE II. *New energy levels of* Pr III – Continued

Configuration	Designation	J	Energy/hc (cm^{-1})
$4f^27s$	$(^3H_6)1/2$	$6\frac{1}{2}$	104598.99
$4f^26d$	$(^3H_6)3/2$	$5\frac{1}{2}$	104904.55
	$(^3H_6)5/2$	$5\frac{1}{2}$	105450.18
	$(^3H_6)3/2$	$4\frac{1}{2}$	105566.62
	$(^3H_6)5/2$	$6\frac{1}{2}$	105632.16
$4f^27s$	$(^3F_3)1/2$	$3\frac{1}{2}$	106665.07
	$(^3F_3)1/2$	$2\frac{1}{2}$	106745.65
	$(^3F_4)1/2$	$4\frac{1}{2}$	107081.94
$4f^26d$	$(^3F_3)3/2$	$3\frac{1}{2}$	107299.07
	$(^3F_4)3/2$	$4\frac{1}{2}$	107854.46
	$(^3F_4)5/2$	$5\frac{1}{2}$	108559.40
$4f^25f$	$(^3H_4)[6]^\circ$	$5\frac{1}{2}$	110295.1
	$[4]^\circ$	$3\frac{1}{2}$	110333.5
	$[7]^\circ$	$6\frac{1}{2}$	110530.9
	$[5]^\circ$	$5\frac{1}{2}$	110881.1
	$[4]^\circ$	$4\frac{1}{2}$	110922.5
	$[6]^\circ$	$6\frac{1}{2}$	111110.3
	$[2]^\circ$	$1\frac{1}{2}$	111268.7
	$[7]^\circ$	$7\frac{1}{2}$	111335.1
	$[3]^\circ$	$3\frac{1}{2}$	111342.8
	$[2]^\circ$	$2\frac{1}{2}$	111494.8
	$[5]^\circ$	$4\frac{1}{2}$	111993.0
	$(^3H_5)[5]^\circ$	$5\frac{1}{2}$	112643.2
	$[7]^\circ$	$6\frac{1}{2}$	112769.7
	$[7]^\circ$	$7\frac{1}{2}$	112896.3
	$[8]^\circ$	$8\frac{1}{2}$	113023.5
	$[5]^\circ$	$4\frac{1}{2}$	113158.8
	$[4]^\circ$	$3\frac{1}{2}$	113291.8
	$[3]^\circ$	$2\frac{1}{2}$	113556.8
	$[6]^\circ$	$6\frac{1}{2}$	113600.3
	$[3]^\circ$	$3\frac{1}{2}$	113630.9
	$[6]^\circ$	$5\frac{1}{2}$	113664.3
	$[4]^\circ$	$4\frac{1}{2}$	113780.5
	$[2]^\circ$	$1\frac{1}{2}$	113825.5
	$[8]^\circ$	$7\frac{1}{2}$	113833.9
	$[2]^\circ$	$2\frac{1}{2}$	113914.1
	$(^3H_6)[8]^\circ$	$8\frac{1}{2}$	114725.6
	$[6]^\circ$	$6\frac{1}{2}$	114797.2
	$[9]^\circ$	$9\frac{1}{2}$	114970.7
	$[4]^\circ$	$4\frac{1}{2}$	115324.3
	$[6]^\circ$	$5\frac{1}{2}$	115403.3
	$[7]^\circ$	$6\frac{1}{2}$	115408.4
	$[3]^\circ$	$3\frac{1}{2}$	115420.8
	$[5]^\circ$	$4\frac{1}{2}$	115499.8
	$(^3F_2)[4]^\circ$	$3\frac{1}{2}$	115670.0
	$(^3H_6)[8]^\circ$	$7\frac{1}{2}$	115672.2
	$[3]^\circ$	$2\frac{1}{2}$	115800.0
	$[5]^\circ$	$5\frac{1}{2}$	115933.2
	$[4]^\circ$	$3\frac{1}{2}$	116021.8
	$[7]^\circ$	$7\frac{1}{2}$	116238.8
	$(^3F_2)[5]^\circ$	$5\frac{1}{2}$	116309.2
	$[4]^\circ$	$4\frac{1}{2}$	116453.2
	$(^3H_6)[9]^\circ$	$8\frac{1}{2}$	116489.8
	$(^3F_2)[3]^\circ$	$2\frac{1}{2}$	116727.1
	$[3]^\circ$	$3\frac{1}{2}$	117044.6
	$(^3F_3)[6]^\circ$	$6\frac{1}{2}$	117248.2
	$[6]^\circ$	$5\frac{1}{2}$	117323.1
	$[1]^\circ$	$1\frac{1}{2}$	117540.5
	$[5]^\circ$	$5\frac{1}{2}$	117574.5
	$[4]^\circ$	$3\frac{1}{2}$	117647.2
	$[3]^\circ$	$2\frac{1}{2}$	117686.4
	$(^3F_4)[6]^\circ$	$6\frac{1}{2}$	117775.3
	$[7]^\circ$	$7\frac{1}{2}$	118063.0
	$(^3F_3)[4]^\circ$	$4\frac{1}{2}$	118081.1
	$[2]^\circ$	$1\frac{1}{2}$	118201.4
	$(^3F_4)[5]^\circ$	$5\frac{1}{2}$	118271.6
	$(^3F_3)[3]^\circ$	$3\frac{1}{2}$	118318.6
	$(^3H_4)[5]^\circ$	$4\frac{1}{2}$	118468.8
	$[7]^\circ$	$6\frac{1}{2}$	118610.9
	$[5]^\circ$	$5\frac{1}{2}$	118879.3
	$(^1G_4)[6]^\circ$	$6\frac{1}{2}$	120498.7
	$[5]^\circ$	$5\frac{1}{2}$	121095.2
	$[7]^\circ$	$7\frac{1}{2}$	121119.2
	$[5]^\circ$	$4\frac{1}{2}$	121382.6
	$[7]^\circ$	$6\frac{1}{2}$	121431.2
	$[6]^\circ$	$5\frac{1}{2}$	121532.5
	$(^1D_2)[1]^\circ$	$1\frac{1}{2}$	128214.2
	$[5]^\circ$	$4\frac{1}{2}$	128352.8
	$[5]^\circ$	$5\frac{1}{2}$	128381.6
	$[4]^\circ$	$3\frac{1}{2}$	128453.2
	$[4]^\circ$	$4\frac{1}{2}$	128568.6
	$(^1I_6)[9]^\circ$	$8\frac{1}{2}$	133194.3
	$[9]^\circ$	$9\frac{1}{2}$	133242.3
	$[8]^\circ$	$7\frac{1}{2}$	133352.2
	$[8]^\circ$	$8\frac{1}{2}$	133373.0
$4f^28s$	$(^3H_4)1/2$	$4\frac{1}{2}$	129106.1
	$(^3H_5)1/2$	$5\frac{1}{2}$	131200.3
	$(^3H_5)1/2$	$4\frac{1}{2}$	131226.3
	$(^3H_6)1/2$	$6\frac{1}{2}$	133393.2
	$(^3H_6)1/2$	$5\frac{1}{2}$	133503.9
	$(^3F_3)1/2$	$3\frac{1}{2}$	135445.2
	$(^3F_4)1/2$	$4\frac{1}{2}$	135868.8

[a] Level values are given to two decimal places when derived from wavelengths > 2100 Å having no hfs.

4. Theoretical Interpretation of the Observed Configurations

For the calculation and diagonalization of energy matrices, computer programs written by Y. Bordarier and A. Carlier at Laboratoire Aimé Cotton, Orsay, France, were used. These programs evaluate the energy formulas given in terms of nj-coefficients, and compiled the output in the form of J-matrices which may then be diagonalized. The large library of matrices assembled at Hebrew University by G. Racah and his co-workers was made available to us by Z. Goldschmit, and is compatible with the above-mentioned programs.

The matrix library tape contains the configurations f^2p and $f(d+s)^2$. For the present work they were combined with configuration interaction (utilizing the formulas for three-electron matrix elements calculated by Fano, Pratts, and Goldschmidt [12]) to study the configuration complex $4f^26p+5d^24f+4f5d6s$. The matrices of $f^2(d+s)$ are also on the library tape, and were used in the study of $4f^26d$, $4f^27s$, and $4f^28s$. The matrices of f^2f' were calculated manually by means of the Racah formalism [13] prior to the acquisition of these programs.

In the present paper, unreduced values for the Slater parameters are used. The convention of multiplying the coefficient martices by arbitrary factors to simplify denominators is unnecessary for computer calculations.

The notations for the parameters in tables III, V, VII, and IX have the following meaning: "A" is an additive constant common to all levels of the configuration; $F^k(l, l')$ and $G^k(l, l')$ are the Slater radial integrals arising from the electrostatic interaction between the electrons l and l'; ζ_l is the parameter of the spin-orbit

TABLE III. *Fitted parameter values and associated standard errors for the* $4f^26p+5d^24f+4f5d6s$ *configurations of* Pr III *and corresponding parameters of* Ce III *and* Pr IV *in units of* cm^{-1}

Parameters	Pr III	Ce III	Pr IV
	$4f^26p$	$4f6p$	$4f^2$
A	67903 ± 90	52001 ± 62	
$E^1(f^2)$	4984 ± 25		5011 ±17
E^2	23.1 ± 0.2		23.1 ± 0.1
E^3	486 ± 2		488 ± 1
α	28 ± 2		24 ± 1
γ	−50 ± 9		−49 ± 6
$F^2(fp)$	6075 ±225	5400 ±450	
G^2	1785 ±140	2450 ±875	
G^4	1531 ±302	945 ±284	
ζ_p	2338 ± 24	2155 ± 33	
ζ_f	751 ± 10	644 ± 10	760 ± 6
	$5d^24f$	$5d^2$	
A	73137 ± 48	46027 ± 67	
$B(d^2)$	406 ± 5	442 ± 3	
C	2021 ± 21	2006 ±111	
$F^2(fd)$	21000 ±284		
F^4	15385 ±431		
G^1	10080 ± 96		
G^3	13954 ±665		
G^5	10825 ±611		
ζ_d	946 ± 23	837 ± 14	
ζ_f	838 ± 19		
E_x	483 ± 55		
	$4f5d6s$	$5d6s$	
A	92316 ± 156	66388 ± 96	
$F^2(fd)$	20790 ±1050		
F^4	15177 Fixed F^2/F^4		
G^1	9905 ± 476		
G^3	13167 Fixed G^1/G^3		
G^5	10825 Fixed G^1/G^5		
$G^2(ds)$	10125 ± 410	11125 ± 705	
$G^3(fs)$	2100 Fixed		
ζ_d	1035 ± 66	927 ± 28	
ζ_f	838 Fixed		
Configuration interaction			
$R^1(fp,d^2)$	−1583 ± 122	3115 ± 105	
$R^3(fp,d^2)$	1655 ± 308	0 Fixed	
$R^1(fp,ds)$	6590 ± 341	5355 ± 730	
$R^3(fp,sd)$	0 Fixed	0 Fixed	
$R^2(dd,ds)$	16940 ± 621	15820 ±1295	
$R^2(fd,fs)$	0 Fixed		
$R^3(fd,sf)$	0 Fixed		
rms error in calculated levels	89 cm^{-1}	47 cm^{-1}	

interaction for the electron l; E^1, E^2, and E^3 are linear combinations of the Slater radial integrals defined by Racah [14] which arise from the electrostatic interaction within an f^n shell; B and C are linear combinations of Slater integrals defined by Racah [13] for the d^n shell; α and γ are two-body effective interaction parameters acting within the f^n shell which have the coefficients $L(L+1)$ and $12g(U)$, respectively, where L refers to the orbital angular momentum in the f^n shell and $g(U)$ are the eigenvalues of the Casimir operator $G(G_2)$ tabulated by Racah [14]; E_x is the two-body effective interaction parameter for nonequivalent electrons proposed by Sack [20] and is used here for the $5d^24f$ configuration; R^k are the radial integrals arising from configuration interaction.

4.1. The $4f^26p+5d^24f+4f5d6s$ Complex

These three configurations are analogous to the Ce III group $4f6p$, $5d^2$, and $5d6s$ treated theoretically by Z. Goldschmidt [15]. She found strong mutual perturbations in Ce III, reporting large mixutres of terms of two configurations in several levels. This accounts for the poor results of Spector's calculation of $4f6p$ alone [16]. The rms error in his calculated levels is 394 cm^{-1}, while that obtained in reference 15 for the mixture of the three configurations is 47 cm^{-1}.

Following the results in Ce III, I have treated the mixed complex of configurations $4f^26p$, $5d^24f$, and $4f5d6s$ in Pr III. Initial parameters for the first diagonalization of the energy matrices were obtained from the following sources for the $5d^24f$ and $4f5d6s$ configurations:

Interaction	Source	Reference
$d-d$	Ce III $5d^2$	15
$d-s$	Ce III $5d6s$	15
$f-s$	Pr III $4f^26s$	19
$d-f$	Pr III $4f^25d$	17
$\zeta_d(5d^2)$	Ce III $5d^2$	15
$\zeta_d(5d)$	Ce III $5d6s$	15
ζ_f	Pr IV $4f6s$	18

The matrices for these configurations were diagonalized without configuration interaction to determine the correspondence with the observed levels. This was accomplished by means of the experimentally identified LS composition of many of the levels. The parameters were then improved by least squares adjustment to fit the observed levels and further improved by several repetitions of these steps. Because of the small number of known levels of $4f5d6s$, fixed ratios were assumed for F^2/F^4, G^1/G^3, and G^1/G^5 of the $f-d$ interaction as well as fixed values of $G^3(f,s)$ and ζ_f. The refined parameter values then served as initial parameters for the first diagonalization with configuration interaction.

Spector has treated the $4f^26p$ configuration of Pr III theoretically [19] and obtained an rms error of 198 cm^{-1} for his calculated levels. His results served here for initial parameters of this configuration.

Initial values for the configuration interaction parameters $R^1(fp,d^2)$ between $4f^26p$ and $5d^24f$, $R^1(fp,ds)$ between $4f^26p$ and $4f5d6s$, and $R^2(d^2,ds)$ between $5d^24f$ and $4f5d6s$ were taken from the Ce III results [15]. All other configuration interaction parameters were initially set equal to zero.

Several sequences of diagonalization and adjustment of the parameters were carried out to obtain conver-

gence before attempting to evaluate the less sensitive interaction parameters. Then the parameters $R^2(fd,fs)$ and $R^3(fd,sf)$ which act between the $5d^24f$ and $4f5d6s$ configurations, and $G^3(fs)$ of the latter configuration were added. These were found to be undefinable in the least squares calculations (their standard errors exceeded their values) because too few levels of $4f5d6s$ are known. They were therefore fixed at the following values:

$$R^2(fd,fs) = R^3(fd,sf) = 0$$
$$G^3(fs) = 2100 \text{ cm}^{-1}.$$

Finally, values for $R^3(fp,d^2)$ and $R^3(fp,sd)$ were sought. The latter was undefinable and was therefore fixed at zero. The iterative fitting procedure was again brought to convergence, with an rms error of 119 cm^{-1} for the calculated levels.

Goldschmidt's success in utilizing the Sack [20] effective two-body interaction operators $E_lL(L+1)$ and $E_sS(S+1)$ acting on the final L and S of the levels of $4f5d$ in Ce III [15] suggested their use for the $4f^26p$ and $5d^24f$ configurations of Pr III. For these configurations, following Sack, the operators are $E_l[L(L+1)-L_c(L_c+1)]$ and $E_s[S(S+1)-S_c(S_c+1)]$, where L_c and S_c refer to the $4f^2$ or $5d^2$ core terms. A well defined value was obtained only for E_s of $5d^24f$. The addition of this parameter reduced the rms error to its final value of 89 cm^{-1}.

In table III the final values for the parameters derived from the mixing of the three configurations are given. In all least squares calculations the ratios F^2/F^4, G^1/G^3, and G^1/G^5 of the $4f5d6s$ configuration were fixed at the values taken by the corresponding parameters of $5d^24f$ in the preceding calculation. Also the parameter ζ_f of $4f5d6s$ was required to be equal to ζ_f in $5d^24f$. The remaining free parameters common to these two configurations, namely F^2, G^1, and ζ_d, took nearly equal values in both configurations. It is interesting to note that they are nearly equal to the corresponding parameters of the $4f5d$ configuration [18] of Pr IV.

Included in table III are the corresponding parameters of Ce III evaluated by Goldschmidt [15] and the parameters of the $4f^2$ configuration of Pr IV [21] included for comparison with $4f^26p$ core interactions.

Table IV contains all the calculated levels of the three configurations, all the experimental levels assigned to these configurations, and the squares of the components of the eigenvectors of the calculated levels (their percentage composition). A maximum of three components is given for each level, but less are shown when the sum represents 90 percent or more of the composition. Where a level contains 20 percent or more of the eigenvectors of two configurations, both are indicated in the column labeled "configuration" by means of an "X".

The highest purity of eigenvectors for $4f^26p$ is of course obtained in J_lj-coupling because of the large value of ζ_p and the small electrostatic interaction between the f and p electrons. The designation of the energy levels in this scheme gives the $4f^2$ core level in parentheses followed by the j of the $6p$ electron (1/2 or 3/2).

The coupling is much less pure in $5d^24f$. Here the electrostatic interactions within the $5d^2$ shell and between $5d$ and $4f$ are both strong. Therefore, no preferred order of coupling of electrons occurs. The basis states are calculated in an LS scheme in which the d electrons are first coupled and the f electron is then added. In table IV the $5d^2$ core term is given in parentheses followed by the final LS term. The large values of $\zeta(5d)$ and $\zeta(4f)$ give rise to intermediate coupling. I transformed the eigenvectors to the $(d^2)J_1(f)j$ scheme and found higher purity for a few levels, but the average purity for the configuration is lower than in the LS scheme.

TABLE IV. *Calculated energy levels and compositions of the mixed* $4f^26p$, $5d^24f$, *and* $4f5d6s$ *configurations of* Pr III.

The $4f^26p$ levels are designated in J_lj-coupling. The levels of $5d^24f$ and $4f5d6s$ are designated in LS-coupling, with those of $4f5d6s$ distinguished by the symbol *. Levels attributed to two configurations contain 20 percent or more of each

J	Levels calculated (cm^{-1})	Levels observed (cm^{-1})	Obs. minus calc.	Configuration			Composition					
				$4f^26p$	$5d^24f$	$4f5d6s$						
0½	63030				X		$(^3F)^2S$	31%,	$(^3F)^4D$	23%,	$(^3F)^2P$	19%
	64988				X		$(^3F)^2S$	41%,	$(^3F)^4D$	30%,	$(^3F_2)3/2$	11%
	66481	66325	−156	X			$(^3F_2)3/2$	81%,	$(^3F)^2S$	4%,	$(^3F)^4D$	3%
	68973				X		$(^1D)^2P$	31%,	$(^3F)^2P$	24%,	$(^3F)^4D$	23%
	70262				X		$(^3F)^4P$	74%,	$(^3F)^2S$	19%,		
	72188				X		$(^3P)^4D$	62%,	$(^3F)^2P$	13%,	$(^3F)^4D$	12%
	74970				X		$(^3F)^2P$	37%,	$(^1D)^2P$	30%,	$(^3P)^4D$	18%
	78311	78313	2	X			$(^1D_2)3/2$	68%,	$(^3P_2)3/2$	11%,	$(^3P_0)1/2$	9%
	79409			X			$(^3P_0)1/2$	72%,	$(^1D_2)3/2$	16%		
	79703	79742	39	X			$(^3P_1)1/2$	79%,	$(^3P_0)1/2$	12%		
	83375			X			$(^3P_1)3/2$	51%,	$(^3P_2)3/2$	35%,	*$(^3P)^4P$	6%
	84984			X			$(^3P_2)3/2$	47%,	$(^3P_1)3/2$	37%,	$(^1G)^2P$	6%
	87650				X		$(^1G)^2P$	91%				
	89556					X	*$(^3D)^4D$	91%				
	92742					X	*$(^3P)^4P$	90%				
	97264					X	*$(^3P)^2P$	90%				
	101423					X	*$(^1P)^2P$	89%,	$(^1S_0)1/2$	5%		
	111001			X			$(^1S_0)1/2$	94%				

TABLE IV. *Calculated energy levels and compositions of the mixed* $4f^26p$, $5d^24f$, *and* 4f5d6s *configurations of* Pr III. — Continued

The $4f^26p$ levels are designated in J_1j-coupling. The levels of $5d^24f$ and $4f5d6s$ are designated in *LS*-coupling, with those of $4f5d6s$ distinguished by the symbol *. Levels attributed to two configurations contain 20 percent or more of each

J	Levels calculated (cm^{-1})	Levels observed (cm^{-1})	Obs. minus calc.	Configuration			Composition					
				$4f^26p$	$5d^24f$	$4f5d6s$						
1½	63142	63221	79	X			$(^3F_2)1/2$	91%				
	65166				X		$(^3F)^4D$	57%,	$(^3P)^4D$	13%,	$(^3F)^2P$	10%
	65639				X		$(^3F)^4F$	76%,	$(^3F_2)3/2$	10%,	$(^3P)^4F$	5%
	66828	66867	39	X			$(^3F_2)3/2$	76%,	$(^3F)^4F$	7%,	$(^3F)^4D$	5%
	67916	67965	49	X			$(^3F_3)3/2$	91%				
	68942				X		$(^3F)^2P$	41%,	$(^1D)^2P$	13%,	$(^3F)^4D$	10%
	69488				X		$(^3F)^4P$	82%,	$(^3F)^4S$	5%,	$(^3F)^2P$	5%
	70631				X		$(^1D)^2D$	44%,	$(^3F)^4S$	16%,	$(^1D)^2P$	14%
	71456	71501	45		X		$(^3P)^2D$	32%,	$(^3F)^4S$	25%,	$(^3P)^4D$	14%
	71988				X		$(^3F)^4S$	35%,	$(^3P)^2D$	17%,	$(^1D)^2D$	10%
	73947				X		$(^3P)^4F$	31%,	$(^3P)^4D$	27%,	$(^3F)^2D$	14%
	74066				X		$(^3P)^4D$	20%,	$(^3P)^2D$	18%,	$(^1D)^2P$	15%
	74509	74464	−45		X		$(^3P)^4F$	45%,	$(^3F)^2D$	26%,	$(^3F)^4F$	7%
	75415	75410	−5	X			$(^1D_2)1/2$	79%,	$(^3P_2)1/2$	8%,	$(^3F)^2D$	5%
	76826	76892	66		X		$(^3F)^2D$	30%,	$(^1D)^2P$	27%,	$(^3F)^2P$	15%
	78963	78889	−74	X			$(^1D_2)3/2$	76%,	$(^3P_2)3/2$	8%,	$(^3P_1)1/2$	4%
	80190	80164	−26	X			$(^3P_1)1/2$	88%,	$(^1D_2)3/2$	5%		
	80878	80898	20	X			$(^3P_2)1/2$	75%,	$(^1D_2)1/2$	7%,	$(^3P_0)3/2$	5%
	82573	82492	−81	X	X		$(^3P_0)3/2$	44%,	$(^1G)^2D$	35%,	$(^1G)^2P$	6%
	82926	83026	100	X			$(^3P_1)3/2$	43%,	$(^3P_0)3/2$	23%,	$(^1G)^2D$	12%
	84003			X		X	$(^3P_1)3/2$	31%,	$*(^3F)^4F$	25%,	$(^1G)^2D$	15%
	84494	84410	−84		X		$*(^3F)^4F$	62%,	$(^3P_1)3/2$	11%,	$(^1G)^2D$	8%
	85279			X			$(^3P_2)3/2$	65%,	$(^1G)^2P$	16%,	$(^1D_2)3/2$	5%
	87031				X		$(^1G)^2P$	62%,	$(^3P_2)3/2$	15%,	$(^1G)^2D$	13%
	89214					X	$*(^1D)^2D$	40%,	$*(^3D)^4D$	37%,	$*(^3F)^4F$	7%
	90681					X	$*(^3D)^4D$	52%,	$*(^1D)^2D$	32%,	$*(^3P)^4P$	4%
	92797					X	$*(^3P)^4P$	76%,	$*(^1P)^2P$	5%,	$*(^3D)^4D$	4%
	95092					X	$*(^3D)^2D$	76%,	$*(^1D)^2D$	7%,	$(^1D)^2D$	6%
	96994					X	$*(^3P)^2P$	67%,	$*(^1P)^2P$	16%,	$*(^3P)^4P$	5%
	103051					X	$*(^1P)^2P$	70%,	$*(^3P)^2P$	19%,	$(^1S_0)3/2$	3%
	114351			X			$(^1S_0)3/2$	96%				
2½	61698	61718	20	X			$(^3H_4)3/2$	72%,	$(^3F_2)1/2$	18%		
	63544	63576	32	X			$(^3F_2)1/2$	75%,	$(^3H_4)3/2$	20%		
	64396	64401	5	X			$(^3F_3)1/2$	75%,	$(^3F)^4D$	7%,	$(^3F)^2F$	6%
	64817	64818	1		X		$(^3F)^2F$	31%,	$(^3F)^4G$	27%,	$(^3F_3)1/2$	16%
	66014	65909	−105		X		$(^3F)^4G$	47%,	$(^3F)^4D$	18%,	$(^1D)^2F$	9%
	66571	66681	110	X	X		$(^3F)^4F$	52%,	$(^3F_2)3/2$	30%,	$(^3F_3)3/2$	5%
	66994	66943	−51		X		$(^3F)^4D$	24%,	$(^3F_2)3/2$	14%,	$(^3F)^2F$	11%
	67361	67395	34	X	X		$(^3F_2)3/2$	44%,	$(^3F)^4F$	22%,	$(^3F)^4D$	14%
	68288			X			$(^3F_3)3/2$	38%,	$(^3F_4)3/2$	30%,	$(^1G_4)3/2$	16%
	68991	68979	−12	X			$(^3F_3)3/2$	41%,	$(^3F_4)3/2$	35%,	$(^1G_4)3/2$	10%
	69359				X		$(^3F)^4P$	36%,	$(^3P)^2D$	22%,	$(^3F)^2D$	13%
	69572	69682	110		X		$(^3P)^4G$	83%,	$(^3F)^4P$	6%,	$(^3F)^4G$	5%
	70369				X		$(^3P)^2D$	46%,	$(^3F)^4P$	35%,	$(^3F)^4D$	7%
	71504	71536	32	X			$(^1G_4)3/2$	61%,	$(^3F_4)3/2$	28%,	$(^1D_2)1/2$	2%
	72007	71995	−12		X		$(^1D)^2D$	26%,	$(^3P)^4D$	17%,	$(^3F)^4P$	16%
	74168	74105	−63		X		$(^3P)^4D$	27%,	$(^3P)^4F$	23%,	$(^1D)^2F$	14%
	74744				X		$(^3P)^4F$	62%,	$(^3P)^4D$	12%,	$(^1D)^2F$	8%
	75354	75561	207		X		$(^3F)^2D$	35%,	$(^1D_2)1/2$	18%,	$(^1D)^2D$	14%
	75782	75615	−167	X			$(^1D_2)1/2$	60%,	$(^1D)^2D$	10%,	$(^3P_2^2)1/2$	6%
	76491				X		$(^3F)^2D$	27%,	$(^1D)^2F$	19%,	$(^3P)^2D$	12%
	77944	77822	−122		X		$(^1G)^2F$	70%,	$(^3F)^2F$	5%,	$(^1G)^2D$	4%
	79360	79367	7	X			$(^1D_2)3/2$	79%,	$(^3P_2)3/2$	7%,	$*(^1D)^2D$	5%
	81472	81405	−67	X			$(^3P_2)1/2$	83%,	$(^1D_2)1/2$	8%		
	83359	83427	68	X			$(^3P_1)3/2$	79%,	$(^1G)^2D$	10%,	$*(^3D)^4D$	3%
	84317			X	X		$(^1G)^2D$	43%,	$(^3P_2)3/2$	20%,	$(^3P_1)3/2$	10%
	84710				X		$(^3P)^2F$	52%,	$(^1S)^2F$	13%,	$(^1G)^2F$	9%
	84986					X	$*(^3F)^4F$	56%,	$(^3P)^2F$	8%,	$(^3P_x)3/2$	7%
	85323	85306	−17	X			$(^3P_2)3/2$	52%,	$(^1G)^2D$	19%,	$*(^3F)^4F$	9%
	85904					X	$*(^3G)^4G$	87%,	$*(^3F)^4F$	7%,		
	88297					X	$*(^1D)^2D$	42%,	$*(^3F)^4F$	18%,	$*(^3F)^2F$	16%
	90038					X	$*(^3F)^2F$	44%,	$*(^3D)^4D$	24%,	$*(^1D)^2D$	9%
	91295					X	$*(^3D)^4D$	56%,	$*(^1D)^2D$	11%,	$(^1S)^2F$	10%
	92422	92555	133		X		$(^1S)^2F$	54%,	$*(^1F)^2F$	13%,	$(^3P)^2F$	11%
	94069					X	$*(^3P)^4P$	69%,	$*(^3D)^2D$	10%,	$(^3P_2)3/2$	3%
	94917					X	$*(^1F)^2F$	50%,	$*(^3D)^2D$	10%,	$*(^3P)^4P$	10%
	97877					X	$*(^3D)^2D$	62%,	$*(^1F)^2F$	16%,	$*(^1D)^2D$	9%

TABLE IV. *Calculated energy levels and compositions of the mixed* 4f²6p, 5d²4f, *and* 4f5d6s *configurations of* Pr III. – Continued

The $4f^26p$ levels are designated in J_1j-coupling. The levels of $5d^25f$ and $4f5d6s$ are designated in *LS*-coupling, with those of $4f5d6s$ distinguished by the symbol *. Levels attributed to two configurations contain 20 percent or more of each

J	Levels calculated (cm^{-1})	Levels observed (cm^{-1})	Obs. minus calc.	Configuration			Composition					
				$4f^26p$	$5d^24f$	$4f5d6s$						
3½	58164	58158	−6	X			$(^3H_4)1/2$	82%,	$(^4F)^4H$	6%,	$(^3H_4)3/2$	4%
	60524	60520	−4		X		$(^3F)^4H$	43%,	$(^3F)^2G$	33%,	$(^3H_4)1/2$	10%
	61560	61605	45	X			$(^3H_4)3/2$	80%,	$(^3F)^2G$	7%,	$(^1G^4)3/2$	2%
	63260	63232	−28		X		$(^3F)^4H$	42%,	$(^3F)^2G$	20%,	$(^3F)^2F$	7%
	63807	63769	−38	X			$(^3H_5)3/2$	47%,	$(^3F_3)1/2$	34%,	$(^3F)^4G$	4%
	64992	64980	−12	X			$(^3F_4)1/2$	46%,	$(^1G_4)1/2$	17%,	$(^3F)^2G$	8%
	65265	65296	31	X			$(^3F_3)1/2$	45%,	$(^3H_5)3/2$	39%,	$(^3F_4)1/2$	6%
	65932	65935	3		X		$(^3F)^2F$	22%,	$(^3F)^4D$	12%,	$(^3F)^2G$	9%
	66949	66853	−96		X		$(^3F)^4G$	47%,	$(^3F_2)3/2$	18%,	$(^3F)^4D$	7%
	67280	67240	−40	X	X		$(^3F_2)3/2$	58%,	$(^3F)^4G$	27%,	$(^3F_3)3/2$	2%
	67624	67679	55	X	X		$(^1G_4)1/2$	32%,	$(^3F)^4F$	32%,	$(^3F_4)1/2$	9%
	68221	68332	111	X	X		$(^3F)^4F$	22%,	$(^3F_3)3/2$	21%,	$(^1G_4)1/2$	18%
	68511	68492	−19	X			$(^3F_3)3/2$	37%,	$(^3F)^4F$	17%,	$(^3F_4)1/2$	10%
	68789	68802	13	X			$(^3F_4)3/2$	29%,	$(^1G_4)3/2$	23%,	$(^3F_3)3/2$	22%
	69184	68987	−197		X		$(^3F)^4D$	19%,	$(^3P)^4G$	15%,	$(^1D)^2G$	14%
	69492	69431	−61		X		$(^3F)^4D$	18%,	$(^4P)^4G$	17%,	$(^1D)^2G$	17%
	71450	71386	−64		X		$(^3P)^4G$	58%,	$(^1D)^2G$	24%,	$(^3P)^2G$	7%
	72005	71979	−26	X			$(^1G_4)3/2$	48%,	$(^3F_4)3/2$	38%,	$(^1G)^2G$	4%
	73316	73378	62		X		$(^1G)^2G$	65%,	$(^3P)^2G$	9%,	$(^1D)^2G$	9%
	74550				X		$(^3P)^4D$	62%,	$(^3F)^4D$	18%,	$(^1D)^2F$	10%
	75309	75294	−15		X		$(^3P)^4F$	74%,	$(^3P)^4D$	7%,	$(^3F)^2F$	5%
	76550				X		$(^1D)^2F$	46%,	$(^4P)^4F$	11%,	$(^3F)^2F$	10%
	78374	78463	89	X	X		$(^1G)^2F$	58%,	$(^1D_2)3/2$	20%,	$(^3P)^2F$	5%
	79226	79396	170	X			$(^1D_2)3/2$	66%,	$(^1G)^2F$	14%,	$(^3P_2)3/2$	7%
	81357				X		$(^3P)^2G$	46%,	$(^3G)^2G$	21%,	$(^1D)^2G$	9%
	84135					X	$*(^3H)^4H$	73%,	$*(^1G)^2G$	19%		
	84418	84431	13	X			$(^3P_2)3/2$	85%,	$(^1D_2)3/2$	9%		
	85860				X		$(^3P)^2F$	57%,	$(^3G)^2F$	11%,	$(^3F)^2F$	10%
	86122					X	$*(^1G)^2G$	32%,	$*(^3G)^4G$	22%,	$*(^3H)^4H$	22%
	86381					X	$*(^3F)^4F$	70%,	$*(^3G)^4G$	15%,	$(^3P)^2F$	4%
	87602	87512	−90			X	$*(^3G)^4G$	52%,	$*(^1G)^2G$	26%,	$*(^3F)^4F$	11%
	90636					X	$*(^3D)^4D$	32%,	$*(^1F)^2F$	29%,	$*(^3F)^2F$	24%
	92022					X	$*(^3F)^2F$	35%,	$*(^3D)^4D$	32%,	$*(^3G)^2G$	15%
	92476	92442	−34			X	$*(^3G)^2G$	53%,	$*(^3D)^4D$	21%,	$*(^1G)^2G$	10%
	94002	93967	−35		X		$(^1S)^2F$	74%,	$*(^3G)^2G$	4%,	$*(^3D)^4D$	4%
	96948	96830	−118			X	$*(^1F)^2F$	51%,	$*(^3F)^2F$	23%,	$(^1D)^2F$	8%
4½	58244	58174	−70	X			$(^3H_4)1/2$	95%				
	60160	60166	6	X			$(^3H_5)1/2$	79%,	$(^3H_4)3/2$	7%,	$(^3F)^4H$	7%
	61332	61357	25	X			$(^3H_4)3/2$	53%,	$(^3F)^4I$	19%,	$(^3H_5)1/2$	12%
	61971	62063	92	X	X		$(^3F)^4I$	44%,	$(^3H_4)3/2$	32%,	$(^3F)^2G$	9%
	62508	62536	28		X		$(^3F)^2G$	33%,	$(^3F)^4H$	27%,	$(^3F)^4I$	27%
	63560	63593	33	X	X		$(^3H_5)3/2$	67%,	$(^3F)^4H$	11%,	$(^3F)^2G$	11%
	64271	64236	−35	X	X		$(^3F)^4H$	46%,	$(^3H_5)3/2$	24%,	$(^3F)^2G$	19%
	64929	64857	−72	X			$(^3F_4)1/2$	57%,	$(^1G_4)1/2$	24%,	$(^3H_6)3/2$	12%
	66953	67049	96	X			$(^3H_6)3/2$	60%,	$(^1G_4)1/2$	12%,	$(^1D)^2H$	9%
	67412	67399	−13		X		$(^1D)^2H$	29%,	$(^3F)^2H$	20%,	$(^3H_6)3/2$	13%
	67815	67871	56	X	X		$(^3F_3)3/2$	48%,	$(^3F)^4G$	26%,	$(^1G_4)1/2$	6%
	68349	68375	26	X			$(^1G_4)1/2$	41%,	$(^3F_4)1/2$	22%,	$(^3F_4)3/2$	15%
	68683	68544	−139	X	X		$(^3F)^4G$	50%,	$(^3F_3)3/2$	35%,	$(^3F_4)3/2$	3%
	69181	69138	−43	X			$(^3F_4)3/2$	36%,	$(^1G_4)3/2$	32%,	$(^3F_3)3/2$	6%
	69529	69686	157		X		$(^3F)^4F$	65%,	$(^3F_4)1/2$	8%,	$(^3P)^4F$	5%
	70999	71021	22		X		$(^3P)^4G$	43%,	$(^3P)^2G$	17%,	$(^1D)^2G$	12%
	71641	71592	−49	X			$(^1G_4)3/2$	51%,	$(^3F_4)3/2$	37%,	$(^3P)^4G$	4%
	73119	73030	−89		X		$(^3P)^4G$	36%,	$(^1G)^2H$	25%,	$(^1G)^2G$	15%
	73690	73606	−84		X		$(^1D)^2G$	42%,	$(^1G)^2H$	12%,	$(^1D)^2H$	12%
	74675				X		$(^3F)^2H$	51%,	$(^1G)^2H$	23%,	$(^1D)^2H$	15%
	75636	75762	126		X		$(^1G)^2G$	38%,	$(^1G)^2H$	21%,	$(^3F)^2H$	9%
	77169				X		$(^3P)^4F$	85%,	$(^3F)^4F$	6%		
	81428				X		$(^3P)^2G$	46%,	$(^1G)^2G$	28%,	$(^1D)^2G$	11%
	84446	84411	−35	X			$(^1I_6)3/2$	78%,	$*(^1H)^2H$	8%,	$*(^3H)^4H$	5%
	85028					X	$*(^1G)^2G$	35%,	$*(^3H)^4H$	34%,	$(^1I_6)3/2$	12%
	86442					X	$*(^3H)^4H$	54%,	$*(^1G)^2G$	24%,	$*(^3F)^4F$	16%
	88134	88220	86			X	$*(^3G)^4G$	57%,	$*(^3F)^4F$	35%		
	89017	88949	−68			X	$*(^3F)^4F$	39%,	$*(^3G)^4G$	35%,	$*(^1G)^2G$	16%
	90557	90629	72			X	$*(^3H)^2H$	79%,	$(^1D)^2H$	5%,	$*(^1G)^2G$	4%
	95075	95148	73			X	$*(^3G)^2G$	77%,	$(^1D)^2G$	8%,	$*(^1G)^2G$	8%
	99782					X	$*(^1H)^2H$	85%,	$(^1I_6)3/2$	6%		

TABLE IV. *Calculated energy levels and compositions of the mixed* $4f^26p$, $5d^24f$, *and* 4f5d6s *configurations of* Pr III. – Continued

The $4f^26p$ levels are designated in J_1j-coupling. The levels of $5d^24f$ and $4f5d6s$ are designated in *LS*-coupling, with those of $4f5d6s$ distinguished by the symbol *. Levels attributed to two configurations contain 20 percent or more of each

J	Levels calculated (cm^{-1})	Levels observed (cm^{-1})	Obs. minus calc.	Configuration			Composition					
				$4f^26p$	$5d^24f$	$4f5d6s$						
5½	60465	60420	−45	X			$(^3H_5)1/2$	94%				
	62243	62241	−2	X			$(^3H_4)3/2$	40%,	$(^3H_6)1/2$	35%,	$(^3H_5)3/2$	15%
	62569	62559	−10	X			$(^3H_6)1/2$	55%,	$(^3H_4)3/2$	37%		
	63811	63817	6	X	X		$(^3F)^4I$	50%,	$(^3H_5)3/2$	24%,	$(^3H_4)3/2$	15%
	64074	64151	77	X	X		$(^3F)^4I$	42%,	$(^3H_5)3/2$	39%,	$(^3F)^4H$	6%
	64951	64865	−86		X		$(^3F)^4H$	73%,	$(^3H_5)3/2$	15%		
	65912	65922	10	X			$(^3H_6)3/2$	88%,	$(^3F)^4H$	4%		
	68184	68238	54		X		$(^3F)^2I$	51%,	$(^1G)^2I$	36%,	$(^3F)^4H$	6%
	68514	68526	12	X			$(^3F_4)3/2$	53%,	$(^1G_4)3/2$	20%,	$(^3F)^4G$	14%
	69455	69409	−46		X		$(^3F)^2H$	37%,	$(^1D)^2H$	25%,	$(^3F)^4G$	11%
	69924	69978	54		X		$(^3F)^4G$	62%,	$(^1D)^2H$	11%,	$(^3P)^4G$	8%
	71714	71736	22	X			$(^1G_4)3/2$	65%,	$(^3F_4)3/2$	29%		
	73535	73609	74		X		$(^3P)^4G$	76%,	$(^3F)^2H$	9%,	$(^1G)^2H$	8%
	75641	75640	−1		X		$(^3F)^2H$	32%,	$(^1D)^2H$	18%,	$(^1G)^2I$	16%
	76097				X		$(^1G)^2H$	56%,	$(^1D)^2H$	27%,	$(^3P)^4G$	9%
	78869	78695	−174		X		$(^1G)^2I$	35%,	$(^3F)^2I$	25%,	$(^3F)^2H$	12%
	80312	80361	49	X			$(^1I_6)1/2$	80%,	$(^3F)^2I$	6%,	$(^1G)^2I$	6%
	83729	83607	−122	X			$(^1I_6)3/2$	87%,	$(^1I_6)1/2$	7%		
	87519					X	$*(^3H)^4H$	95%				
	90049	90120	71			X	$*(^3G)^4G$	96%				
	93283	93296	13			X	$*(^3H)^2H$	80%,	$*(^1H)^2H$	9%,	$*(^3H)^4H$	5%
	99971					X	$*(^1H)^2H$	82%,	$*(^3H)^2H$	10%		
6½	62725	62679	−46	X			$(^3H_6)1/2$	89%,	$(^3H_6)3/2$	6%		
	64218	64215	−3	X			$(^3H_5)3/2$	86%,	$(^3H_6)3/2$	8%		
	65944	65967	23		X		$(^3F)^4I$	86%,	$(^3F)^4H$	5%		
	66091	66148	57	X	X		$(^3H_6)3/2$	51%,	$(^3F)^4H$	25%,	$(^3H_5)3/2$	12%
	66872	66736	−136	X	X		$(^3F)^4H$	53%,	$(^3H_6)3/2$	32%,	$(^3F)^4I$	6%
	70452	70381	−71		X		$(^3F)^2I$	53%,	$(^1G)^2I$	29%,	$(^3F)^4H$	12%
	77201				X		$(^1G)^2K$	96%				
	79246	79136	−110		X		$(^1G)^2I$	51%,	$(^3F)^2I$	26%,	$(^1I_6)1/2$	17%
	80743	80989	246	X	X		$(^1I_6)1/2$	70%,	$(^1G)^2I$	12%,	$(^3F)^2I$	9%
	83713	83703	−10	X			$(^1I_6)3/2$	87%,	$(^1I_6)1/2$	11%		
	89758					X	$*(^3H)^4H$	100%				
7½	66298	66301	3	X			$(^3H_6)3/2$	96%				
	68285	68305	20		X		$(^3F)^4I$	95%				
	79787				X		$(^1G)^2K$	98%				
	84999	84992	−7	X			$(^1I_6)3/2$	98%				

The $5d^24f$ configuration is illustrated in figure 1. The observed levels are represented by solid lines and the calculated positions of unknown levels are given as dashed lines. The term designations represent the major components, although in many cases these are less than 50 percent. The identity of a unique major component in some cases is impossible. In spite of the intermediate coupling, the low-lying quartets exhibit a regularity in their structure characteristic of *LS*-coupling. This is also true of the equally complex $4f^25d$ configuration of the same ion [1]. Judd has shown that this structure arises from the near equality of $\zeta(4f)$ and $\zeta(5d)$, which results in nearly null non-diagonal matrix elements between terms of maximum multiplicity [22]. The structure of the $(^3F)^4H^0$ term is distorted by the strong mixture with $(^3F)^2G^0$.

The coupling in $4f5d6s$ is *LS*, but not very pure because of the large spin-orbit interactions. The basis states were constructed by first coupling the *f* and *d* electrons to form parent terms and then adding the *s* electron. If more levels had been found, it would probably have been possible to define parameters E_l and E_s for this configuration since they have been essential to other configurations of Pr III and Ce III containing both $4f$ and $5d$ electrons.

4.2. The $4f^25f$ Configuration

This is a well-isolated configuration which is quite amenable to individual treatment. The correspond-

TABLE V. *Fitted parameter values and associated standard errors for the 4f²5f configuration of* Pr III *and corresponding parameters of* Ce III *in units of cm⁻¹*

Parameters	Pr III	Ce III
	$4f^25f$	$4f5f$
A	118394 ± 16	101544 ± 12
$E^1(f^2)$	4983 9	
E^2	22.99 ± 0.05	
E^3	479 ± 1	
α	22.7 ± 0.4	
γ	−56 Fixed	
$F^2(ff')$	3150 ± 53	3150 ± 90
F^4	1870 ± 160	1420 ± 220
F^6	490 ± 190	736 ± ?
G^0	931 ± 9	1175 ± 14
G^2	1511 ± 71	1530 ± 110
G^4	1220 ± 170	870 ± 330
G^6	847 ± 140	736 ± ?
$\zeta_f(f^2)$	760 ± 2	639 ± 7
$\zeta_{f'}$	22 ± 3	26 ± 8
rms error in calculated levels	28 cm⁻¹	39 cm⁻¹

ing configuration $4f5f$ of Ce III reported in reference 3 was treated theoretically by Spector [16], who obtained an rms error in the level predictions of 39 cm⁻¹.

As was found in the Ce III work, the highest purity of eigenvectors results from the use of the J_1l-coupling scheme. However, due to the large value of the exchange parameter $G^0(ff')$, substantial LS-components are obtained when the calculation is carried out in the LS-scheme. Analogous to Ce III, this condition permitted the experimental assignment of many LS terms on the basis of line intensities due to transitions to the LS-coupled $4f^25d$ configuration. These LS designations were essential in establishing the correspondence between the observed and calculated levels.

Initial parameter values were obtained from the $4f^2$ configuration of Pr IV for the $4f^2$ core interactions and from Spector's results in Ce III for the f-f' interaction as well as for $\zeta(5f)$.

Because no levels based on $4f^2(^3P)$ or (^1S) are known only 4 electrostatic core parameters could be fit to the 5 observed core terms. Therefore the "effective" interaction parameter γ was fixed at -56 cm⁻¹, the value obtained by S. Feneuille and N. Pelletier-Allard [23] in a recent calculation of $4f^2(6s+5d)$ of Pr III. The free parameters did not change significantly from their initial values.

All observed levels of odd parity in this region were fitted to the $4f^25f$ configuration. The final rms error in the calculated level positions was 28 cm⁻¹. The resulting parameters are given in table V along with the corresponding ones of $4f5f$ of Ce III.

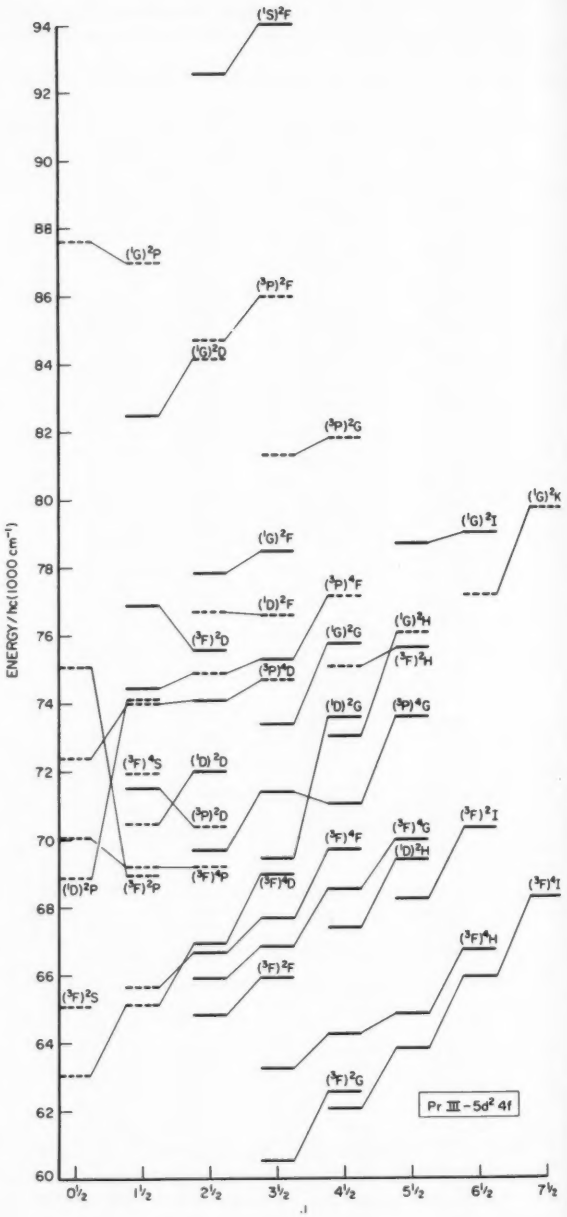

FIGURE 1. *Energy levels of the* $5d^24f$ *configuration of* Pr III.
Levels not observed are represented by dashed lines at their calculated positions.

The calculated and observed energy levels and eigenvectors of $4f^25f$ in J_1l-coupling are given in table VI. The designations show the $4f^2$ core level followed by the quantum number $K=(J_1+l)$ in square brackets. Because of the importance of the LS-coupling designations in the theoretical analysis they are included in a column containing the largest component in this scheme.

TABLE VI. *Calculated energy levels and compositions of the* $4f^2 5f$ *configuration of* Pr III.

Designations are in J_1l-coupling

J	Levels calculated (cm^{-1})	Levels observed (cm^{-1})	Obs. minus Calc.	Composition in J_1l-coupling	Largest component in LS-coupling
$0\frac{1}{2}$	111748			$^3H_4[1]$ 92%	$(^3H)^4D$ 92%
	115693			$^3F_2[1]$ 85%, $^3F_3[0]$ 5%	$(^3F)^2S$ 41%
	116909			$^3F_3[0]$ 70%, $^3F_4[1]$ 15%, $^3F_3[1]$ 8%	$(^3F)^4P$ 60%
	117392			$^3F_3[1]$ 78%, $^3F_3[0]$ 10%, $^3F_2[1]$ 7%	$(^3F)^4D$ 65%
	118943			$^3F_4[1]$ 70%, $^3F_3[0]$ 14%, $^3F_3[1]$ 7%	$(^3F)^2P$ 61%
	120507			$^1G_4[1]$ 85%, $^3F_4[1]$ 12%	$(^1G)^2P$ 80%
	128370			$^1D_2[1]$ 89%, $^3P_2[1]$ 6%	$(^1D)^2P$ 88%
	134088			$^3P_2[1]$ 93%	$(^3P)^4D$ 92%
$1\frac{1}{2}$	111267	111269	2	$^3H_4[2]$ 92%	$(^3H)^4F$ 80%
	111755			$^3H_4[1]$ 90%	$(^3H)^4D$ 54%
	113803	113826	23	$^3H_5[2]$ 93%	$(^3H)^2D$ 45%
	115948			$^3F_2[1]$ 77%, $^3F_4[1]$ 10%, $^3F_2[2]$ 4%	$(^3F)^4P$ 70%
	116812			$^3F_2[2]$ 82%, $^3F_2[1]$ 3%, $^3F_3[2]$ 3%	$(^3F)^2D$ 37%
	117552	117540	−12	$^3F_3[1]$ 26%, $^3F_4[1]$ 22%, $^3F_4[2]$ 21%	$(^3F)^2P$ 24%
	118154	118201	47	$^3F_3[2]$ 59%, $^3F_3[1]$ 25%, $^1G_4[1]$ 7%	$(^3F)^4F$ 34%
	118260			$^3F_4[2]$ 38%, $^3F_3[1]$ 22%, $^3F_3[2]$ 20%	$(^3F)^4D$ 39%
	119010			$^3F_4[1]$ 31%, $^3F_3[1]$ 20%, $^3F_2[1]$ 14%	$(^3F)^4S$ 62%
	121489			$^1G_4[1]$ 48%, $^3F_4[1]$ 27%, $^1G_4[2]$ 15%	$(^1G)^2P$ 43%
	122588			$^1G_4[2]$ 56%, $^3F_4[2]$ 25%, $^1G_4[1]$ 10%	$(^1G)^2D$ 51%
	128163	128214	51	$^1D_2[1]$ 84%, $^3P_2[1]$ 7%	$(^1D)^2P$ 83%
	128942			$^1D_2[2]$ 85%, $^3P_2[2]$ 6%	$(^1D)^2D$ 83%
	132798			$^3P_1[2]$ 89%, $^3P_2[2]$ 11%	$(^3P)^4F$ 62%
	133895			$^3P_2[2]$ 63%, $^3P_2[1]$ 23%, $^3P_1[2]$ 7%	$(^3P)^2D$ 64%
	134173			$^3P_2[1]$ 69%, $^3P_2[2]$ 19%, $^1D_2[1]$ 4%	$(^3P)^4D$ 74%
$2\frac{1}{2}$	111489	111495	6	$^3H_4[2]$ 64%, $^3H_4[3]$ 28%	$(^3H)^4F$ 59%
	111928			$^3H_4[3]$ 63%, $^3H_4[2]$ 28%	$(^3H)^4G$ 52%
	113542	113557	15	$^3H_5[3]$ 45%, $^3H_5[2]$ 44%, $^3F_2[2]$ 6%	$(^3H)^4D$ 23%
	113902	113914	12	$^3H_5[2]$ 46%, $^3H_5[3]$ 45%	$(^3H)^2F$ 38%
	115831	115800	−31	$^3H_6[3]$ 48%, $^3F_2[2]$ 43%	$(^3H)^2D$ 47%
	116471			$^3H_6[3]$ 38%, $^3F_2[2]$ 23%, $^3F_2[3]$ 18%	$(^3F)^4P$ 26%
	116711	116727	16	$^3F_2[3]$ 66%, $^3F_3[3]$ 9%, $^3F_2[2]$ 6%	$(^3F)^4G$ 50%
	117609			$^3F_3[2]$ 51%, $^3F_3[3]$ 26%, $^1G_4[3]$ 6%	$(^3F)^2F$ 30%
	117651	117686	35	$^3F_3[3]$ 33%, $^3F_4[2]$ 14%, $^3F_2[2]$ 13%	$(^3F)^4D$ 42%
	118612			$^3F_3[3]$ 32%, $^3F_4[3]$ 26%, $^3F_4[2]$ 13%	$(^3F)^4F$ 54%
	118952			$^3F_4[2]$ 51%, $^3F_4[3]$ 22%, $^1G_4[3]$ 10%	$(^3F)^2D$ 31%
	120686			$^1G_4[3]$ 57%, $^3F_4[3]$ 20%, $^1G_4[2]$ 17%	$(^1G)^2F$ 53%
	121763			$^1G_4[2]$ 66%, $^3F_4[3]$ 15%, $^1G_4[3]$ 7%	$(^1G)^2D$ 64%
	128590			$^1D_2[3]$ 85%, $^3P_2[3]$ 9%	$(^1D)^2F$ 83%
	128833			$^1D_2[2]$ 84%, $^3P_2[2]$ 7%	$(^1D)^2D$ 82%
	132127			$^3P_0[3]$ 86%, $^3P_1[3]$ 10%	$(^3P)^4G$ 64%
	132709			$^3P_1[3]$ 86%, $^3P_0[3]$ 8%	$(^3P)^2D$ 37%
	133044			$^3P_1[2]$ 64%, $^1I_6[3]$ 18%, $^3P_2[2]$ 13%	$(^3P)^4F$ 28%
	133832			$^3P_2[3]$ 45%, $^1I_6[3]$ 41%, $^3P_2[2]$ 4%	$(^1I)^2F$ 41%
	134221			$^3P_2[2]$ 54%, $^3P_1[2]$ 20%, $^3P_2[3]$ 12%	$(^3P)^4D$ 55%
	136510			$^1I_6[3]$ 37%, $^3P_2[3]$ 29%, $^3P_2[2]$ 24%	$(^3P)^2F$ 52%
	163236			$^1S_0[3]$ 99%	$(^1S)^2F$ 99%
$3\frac{1}{2}$	110340	110334	−6	$^3H_4[4]$ 91%	$(^3H)^4H$ 81%
	111381	111343	−38	$^3H_4[3]$ 87%, $^3H_4[4]$ 4%	$(^3H)^2G$ 40%
	113308	113292	−16	$^3H_5[4]$ 50%, $^3H_5[3]$ 46%	$(^3H)^4F$ 44%
	113639	113631	−8	$^3H_5[3]$ 46%, $^3H_5[4]$ 40%, $^3F_3[4]$ 3%	$(^3H)^4G$ 51%
	115405	115421	16	$^3H_6[3]$ 36%, $^3H_6[4]$ 28%, $^3F_2[3]$ 27%	$(^3H)^4D$ 35%
	115672	115670	−2	$^3F_2[4]$ 89%, $^3F_3[4]$ 4%	$(^3F)^4H$ 82%
	116021	116022	1	$^3H_6[3]$ 41%, $^3H_6[4]$ 39%, $^3F_4[3]$ 4%	$(^3H)^2F$ 42%
	117029	117045	16	$^3F_2[3]$ 57%, $^3H_6[4]$ 25%, $^3F_3[3]$ 5%	$(^3F)^4G$ 21%
	117671	117647	−24	$^3F_3[4]$ 64%, $^3F_3[3]$ 10%, $^1G_4[3]$ 8%	$(^3F)^2F$ 33%
	118143			$^3F_4[3]$ 26%, $^1G_4[3]$ 19%, $^3F_4[4]$ 17%	$(^3F)^4D$ 40%
	118321	118319	−2	$^3F_3[3]$ 60%, $^3F_3[4]$ 16%, $^3F_4[4]$ 7%	$(^3F)^2G$ 41%
	118967			$^3F_4[4]$ 47%, $^3F_4[3]$ 21%, $^1G_4[4]$ 18%	$(^3F)^4F$ 41%
	121401			$^1G_4[3]$ 41%, $^3F_4[3]$ 29%, $^1G_4[4]$ 23%	$(^1G)^2F$ 36%
	121599			$^1G_4[4]$ 50%, $^3F_4[4]$ 21%, $^1G_4[3]$ 17%	$(^1G)^2G$ 45%
	128456	128453	−3	$^1D_2[4]$ 87%, $^3P_2[4]$ 6%,	$(^1D)^2G$ 86%
	129012			$^1D_2[3]$ 88%, $^3P_2[3]$ 6%	$(^1D)^2F$ 86%
	132256			$^3P_0[3]$ 76%, $^3P_1[4]$ 8%, $^3P_1[3]$ 8%	$(^3P)^4G$ 41%
	132760			$^3P_1[4]$ 62%, $^1I_6[4]$ 25%, $^1I_6[3]$ 6%	$(^3P)^2G$ 37%
	132869			$^3P_1[3]$ 72%, $^3P_0[3]$ 11%, $^3P_1[4]$ 8%	$(^3P)^4D$ 53%

TABLE VI. *Calculated energy levels and compositions of the* $4f^25f$ *configuration of* Pr III.—Continued

Designations are in J_1l-coupling

J	Levels calculated (cm^{-1})	Levels observed (cm^{-1})	Obs. minus Calc.	Composition in J_1l-coupling	Largest component in LS-coupling
	133585			$^1I_6[3]$ 42%, $^3P_2[4]$ 33%, $^1I_6[4]$ 17%	$(^1I)^2F$ 42%
	134108			$^3P_2[3]$ 75%, $^3P_2[4]$ 11%, $^1D_2[3]$ 7%	$(^3P)^4F$ 54%
	134896			$^1I_6[4]$ 48%, $^3P_1[4]$ 19%, $^1I_6[3]$ 10%	$(^1I)^2G$ 48%
	136377			$^3P_2[4]$ 45%, $^1I_6[3]$ 37%, $^3P_2[3]$ 11%	$(^3P)^2F$ 54%
	163249			$^1S_0[3]$ 99%	$(^1S)^2F$ 99%
$4\frac{1}{2}$	110906	110922	16	$^3H_4[4]$ 66%, $^3H_4[5]$ 21%, $^3H_5[5]$ 8%	$(^3F)^4H$ 70%
	111915	111993	78	$^3H_4[5]$ 72%, $^3H_4[4]$ 25%	$(^3F)^2I$ 58%
	113154	113159	5	$^3H_5[5]$ 62%, $^3H_5[4]$ 26%, $^3H_4[4]$ 6%	undefined
	113783	113780	−3	$^3H_5[4]$ 66%, $^3H_5[5]$ 28%	$(^3H)^2H$ 35%
	115334	115324	−10	$^3H_6[4]$ 46%, $^3H_6[5]$ 26%, $^3F_2[4]$ 18%	$(^3H)^4F$ 35%
	115519	115500	−19	$^3H_6[5]$ 59%, $^3H_6[4]$ 36%	$(^3H)^2G$ 54%
	115841			$^3F_2[5]$ 87%, $^3F_2[4]$ 3%	$(^3H)^4H$ 71%
	116456	116453	−3	$^3F_2[4]$ 52%, $^3F_3[5]$ 20%, $^3F_3[4]$ 7%	$(^3P)^4H$ 54%
	117516			$^3F_3[5]$ 44%, $^3F_2[4]$ 17%, $^3F_4[5]$ 11%	$(^3F)^2H$ 36%
	118076	118081	5	$^3F_3[4]$ 40%, $^3F_4[5]$ 18%, $^3F_4[4]$ 16%	$(^3F)^2G$ 36%
	118495	118469	−26	$^3F_4[5]$ 36%, $^3F_3[5]$ 32%, $^3F_3[4]$ 14%	$(^3F)^4G$ 36%
	118911			$^3F_4[4]$ 43%, $^3F_3[4]$ 24%, $^1G_4[4]$ 22%	$(^3F)^4F$ 65%
	121376	121383	7	$^1G_4[5]$ 51%, $^3F_4[5]$ 21%, $^1G_4[4]$ 14%	$(^1G)^2H$ 46%
	122121			$^1G_4[4]$ 50%, $^3F_4[4]$ 24%, $^1G_4[5]$ 14%	$(^1G)^2G$ 45%
	128360	128353	−7	$^1D_2[5]$ 78%, $^1D_2[4]$ 10%, $^3P_2[5]$ 7%	$(^1D)^2H$ 77%
	128584	128569	−15	$^1D_2[4]$ 79%, $^1D_2[5]$ 11%, $^3P_2[4]$ 6%	$(^1D)^2G$ 78%
	132719			$^3P_1[4]$ 89%, $^1I_6[4]$ 9%	$(^3P)^4G$ 48%
	133285			$^1I_6[5]$ 80%, $^3P_2[5]$ 11%	$(^1I)^2H$ 80%
	133459			$^1I_6[4]$ 43%, $^3P_2[5]$ 29%, $^1I_6[5]$ 17%	$(^1I)^2G$ 43%
	134030			$^3P_2[4]$ 90%	$(^3P)^4F$ 65%
	135078			$^3P_2[5]$ 52%, $^1I_6[4]$ 37%, $^3P_1[4]$ 5%	$(^3P)^2G$ 54%
$5\frac{1}{2}$	110308	110295	−13	$^3H_4[6]$ 83%, $^3H_4[5]$ F3%	$(^3H)^4K$ 74%
	110876	110881	5	$^3H_4[5]$ 78%, $^3H_4[6]$ 12%	$(^3H)^2I$ 41%
	112636	112643	7	$^3H_5[5]$ 66%, $^3H_5[6]$ 29%	$(^3H)^4H$ 61%
	113664	113664	0	$^3H_5[6]$ 61%, $^3H_5[5]$ 28%, $^3H_4[5]$ 4%	$(^3H)^4I$ 67%
	115402	115403	1	$^3H_6[6]$ 64%, $^3H_6[5]$ 21%, $^3F_4[5]$ 5%	$(^3H)^2H$ 34%
	115934	115933	−1	$^3H_6[5]$ 50%, $^3H_6[6]$ 19%, $^3F_3[5]$ 6%	$(^3H)^4G$ 41%
	116276	116309	33	$^3F_2[5]$ 63%, $^3H_6[5]$ 11%, $^3H_6[6]$ 10%	$(^3F)^4I$ 31%
	117320	117323	3	$^3F_3[6]$ 35%, $^3F_3[5]$ 26%, $^3F_4[6]$ 22%	$(^3F)^4H$ 28%
	117577	117574	−3	$^3F_3[5]$ 51%, $^3F_3[6]$ 32%, $^1G_4[6]$ 6%	$(^3F)^2I$ 48%
	118304	118272	−32	$^3F_4[5]$ 22%, $^3F_4[6]$ 17%, $^1G_4[5]$ 14%	$(^3F)^4G$ 32%
	118926	118879	−47	$^3F_4[5]$ 35%, $^1G_4[6]$ 19%, $^3F_4[6]$ 18%	$(^3F)^2H$ 37%
	121078	121095	17	$^1G_4[5]$ 45%, $^3F_4[5]$ 23%, $^1G_4[6]$ 19%	$(^1G)^2H$ 40%
	121546	121532	−14	$^1G_4[6]$ 35%, $^3F_4[6]$ 31%, $^1G_4[5]$ 26%	$(^1G)^2I$ 31%
	128364	128382	18	$^1D_2[5]$ 89%, $^3P_2[5]$ 8%	$(^1D)^2H$ 88%
	133162			$^1I_6[6]$ 83%, $^1I_6[5]$ 16%	$(^1I)^2I$ 83%
	133322			$^1I_6[5]$ 76%, $^1I_6[6]$ 16%	$(^1I)^2H$ 76%
	133955			$^3P_2[5]$ 84%, $^1D_2[5]$ 8%	$(^3P)^4G$ 83%
$6\frac{1}{2}$	110535	110531	−4	$^3H_4[7]$ 97%	$(^3H)^4L$ 89%
	111115	111110	−5	$^3H_4[6]$ 87%, $^3H_5[7]$ 8%	$(^3H)^4K$ 59%
	112756	112770	14	$^3H_5[7]$ 51%, $^3H_5[6]$ 38%	$(^3H)^2I$ 39%
	113570	113600	30	$^3H_5[6]$ 49%, $^3H_5[7]$ 37%, $^3H_6[6]$ 9%	$(^3H)^2K$ 43%
	114792	114797	5	$^3H_6[6]$ 69%, $^3H_6[7]$ B4%	$(^3H)^4H$ 48%
	115369	115408	39	$^3H_6[7]$ 64%, $^3H_6[6]$ 19%, $^3F_3[6]$ 8%	$(^3H)^4I$ 60%
	117263	117248	−15	$^3F_3[6]$ 56%, $^3F_4[6]$ 29%, $^1G_4[6]$ 11%	$(^3F)^4H$ 54%
	117762	117775	13	$^3F_4[7]$ 28%, $^3F_4[6]$ 28%, $^3F_3[6]$ 21%	$(^3F)^4I$ 61%
	118629	118611	−18	$^3F_4[7]$ 36%, $^1G_4[7]$ 25%, $^3F_4[6]$ 19%	$(^3F)^2I$ 55%
	120502	120499	−3	$^1G_4[6]$ 61%, $^3F_4[6]$ 21%, $^1G_4[7]$ 15%	$(^1G)^2I$ 56%
	121437	121431	−6	$^1G_4[7]$ 50%, $^3F_4[7]$ 30%, $^1G_4[6]$ 14%	$(^1G)^2K$ 44%
	132708			$^1I_6[7]$ 100%	$(^1I)^2K$ 100%
	133181			$^1I_6[6]$ 99%	$(^1I)^2I$ 99%
$7\frac{1}{2}$	111339	111335	−4	$^3H_4[7]$ 82%, $^3H_5[8]$ 16%	$(^3H)^4L$ 67%
	112895	112896	1	$^3H_5[7]$ 88%, $^3H_6[8]$ 6%	$(^3H)^4K$ 72%
	113832	113834	2	$^3H_5[8]$ 79%, $^3H_4[7]$ 15%	$(^3H)^2L$ 76%
	115666	115672	6	$^3H_6[8]$ 71%, $^3H_6[7]$ 14%, $^3H_5[7]$ 5%	$(^3H)^2K$ 57%
	116196	116239	43	$^3H_6[7]$ 78%, $^3H_6[8]$ 17%	$(^3H)^4I$ 72%
	118051	118063	12	$^3F_4[7]$ 70%, $^1G_4[7]$ 19%, $^3H_6[8]$ 2%	$(^3F)^4I$ 65%
	121087	121119	32	$^1G_4[7]$ 73%, $^3F_4[7]$ 23%	$(^1G)^2K$ 67%
	132780			$^1I_6[7]$ 98%	$(^1I)^2K$ 98%
	133421	133352	−69	$^1I_6[8]$ 98%	$(^1I)^2L$ 98%

TABLE VI. *Calculated energy levels and compositions of the* $4f^25f$ *configuration of* Pr III.—Continued

Designations are in J_1l-coupling

J	Levels calculated (cm^{-1})	Levels observed (cm^{-1})	Obs. minus Calc.	Composition in J_1l-coupling	Largest component in LS-coupling
$8\frac{1}{2}$	113026	113024	−2	$^3H_5[8]$ 94%	$(^3H)^4L$ 94%
	114733	114726	−7	$^3H_6[8]$ 95%	$(^3H)^4K$ 95%
	116497	116490	−7	$^3H_6[9]$ 89%, $^3H_5[8]$ 6%	$(^3H)^2L$ 89%
	133120	133194	74	$^1I_6[9]$ 98%	$(^1I)^2M$ 98%
	133438	133373	−65	$^1I_6[8]$ 97%	$(^1I)^2L$ 97%
$9\frac{1}{2}$	114978	114971	−7	$^3H_6[9]$ 100%	$(^3H)^4L$ 100%
	133191	133242	51	$^1I_6[9]$ 100%	$(^1I)^2M$ 100%

The energy level structure of $4f^25f$ is shown in figure 2 in J_1l-coupling. Pairs of levels of equal J_1 and K are connected and the $4f^2$ core is indicated. The experimentally derived levels are drawn with solid lines, and those not found are drawn with dashed lines at their calculated positions. By comparing this structure with that of $4f5f$ of Ce III shown in figure 4 of reference 3, we note a decrease in the pair splittings in Pr III, indicating a trend with increasing Z to purer J_1l coupling. The electrostatic parameter $G^0(ff')$ has decreased by 20 percent from its value in Ce III while $F^2(ff')$ remains unchanged.

4.3. The $4f^26d$ and $4f^27s$ Configurations

Levels of both of these configurations were given in ref. 2, but were all designated as $4f^26d$. They were derived from transitions to $4f^26p$. No distinction between configurations was evident from relative line intensities.

The present analysis of this transition array revealed 26 more levels belonging to the upper two configurations. A clue as to the designation of these levels is the fact that nearly all observed transitions from a given upper level has the same $4f^2$ core level of $4f^26p$ in common. This arises from the condition that both the upper and lower configurations exhibit good J_1j-coupling.

The two configurations $4f^26d$ and $4f^27s$ were expected to overlap because of the arrangement of the corresponding Ce III configurations $4f6d$ and $4f7s$. To unravel them, I calculated their energy levels using the parameters of Ce III for the f-d and f-s interactions, and compared the result with the known levels. It was then possible to recognize the level groupings in the two configurations.

For both configurations, levels based only on the two core levels ^3H and ^3F are known. Therefore, only one core electrostatic parameter, namely E^3, could be determined. The ratios E^1/E^3 and E^1/E^2 were fixed at the values 10.3 and 216, respectively. These ratios are nearly equal in the configurations [17, 23] $4f^3$, $4f^2(5d+6s)$, and $4f^26p$ (table III of present work) of Pr III, and $4f^2$ of Pr IV(see table III). The parameters α and γ of the $4f^2$ core were fixed at the values found in $4f^26s$ of Pr III [23].

The least squares adjustment of the $4f$-$6d$ and $4f$-$7s$ interaction parameters produced the well-defined values given in tables VII and IX. The corresponding parameters of $4f6d$ in Ce III are also given. A diagonalization with these final parameters provided the calculated levels and eigenvectors in J_1j-coupling shown in table VIII for the $4f^2(^3H,^3F)6d$ levels. A complete listing of the calculated results is not given because of the small number of known levels. The eigenvectors were also calculated in the J_1l-coupling scheme. The overall purity of levels was found to be lower than in J_1j, as is the case in Ce III for $4f6d$ [16].

A diagram of the configurations $4f^2(^3H, ^3F)$ $6d$ and $7s$ is given in figure 3. As in figures 1 and 2, observed levels are given as solid lines while those not yet located are represented by dashed lines at their calculated positions. Levels are connected which are based on the same J_1 core level.

TABLE VII. *Fitted parameter values and associated standard errors for the* $4f^26d$ *configuration of* Pr III *and corresponding parameters of* Ce III *in units of* cm^{-1}.

Parameters	Pr III	Ce III
	$4f^26d$	$4f6d$
A	108321 ± 20	91509 ± 36
$E^1(f^2)$	4927 Fixed E^1/E^3	
E^2	22.8 Fixed E^2/E^3	
E^3	479 ± 2	
α	23 Fixed	
γ	−56 Fixed	
$F^2(fd)$	4070 ± 100	3260 ± 320
F^4	2500 ± 190	1730 ± 690
G^1	1396 ± 60	1330 ± 180
G^3	1500 ± 220	540 ± 690
G^5	2590 ± 160	1980 ± 610
ζ_f	766 ± 3	642 ± 20
ζ_d	197 ± 7	239 ± 36
rms error in calculated levels	31 cm^{-1}	139 cm^{-1}

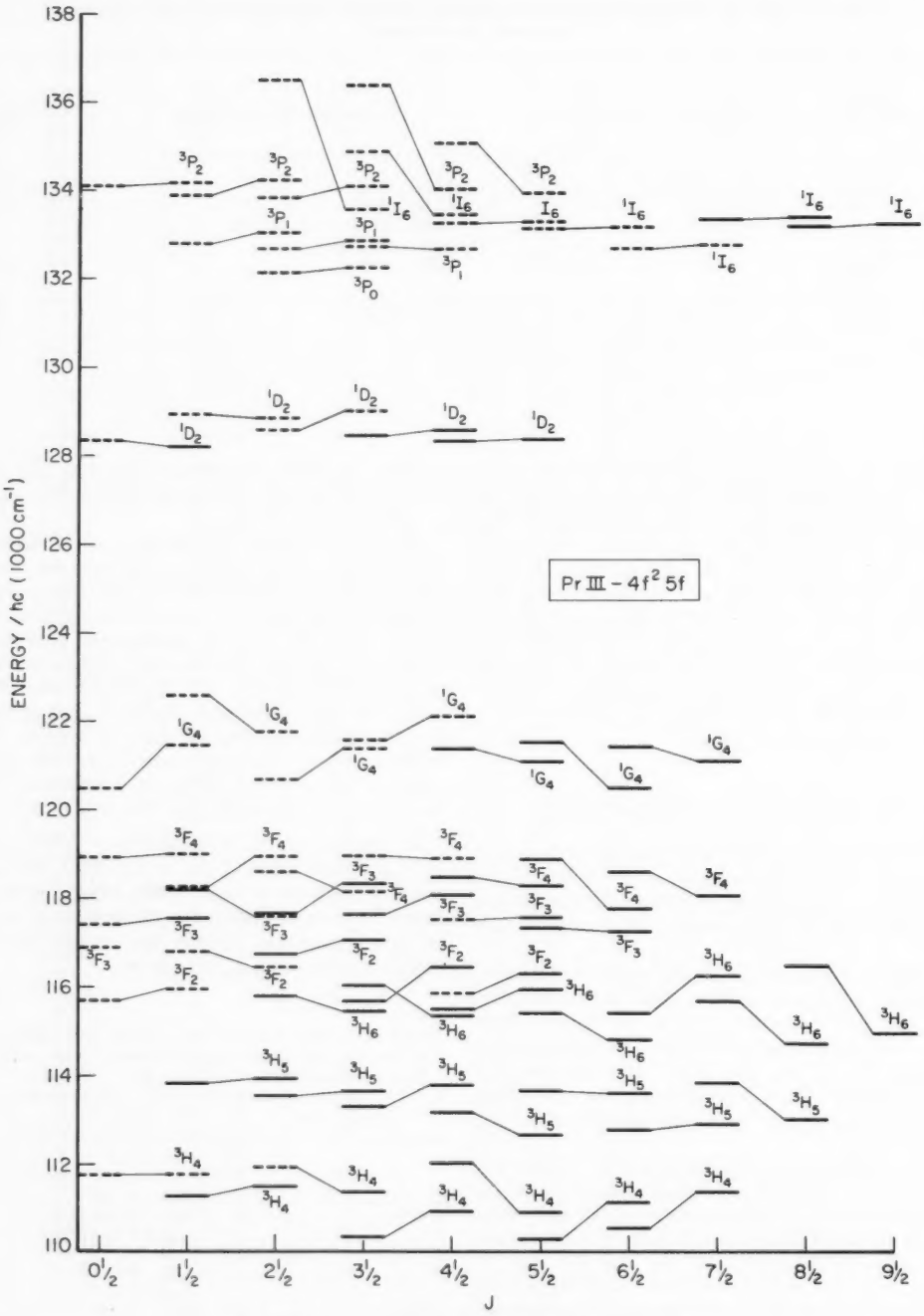

FIGURE 2. *Energy levels of the* $4f^25f$ *configuration of* Pr III.
Pairs of levels of identical $4f^3$ core and quantum number K in the J_1l-coupling scheme are connected. Levels not observed are represented by dashed lines at their calculated positions.

TABLE VIII. *Calculated energy levels and compositions of the* $4f^26d$ *configuration of* Pr III.

Designations are in J_1j-coupling. Only levels built primarily on $4f^2(^3H)$ and $4f^2(^3F)$ core levels are given.

J	Levels calculated (cm^{-1})	Levels observed (cm^{-1})	Obs. minus calc.	Composition in J_1j-coupling
$0^1/_2$	105740			$(^3F_2)3/2$ 92%
	105973			$(^3F_2)5/2$ 93%
	107684			$(^3F_3)5/2$ 99%
$1^1/_2$	101658			$(^3H_4)5/2$ 97%
	106059			$(^3F_2)3/2$ 92%
	106154			$(^3F_2)5/2$ 94%
	107120			$(^3F_3)3/2$ 96%
	107844			$(^3F_3)5/2$ 82%, $(^3F_4)5/2$ 7%, $(^3F_3)3/2$ 4%
	108345			$(^3F_4)5/2$ 56%, $(^1G_4)5/2$ 31%, $(^3F_3)5/2$ 10%
$2^1/_2$	101071	101071	0	$(^3H_4)3/2$ 50%, $(^3H_4)5/2$ 45%
	101715	101666	−49	$(^3H_4)5/2$ 52%, $(^3H_4)3/2$ 43%
	104106			$(^3H_5)5/2$ 94%
	105741			$(^3F_2)3/2$ 85%, $(^3F_2)5/2$ 8%
	106369			$(^3F_2)5/2$ 87%, $(^3F_2)3/2$ 6%
	107280			$(^3F_3)3/2$ 83%, $(^3F_3)5/2$ 6%, $(^3F_4)5/2$ 4%
	107600			$(^3F_4)3/2$ 62%, $(^1G_4)3/2$ 26%, $(^3F_3)3/2$ 6%
	107799			$(^3F_3)5/2$ 75%, $(^3F_3)3/2$ 8%, $(^1G_4)5/2$ 7%
	108809			$(^3F_4)5/2$ 52%, $(^1G_4)5/2$ 25%, $(^3F_3)5/2$ 14%
$3^1/_2$	100783	100789	6	$(^3H_4)3/2$ 65%, $(^3H_4)5/2$ 31%
	101477	101446	−31	$(^3H_4)5/2$ 64%, $(^3H_4)3/2$ 28%
	103361	103309	−52	$(^3H_5)3/2$ 93%
	103955	103896	−59	$(^3H_5)5/2$ 95%
	105514			$(^3F_2)3/2$ 89%, $(^3F_2)5/2$ 7%,
	106433			$(^3F_2)5/2$ 77%, $(^3F_3)3/2$ 13%
	106496			$(^3H_6)5/2$ 86%, $(^3F_3)3/2$ 5%
	107328	107299	−29	$(^3F_3)3/2$ 64%, $(^3F_4)3/2$ 8%, $(^3F_3)5/2$ 8%
	107890			$(^3F_4)3/2$ 34%, $(^3F_4)5/2$ 26%, $(^1G_4)3/2$ 19%
	108173			$(^3F_3)5/2$ 54%, $(^3F_3)3/2$ 12%, $(^3F_4)3/2$ 11%
	108305			$(^1G_4)5/2$ 30%, $(^3F_4)5/2$ 27%, $(^3F_3)5/2$ 25%
$4^1/_2$	100415	100430	15	$(^3H_4)3/2$ 96%,
	100954	100947	−7	$(^3H_4)5/2$ 94%
	102853	102830	−23	$(^3H_5)3/2$ 79%, $(^3H_5)5/2$ 18%,
	103327	103335	8	$(^3H_5)5/2$ 74%, $(^3H_5)3/2$ 18%
	105519	105567	48	$(^3H_6)3/2$ 96%
	106245			$(^3F_2)5/2$ 61%, $(^3H_6)5/2$ 25%, $(^3F_3)3/2$ 8%
	106346			$(^3H_6)5/2$ 69%, $(^3F_2)5/2$
	107190			$(^3F_3)3/2$ 54%, $(^3F_4)3/2$ 19%, $(^1G_4)3/2$ 12%
	107819			$(^3F_3)5/2$ 83%, $(^1G_4)3/2$ 8%
	107872	107854	−18	$(^3F_4)3/2$ 32%, $(^3F_3)3/2$ 20%, $(^1G_4)3/2$ 13%
	108600			$(^3F_4)5/2$ 42%, $(^1G_4)5/2$ 33%, $(^3F_3)3/2$ 9%
$5^1/_2$	100617	100625	8	$(^3H_4)3/2$ 96%
	101165	101165	0	$(^3H_4)5/2$ 94%
	102639	102617	−22	$(^3H_5)3/2$ 95%
	103336	103344	8	$(^3H_5)5/2$ 96%
	104924	104905	−19	$(^3H_6)3/2$ 93%
	105458	105450	−8	$(^3H_6)5/2$ 82%
	107403			$(^3F_3)5/2$ 67%, $(^3F_4)3/2$ 24%
	107720			$(^3F_4)3/2$ 29%, $(^3F_4)5/2$ 20%, $(^3F_3)5/2$ 19%
	108527	108559	32	$(^3F_4)5/2$ 42%, $(^1G_4)5/2$ 21%, $(^1G_4)3/2$ 15%
$6^1/_2$	101667	101680	13	$(^3H_4)5/2$ 84%, $(^3H_5)3/2$ 10%
	102988	102982	−6	$(^3H_5)3/2$ 51%, $(^3H_5)5/2$ 47%
	103764	103805	41	$(^3H_5)5/2$ 48%, $(^3H_5)3/2$ 39%
	105020	105019	−1	$(^3H_6)3/2$ 86%, $(^3H_6)5/2$ 13%
	105644	105632	−12	$(^3H_6)5/2$ 85%, $(^3H_6)3/2$ 12%
	107979			$(^3F_4)5/2$ 70%, $(^1G_4)5/2$ 27%
$7^1/_2$	103488	103484	−4	$(^3H_5)5/2$ 95%
	105080	105050	−30	$(^3H_6)5/2$ 57%, $(^3H_6)3/2$ 42%
	106356			$(^3H_6)3/2$ 54%, $(^3H_6)5/2$ 41%
$8^1/_2$	105513			$(^3H_6)5/2$ 100%

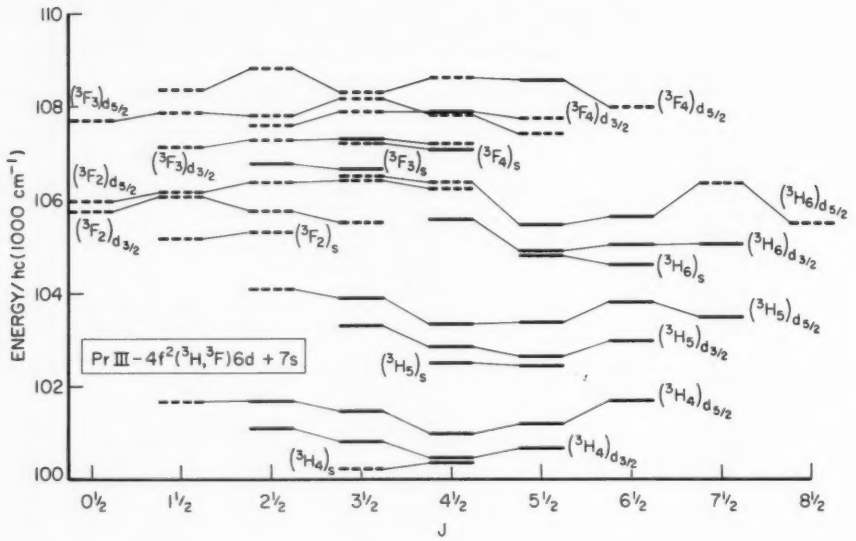

FIGURE 3. *Energy levels of the* $4f^2 6d$ *and* $4f^2 7s$ *configurations of* Pr III designated in $J_1 j$-coupling. The $4f^2$ core levels are given in parentheses followed by subscript d or s for the $6d$ or $7s$ configurations.
Levels not observed are represented by dashed lines at their calculated positions.

4.4. The $4f^2 8s$ Configuration

Only a few high-lying levels were found by adding the vacuum ultraviolet lines of Pr III to the $4f^2 6p$ group. These were characterized by the strict adherence of the observed lines to core level selection rules in $J_1 j$-coupling. They were therefore either $4f^2 7d$ or $4f^2 8s$ levels. Their pair structure suggested the latter configuration and I attempted to fit them accordingly.

Here again, only levels based on the ^3H and ^3F core levels were found. Therefore, the same fixed conditions on $4f^2$ core parameters were used as for $4f^2 6d$ and $4f^2 7s$. The results of least squares fitting of the remaining parameters are given in table IX. The free core parameters E^3 and ζ_{4f} are practically identical to those found for $4f^2 6d$ and $4f^2 7s$. Also, the parameter $G^3(fs)$ shows the same fractional increase from the Ce III value as does the same parameter of $4f^2 7s$ and $4f^2 6s$. These results strongly support the interpretation of these levels as $4f^2 8s$.

TABLE IX. *Fitted parameter values and associated standard errors for the* $4f^2 7s$ *and* $4f^2 8s$ *configurations of* Pr III *in units of* cm^{-1}.

Parameters	Pr III		Pr III	
	$4f^2 7s$		$4f^2 8s$	
A	107226	±32	135946	±8
$E^1(f^2)$	4950	Fixed E^1/E^3	4936	Fixed E^1/E^3
E^2	22.9	Fixed E^2/E^3	22.8	Fixed E^2/E^3
E^3	482	±2	480.3	±0.7
α	23	Fixed	23	Fixed
γ	−56	Fixed	−56	Fixed
$G^3(fs)$	590	±110	350	±28
ζ_f	768	±6	761	±1
rms error in calculated levels	19 cm^{-1}		7 cm^{-1}	

5. The Ionization Energy

The present extension of the analysis of Pr III provides a three member $4f^2 ns$ series ($n = 6, 7, 8$) which is suitable for a determination of the ionization energy of this ion.

The levels based on the ^3H core term are available in the three configurations, and the purity of these levels is above 90 percent (in contrast to the ^3F levels). Therefore, for the series terms I used the center of gravity of the levels built on the ^3H core. For the missing level in $4f^2(^3H)7s$ and $4f^2(^3H)8s$ the calculated position was substituted. The centers of gravity of

$4f^2(^3H)6s$, $7s$, and $8s$ and the fitted effective principal quantum numbers are:

Configuration	c.g. (cm^{-1})	n^*
$4f^2(^3H)6s$	31137	2.6045
$4f^2(^3H)7s$	102738	3.6535
$4f^2(^3H)8s$	131507	4.6732

The Ritz formula to which these values are fitted is:

$$T=-9R/(n-3.2959-6.8432\times10^{-7}\,T)^2.$$

To reduce the limit of this series to the lowest limit corresponding to the ionization energy, the center of gravity of the ^3H term of $4f^2$ observed in Pr IV [18] was subtracted. This gives the value of 174284 cm^{-1} for the lowest series limit of Pr III.

The error resulting from the use of this three term series may be estimated from La III [24], where a four term ns series ($n=6$, 7, 8, 9) is known. The ionization energy derived from this series agrees with those obtained with nf and ng series to within 10 cm^{-1}. By using only the first three terms of the ns series in La III one obtains a value for the ionization energy differing from that given by the four term series by -115 cm^{-1}. I therefore added an equivalent fractional amount to the calculated ionization energy of Pr III obtained from the three term series and estimate the uncertainty to be equal to this quantity. This gives the ionization energy of Pr III as 21.625 eV (174420 cm^{-1}) with an estimated uncertainty of 0.016 eV (130 cm^{-1}).

This procedure for estimating the correction for the quadratic term in the quantum defect is valid if series of this kind generally exhibit the same behavior. It was noted in reference 10 that an examination of the curves of the quantum defect (σ) versus term energy (T) for the ns series of a large number of alkali-like atoms shows that their shapes are similar, and for the same period are practically identical (see table IV of ref. 10). Therefore, the use of the four-member series in La III to estimate the error in the ionization energy derived from a three-member series in Pr III is reasonable.

I am pleased to thank Prof. R. Chabbal, Director of Laboratoire Aimé Cotton, Orsay, France, for making available the excellent computer programs for calculating energy matrices written by Y. Bordarier and A. Carlier of his staff. My first experience with these programs was gained at his laboratory where part of the present theoretical analysis was carried out.

I also thank Mrs. Z. Goldschmidt for providing NBS with the library of energy matrices compiled at Hebrew University, Jerusalem, Israel, by Prof. G. Racah and his co-workers.

The assistance of Dr. R. Cowan of the Los Alamos Scientific Laboratory in checking for errors in the energy matrices by independently calculating them was extremely valuable.

Dr. V. Kaufman generously contributed the exposures of the Pr spark made with the Eagle vacuum spectrograph.

6. References

[1] Sugar, J., Johns Hopkins Spectroscopic Rept. No. 22 (1961).
[2] Sugar, J., J. Opt. Soc. Am. **53,** 831 (1963).
[3] Sugar, J., J. Opt. Soc. Am. **55,** 33 (1965).
[4] Kaufman, V., and Andrew, K. L., J. Opt. Soc. Am. **52,** 1223 (1962).
[5] Kaufman, V., Radziemski, L. J., Jr., and Andrew, K L., J. Opt. Soc. Am. **56,** 911 (1966).
[6] Kaufman, V., and Ward, J. F., J. Opt. Soc. Am. **56,** 1591 (1966).
[7] Kaufman, V., and Ward, J. F., Appl. Opt. 6, 43 (1967).
[8] Edlén, B., Rep. Prog. Phys. **26,** 181 (1963).
[9] The present work extended through two generations of computer programs for energy level searching. The first was written by G. Racah at NBS for the IBM 7090, and the second by J. Tech of NBS for the UNIVAC 1108.
[10] Reader, J. and Sugar, J., Phys. Rev. **137,** B784 (1965).
[11] Racah, G., Bull. Res. Counc. of Israel **8F,** 1 (1959).
[12] Fano, U., Pratts, F., and Goldschmidt, Z., Phys. Rev. **129,** 2643 (1963).
[13] Racah, G., Phys. Rev. **62,** 438 (1942).
[14] Racah, G., Phys. Rev. **76,** 1352 (1949).
[15] Goldschmidt, Z. B., Spectroscopic and Group Theoretical Methods in Physics, edited by F. Bloch et. al. (John Wiley & Sons, Inc., New York, 1968).
[16] Spector N., J. Opt. Soc. Am. **55,** 492 (1965).
[17] Trees, R. E., J. Opt. Soc. Am. **54,** 651 (1964).
[18] Sugar J., J. Opt. Soc. Am. **55,** 1058 (1965).
[19] Spector N., J. Opt. Soc. Am. **54,** 1359 (1964).
[20] Sack, N., Phys. Rev. **102,** 1302 (1956).
[21] The parameters of $4f^2$ for Pr IV given in table III differ from those in ref. 18 where γ was ignored.
[22] Judd, B. R., J. Opt. Soc. Am. **58,** 1311 (1968).
[23] Feneuille, S., and Pelletier-Allard N., Physica **40,** 347 (1969) The parameter γ was added in $4f^26s$. The calculation of $4f^25d$ was greatly improved by the addition of two-body effective parameters for nonequivalent electrons.
[24] Sugar J., and Kaufman, V., J. Opt. Soc. Am. **55,** 1283 (1965).

TABLE X. *Observed spectral lines of* Pr III *in the vacuum ultra violet region*

λ_{vac} Å	Intensity	σ (cm^{-1})	Classification [a]	λ_{vac} Å	Intensity	σ (cm^{-1})	Classification [a]
2103.455	3	47540.8	$23844\,{}_{9/2} - 71385^{\circ}{}_{7/2}$	2085.148	2	47958.2	
2102.907	20	47553.2		2084.954	10	47962.7	
2102.492	3	47562.6		2084.699	3	47968.5	$23532\,{}_{5/2} - 71501^{\circ}{}_{3/2}$
2101.877	10	47576.5					$25409\,{}_{7/2} - 73378^{\circ}{}_{7/2}$
2101.778	100	47578.8	$23442\,{}_{11/2} - 71021^{\circ}{}_{9/2}$	2084.344	60	47976.7	$14558\,{}_{9/2} - 62535^{\circ}{}_{9/2}$
2101.651	2	47581.6		2083.504	1	47996.1	$25033\,{}_{9/2} - 73029^{\circ}{}_{9/2}$
2099.948	5	47620.2	$25409\,{}_{7/2} - 73029^{\circ}{}_{9/2}$	2083.412	1	47998.2	$19872\,{}_{7/2} - 67870^{\circ}{}_{9/2}$
2099.757	50	47624.6		2083.123	400	48004.8	$13352\,{}_{11/2} - 61357^{\circ}{}_{9/2}$
2099.757	50	47624.6	$29267\,{}_{5/2} - 76892^{\circ}{}_{3/2}$	2082.879	2	48010.5	
2099.402	200	47632.6	$16135\,{}_{7/2} - 63768^{\circ}{}_{7/2}$	2082.810	3	48012.1	$21418\,{}_{5/2} - 69431^{\circ}{}_{7/2}$
2098.974	3	47642.3		2082.653	3	48015.7	
2098.903	20	47643.9	$20848\,{}_{5/2} - 68492^{\circ}{}_{7/2}$	2081.788	2	48035.6	$27604\,{}_{9/2} - 75640^{\circ}{}_{11/2}$
2098.523	100	47652.6	$21755\,{}_{11/2} - 69408^{\circ}{}_{11/2}$	2080.866	1	48056.9	
2098.275	5	47658.2	$26446\,{}_{7/2} - 74105^{\circ}{}_{5/2}$	2080.280	30	48070.4	$21611\,{}_{5/2} - 69681^{\circ}{}_{5/2}$
2097.806	100	47668.8	$17627\,{}_{9/2} - 65295^{\circ}{}_{7/2}$	2079.497	100	48088.6	$23647\,{}_{13/2} - 71736^{\circ}{}_{11/2}$
2097.601	1000	47673.5	$12846\,{}_{9/2} - 60520^{\circ}{}_{7/2}$	2079.441	300	48089.8	$19308\,{}_{11/2} - 67398^{\circ}{}_{9/2}$
2097.513	500	47675.5	$14859\,{}_{11/2} - 62535^{\circ}{}_{9/2}$	2079.020	1	48099.6	$16135\,{}_{7/2} - 64235^{\circ}{}_{9/2}$
2097.284	20	47680.7	$18241\,{}_{11/2} - 65922^{\circ}{}_{11/2}$	2078.645	20	48108.3	$27452\,{}_{5/2} - 75560^{\circ}{}_{5/2}$
2097.234	100	47681.8	$14558\,{}_{9/2} - 62240^{\circ}{}_{11/2}$	2078.489	20	48111.9	$31254\,{}_{7/2} - 79366^{\circ}{}_{5/2}$
2097.160	40	47683.5	$21294\,{}_{7/2} - 68978^{\circ}{}_{5/2}$	2078.426	3	48113.3	
2097.075	5	47685.5	$24309\,{}_{3/2} - 71994^{\circ}{}_{5/2}$	2077.544	60	48133.8	$23844\,{}_{9/2} - 71978^{\circ}{}_{7/2}$
2096.985	5	47687.5		2077.450	40	48135.9	$21294\,{}_{7/2} - 69431^{\circ}{}_{7/2}$
2096.890	5	47689.7	$27604\,{}_{9/2} - 75294^{\circ}{}_{7/2}$	2077.337	3	48138.6	$20848\,{}_{5/2} - 68987^{\circ}{}_{7/2}$
2096.832	200	47691.0	$18990\,{}_{7/2} - 66681^{\circ}{}_{5/2}$	2076.841	200	48150.0	$23442\,{}_{11/2} - 71592^{\circ}{}_{9/2}$
2096.787	6	47692.0	$21294\,{}_{7/2} - 68987^{\circ}{}_{7/2}$	2076.505	3	48157.8	$27604\,{}_{9/2} - 75762^{\circ}{}_{9/2}$
2096.496	400	47698.6	$14859\,{}_{11/2} - 62558^{\circ}{}_{13/2}$	2076.358	100	48161.2	$45805\,{}_{9/2} - 93967^{\circ}{}_{7/2}$
2094.953	20	47733.8	$23651\,{}_{7/2} - 71385^{\circ}{}_{7/2}$	2075.991	300	48169.8	$19700\,{}_{11/2} - 67870^{\circ}{}_{9/2}$
2094.676	400	47740.1	$19308\,{}_{11/2} - 67049^{\circ}{}_{9/2}$	2075.747	500	48175.4	$15045\,{}_{5/2} - 63221^{\circ}{}_{3/2}$
2094.155	4000	47752.0	$17113\,{}_{13/2} - 64865^{\circ}{}_{11/2}$	2074.851	5	48196.2	
2093.909	5	47757.6		2073.739	20	48222.1	$21755\,{}_{11/2} - 69978^{\circ}{}_{11/2}$
2093.424	40	47768.6		2073.462	200	48228.5	$20315\,{}_{9/2} - 68544^{\circ}{}_{9/2}$
2092.509	10	47789.5		2073.215	3	48234.3	
2091.826	30	47805.1	$20160\,{}_{3/2} - 67965^{\circ}{}_{3/2}$	2072.886	10	48241.9	$24788\,{}_{9/2} - 73029^{\circ}{}_{9/2}$
2091.758	20	47806.7	$19872\,{}_{7/2} - 67679^{\circ}{}_{7/2}$	2072.580	15	48249.0	
2091.411	4000	47814.6	$18921\,{}_{15/2} - 66735^{\circ}{}_{13/2}$	2072.534	400	48250.1	$18990\,{}_{7/2} - 67240^{\circ}{}_{7/2}$
2091.238	100	47818.6	$14859\,{}_{11/2} - 62678^{\circ}{}_{13/2}$	2071.991	80	48262.8	$21418\,{}_{5/2} - 69681^{\circ}{}_{5/2}$
2090.153	20	47843.4	$21294\,{}_{7/2} - 69138^{\circ}{}_{9/2}$	2071.533	5	48273.4	$22747\,{}_{9/2} - 71021^{\circ}{}_{9/2}$
2089.744	1	47852.7	$23532\,{}_{5/2} - 71385^{\circ}{}_{7/2}$	2070.768	50	48291.3	$15525\,{}_{11/2} - 63816^{\circ}{}_{11/2}$
2089.473	10	47859.0	$18063\,{}_{9/2} - 65922^{\circ}{}_{11/2}$	2070.649	200	48294.0	$23442\,{}_{11/2} - 71736^{\circ}{}_{11/2}$
2089.306	5	47862.8	$18990\,{}_{7/2} - 66852^{\circ}{}_{7/2}$	2070.338	50	48301.3	$16516\,{}_{7/2} - 64817^{\circ}{}_{5/2}$
2088.848	2	47873.3	$21535\,{}_{9/2} - 69408^{\circ}{}_{11/2}$	2070.042	400	48308.2	$17627\,{}_{9/2} - 65935^{\circ}{}_{7/2}$
2088.769	10	47875.1	$32288\,{}_{3/2} - 80164^{\circ}{}_{3/2}$	2069.258	50	48326.5	$23651\,{}_{7/2} - 71978^{\circ}{}_{7/2}$
2088.632	10	47878.2		2068.559	30	48342.8	$23651\,{}_{7/2} - 71994^{\circ}{}_{5/2}$
2088.346	400	47884.8	$16516\,{}_{7/2} - 64401^{\circ}{}_{5/2}$	2068.261	200	48349.8	$39870\,{}_{9/2} - 88220^{\circ}{}_{9/2}$
2088.042	5	47891.8	$23844\,{}_{9/2} - 71736^{\circ}{}_{11/2}$	2067.712	200	48362.6	$15454\,{}_{13/2} - 63816^{\circ}{}_{11/2}$
2087.387	4	47906.8	$18241\,{}_{11/2} - 66148^{\circ}{}_{13/2}$	2067.034	200	48378.5	
2087.300	4	47908.8		2066.270	10	48396.4	
2087.200	4	47911.1		2065.895	300	48405.2	$18990\,{}_{7/2} - 67395^{\circ}{}_{5/2}$
2086.712	10	47922.3	$20315\,{}_{9/2} - 68238^{\circ}{}_{11/2}$	2065.177	5	48422.0	$27138\,{}_{7/2} - 75560^{\circ}{}_{5/2}$
2085.246	30	47956.0	$28936\,{}_{3/2} - 76892^{\circ}{}_{3/2}$	2064.736	1000	48432.3	$17534\,{}_{15/2} - 65967^{\circ}{}_{13/2}$

[a] For doubly-classified lines, the wavelength is entered only once.

TABLE X. *Observed spectral lines of* Pr III *in the vacuum ultra violet region*—Continued

λ_{vac} Å	Intensity	σ (cm^{-1})	Classification [a]	λ_{vac} Å	Intensity	σ (cm^{-1})	Classification [a]
2064.291	2	48442.8	$21535\ _{9/2} - 69978^{\circ}_{11/2}$	2048.425	10	48818.0	$20160\ _{3/2} - 68978^{\circ}_{5/2}$
2064.176	10	48445.5	$23532\ _{5/2} - 71978^{\circ}_{7/2}$	2048.148	100	48824.6	$19700\ _{11/2} - 68525^{\circ}_{11/2}$
2063.966	5	48450.4	$23050\ _{3/2} - 71501^{\circ}_{3/2}$	2047.788	20	48833.2	$20848\ _{5/2} - 69681^{\circ}_{5/2}$
2063.765	2	48455.1		2047.369	80	48843.2	$19700\ _{11/2} - 68544^{\circ}_{9/2}$
2063.592	1	48459.2	$19872\ _{7/2} - 68331^{\circ}_{7/2}$	2047.331	1	48844.1	
2063.478	3	48461.9	$23532\ _{5/2} - 71994^{\circ}_{5/2}$	2047.208	2	48847.0	$26446\ _{7/2} - 75294^{\circ}_{7/2}$
2063.161	4	48469.3	$18211\ _{5/2} - 66681^{\circ}_{5/2}$	2046.923	70	48853.8	$17113\ _{13/2} - 65967^{\circ}_{13/2}$
2062.870	200	48476.2	$27138\ _{7/2} - 75614^{\circ}_{5/2}$	2046.754	10	48857.8	$22527\ _{7/2} - 71385^{\circ}_{7/2}$
2062.457	200	48485.9	$20315\ _{9/2} - 68801^{\circ}_{7/2}$	2046.692	20	48859.3	$29835\ _{9/2} - 78694^{\circ}_{11/2}$
			$23050\ _{3/2} - 71536^{\circ}_{5/2}$	2046.390	10	48866.5	
2061.421	80	48510.2	$12846\ _{9/2} - 61357^{\circ}_{9/2}$	2045.914	10	48877.9	$19360\ _{13/2} - 68238^{\circ}_{11/2}$
2060.746	20	48526.1		2045.564	2	48886.3	
2060.636	10	48528.7	$25934\ _{5/2} - 74463^{\circ}_{3/2}$	2045.465	200	48888.6	$13352\ _{11/2} - 62240^{\circ}_{11/2}$
2060.569	30	48530.3	$15045\ _{5/2} - 63576^{\circ}_{5/2}$	2044.686	10	48907.3	$24470\ _{7/2} - 73378^{\circ}_{7/2}$
2060.054	1	48542.4		2044.070	1	48922.0	
2059.891	10	48546.2		2043.773	500	48929.1	$19872\ _{7/2} - 68801^{\circ}_{7/2}$
2059.245	4000	48561.5	$19308\ _{11/2} - 67870^{\circ}_{9/2}$	2043.103	50	48945.2	$19360\ _{13/2} - 68305^{\circ}_{15/2}$
2058.796	60	48572.1		2042.616	400	48956.8	$14859\ _{11/2} - 63816^{\circ}_{11/2}$
2058.663	30	48575.2	$25033\ _{9/2} - 73609^{\circ}_{11/2}$	2041.925	2	48973.4	
2058.371	10	48582.1	$35828\ _{9/2} - 84410^{\circ}_{9/2}$	2039.381	200	49034.5	$14558\ _{9/2} - 63593^{\circ}_{9/2}$
2058.090	5	48588.7		2038.682	1	49051.3	
2057.554	100	48601.4	$35828\ _{9/2} - 84430^{\circ}_{7/2}$	2038.366	1	49058.9	
2057.042	10	48613.5	$17534\ _{15/2} - 66148^{\circ}_{13/2}$	2037.578	3	49077.9	
2056.771	5	48619.9	$19872\ _{7/2} - 68492^{\circ}_{7/2}$	2036.415	20 *c l*	49105.9	$19872\ _{7/2} - 68978^{\circ}_{5/2}$
2056.545	30	48625.2	$15525\ _{11/2} - 64150^{\circ}_{11/2}$	2036.103	1	49113.4	
2056.409	30	48628.4	$29835\ _{9/2} - 78463^{\circ}_{7/2}$	2036.061	100	49114.4	$19872\ _{7/2} - 68987^{\circ}_{7/2}$
2056.326	100	48630.4	$30505\ _{11/2} - 79136^{\circ}_{13/2}$	2035.210	10	49135.0	
2054.597	50	48671.4	$20315\ _{9/2} - 68987^{\circ}_{7/2}$	2034.894	100	49142.6	$21238\ _{13/2} - 70381^{\circ}_{13/2}$
2054.509	1000	48673.4	$14558\ _{9/2} - 63232^{\circ}_{7/2}$	2034.290	1	49157.2	$18241\ _{11/2} - 67398^{\circ}_{9/2}$
2054.168	200	48681.5	$16135\ _{7/2} - 64817^{\circ}_{5/2}$	2034.186	7	49159.7	$16135\ _{7/2} - 65295^{\circ}_{7/2}$
2053.815	10	48689.9	$15525\ _{11/2} - 64215^{\circ}_{13/2}$	2033.950	2000	49165.4	$19360\ _{13/2} - 68525^{\circ}_{11/2}$
2053.531	1000	48696.6	$15454\ _{13/2} - 64150^{\circ}_{11/2}$	2033.719	10	49171.0	
2052.953	2000	48710.3	$13352\ _{11/2} - 62062^{\circ}_{9/2}$	2033.478	40	49176.8	$18063\ _{9/2} - 67240^{\circ}_{7/2}$
			$15525\ _{11/2} - 64235^{\circ}_{9/2}$	2033.207	200	49183.4	$13352\ _{11/2} - 62535^{\circ}_{9/2}$
2052.434	2	48722.6	$15045\ _{5/2} - 63768^{\circ}_{7/2}$				$18211\ _{5/2} - 67395^{\circ}_{5/2}$
2052.198	3	48728.2		2033.129	50	49185.3	$23844\ _{9/2} - 73029^{\circ}_{9/2}$
2052.131	3	48729.8		2033.015	100	49188.0	$17113\ _{13/2} - 66301^{\circ}_{15/2}$
2052.078	10	48731.1	$18211\ _{5/2} - 66943^{\circ}_{5/2}$	2032.480	200	49201.0	$17534\ _{15/2} - 66735^{\circ}_{13/2}$
2052.045	1	48731.9		2032.253	400	49206.5	$13352\ _{11/2} - 62558^{\circ}_{11/2}$
2051.988	100	48733.2	$14859\ _{11/2} - 63593^{\circ}_{9/2}$	2032.117	1000	49209.8	$14558\ _{9/2} - 63768^{\circ}_{7/2}$
2051.736	200	48739.2	$21238\ _{13/2} - 69978^{\circ}_{11/2}$	2031.865	400	49215.9	$12846\ _{9/2} - 62062^{\circ}_{9/2}$
2050.969	20	48757.4		2031.558	1	49223.3	$22277\ _{3/2} - 71501^{\circ}_{3/2}$
2050.911	10	48758.8	$12846\ _{9/2} - 61605^{\circ}_{7/2}$	2031.455	400	49225.8	$17627\ _{9/2} - 66852^{\circ}_{7/2}$
2050.812	400	48761.2	$15454\ _{13/2} - 64215^{\circ}_{13/2}$	2031.256	10	49230.6	$22747\ _{9/2} - 71978^{\circ}_{7/2}$
2050.587	200	48766.5	$17534\ _{15/2} - 66301^{\circ}_{15/2}$	2030.131	100	49257.9	$14558\ _{9/2} - 63816^{\circ}_{11/2}$
2050.036	20	48779.6	$16516\ _{7/2} - 65295^{\circ}_{7/2}$	2029.983	2	49261.5	
2049.624	20	48789.4	$18063\ _{9/2} - 66852^{\circ}_{7/2}$	2029.814	7	49265.6	$19872\ _{7/2} - 69138^{\circ}_{9/2}$
2048.865	400	48807.5	$18241\ _{11/2} - 67049^{\circ}_{9/2}$	2029.694	2	49268.5	
2048.798	100	48809.1	$17113\ _{13/2} - 65922^{\circ}_{11/2}$	2029.540	20	49272.2	$35137\ _{3/2} - 84409^{\circ}_{3/2}$
2048.630	1	48813.1		2029.192	300	49280.7	

[a] For doubly-classified lines, the wavelength is entered only once.

TABLE X. *Observed spectral lines of* Pr III *in the vacuum ultra violet region*—Continued

λ_{vac} Å	Intensity	σ (cm^{-1})	Classification [a]	λ_{vac} Å	Intensity	σ (cm^{-1})	Classification [a]
							$17627\ ^{9/2} - 67398^{\circ}_{9/2}$
2028.959	2	49286.4					
2028.926	5	49287.2	$44679\ ^{7/2} - 93967^{\circ}_{7/2}$	2009.107	40	49773.4	$16135\ ^{7/2} - 65909^{\circ}_{5/2}$
2028.780	100	49290.7	$14859\ ^{11/2} - 64150^{\circ}_{11/2}$	2008.066	10	49799.2	$16135\ ^{7/2} - 65935^{\circ}_{7/2}$
2028.209	40	49304.6	$22080\ ^{7/2} - 71385^{\circ}_{7/2}$	2007.738	20	49807.3	$18063\ ^{9/2} - 67870^{\circ}_{9/2}$
2027.315	3	49326.3	$13352\ ^{11/2} - 62678^{\circ}_{13/2}$	2006.763	1	49831.5	
2027.194	40	49329.3		2006.565	30	49836.4	$21755\ ^{11/2} - 71592^{\circ}_{9/2}$
2027.102	300	49331.5	$15525\ ^{11/2} - 64857^{\circ}_{9/2}$	2006.072	10	49848.7	
2026.948	10	49335.3	$18063\ ^{9/2} - 67398^{\circ}_{9/2}$	2005.817	30	49855.0	$30505\ ^{11/2} - 80360^{\circ}_{11/2}$
2026.694	10	49341.4	$18990\ ^{7/2} - 68331^{\circ}_{7/2}$	2004.416	10	49889.8	$21611\ ^{5/2} - 71501^{\circ}_{3/2}$
2026.007	30 *c l*	49358.2		2003.908	20	49902.5	
2025.296	30	49375.5	$14859\ ^{11/2} - 64235^{\circ}_{9/2}$	2003.001	10	49925.1	$21611\ ^{5/2} - 71536^{\circ}_{5/2}$
2024.954	100	49383.8	$18921\ ^{15/2} - 68305^{\circ}_{13/2}$	2002.296	2	49942.7	
2024.812	2	49387.3		2001.839	1	49954.1	
2024.573	20 *c l*	49393.1	$16516\ ^{7/2} - 65909^{\circ}_{5/2}$	2001.548	10	49961.3	$23647\ ^{13/2} - 73609^{\circ}_{11/2}$
2024.540	400	49393.9	$12846\ ^{9/2} - 62240^{\circ}_{11/2}$	2001.441	40	49964.0	
2024.298	70	49399.8		2001.049	5	49973.8	$28720\ ^{9/2} - 78694^{\circ}_{11/2}$
2023.848	10	49410.8	$15454\ ^{13/2} - 64865^{\circ}_{11/2}$	2000.784	2	49980.4	$21755\ ^{11/2} - 71736^{\circ}_{11/2}$
2023.390	10	49422.0	$17627\ ^{9/2} - 67049^{\circ}_{9/2}$	2000.587	200	49985.3	$19700\ ^{11/2} - 69686^{\circ}_{9/2}$
2023.005	200	49431.4	$29263\ ^{13/2} - 78694^{\circ}_{11/2}$	2000.462	20	49988.4	$18990\ ^{7/2} - 68978^{\circ}_{5/2}$
2022.766	70	49437.3	$19700\ ^{11/2} - 69138^{\circ}_{9/2}$	2000.116	400	49997.1	$14859\ ^{11/2} - 64857^{\circ}_{9/2}$
							$18990\ ^{7/2} - 68987^{\circ}_{7/2}$
2022.370	3	49446.9					
2022.027	1	49455.3	$22080\ ^{7/2} - 71536^{\circ}_{5/2}$	1999.902	30	50002.4	$24461\ ^{5/2} - 74463^{\circ}_{3/2}$
2021.544	50	49467.1	$22527\ ^{7/2} - 71994^{\circ}_{5/2}$	1999.795	100	50005.1	$14859\ ^{11/2} - 64865^{\circ}_{11/2}$
2021.249	1	49474.4		1998.905	30	50027.4	
2020.778	10	49485.9	$21535\ ^{9/2} - 71021^{\circ}_{9/2}$	1998.598	10	50035.1	
2018.512	1	49541.4		1998.301	1	50042.5	
2018.385	10	49544.6	$26095\ ^{11/2} - 75640^{\circ}_{11/2}$	1998.064	400	50048.4	$19360\ ^{13/2} - 69408^{\circ}_{11/2}$
2017.745	30	49560.3	$29835\ ^{9/2} - 79395^{\circ}_{7/2}$	1997.912	20	50052.2	$17627\ ^{9/2} - 67679^{\circ}_{7/2}$
2016.711	100	49585.7		1996.715	30	50082.3	$21418\ ^{5/2} - 71501^{\circ}_{3/2}$
2016.637	2	49587.5	$23442\ ^{11/2} - 73029^{\circ}_{9/2}$	1996.423	3	50089.6	
2016.463	1	49591.8	$14558\ ^{9/2} - 64150^{\circ}_{11/2}$	1996.023	5 *c l*	50099.6	$19308\ ^{11/2} - 69408^{\circ}_{11/2}$
2015.591	100	49613.2	$17627\ ^{9/2} - 67240^{\circ}_{7/2}$	1995.989	10	50100.5	
2015.488	200	49615.8	$18063\ ^{9/2} - 67679^{\circ}_{7/2}$	1995.216	100	50119.9	$18211\ ^{5/2} - 68331^{\circ}_{7/2}$
2015.267	20	49621.2	$29267\ ^{5/2} - 78889^{\circ}_{3/2}$	1994.856	1	50128.9	
2015.214	100	49622.5	$17113\ ^{13/2} - 66735^{\circ}_{13/2}$	1994.692	400	50133.0	$18241\ ^{11/2} - 68374^{\circ}_{9/2}$
2014.946	100	49629.1	$18241\ ^{11/2} - 67870^{\circ}_{9/2}$	1994.027	20	50149.8	$31254\ ^{7/2} - 81404^{\circ}_{5/2}$
2014.405	2	49642.4		1993.422	300 *c l*	50165.0	$16516\ ^{7/2} - 66681^{\circ}_{5/2}$
2013.897	5	49655.0		1993.346	100 *c l*	50166.9	$23442\ ^{11/2} - 73609^{\circ}_{11/2}$
2013.015	100	49676.7	$14558\ ^{9/2} - 64235^{\circ}_{9/2}$	1991.983	10	50201.2	$21535\ ^{9/2} - 71736^{\circ}_{11/2}$
2012.896	30	49679.7	$25934\ ^{5/2} - 75614^{\circ}_{5/2}$	1991.836	6	50204.9	$25409\ ^{7/2} - 75614^{\circ}_{5/2}$
2011.593	100	49711.8	$12846\ ^{9/2} - 62558^{\circ}_{11/2}$	1991.622	60	50210.3	
2011.388	3	49716.9	$22277\ ^{3/2} - 71994^{\circ}_{5/2}$	1991.509	30	50213.2	$24250\ ^{3/2} - 74463^{\circ}_{3/2}$
2011.008	1	49726.3	$21294\ ^{7/2} - 71021^{\circ}_{9/2}$	1991.049	1	50224.8	
			$23651\ ^{7/2} - 73378^{\circ}_{7/2}$	1990.959	3	50227.0	
2010.696	20	49734.0		1989.646	50	50260.2	$25033\ ^{9/2} - 75294^{\circ}_{7/2}$
2010.339	80	49742.8	$28720\ ^{9/2} - 78463^{\circ}_{7/2}$	1989.319	300	50268.5	$18063\ ^{9/2} - 68331^{\circ}_{7/2}$
2009.905	80	49753.6	$18211\ ^{5/2} - 67965^{\circ}_{3/2}$	1988.770	6	50282.3	$22747\ ^{9/2} - 73029^{\circ}_{9/2}$
2009.579	40	49761.7		1988.707	2	50283.9	$18241\ ^{11/2} - 68525^{\circ}_{11/2}$
2009.467	5	49764.4	$23844\ ^{9/2} - 73609^{\circ}_{11/2}$	1988.247	10	50295.6	
2009.177	40	49771.6	$15045\ ^{5/2} - 64817^{\circ}_{5/2}$	1988.139	300	50298.3	$14558\ ^{9/2} - 64857^{\circ}_{9/2}$

[a] For doubly-classified lines, the wavelength is entered only once.

TABLE X. *Observed spectral lines of* Pr III *in the vacuum ultra violet region*—Continued

λ_{vac} Å	Intensity	σ (cm^{-1})	Classification [a]	λ_{vac} Å	Intensity	σ (cm^{-1})	Classification [a]
1987.631	40	50311.2	$18063\ _{9/2} - 68374^{\circ}{}_{9/2}$	1967.373	1	50829.2	
1987.542	2	50313.4		1967.233	1	50832.8	$24461\ _{5/2} - 75294^{\circ}{}_{7/2}$
1985.995	5	50352.6	$21148\ _{3/2} - 71501^{\circ}{}_{3/2}$	1966.710	2	50846.3	$21148\ _{3/2} - 71994^{\circ}{}_{5/2}$
			$25409\ _{7/2} - 75762^{\circ}{}_{9/2}$	1966.502	3	50851.7	$24788\ _{9/2} - 75640^{\circ}{}_{11/2}$
1985.023	1	50377.2	$19308\ _{11/2} - 69686^{\circ}{}_{9/2}$	1966.208	40	50859.3	$27604\ _{9/2} - 78463^{\circ}{}_{7/2}$
1984.870	10	50381.1					$36652\ _{5/2} - 87511^{\circ}{}_{7/2}$
1984.698	20	50385.5	$12846\ _{9/2} - 63232^{\circ}{}_{7/2}$	1965.970	80	50865.5	$17627\ _{9/2} - 68492^{\circ}{}_{7/2}$
1984.380	4	50393.6		1965.346	1	50881.6	
1984.348	2 *c l*	50394.4		1963.974	2	50917.2	$17627\ _{9/2} - 68544^{\circ}{}_{9/2}$
1984.250	50	50396.9	$15525\ _{11/2} - 65922^{\circ}{}_{11/2}$	1963.911	2	50918.8	
1983.311	10	50420.7	$14558\ _{9/2} - 64979^{\circ}{}_{7/2}$	1963.786	100 *c l*	50922.0	$12846\ _{9/2} - 63768^{\circ}{}_{7/2}$
1983.066	2	50427.0	$16516\ _{7/2} - 66943^{\circ}{}_{5/2}$	1963.731	20 *c l*	50923.5	$18063\ _{9/2} - 68987^{\circ}{}_{7/2}$
1982.981	300	50429.1	$18063\ _{9/2} - 68492^{\circ}{}_{7/2}$	1963.401	100	50932.0	
1982.785	2	50434.1	$23175\ _{13/2} - 73609^{\circ}{}_{11/2}$	1962.747	4	50949.0	$22080\ _{7/2} - 73029^{\circ}{}_{9/2}$
1982.492	5	50441.6	$15525\ _{11/2} - 65967^{\circ}{}_{13/2}$	1962.418	10	50957.5	$25934\ _{5/2} - 76892^{\circ}{}_{3/2}$
1982.428	1	50443.2	$21535\ _{9/2} - 71978^{\circ}{}_{7/2}$	1961.929	200	50970.2	$12846\ _{9/2} - 63816^{\circ}{}_{11/2}$
1981.580	100	50464.8	$13352\ _{11/2} - 63816^{\circ}{}_{11/2}$	1961.265	3	50987.5	
1981.449	2	50468.1	$15454\ _{13/2} - 65922^{\circ}{}_{11/2}$	1960.735	10	51001.3	
1981.140	4	50476.0		1959.961	30	51021.4	$19360\ _{13/2} - 70381^{\circ}{}_{13/2}$
1980.950	10	50480.8	$18063\ _{9/2} - 68544^{\circ}{}_{9/2}$	1959.874	10 *b l*	51023.7	$45807\ _{5/2} - 96830^{\circ}{}_{7/2}$
1980.867	2	50483.0	$30505\ _{11/2} - 80988^{\circ}{}_{13/2}$	1958.687	2	51054.6	$23050\ _{3/2} - 74105^{\circ}{}_{5/2}$
1980.287	200	50497.7		1958.387	100	51062.4	$14859\ _{11/2} - 65922^{\circ}{}_{11/2}$
1980.191	100 *h*	50500.2	$38448\ _{9/2} - 88948^{\circ}{}_{9/2}$	1958.053	2	51071.1	
1979.745	5 *b l*	50511.6		1958.001	1	51072.5	$19308\ _{11/2} - 70381^{\circ}{}_{13/2}$
1979.692	20	50512.9	$15454\ _{13/2} - 65967^{\circ}{}_{13/2}$	1957.908	3	51074.9	$18063\ _{9/2} - 69138\ _{9/2}$
1978.427	200	50545.2	$16135\ _{7/2} - 66681^{\circ}{}_{5/2}$	1957.338	1	51089.8	$24470\ _{7/2} - 75560^{\circ}{}_{5/2}$
1975.850	2	50611.1	$17627\ _{9/2} - 68238^{\circ}{}_{11/2}$	1957.073	6	51096.7	
1975.782	4	50612.9		1957.039	3	51097.6	$29263\ _{13/2} - 80360^{\circ}{}_{11/2}$
1975.582	200	50618.0	$19360\ _{13/2} - 69978^{\circ}{}_{11/2}$	1956.957	20	51099.7	$24461\ _{5/2} - 75560^{\circ}{}_{5/2}$
1975.424	3	50622.0		1956.672	5	51107.2	$14859\ _{11/2} - 65967^{\circ}{}_{13/2}$
1973.849	3	50662.4		1955.992	15	51124.9	$17113\ _{13/2} - 68238^{\circ}{}_{11/2}$
1973.590	2	50669.1	$19308\ _{11/2} - 69978^{\circ}{}_{11/2}$	1955.521	3	51137.3	
1973.367	10	50674.8	$28720\ _{9/2} - 79395^{\circ}{}_{7/2}$	1955.268	3	51143.9	$24470\ _{7/2} - 75614^{\circ}{}_{5/2}$
1972.857	10	50687.9	$20848\ _{5/2} - 71536^{\circ}{}_{5/2}$	1954.535	10	51163.1	$16516\ _{7/2} - 67679^{\circ}{}_{7/2}$
1972.617	5	50694.1	$15454\ _{13/2} - 66148^{\circ}{}_{13/2}$	1954.455	60 *w*	51165.2	
1972.200	30	50704.8	$17627\ _{9/2} - 68331^{\circ}{}_{7/2}$	1954.386	20	51167.0	$18241\ _{11/2} - 69408^{\circ}{}_{11/2}$
1971.913	2	50712.2		1954.196	40	51171.9	
1971.730	15	50716.9	$16135\ _{7/2} - 66852^{\circ}{}_{7/2}$	1954.092	2	51174.7	$17627\ _{9/2} - 68801^{\circ}{}_{7/2}$
1971.636	200	50719.3		1953.531	20	51189.4	
1971.287	4	50728.3	$25033\ _{9/2} - 75762^{\circ}{}_{9/2}$	1953.321	5	51194.9	
1971.248	4	50729.3		1952.395	1	51219.1	$18211\ _{5/2} - 69431^{\circ}{}_{7/2}$
1970.573	80	50746.7	$12846\ _{9/2} - 63593^{\circ}{}_{9/2}$	1951.968	2	51230.3	
1970.091	1	50759.1	$39870\ _{9/2} - 90629^{\circ}{}_{9/2}$	1951.018	200 *b l*	51255.3	
1969.791	40	50766.8	$18211\ _{5/2} - 68978^{\circ}{}_{5/2}$	1950.864	1	51259.3	$16135\ _{7/2} - 67395^{\circ}{}_{5/2}$
1969.650	20	50770.4	$17534\ _{15/2} - 68305^{\circ}{}_{13/2}$	1949.759	100	51288.4	$14859\ _{11/2} - 66148^{\circ}{}_{13/2}$
1969.468	10	50775.1	$18211\ _{5/2} - 68987^{\circ}{}_{7/2}$	1949.156	60	51304.3	$12846\ _{9/2} - 64150^{\circ}{}_{11/2}$
1968.530	60	50799.3		1948.364	10	51325.1	$27138\ _{7/2} - 78463^{\circ}{}_{7/2}$
1968.227	40	50807.2	$16135\ _{7/2} - 66943^{\circ}{}_{5/2}$	1947.036	10	51360.1	$17627\ _{9/2} - 68987^{\circ}{}_{7/2}$
1967.608	10	50823.1	$24470\ _{7/2} - 75294^{\circ}{}_{7/2}$	1946.900	1	51363.7	$14558\ _{9/2} - 65922^{\circ}{}_{11/2}$
1967.447	20	50827.3		1946.830	3	51365.6	

[a] For doubly-classified lines, the wavelength is entered only once.

TABLE X. *Observed spectral lines of* Pr III *in the vacuum ultra violet region*—Continued

λ_{vac} Å	Intensity	σ (cm^{-1})	Classification [a]	λ_{vac} Å	Intensity	σ (cm^{-1})	Classification [a]
							$23532\ _{5/2} - 75560^{\circ}_{5/2}$
1946.417	80	51376.4	$14558\ _{9/2} - 65935^{\circ}_{7/2}$				
1945.646	2	51396.8		1921.828	2	52033.8	
1945.053	1	51412.5	$17113\ _{13/2} - 68525^{\circ}_{11/2}$	1921.763	50	52035.6	$19700\ _{11/2} - 71736^{\circ}_{11/2}$
1943.835	8	51444.7	$18241\ _{11/2} - 69686^{\circ}_{9/2}$	1920.869	1	52059.8	
1943.650	4	51449.6	$23844\ _{9/2} - 75294^{\circ}_{7/2}$	1919.639	1	52093.1	
1943.293	10	51459.0		1919.162	30	52106.1	$19872\ _{7/2} - 71978^{\circ}_{7/2}$
1943.248	30	51460.2	$18921\ _{15/2} - 70381^{\circ}_{13/2}$	1918.562	100	52122.4	$19872\ _{7/2} - 71994^{\circ}_{5/2}$
1941.939	2	51494.9	$21535\ _{9/2} - 73029^{\circ}_{9/2}$	1917.201	1	52159.4	
1941.556	100	51505.1	$13352\ _{11/2} - 64857^{\circ}_{9/2}$	1916.741	4	52171.9	$31254\ _{7/2} - 83426^{\circ}_{5/2}$
1941.250	2	51513.2	$13352\ _{11/2} - 64865^{\circ}_{11/2}$	1916.507	1	52178.3	
1940.930	2	51521.7		1916.106	50	52189.2	$14859\ _{11/2} - 67049^{\circ}_{9/2}$
1940.853	5	51523.7	$15525\ _{11/2} - 67049^{\circ}_{9/2}$	1915.296	1	52211.2	
1940.770	2	51525.9		1914.681	2	52228.0	$27138\ _{7/2} - 79366^{\circ}_{5/2}$
1939.299	100	51565.0		1913.964	70	52247.6	
1939.161	10	51568.7		1913.622	1	52256.9	$27138\ _{7/2} - 79395^{\circ}_{7/2}$
1937.726	20	51606.9		1913.339	2	52264.6	
1937.127	10	51622.8	$18063\ _{9/2} - 69686^{\circ}_{9/2}$	1913.284	100 *b l*	52266.2	
1936.659	40	51635.3	$15045\ _{5/2} - 66681^{\circ}_{5/2}$	1912.698	5	52282.2	
1936.478	3	51640.1	$28720\ _{9/2} - 80360^{\circ}_{11/2}$	1912.651	20	52283.4	$19308\ _{11/2} - 71592^{\circ}_{9/2}$
1936.375	1	51642.9		1911.251	3	52321.8	
1935.588	30	51663.9	$19872\ _{7/2} - 71536^{\circ}_{5/2}$	1910.242	2	52349.4	$15045\ _{5/2} - 67395^{\circ}_{5/2}$
1935.290	1	51671.8	$38448\ _{9/2} - 90119^{\circ}_{11/2}$	1910.093	1	52353.5	
1933.865	10	51709.9	$35801\ _{7/2} - 87511^{\circ}_{7/2}$	1909.895	3	52358.9	$23050\ _{3/2} - 75409^{\circ}_{3/2}$
1933.775	100	51712.3	$19308\ _{11/2} - 71021^{\circ}_{9/2}$	1909.471	200	52370.5	$21238\ _{13/2} - 73609^{\circ}_{11/2}$
1933.491	1	51719.9	$19872\ _{7/2} - 71592^{\circ}_{9/2}$	1909.258	300	52376.4	$19360\ _{13/2} - 71736^{\circ}_{11/2}$
1932.872	8	51736.5	$18241\ _{11/2} - 69978^{\circ}_{11/2}$	1907.956	4	52412.1	$25409\ _{7/2} - 77822^{\circ}_{5/2}$
1932.181	5 *b l*	51755.0		1907.054	10	52436.9	
1931.739	5	51766.8	$21611\ _{5/2} - 73378^{\circ}_{7/2}$	1906.750	10 *b l*	52445.3	
1931.368	1	51776.8		1906.126	2	52462.4	$16516\ _{7/2} - 68978^{\circ}_{5/2}$
1930.813	40	51791.6		1906.040	40	52464.8	$23175\ _{13/2} - 75640^{\circ}_{11/2}$
1930.349	10	51804.1	$17627\ _{9/2} - 69431^{\circ}_{7/2}$	1905.819	20 *h*	52470.9	$16516\ _{7/2} - 68987^{\circ}_{7/2}$
1930.001	3	51813.4		1905.688	10	52474.5	
1929.920	20	51815.6	$16516\ _{7/2} - 68331^{\circ}_{7/2}$	1904.981	1	52494.0	$21611\ _{5/2} - 74105^{\circ}_{5/2}$
1929.706	30	51821.4	$15045\ _{5/2} - 66867^{\circ}_{3/2}$	1904.862	3	52497.2	
1928.246	7	51860.6		1904.625	1	52503.8	
1927.821	20	51872.0		1904.212	4	52515.2	
1927.774	20	51873.3	$15525\ _{11/2} - 67398^{\circ}_{9/2}$	1903.356	60	52538.8	$14859\ _{11/2} - 67398^{\circ}_{9/2}$
1927.678	4	51875.9	$14859\ _{11/2} - 66735^{\circ}_{13/2}$	1903.115	10 *c l*	52545.4	
1927.095	300	51891.6	$19700\ _{11/2} - 71592^{\circ}_{9/2}$	1903.083	10 *c l*	52546.3	$18990\ _{7/2} - 71536^{\circ}_{5/2}$
1926.884	3	51897.3	$15045\ _{5/2} - 66943^{\circ}_{5/2}$	1902.215	2	52570.3	$13352\ _{11/2} - 65922^{\circ}_{11/2}$
1925.579	3 *b l*	51932.4		1901.979	4	52576.8	
1925.184	10	51943.1	$27452\ _{5/2} - 79395^{\circ}_{7/2}$	1901.715	7	52584.1	
1924.451	30	51962.9	$23651\ _{7/2} - 75614^{\circ}_{5/2}$	1900.811	5	52609.1	
1923.365	300	51992.2	$23647\ _{13/2} - 75640^{\circ}_{11/2}$	1900.561	1	52616.0	
1923.154	2	51997.9		1899.627	1	52641.9	$24250\ _{3/2} - 76892^{\circ}_{3/2}$
1922.689	200	52010.5	$12846\ _{9/2} - 64857^{\circ}_{9/2}$	1899.491	5	52645.7	
1922.459	3	52016.7	$26446\ _{7/2} - 78463^{\circ}_{7/2}$	1898.200	80	52681.5	$14558\ _{9/2} - 67240^{\circ}_{7/2}$
1922.394	1	52018.5	$12846\ _{9/2} - 64865^{\circ}_{11/2}$	1898.020	5	52686.5	$21418\ _{5/2} - 74105^{\circ}_{5/2}$
1922.178	20	52024.3	$22080\ _{7/2} - 74105^{\circ}_{5/2}$				$34825\ _{7/2} - 87511^{\circ}_{7/2}$
1922.047	10	52027.9	$16516\ _{7/2} - 68544^{\circ}_{9/2}$	1897.082	1	52712.5	$15525\ _{11/2} - 68238^{\circ}_{11/2}$

[a] For doubly-classified lines, the wavelength is entered only once.

TABLE X. *Observed spectral lines of* Pr III *in the vacuum ultra violet region*—Continued

λ_{vac} Å	Intensity	σ (cm^{-1})	Classification [a]	λ_{vac} Å	Intensity	σ (cm^{-1})	Classification [a]
1896.430	6 *c l*	52730.6		1880.571	10	53175.3	
1896.409	2 *c l*	52731.2		1879.845	4	53195.9	$35024\ ^{7/2} - 88220^{\circ}\ _{9/2}$
1896.290	1	52734.6		1879.786	4	53197.5	$30505\ ^{11/2} - 83703^{\circ}\ _{13/2}$
1895.474	2	52757.2		1879.673	1	53200.7	
1895.146	1	52766.4	$22527\ ^{7/2} - 75294^{\circ}\ _{7/2}$	1879.571	2 *c l*	53203.6	
1894.672	2	52779.6	$18241\ ^{11/2} - 71021^{\circ}\ _{9/2}$	1879.542	5	53204.4	
1894.520	1	52783.8	$15454\ ^{13/2} - 68238^{\circ}\ _{11/2}$	1879.235	20	53213.1	$22080\ ^{7/2} - 75294^{\circ}\ _{7/2}$
1894.358	3	52788.3		1878.823	10	53224.8	
1893.864	3	52802.1		1878.459	20	53235.1	
1893.751	1	52805.2		1877.694	10	53256.8	$20848\ ^{5/2} - 74105^{\circ}\ _{5/2}$
1893.569	3	52810.3	$21294\ ^{7/2} - 74105^{\circ}\ _{5/2}$	1877.280	5	53268.5	$17113\ ^{13/2} - 70381^{\circ}\ _{13/2}$
1893.334	1 *h*	52816.9		1876.933	100 *b l*	53278.4	
1893.181	10 *h*	52821.2		1876.675	2	53285.7	$15045\ ^{5/2} - 68331^{\circ}\ _{7/2}$
1892.506	60	52840.0	$14558\ ^{9/2} - 67398^{\circ}\ _{9/2}$	1876.549	20	53289.3	$18211\ ^{5/2} - 71501^{\circ}\ _{3/2}$
1892.266	1	52846.7	$17534\ ^{15/2} - 70381^{\circ}\ _{13/2}$	1875.754	8	53311.9	$14558\ ^{9/2} - 67870^{\circ}\ _{9/2}$
1892.183	5	52849.0	$15525\ ^{11/2} - 68374^{\circ}\ _{9/2}$	1875.388	10	53322.3	$18063\ ^{9/2} - 71385^{\circ}\ _{7/2}$
1892.050	4	52852.7	$21611\ ^{5/2} - 74463^{\circ}\ _{3/2}$	1875.309	20	53324.6	$18211\ ^{5/2} - 71536^{\circ}\ _{5/2}$
1891.609	2	52865.0	$17113\ ^{13/2} - 69978^{\circ}\ _{11/2}$	1874.981	20	53333.9	
1890.948	5	52883.5		1874.079	60	53359.5	$23532\ ^{5/2} - 76892^{\circ}\ _{3/2}$
1890.827	200	52886.9		1873.997	20	53361.9	
1890.665	2	52891.4		1873.914	5 *b l*	53364.2	
1889.832	2	52914.8	$16516\ ^{7/2} - 69431^{\circ}\ _{7/2}$	1873.470	5	53376.9	
1889.674	60	52919.2		1873.434	7	53377.9	$14859\ ^{11/2} - 68238^{\circ}\ _{11/2}$
1888.294	30	52957.8	$18063\ ^{9/2} - 71021^{\circ}\ _{9/2}$	1873.146	2	53386.1	
1887.490	1	52980.4	$27380\ ^{11/2} - 80360^{\circ}\ _{11/2}$	1872.737	200	53397.8	
1887.180	10	52989.1		1871.878	20	53422.3	
1886.792	4	53000.0	$15525\ ^{11/2} - 68525^{\circ}\ _{11/2}$	1870.826	5	53452.3	
1886.624	10	53004.7	$18990\ ^{7/2} - 71994^{\circ}\ _{5/2}$	1870.354	1	53465.8	
1886.491	7	53008.5		1869.803	2	53481.6	
1886.412	5	53010.7	$14859\ ^{11/2} - 67870^{\circ}\ _{9/2}$	1868.246	1	53526.1	
1886.132	1	53018.6	$15525\ ^{11/2} - 68544^{\circ}\ _{9/2}$	1867.982	5	53533.7	$22080\ ^{7/2} - 75614^{\circ}\ _{5/2}$
1885.940	3	53024.0		1867.565	200	53545.7	$16135\ ^{7/2} - 69681^{\circ}\ _{5/2}$
1885.869	4	53026.0		1867.224	5	53555.4	
1885.328	3	53041.2	$26095\ ^{11/2} - 79136^{\circ}\ _{13/2}$	1866.957	5	53563.1	
1885.015	5	53050.0		1866.678	1	53571.1	$24250\ ^{3/2} - 77822^{\circ}\ _{5/2}$
1884.653	3	53060.2		1866.179	30	53585.4	
1884.399	20	53067.3		1865.842	4	53595.1	
1884.152	10	53074.3		1865.698	5	53599.2	
1884.105	1	53075.6	$12846\ ^{9/2} - 65922^{\circ}\ _{11/2}$	1865.530	10 *c l*	53604.1	
1883.789	3	53084.5		1865.503	10 *c l*	53604.8	
1883.700	50 *c l*	53087.0	$22527\ ^{7/2} - 75614^{\circ}\ _{5/2}$	1865.232	20	53612.6	$15525\ ^{11/2} - 69138^{\circ}\ _{9/2}$
1883.647	50 *c l*	53088.5	$12846\ ^{9/2} - 65935^{\circ}\ _{7/2}$	1865.139	40	53615.3	$20848\ ^{5/2} - 74463^{\circ}\ _{3/2}$
1883.315	2	53097.9		1865.061	2	53617.6	
1883.184	50	53101.6	$30505\ ^{11/2} - 83607^{\circ}\ _{11/2}$	1864.141	50 *b l*	53644.0	
1883.007	1	53106.5		1863.670	20	53657.6	$35291\ ^{9/2} - 88948^{\circ}\ _{9/2}$
1882.932	2	53108.7		1863.393	20	53665.5	$14859\ ^{11/2} - 68525^{\circ}\ _{11/2}$
1882.843	3	53111.2		1863.347	5	53666.9	
1882.031	20	53134.1		1863.289	10	53668.5	
1881.224	500	53156.9	$25979\ ^{15/2} - 79136^{\circ}\ _{13/2}$	1863.044	100	53675.6	$24788\ ^{9/2} - 78463^{\circ}\ _{7/2}$
1880.919	10	53163.5	$16516\ ^{7/2} - 69681^{\circ}\ _{5/2}$	1862.028	4 *h*	53704.9	

[a] For doubly-classified lines, the wavelength is entered only once.

TABLE X. *Observed spectral lines of* Pr III *in the vacuum ultra violet region*—Continued

λ_{vac} Å	Intensity	σ (cm^{-1})	Classification [a]	λ_{vac} Å	Intensity	σ (cm^{-1})	Classification [a]
1861.467	60	53721.1	$19308\ ^{11/2}-\ 73029^{\circ}\ _{9/2}$	1843.574	4	54242.5	
1861.040	10	53733.4		1843.356	10	54248.9	$19360\ ^{13/2}-\ 73609^{\circ}\ _{11/2}$
1860.876	30	53738.1		1842.950	10	54260.8	$21148\ ^{3/2}-\ 75409^{\circ}\ _{3/2}$
1860.257	10	53756.0	$15045\ ^{5/2}-\ 68801^{\circ}\ _{7/2}$	1842.789	200	54265.6	$21294\ ^{7/2}-\ 75560^{\circ}\ _{5/2}$
1860.167	100	53758.6	$17627\ ^{9/2}-\ 71385^{\circ}\ _{7/2}$				$26095\ ^{11/2}-\ 80360^{\circ}\ _{11/2}$
			$21535\ ^{9/2}-\ 75294^{\circ}\ _{7/2}$	1842.365	60	54278.1	$14859\ ^{11/2}-\ 69138^{\circ}\ _{9/2}$
1859.679	40*h*	53772.7	$14558\ ^{9/2}-\ 68331^{\circ}\ _{7/2}$	1842.235	5	54281.9	
1859.328	5	53782.9	$18211\ ^{5/2}-\ 71994^{\circ}\ _{5/2}$	1841.926	1	54291.0	$35828\ ^{9/2}-\ 90119^{\circ}\ _{11/2}$
1859.270	5	53784.6		1841.729	2	54296.8	
1858.198	10	53815.6	$14558\ ^{9/2}-\ 68374^{\circ}\ _{9/2}$	1841.514	6	54303.1	$20160\ ^{3/2}-\ 74463^{\circ}\ _{3/2}$
1857.791	5*w*	53827.4		1841.463	2	54304.6	
1857.615	5	53832.5		1841.311	2	54309.1	
1857.212	10	53844.1		1840.954	10 *c l*	54319.7	$21294\ ^{7/2}-\ 75614^{\circ}\ _{5/2}$
1857.044	1*h*	53849.0		1840.585	1	54330.6	
1856.931	1	53852.3		1840.136	3	54343.8	
1856.144	10	53875.1	$21418\ ^{5/2}-\ 75294^{\circ}\ _{7/2}$	1839.547	2	54361.2	
1856.053	10	53877.8		1838.456	200	54393.5	$12846\ ^{9/2}-\ 67240^{\circ}\ _{7/2}$
1855.878	10 *c l*	53882.8	$15525\ ^{11/2}-\ 69408^{\circ}\ _{11/2}$	1838.198	50	54401.1	$21238\ ^{13/2}-\ 75640^{\circ}\ _{11/2}$
1855.601	2	53890.9		1837.984	20	54407.4	
1855.511	10*h*	53893.5		1837.352	3	54426.2	
1855.117	3	53905.0	$30505\ ^{11/2}-\ 84410^{\circ}\ _{9/2}$	1837.311	1	54427.4	
1855.004	30	53908.2	$19700\ ^{11/2}-\ 73609^{\circ}\ _{11/2}$	1837.189	2	54431.0	
1854.181	5 *c l*	53932.2		1837.074	6	54434.4	
1853.958	10*h*	53938.6		1836.887	3	54439.9	
1853.754	1	53944.6	$20160\ ^{3/2}-\ 74105^{\circ}\ _{5/2}$	1836.705	3	54445.3	$20848\ ^{5/2}-\ 75294^{\circ}\ _{7/2}$
1853.326	4	53957.0	$25409\ ^{7/2}-\ 79366^{\circ}\ _{5/2}$	1836.635	5	54447.4	
1853.288	4	53958.2		1836.471	7	54452.3	$15525\ ^{11/2}-\ 69978^{\circ}\ _{11/2}$
1853.078	4	53964.3		1835.696	2	54475.2	
1852.481	2	53981.7		1835.657	1	54476.4	
1852.409	2*h*	53983.8		1835.219	1	54489.4	
1851.891	1	53998.8	$21294\ ^{7/2}-\ 75294^{\circ}\ _{7/2}$	1834.398	8	54513.8	
1850.099	8	54051.2	$31254\ ^{7/2}-\ 85306^{\circ}\ _{5/2}$	1833.240	100	54548.2	
1849.381	10	54072.1		1833.120	100	54551.8	
1849.277	2	54075.2		1832.466	2	54571.3	
1848.358	4	54102.1		1832.331	15	54575.3	$29835\ ^{9/2}-\ 84410^{\circ}\ _{9/2}$
1848.161	2	54107.8		1831.264	4	54607.1	
1847.484	10	54127.7		1831.212	8	54608.6	
1847.308	10 *b l*	54132.8		1830.872	50	54618.8	$23844\ ^{9/2}-\ 78463^{\circ}\ _{7/2}$
1847.196	20 *c l*	54136.1		1830.727	1	54623.1	$17113\ ^{13/2}-\ 71736^{\circ}\ _{11/2}$
1847.167	2	54137.0		1830.593	100*h*	54627.1	
1847.014	10	54141.4		1830.311	20	54635.5	$15045\ ^{7/2}-\ 69681^{\circ}\ _{5/2}$
1846.935	20	54143.8		1829.742	10*h*	54652.5	
1846.836	40	54146.6		1829.313	100*h*	54665.3	
1846.378	20	54160.1		1828.849	5 *b l*	54679.2	
1846.187	6	54165.7		1828.589	1	54687.0	
1845.896	1	54174.2		1828.196	2	54698.7	$78694^{\circ}\ _{11/2}-133393\ ^{13/2}$
1844.951	2	54202.0		1828.045	2	54703.2	
1844.862	3	54204.6		1827.758	4	54711.8	
1844.590	1	54212.6		1826.966	10	54735.6	
1843.910	20	54232.6	$19872\ ^{7/2}-\ 74105^{\circ}\ _{5/2}$	1825.989	2	54764.8	

[a] For doubly-classified lines, the wavelength is entered only once.

TABLE X. *Observed spectral lines of* Pr III *in the vacuum ultra violet region*—Continued

λ_{vac} Å	Intensity	σ (cm^{-1})	Classification [a]	λ_{vac} Å	Intensity	σ (cm^{-1})	Classification [a]
1825.792	1	54770.8		1798.347	20	55606.6	
1825.215	2	54788.1	$18241\ _{11/2}-\ 73029^{\circ}_{9/2}$	1797.273	20	55639.8	
1823.960	3	54825.8		1797.085	20	55645.7	$12846\ _{9/2}-\ 68492^{\circ}_{7/2}$
1823.855	15	54828.9	$35291\ _{9/2}-\ 90119^{\circ}_{11/2}$	1797.011	1	55648.0	
1823.703	60	54833.5		1795.721	2	55687.9	
1823.561	30	54837.8		1795.662	10	55689.8	$28720\ _{9/2}-\ 84410^{\circ}_{9/2}$
1822.640	2	54865.5		1794.822	10	55715.8	$22747\ _{9/2}-\ 78463^{\circ}_{7/2}$
1822.514	20	54869.3	$16516\ _{7/2}-\ 71385^{\circ}_{7/2}$	1794.614	40*h*	55722.3	
1821.782	4	54891.3		1794.164	1	55736.3	
1821.451	8	54901.3		1793.973	40	55742.2	$19872\ _{7/2}-\ 75614^{\circ}_{5/2}$
1821.333	1	54904.8		1793.695	100	55750.8	
1820.860	50	54919.1		1793.502	40	55756.8	
1820.296	4	54936.1		1792.983	10	55773.0	
1819.595	30	54957.3	$26446\ _{7/2}-\ 81404^{\circ}_{5/2}$	1792.794	3	55778.8	
1819.292	15	54966.4	$18063\ _{9/2}-\ 73029^{\circ}_{9/2}$	1792.569	1	55785.9	$13352\ _{11/2}-\ 69138^{\circ}_{5/2}$
1819.259	10	54967.4		1792.101	1	55800.4	
1818.913	10	54977.9		1791.938	30	55805.5	
1818.031	10*b l*	55004.6		1791.690	80	55813.2	
1817.401	3	55023.6		1791.274	2	55826.2	
1817.344	7	55025.4		1790.071	2	55863.7	
1817.023	1	55035.1		1790.027	3	55865.1	
1816.643	400	55046.6	$23647\ _{13/2}-\ 78694^{\circ}_{11/2}$	1789.955	1	55867.3	
1816.484	2	55051.4		1789.656	5	55876.7	
1815.721	30	55074.5		1789.247	1	55889.4	$19872\ _{7/2}-\ 75762^{\circ}_{9/2}$
1815.025	4	55095.7		1789.129	1	55893.1	$18211\ _{5/2}-\ 74105^{\circ}_{5/2}$
1814.295	40	55117.8	$14859\ _{11/2}-\ 69978^{\circ}_{11/2}$	1788.462	2	55914.0	$36640\ _{7/2}-\ 92554^{\circ}_{5/2}$
1812.375	20	55176.2		1787.770	3	55935.6	$22527\ _{7/2}-\ 78463^{\circ}_{7/2}$
1811.894	200*w*	55190.9		1787.635	1	55939.8	
1810.775	50	55225.0		1787.154	15	55954.9	$12846\ _{9/2}-\ 68801^{\circ}_{7/2}$
1810.611	3	55230.0		1786.964	4	55960.8	$23175\ _{13/2}-\ 79136^{\circ}_{13/2}$
1809.556	4	55262.2	$23050\ _{3/2}-\ 78312^{\circ}_{1/2}$	1786.691	10*h*	55969.4	
1808.516	15	55293.9	$22527\ _{7/2}-\ 77822^{\circ}_{5/2}$	1786.141	70	55986.6	
1808.106	30	55306.5		1785.885	10	55994.6	$25409\ _{7/2}-\ 81404^{\circ}_{5/2}$
1807.913	4	55312.4		1785.330	1	56012.0	
1807.776	1	55316.6		1780.963	10*b l*	56149.4	
1805.481	5	55386.9		1780.596	5	56161.0	$14859\ _{11/2}-\ 71021^{\circ}_{9/2}$
1804.775	40	55408.6		1780.210	10	56173.1	
1804.354	10	55421.5	$19872\ _{7/2}-\ 75294^{\circ}_{7/2}$	1779.460	4	56196.8	
1803.399	2	55450.8		1779.025	2	56210.6	$21611\ _{5/2}-\ 77822^{\circ}_{5/2}$
1803.231	3*b l*	55456.0		1778.732	1	56219.8	
1803.100	3*b l*	55460.0		1778.422	1	56229.6	
1802.430	20*b l*	55480.6		1777.716	4	56251.9	$18211\ _{5/2}-\ 74463^{\circ}_{3/2}$
1802.292	20	55484.9	$12846\ _{9/2}-\ 68331^{\circ}_{7/2}$	1777.452	2	56260.3	
1802.186	5	55488.2	$23647\ _{13/2}-\ 79136^{\circ}_{13/2}$	1776.879	20	56278.4	
1801.964	1	55495.0		1776.515	15*h*	56290.0	
1801.172	100	55519.4	$23175\ _{13/2}-\ 78694^{\circ}_{11/2}$	1774.491	5	56354.2	
			$38448\ _{9/2}-\ 93967^{\circ}_{7/2}$	1774.257	1	56361.6	
1800.902	20	55527.7	$12846\ _{9/2}-\ 68374^{\circ}_{9/2}$	1773.023	7	56400.8	
1800.839	10	55529.7		1772.390	1	56421.0	$38726\ _{7/2}-\ 95147^{\circ}_{9/2}$
1799.453	1	55572.4		1772.129	3	56429.3	

[a] For doubly-classified lines, the wavelength is entered only once.

TABLE X. *Observed spectral lines of* Pr III *in the vacuum ultra violet region*—Continued

λ_{vac} Å	Intensity	σ (cm^{-1})	Classification [a]	λ_{vac} Å	Intensity	σ (cm^{-1})	Classification [a]
1771.958	4	56434.7		1740.056	1	57469.4	
1771.680	1	56443.6		1739.840	200	57476.6	
1771.545	15	56447.9		1738.971	30	57505.3	
1771.483	10	56449.9		1737.972	5*h*	57538.3	
1771.328	4	56454.8		1736.996	10	57570.6	
1769.398	100	56516.4	$23844_{9/2} - 80360^{\circ}_{11/2}$	1736.747	5	57578.9	
1769.064	20	56527.1	$21294_{7/2} - 77822^{\circ}_{5/2}$	1736.646	200	57582.2	
1768.618	7	56541.3		1735.801	4	57610.3	
1768.479	10	56545.8		1735.757	1	57611.8	
1768.114	5	56557.4		1734.029	2	57669.2	$13352_{11/2} - 71021^{\circ}_{9/2}$
1766.432	3	56611.3	$22277_{3/2} - 78889^{\circ}_{3/2}$	1732.382	20	57724.0	$25979_{15/2} - 83703^{\circ}_{13/2}$
1765.543	2	56639.8		1731.526	2	57752.5	$23651_{7/2} - 81404^{\circ}_{5/2}$
1765.299	1	56647.6	$22747_{9/2} - 79395^{\circ}_{7/2}$	1731.442	2	57755.3	$21611_{5/2} - 79366^{\circ}_{5/2}$
1765.087	4	56654.4	$36642_{13/2} - 93296^{\circ}_{11/2}$	1729.702	3	57813.4	$23175_{13/2} - 80988^{\circ}_{13/2}$
1764.859	10*h*	56661.7		1728.302	1	57860.3	$21535_{9/2} - 79395^{\circ}_{7/2}$
1763.122	20	56717.6		1727.281	1	57894.4	
1763.005	1	56721.3		1727.194	1	57897.4	$21238_{13/2} - 79136_{13/2}$
1762.665	7	56732.3	$14859_{11/2} - 71592^{\circ}_{9/2}$	1725.553	3*b l*	57952.4	
1761.668	20	56764.4		1724.116	1	58000.7	
1761.052	2	56784.2		1723.641	10	58016.7	
1760.859	10	56790.5		1722.693	2	58048.6	
1760.518	10*h*	56801.5		1722.011	15	58071.6	$21294_{7/2} - 79366^{\circ}_{5/2}$
1759.916	1	56820.9		1721.800	1	58078.8	
1759.318	30	56840.2		1721.473	1	58089.8	
1759.278	10*c l*	56841.5		1721.102	5*h*	58102.3	
1758.351	5	56871.5		1720.034	2	58138.4	
1758.277	1	56873.9		1719.940	4	58141.6	
1758.196	7	56876.5	$14859_{11/2} - 71736^{\circ}_{11/2}$	1717.770	200	58215.0	$30733_{11/2} - 88948^{\circ}_{9/2}$
1755.522	20	56963.1		1717.152	1	58236.0	
1755.445	4	56965.6	$31254_{7/2} - 88220^{\circ}_{9/2}$	1715.471	5	58293.0	
1754.934	10*h*	56982.2		1713.147	4	58372.1	
1754.583	200	56993.6		1712.848	60*h*	58382.3	$38448_{9/2} - 96830^{\circ}_{7/2}$
1753.297	10	57035.4		1712.381	1	58398.2	
1750.486	5*c l*	57127.0		1712.058	1	58409.2	
1750.462	5*c l*	57127.8	$71978^{\circ}_{7/2} - 129106_{9/2}$	1711.408	2*h*	58431.4	
1749.160	2	57170.3	$35384_{5/2} - 92554^{\circ}_{5/2}$	1710.139	2	58474.8	
1748.330	5	57197.4		1709.377	5*h*	58500.8	
1747.949	100	57209.9		1707.514	1	58564.7	$24461_{5/2} - 83025^{\circ}_{3/2}$
1746.225	1	57266.4		1706.743	10	58591.1	$19872_{7/2} - 78463^{\circ}_{7/2}$
1745.879	3	57277.7	$21611_{5/2} - 78889^{\circ}_{3/2}$	1705.705	50*h*	58626.8	$28885_{9/2} - 87511^{\circ}_{7/2}$
1745.474	10*h*	57291.0		1702.266	1	58745.2	$21418_{5/2} - 80164^{\circ}_{3/2}$
1745.329	2	57295.8		1700.952	20	58790.6	$28720_{9/2} - 87511^{\circ}_{7/2}$
1744.571	4	57320.7		1700.128	1	58819.1	$24788_{9/2} - 83607^{\circ}_{11/2}$
1743.957	3	57340.9	$23647_{13/2} - 80988^{\circ}_{13/2}$	1699.416	3	58843.7	
1743.758	1	57347.4		1698.689	10	58868.9	
1743.377	400	57359.9	$32760_{13/2} - 90119^{\circ}_{11/2}$	1697.558	3	58908.1	
1742.574	2	57386.4		1696.079	15	58959.5	
1742.073	10	57402.9	$18211_{5/2} - 75614^{\circ}_{5/2}$	1694.896	1	59000.7	$25409_{7/2} - 84410^{\circ}_{9/2}$
1741.563	1	57419.7	$14558_{9/2} - 71978^{\circ}_{7/2}$	1694.547	100	59012.8	$25979_{15/2} - 84992^{\circ}_{15/2}$
1740.471	1	57455.7	$21238_{13/2} - 78694^{\circ}_{11/2}$	1692.766	30	59074.9	

[a] For doubly-classified lines, the wavelength is entered only once.

TABLE X. *Observed spectral lines of* Pr III *in the vacuum ultra violet region*—Continued

λ_{vac} Å	Intensity	σ (cm^{-1})	Classification [a]	λ_{vac} Å	Intensity	σ (cm^{-1})	Classification [a]
1691.726	10	59111.2		1521.236	10	65736.0	
1689.800	2	59178.6		1520.128	1	65783.9	$13352\ _{11/2}-\ 79136^{\circ}{}_{13/2}$
1687.085	1	59273.8		1520.030	3	65788.2	
1685.905	1	59315.3	$20848\ _{5/2}-\ 80164^{\circ}{}_{3/2}$	1519.247	100	65822.1	
1685.033	2	59346.0	$35801\ _{7/2}-\ 95147^{\circ}{}_{9/2}$	1518.966	4*h*	65834.2	
1684.583	1	59361.9		1518.655	2	65847.7	$12846\ _{9/2}-\ 78694^{\circ}{}_{11/2}$
1683.887	5	59386.4	$30733\ _{11/2}-\ 90119^{\circ}{}_{11/2}$	1518.560	2	65851.9	$15045\ _{5/2}-\ 80897^{\circ}{}_{3/2}$
1681.073	1*h*	59485.8		1518.374	1	65859.9	
1680.841	8	59494.0	$19872\ _{7/2}-\ 79366^{\circ}{}_{5/2}$	1518.212	1	65867.0	
1679.872	1	59528.3		1518.142	40*h*	65870.0	
1677.314	20*h*	59619.1		1517.622	20*h*	65892.6	
1676.900	30	59633.8	$71592^{\circ}{}_{9/2}-131226\ _{9/2}$	1517.441	10	65900.4	$21611\ _{5/2}-\ 87511^{\circ}{}_{7/2}$
1676.363	3	59653.0		1517.341	100*h*	65904.8	
1674.074	4*h*	59734.5		1516.753	5	65930.3	$65295^{\circ}{}_{7/2}-131226\ _{9/2}$
1673.663	1	59749.2		1516.533	40*w*	65939.9	
1672.914	4	59775.9	$19360\ _{13/2}-\ 79136^{\circ}{}_{13/2}$	1516.365	1	65947.2	
1671.427	20	59829.1		1515.694	15	65976.4	$21535\ _{9/2}-\ 87511^{\circ}{}_{7/2}$
1667.796	4	59959.4	$23647\ _{13/2}-\ 83607^{\circ}{}_{11/2}$	1514.893	50*b l*	66011.3	
1666.198	7	60016.9		1513.746	10*h*	66061.3	
1666.118	1	60019.8		1513.602	5	66067.6	
1665.129	8	60055.4	$23647\ _{13/2}-\ 83703^{\circ}{}_{13/2}$	1513.530	5*w*	66070.7	$18921\ _{15/2}-\ 84992^{\circ}{}_{15/2}$
1663.639	1	60109.2		1512.678	1	66107.9	$26446\ _{7/2}-\ 92554^{\circ}{}_{5/2}$
1660.981	3	60205.4	$71021^{\circ}{}_{9/2}-131226\ _{9/2}$	1512.632	1	66109.9	
1657.206	2	60342.5		1512.206	100*w*	66128.6	$14859\ _{11/2}-\ 80988^{\circ}{}_{13/2}$
1654.182	3	60452.8	$18241\ ^{11/2}-\ 78694^{\circ}{}_{11/2}$	1511.988	10	66138.1	
1653.351	2	60483.2		1511.274	4	66169.3	$18241\ _{11/2}-\ 84410^{\circ}{}_{9/2}$
1649.187	400*w*	60635.9		1510.693	10*h*	66194.8	
1648.067	3	60677.2	$18211\ _{5/2}-\ 78889^{\circ}{}_{3/2}$	1509.987	4	66225.7	
1645.043	1	60788.7		1509.565	50*h*	66244.2	
1630.147	5*h*	61344.2	$23647\ _{13/2}-\ 84992^{\circ}{}_{15/2}$	1509.155	2 *c l*	66262.2	$28885\ _{9/2}-\ 95147^{\circ}{}_{9/2}$
1627.434	200*h*	61446.4	$35384\ _{5/2}-\ 96830^{\circ}{}_{7/2}$	1508.867	7*w*	66274.9	$23844\ _{9/2}-\ 90119^{\circ}{}_{11/2}$
1624.969	1	61539.6	$35291\ _{9/2}-\ 96830^{\circ}{}_{7/2}$	1508.327	3	66298.6	
1622.622	1	61628.6	$19360\ _{13/2}-\ 80988^{\circ}{}_{13/2}$	1508.074	20*h*	66309.7	
1621.248	100	61680.9	$33466\ _{11/2}-\ 95147^{\circ}{}_{9/2}$	1506.863	3	66363.0	$27604\ _{9/2}-\ 93967^{\circ}{}_{7/2}$
1614.502	2	61938.6		1506.805	1	66365.6	$44903\ _{5/2}-111268^{\circ}{}_{3/2}$
1611.809	100 *c l*	62042.1		1506.425	2	66382.3	
1604.766	1	62314.4		1505.774	3	66411.0	
1594.572	10	62712.7	$31254\ _{7/2}-\ 93967^{\circ}{}_{7/2}$	1505.654	300	66416.3	
1589.553	2	62910.8		1505.409	5	66427.1	$28720\ _{9/2}-\ 95147^{\circ}{}_{9/2}$
1580.105	3	63286.9	$29267\ _{5/2}-\ 92554^{\circ}{}_{5/2}$	1505.329	20*h*	66430.7	
1579.856	1	63296.9		1504.783	30	66454.8	$67049^{\circ}{}_{9/2}-133503\ _{11/2}$
1574.825	1	63499.1		1504.761	400*w*	66455.7	
1573.388	10*h*	63557.1	$28885\ _{9/2}-\ 92441^{\circ}{}_{7/2}$	1504.662	2	66460.1	$69408^{\circ}{}_{11/2}-135868\ _{9/2}$
1569.341	1	63721.0	$28720\ _{9/2}-\ 92441^{\circ}{}_{7/2}$	1504.398	400 *b l*	66471.8	$23647\ _{13/2}-\ 90119^{\circ}{}_{11/2}$
1531.171	5	65309.5		1504.269	1	66477.5	
1529.851	1	65365.8	$18241\ _{11/2}-\ 83607^{\circ}{}_{11/2}$	1504.086	8	66485.6	$46673\ _{7/2}-113158^{\circ}{}_{9/2}$
1522.489	2*h*	65681.9		1503.607	20	66506.7	$25934\ _{5/2}-\ 92441^{\circ}{}_{7/2}$
1522.241	100*h*	65692.6	$27604\ _{9/2}-\ 93296^{\circ}{}_{11/2}$	1503.422	100 *c l*	66514.9	$27452\ _{5/2}-\ 93967^{\circ}{}_{7/2}$
			$22527\ _{7/2}-\ 88220^{\circ}{}_{9/2}$	1502.967	10	66535.1	
1521.417	3	65728.2		1502.807	2	66542.1	

[a] For doubly-classified lines, the wavelength is entered only once.

TABLE X. *Observed spectral lines of* Pr III *in the vacuum ultra violet region*—Continued

λ_{vac} Å	Intensity	σ (cm^{-1})	Classification [a]	λ_{vac} Å	Intensity	σ (cm^{-1})	Classification [a]
1502.688	10	66547.4	$62558^{\circ}_{11/2}$–$129106_{9/2}$	1487.561	15	67224.1	
1502.435	3	66558.6		1487.137	100*h*	67243.3	
1502.305	10	66564.4		1486.827	1	67257.3	
1501.676	10	66592.3		1486.630	20*h*	67266.2	
1501.054	20	66619.8	$25934_{5/2} - 92554^{\circ}_{5/2}$	1486.538	5	67270.4	
1500.901	3*w*	66626.6		1485.425	200	67320.8	
1500.675	10	66636.7		1484.932	20	67343.2	$68525^{\circ}_{11/2}$–$135868_{9/2}$
1500.445	20*h*	66646.9		1484.661	50	67355.4	$66148^{\circ}_{13/2}$–$133503_{11/2}$
1500.080	50	66663.1	$44679_{7/2}$ –$111342^{\circ}_{7/2}$	1484.298	300*w*	67371.9	$22747_{9/2} - 90119^{\circ}_{11/2}$
1499.756	50*w*	66677.5	$23442_{11/2} - 90119^{\circ}_{11/2}$	1484.211	3	67375.9	
1499.586	3*h*	66685.1	$21535_{9/2} - 88220^{\circ}_{9/2}$	1484.046	3	67383.4	$63816^{\circ}_{11/2}$–$131200_{11/2}$
1499.112	2	66706.2		1483.825	7	67393.4	
1498.566	4	66730.5	$69138^{\circ}_{9/2}$ –$135868_{9/2}$	1483.598	10	67403.7	
1498.426	1	66736.7		1483.508	5	67407.8	$25033_{9/2} - 92441^{\circ}_{7/2}$
1497.724	1	66768.0	$66735^{\circ}_{13/2}$–$133503_{11/2}$	1483.470	8	67409.5	$63816^{\circ}_{11/2}$–$131226_{9/2}$
1497.352	3	66784.6	$23844_{9/2} - 90629^{\circ}_{9/2}$	1483.400	10	67412.7	
1496.880	7	66805.6		1482.662	3	67446.2	
1496.831	8	66807.8		1482.585	10	67449.8	
1496.247	20	66833.9		1482.548	1	67451.4	
1495.999	200	66845.0		1482.417	20	67457.4	$17534_{15/2} - 84992^{\circ}_{15/2}$
1495.547	30	66865.2	$62240^{\circ}_{11/2}$–$129106_{9/2}$	1482.127	10	67470.6	$65922^{\circ}_{11/2}$–$133393_{13/2}$
1495.506	7	66867.0		1481.704	3	67489.9	
1495.220	200	66879.8		1481.609	1	67494.2	$68374^{\circ}_{9/2}$ –$135868_{9/2}$
1495.047	2*h*	66887.5		1481.475	7	67500.3	$61605^{\circ}_{7/2}$ –$129106_{9/2}$
1494.944	20*h*	66892.1		1481.193	5	67513.1	
1494.747	10	66901.0	$68544^{\circ}_{9/2}$ –$135445_{7/2}$	1481.123	5	67516.3	
1494.200	40*w*	66925.4	$21294_{7/2} - 88220^{\circ}_{9/2}$	1481.035	40	67520.3	$26446_{7/2} - 93967^{\circ}_{7/2}$
1493.724	4 *c l*	66946.8		1480.953	3	67524.1	
1493.694	10 *c l*	66948.1		1480.527	2	67543.5	$27604_{9/2} - 95147^{\circ}_{9/2}$
1493.590	5	66952.8	$68492^{\circ}_{7/2}$ –$135445_{7/2}$	1480.093	10*h*	67563.3	
1492.951	4	66981.4		1479.953	10	67569.7	
1492.874	60	66984.9	$64215^{\circ}_{13/2}$–$131200_{11/2}$	1479.887	40	67572.7	
1492.352	100*w*	67008.3	$13352_{11/2} - 80360^{\circ}_{11/2}$	1479.849	2	67574.5	$67870^{\circ}_{9/2}$ –$135445_{7/2}$
1491.830	3	67031.8	$25409_{7/2} - 92441^{\circ}_{7/2}$	1479.695	20	67581.5	$65922^{\circ}_{11/2}$–$133503_{11/2}$
1491.713	10*h*	67037.0		1479.549	10 *b l*	67588.2	
1490.867	7	67075.1	$64150^{\circ}_{11/2}$–$131226_{9/2}$	1479.300	2	67599.5	
1490.494	50	67091.8	$66301^{\circ}_{15/2}$–$133393_{13/2}$	1479.136	10	67607.0	$63593^{\circ}_{9/2}$ –$131200_{11/2}$
1490.431	2	67094.7		1479.083	20	67609.4	
1490.014	3*h*	67113.5	$68331^{\circ}_{7/2}$ –$135445_{7/2}$	1478.974	2	67614.4	
1489.937	50*h*	67116.9		1478.835	5	67620.8	
1489.689	3	67128.1		1478.618	3	67630.7	$68238^{\circ}_{11/2}$–$135868_{9/2}$
1489.567	200	67133.6		1478.572	8	67632.8	$63593^{\circ}_{9/2}$ –$131226_{9/2}$
1489.319	40	67144.8	$25409_{7/2} - 92554^{\circ}_{5/2}$	1478.527	20	67634.9	
1489.187	4*h*	67150.7		1478.436	10	67639.0	$19872_{7/2} - 87511^{\circ}_{7/2}$
1489.073	10*h*	67155.9		1478.324	20	67644.2	
1488.984	100*h*	67159.9		1478.253	10	67647.4	
1488.202	1	67195.2		1478.120	100	67653.5	$24788_{9/2} - 92441^{\circ}_{7/2}$
1488.071	30	67201.1	$26095_{11/2} - 93296^{\circ}_{11/2}$	1478.048	20	67656.8	
1487.843	20	67211.4		1477.977	20 *b l*	67660.0	
1487.723	8	67216.8		1477.650	8	67675.0	

[a] For doubly-classified lines, the wavelength is entered only once.

TABLE X. *Observed spectral lines of* Pr III *in the vacuum ultra violet region*—Continued

λ_{vac} Å	Intensity	σ (cm^{-1})	Classification [a]	λ_{vac} Å	Intensity	σ (cm^{-1})	Classification [a]
1477.559	6	67679.2		1466.320	1	68197.9	
1477.506	3	67681.6		1466.011	1	68212.3	
1477.109	15	67699.8		1465.984	1	68213.6	
1477.046	7	67702.7		1465.899	2	68217.5	
1476.843	30	67712.0	$45844_{3/2} - 113556^{\circ}_{5/2}$	1465.216	2	68249.3	$15454_{13/2} - 83703^{\circ}_{13/2}$
1476.566	2	67724.7		1465.124	200	68253.6	
1476.516	10	67727.0		1465.021	200	68258.4	
1476.274	200	67738.1		1464.853	3	68266.2	
1475.801	4	67759.8		1464.742	5 *b l*	68271.4	
1475.700	10	67764.4		1464.502	60*w*	68282.6	
1475.562	10	67770.8		1464.400	1	68287.3	
1475.508	20*h*	67773.3		1464.013	40	68305.4	
1475.411	200	67777.7		1463.825	100	68314.2	
1474.094	50	67838.3		1463.756	10	68317.4	
1474.013	100	67842.0		1463.554	400	68326.8	
1473.818	200*w*	67851.0		1463.332	200	68337.2	
1473.720	4*h*	67855.5		1463.233	400	68341.8	
1473.364	2	67871.9		1462.700	30	68366.7	
1473.155	2	67881.5	$22747_{9/2} - 90629^{\circ}_{9/2}$	1462.585	20	68372.1	
1472.995	1	67888.9		1462.155	50	68392.2	
1472.456	1	67913.7		1462.019	1	68398.6	
1472.332	20	67919.5		1461.616	100*h*	68417.4	
1472.142	1	67928.2		1461.504	1	68422.7	
1472.102	2	67930.1		1461.405	4	68427.3	
1471.895	3	67939.6		1461.218	2	68436.0	
1471.767	30	67945.5	$28885_{9/2} - 96830^{\circ}_{7/2}$	1460.632	2	68463.5	
1471.518	3	67957.0		1460.440	2	68472.5	
1471.255	5	67969.2		1460.223	1	68482.7	
1470.908	3	67985.2		1460.050	40	68490.8	
1470.805	80	67990.0		1459.674	40	68508.4	$24788_{9/2} - 93296^{\circ}_{11/2}$
1470.324	10	68012.2		1459.405	3	68521.1	
1470.261	20 *b l*	68015.1		1459.339	100	68524.2	
1470.045	3*w*	68025.1		1459.257	2*h*	68528.0	$64865^{\circ}_{11/2} - 133393_{13/2}$
1469.887	2	68032.4	$25934_{5/2} - 93967^{\circ}_{7/2}$	1459.033	1	68538.5	
1469.649	2	68043.4		1458.771	8	68550.8	
1469.511	7	68049.8	$67395^{\circ}_{5/2} - 135445_{7/2}$	1458.701	2	68554.1	
1469.369	3	68056.4		1458.614	30*h*	68558.2	
1468.902	60	68078.1		1458.202	10	68577.6	
1468.779	10	68083.8	$24470_{7/2} - 92554^{\circ}_{5/2}$	1458.130	100	68581.0	
1468.573	5*w*	68093.3	$24461_{5/2} - 92554^{\circ}_{5/2}$	1457.894	2	68592.1	$66852^{\circ}_{7/2} - 135445_{7/2}$
1468.399	200	68101.4	$22527_{7/2} - 90629^{\circ}_{9/2}$	1457.784	10	68597.3	$23844_{9/2} - 92441^{\circ}_{7/2}$
1468.227	20	68109.3	$28720_{9/2} - 96830^{\circ}_{7/2}$	1457.512	30	68610.1	
1467.698	100*h*	68133.9		1457.433	4*h*	68613.8	
1467.646	3	68136.3		1457.357	3*h*	68617.4	
1467.595	10	68138.7		1457.257	5	68622.1	
1467.409	4	68147.3		1456.949	40	68636.6	
1467.247	3	68154.8		1456.787	1	68644.2	
1467.153	7	68159.2		1456.738	1	68646.5	$64857^{\circ}_{9/2} - 133503_{11/2}$
1467.081	10*h*	68162.6		1456.574	2	68654.2	
1466.971	2	68167.7		1455.583	30	68701.0	$26446_{7/2} - 95147^{\circ}_{9/2}$

[a] For doubly-classified lines, the wavelength is entered only once.

TABLE X. *Observed spectral lines of* Pr III *in the vacuum ultra violet region*—Continued

λ_{vac} Å	Intensity	σ (cm^{-1})	Classification [a]	λ_{vac} Å	Intensity	σ (cm^{-1})	Classification [a]
1454.957	400 *b l*	68730.6		1440.844	1 *h*	69403.8	
1454.832	4	68736.4		1440.733	10 *h*	69409.1	
1454.775	5	68739.2		1440.234	5	69433.2	
1454.602	5	68747.3	$46673_{7/2} - 115420^{\circ}_{7/2}$	1439.922	30	69448.2	$18063_{9/2} - 87511^{\circ}_{7/2}$
			$14859_{11/2} - 83607^{\circ}_{11/2}$	1439.540	100	69466.6	
1454.265	20	68763.2		1439.420	10 *h*	69472.4	
1454.029	40	68774.4		1438.925	2	69496.3	$24470_{7/2} - 93967^{\circ}_{7/2}$
1453.934	5	68778.9		1438.766	3	69504.0	$23050_{3/2} - 92554^{\circ}_{5/2}$
1453.705	7	68789.8	$16516_{7/2} - 85306^{\circ}_{5/2}$	1438.719	5	69506.3	$24461_{5/2} - 93967^{\circ}_{7/2}$
1453.541	15	68797.5		1438.532	20 *h*	69515.3	
1453.405	30	68803.9		1438.037	50 *h*	69539.2	
1453.094	20 *h*	68818.7		1437.871	1	69547.3	
1453.014	100 *h*	68822.5		1437.405	7	69569.8	
1452.887	40	68828.5		1435.977	10	69639.0	
1452.569	1	68843.6	$14859_{11/2} - 83703^{\circ}_{13/2}$	1434.845	40	69693.9	$45805_{9/2} - 115499^{\circ}_{9/2}$
1452.478	1	68847.8		1434.629	40 *h*	69704.4	
1452.352	400	68853.8		1434.540	5 *h*	69708.8	
1452.005	8 *h*	68870.3		1434.187	20 *h*	69725.9	
1451.783	100	68880.8	$21238_{13/2} - 90119^{\circ}_{11/2}$	1434.090	10 *h*	69730.6	
1451.358	300 *h*	68901.0		1433.936	20	69738.1	$25409_{7/2} - 95147^{\circ}_{9/2}$
1451.193	30	68908.8	$23532_{5/2} - 92441^{\circ}_{7/2}$	1432.971	5 *h*	69785.1	
1450.960	4 *h*	68919.9		1432.015	5 *h*	69831.7	
1450.500	2	68941.7		1431.711	5 *w*	69846.5	
1450.403	4	68946.4		1431.554	3	69854.1	$23442_{11/2} - 93296^{\circ}_{11/2}$
1450.241	10 *h*	68954.0		1431.244	20	69869.3	$61357^{\circ}_{9/2} - 131226_{9/2}$
1448.814	5	69022.0	$23532_{5/2} - 92554^{\circ}_{5/2}$	1431.103	40	69876.2	
1448.524	10 *h*	69035.8		1431.014	100	69880.5	
1448.168	100	69052.8	$26095_{11/2} - 95147^{\circ}_{9/2}$	1430.930	3	69884.6	$17627_{9/2} - 87511^{\circ}_{7/2}$
1447.963	4	69062.5		1430.543	5	69903.5	
1447.616	100	69079.1		1430.329	20	69914.0	$22527_{7/2} - 92441^{\circ}_{7/2}$
1447.301	3	69094.1	$21535_{9/2} - 90629^{\circ}_{9/2}$	1430.158	300	69922.3	
1446.361	1	69139.0	$48401_{3/2} - 117540^{\circ}_{3/2}$	1429.627	1	69948.3	
1445.822	50 *h*	69164.8		1428.703	3	69993.6	$45807_{5/2} - 115800^{\circ}_{5/2}$
1445.659	4	69172.6		1428.018	40	70027.1	$22527_{7/2} - 92554^{\circ}_{5/2}$
1445.517	300	69179.4	$24788_{9/2} - 93967^{\circ}_{7/2}$	1427.709	20	70042.3	
1445.279	2	69190.8		1427.561	3	70049.5	
1445.033	3 *h*	69202.6		1427.014	100	70076.4	
1444.551	50 *h*	69225.7		1426.067	100	70122.9	$23844_{9/2} - 93967^{\circ}_{7/2}$
1444.331	2	69236.2		1424.775	2	70186.5	
1444.106	20	69247.0		1424.001	1	70224.7	
1443.659	2 *h*	69268.4	$64235^{\circ}_{9/2} - 133503_{11/2}$	1423.653	5	70241.8	
1443.470	400	69277.5		1423.393	3	70254.7	
1443.005	1	69299.8	$18211_{5/2} - 87511^{\circ}_{7/2}$	1423.187	4 *h*	70264.8	
1442.865	3 *h*	69306.6		1423.114	2 *h*	70268.4	
1442.750	5 *h*	69312.1		1422.943	2	70276.9	$22277_{3/2} - 92554^{\circ}_{5/2}$
1442.290	10	69334.2	$21294_{7/2} - 90629^{\circ}_{9/2}$	1422.718	10	70288.0	
1442.085	7	69344.0		1422.551	10 *h*	70296.2	
1441.730	7	69361.1		1422.079	3 *h*	70319.6	
1441.388	20	69377.6	$27452_{5/2} - 96830^{\circ}_{7/2}$	1421.745	10	70336.1	
1440.948	20 *h*	69398.8		1421.636	20	70341.5	

[a] For doubly-classified lines, the wavelength is entered only once.

TABLE X. *Observed spectral lines of* Pr III *in the vacuum ultra violet region*—Continued

λ_{vac} Å	Intensity	σ (cm^{-1})	Classification[a]	λ_{vac} Å	Intensity	σ (cm^{-1})	Classification[a]
1421.479	1	70349.3		1406.681	15	71089.3	
1421.262	100	70360.0	$24788\ ^{9/2} - 95147^{\circ}\ ^{9/2}$	1406.071	15	71120.2	$44679\ ^{7/2} - 115800^{\circ}\ ^{5/2}$
1420.795	15	70383.1	$26446\ ^{7/2} - 96830^{\circ}\ ^{7/2}$	1405.544	50	71146.8	$21294\ ^{7/2} - 92441^{\circ}\ ^{7/2}$
1420.334	5	70406.0		1405.434	2	71152.4	$62240^{\circ}\ ^{11/2} - 133393\ ^{13/2}$
1420.071	50*h*	70419.0	$19700\ ^{11/2} - 90119^{\circ}\ ^{11/2}$	1405.100	1	71169.3	
1420.021	10 *c l*	70421.5		1404.974	30	71175.7	
1418.966	7	70473.8	$22080\ ^{7/2} - 92554^{\circ}\ ^{5/2}$	1404.747	300	71187.2	
1418.477	2	70498.1		1404.102	20	71219.9	$22747\ ^{9/2} - 93967^{\circ}\ ^{7/2}$
1417.458	1	70548.8	$22747\ ^{9/2} - 93296^{\circ}\ ^{11/2}$	1403.981	300	71226.0	
1417.081	20	70567.6		1403.868	4	71231.8	
1416.779	20	70582.6		1403.598	60	71245.5	
1416.165	5	70613.2		1403.310	100	71260.1	$21294\ ^{7/2} - 92554^{\circ}\ ^{5/2}$
1415.874	1	70627.8	$64817^{\circ}\ ^{5/2} - 135445\ ^{7/2}$	1403.171	100	71267.2	
1415.756	300	70633.6		1402.907	40	71280.6	
1414.393	3	70701.7		1402.743	20	71288.9	$40205\ ^{3/2} - 111494^{\circ}\ ^{5/2}$
1414.230	2	70709.8		1402.599	3	71296.2	
1414.137	50	70714.5	$62678^{\circ}\ ^{13/2} - 133393\ ^{13/2}$	1402.458	8	71303.4	$23844\ ^{9/2} - 95147^{\circ}\ ^{9/2}$
1413.766	3	70733.1		1402.122	8	71320.5	$19308\ ^{11/2} - 90629^{\circ}\ ^{9/2}$
1413.674	10	70737.7		1402.047	100 *c l*	71324.3	
1413.359	5	70753.4		1402.030	30 *c l*	71325.2	
1413.235	3*h*	70759.6	$19360\ ^{13/2} - 90119^{\circ}\ ^{11/2}$	1401.774	3	71338.2	
1412.825	400	70780.2		1401.405	4	71357.0	
1412.655	5*h*	70788.7		1401.176	100	71368.6	
1412.492	3	70796.9		1400.611	20*h*	71397.4	
1412.297	20	70806.6	$60419^{\circ}\ ^{11/2} - 131226\ ^{9/2}$	1400.434	7	71406.4	$21148\ ^{3/2} - 92554^{\circ}\ ^{5/2}$
1412.087	10	70817.2		1400.359	7*h*	71410.3	
1411.924	20	70825.3	$62678^{\circ}\ ^{13/2} - 133503\ ^{11/2}$	1400.160	3	71420.4	$25409\ ^{7/2} - 96830^{\circ}\ ^{7/2}$
1411.819	20	70830.6	$21611\ ^{5/2} - 92441^{\circ}\ ^{7/2}$	1399.141	5	71472.4	$39870\ ^{9/2} - 111342^{\circ}\ ^{7/2}$
1411.732	100*h*	70835.0		1398.824	40	71488.6	
1411.399	10 *c l*	70851.7		1398.695	5	71495.2	
1411.372	3 *c l*	70853.0		1398.619	40	71499.1	
1411.184	2	70862.5		1397.919	2	71534.9	
1410.745	10	70884.5	$50647\ ^{11/2} - 121532^{\circ}\ ^{11/2}$	1397.770	4	71542.5	
1410.651	100	70889.3	$64979^{\circ}\ ^{7/2} - 135868\ ^{9/2}$	1397.421	100*h*	71560.4	
1410.528	10 *b l*	70895.4	$25934\ ^{5/2} - 96830^{\circ}\ ^{7/2}$	1397.344	20	71564.3	
1410.304	60	70906.7	$21535\ ^{9/2} - 92441^{\circ}\ ^{7/2}$	1397.227	5	71570.3	
1409.801	100*h*	70932.0	$58174^{\circ}\ ^{9/2} - 129106\ ^{9/2}$	1396.842	7	71590.0	
1409.708	5	70936.7		1396.444	50	71610.5	
1409.535	3	70945.4	$62558^{\circ}\ ^{11/2} - 133503\ ^{11/2}$	1396.219	20	71622.0	
1409.479	20	70948.2	$58158^{\circ}\ ^{7/2} - 129106\ ^{9/2}$	1395.722	2	71647.5	
1408.544	3	70995.3	$16516\ ^{7/2} - 87511^{\circ}\ ^{7/2}$	1395.658	5	71650.8	
1408.221	10	71011.6	$64857^{\circ}\ ^{9/2} - 135868\ ^{9/2}$	1395.383	8	71664.9	
1407.904	2	71027.6		1395.316	3	71668.4	
1407.773	20	71034.2	$60166^{\circ}\ ^{9/2} - 131200\ ^{11/2}$	1395.196	4*h*	71674.5	
1407.574	3	71044.2	$64401^{\circ}\ ^{5/2} - 135445\ ^{7/2}$	1394.784	10	71695.7	$45844\ ^{3/2} - 117540^{\circ}\ ^{3/2}$
1407.485	30*h*	71048.7		1394.718	20*h*	71699.1	
1407.352	6	71055.4		1394.585	60	71705.9	$20848\ ^{5/2} - 92554^{\circ}\ ^{5/2}$
1407.283	10 *c l*	71058.9	$13352\ ^{11/2} - 84410^{\circ}\ ^{9/2}$				$23442\ ^{11/2} - 95147^{\circ}\ ^{9/2}$
1407.260	10 *c l*	71060.1	$60166^{\circ}\ ^{9/2} - 131226\ ^{9/2}$	1394.540	2	71708.2	
1407.212	5	71062.5	$40205\ ^{3/2} - 111268^{\circ}\ ^{3/2}$	1394.435	3	71713.6	

[a] For doubly-classified lines, the wavelength is entered only once.

TABLE X. *Observed spectral lines of* Pr III *in the vacuum ultra violet region*—Continued

λ_{vac} Å	Intensity	σ (cm^{-1})	Classification [a]	λ_{vac} Å	Intensity	σ (cm^{-1})	Classification [a]
1394.323	20	71719.4		1370.129	2	72985.8	$23844\ _{9/2} - 96830^{\circ}{}_{7/2}$
1393.964	20	71737.9		1368.661	100*h*	73064.1	
1393.905	4	71740.9		1367.730	5	73113.8	
1393.526	2	71760.4		1366.761	3	73165.7	
1393.452	100	71764.2		1366.522	3	73178.5	$23651\ _{7/2} - 96830^{\circ}{}_{7/2}$
1392.825	100	71796.5	$25033\ _{9/2} - 96830^{\circ}{}_{7/2}$	1366.392	200	73185.4	
1392.651	3	71805.5		1364.645	1	73279.1	
1392.367	1	71820.1		1364.382	2	73293.2	
1390.762	3	71903.0		1364.303	1	73297.5	$39725\ _{15/2} - 113023^{\circ}{}_{17/2}$
1390.367	100	71923.4		1363.020	2	73366.5	
1390.301	2	71926.9		1362.453	40*h*	73397.0	
1390.089	5	71937.8		1362.371	20*h*	73401.4	$44679\ _{7/2} - 118081^{\circ}{}_{9/2}$
1389.786	7	71953.5		1362.113	1	73415.4	$44903\ _{5/2} - 118318^{\circ}{}_{7/2}$
1389.588	100*h*	71963.8		1361.813	2	73431.5	
1389.240	7*w*	71981.8		1359.082	3*h*	73579.1	
1388.403	2	72025.2		1359.003	30*h*	73583.4	
1388.073	1	72042.3	$24788\ _{9/2} - 96830^{\circ}{}_{7/2}$	1358.233	2	73625.1	
1388.004	1	72045.9		1356.483	200*h*	73720.0	
1387.775	40	72057.8	$21238\ _{13/2} - 93296^{\circ}{}_{11/2}$	1356.355	2*h*	73727.0	$40098\ _{5/2} - 113825^{\circ}{}_{3/2}$
1387.268	4	72084.1	$16135\ _{7/2} - 88220^{\circ}{}_{9/2}$	1355.383	1	73779.9	
1387.136	2	72091.0		1355.214	3	73789.1	$44679\ _{7/2} - 118468^{\circ}{}_{9/2}$
1386.163	3	72141.6	$44903\ _{5/2} - 117044^{\circ}{}_{7/2}$	1354.815	2	73810.8	
1385.459	5*h*	72178.2		1353.997	2	73855.4	
1384.669	3	72219.4		1353.601	10*h*	73877.0	
1383.796	10	72265.0		1353.151	3	73901.6	
1383.656	300*h*	72272.3		1352.987	2	73910.5	$39870\ _{9/2} - 113780^{\circ}{}_{9/2}$
1383.608	2	72274.8	$45805\ _{9/2} - 118081^{\circ}{}_{9/2}$	1352.697	600	73926.4	
1382.351	2	72340.5		1352.511	300	73936.5	$19360\ _{13/2} - 93296^{\circ}{}_{11/2}$
1382.193	2	72348.8		1350.905	1	74024.4	
1382.045	1	72356.5	$45844\ _{3/2} - 118201^{\circ}{}_{3/2}$	1350.326	10*h*	74056.2	
1381.886	2	72364.9	$44679\ _{7/2} - 117044^{\circ}{}_{7/2}$	1350.171	20	74064.7	
1381.816	4	72368.5		1349.740	1	74088.3	$61357^{\circ}{}_{9/2} - 135445\ _{7/2}$
1381.446	100	72387.9	$18241\ _{11/2} - 90629^{\circ}{}_{9/2}$	1349.618	7	74095.0	$19872\ _{7/2} - 93967^{\circ}{}_{7/2}$
1381.209	10	72400.3	$22747\ _{9/2} - 95147^{\circ}{}_{9/2}$	1349.334	7	74110.6	$38785\ _{15/2} - 112896^{\circ}{}_{15/2}$
1380.107	40*h*	72458.2		1349.059	5	74125.7	
1379.958	3	72466.0	$45805\ _{9/2} - 118271^{\circ}{}_{11/2}$	1347.513	10	74210.8	$36670\ _{11/2} - 110881^{\circ}{}_{11/2}$
1378.385	1	72548.7	$38785\ _{15/2} - 111335^{\circ}{}_{15/2}$	1347.328	5	74221.0	
1377.992	15	72569.4	$19872\ _{7/2} - 92441^{\circ}{}_{7/2}$	1347.162	30	74230.1	$18211\ _{5/2} - 92441^{\circ}{}_{7/2}$
1377.425	20	72599.2		1345.174	100*h*	74339.8	$39485\ _{1/2} - 113825^{\circ}{}_{3/2}$
1376.770	15	72633.8	$38701\ _{13/2} - 111335^{\circ}{}_{15/2}$	1345.087	200*w*	74344.6	
1376.032	8	72672.7	$21294\ _{7/2} - 93967^{\circ}{}_{7/2}$	1344.704	5	74365.8	
1375.992	4	72674.8		1344.323	10	74386.9	
1375.847	1	72682.5	$19872\ _{7/2} - 92554^{\circ}{}_{5/2}$	1342.855	10	74468.2	$36642\ _{13/2} - 111110^{\circ}{}_{13/2}$
1374.618	20*h*	72747.5		1342.259	100	74501.3	
1374.199	2	72769.7		1338.810	4	74693.2	$36642\ _{13/2} - 111335^{\circ}{}_{15/2}$
1373.939	10	72783.4	$44903\ _{5/2} - 117686^{\circ}{}_{5/2}$	1338.568	2*h*	74706.7	
1372.124	3*h*	72879.7		1337.468	40*h*	74768.1	
1371.420	100*h*	72917.1		1335.134	100	74898.8	$38701\ _{13/2} - 113600^{\circ}{}_{13/2}$
1371.220	2*h*	72927.8		1334.983	10	74907.3	
1370.471	15	72967.6	$44679\ _{7/2} - 117647^{\circ}{}_{7/2}$	1334.811	2	74917.0	

[a] For doubly-classified lines, the wavelength is entered only once.

TABLE X. *Observed spectral lines of* Pr III *in the vacuum ultra violet region* – Continued

λ_{vac} Å	Intensity	σ (cm^{-1})	Classification [a]	λ_{vac} Å	Intensity	σ (cm^{-1})	Classification [a]
1333.802	20*h*	74973.6		1294.456	2	77252.5	
1332.359	1	75054.8	$18241_{11/2}-93296^{\circ}_{11/2}$	1294.103	3	77273.6	$36640_{7/2}-113914^{\circ}_{5/2}$
1331.490	1	75103.8	$15525_{11/2}-90629^{\circ}_{9/2}$	1294.043	10	77277.2	$13352_{11/2}-90629^{\circ}_{9/2}$
1330.985	60	75132.3	$38701_{13/2}-113833^{\circ}_{15/2}$	1293.079	5	77334.8	$40205_{3/2}-117540^{\circ}_{3/2}$
1329.459	1	75218.6		1292.456	3*h*	77372.1	
1328.452	30	75275.6	$38549_{1/2}-113825^{\circ}_{3/2}$	1292.062	1	77395.7	$15045_{5/2}-92441^{\circ}_{7/2}$
1328.207	5	75289.5	$45805_{9/2}-121095^{\circ}_{11/2}$	1291.104	20	77453.1	$38785_{15/2}-116238^{\circ}_{15/2}$
1325.155	4	75462.9	$41026_{17/2}-116489^{\circ}_{17/2}$				$39870_{9/2}-117323^{\circ}_{11/2}$
1324.595	50*h*	75494.8		1289.817	1	77530.4	
1322.376	1	75621.4		1288.999	2	77579.6	$37919_{7/2}-115499^{\circ}_{9/2}$
1321.520	5	75670.4	$39732_{11/2}-115403^{\circ}_{11/2}$	1287.736	2*h*	77655.7	
1319.844	1	75766.5	$39732_{11/2}-115499^{\circ}_{9/2}$	1286.935	300	77704.0	$38785_{15/2}-116489^{\circ}_{17/2}$
1319.796	1	75769.3	$14859_{11/2}-90629^{\circ}_{9/2}$	1286.530	40*h*	77728.5	
1316.719	3	75946.4	$39725_{13/2}-115672^{\circ}_{15/2}$	1286.233	1	77746.4	
1316.264	1	75972.6	$36670_{11/2}-112643^{\circ}_{11/2}$	1284.023	10	77880.2	$37919_{7/2}-115800^{\circ}_{5/2}$
1315.596	1	76011.2	$38785_{15/2}-114797^{\circ}_{13/2}$	1278.394	3*h*	78223.1	
1314.573	2	76070.3	$14558_{9/2}-90629^{\circ}_{9/2}$	1277.726	2	78264.0	
1314.136	20	76095.6	$38701_{13/2}-114797^{\circ}_{13/2}$	1277.553	50*h*	78274.6	
1313.582	10	76127.7	$36642_{13/2}-112769^{\circ}_{13/2}$	1277.286	30	78291.0	
1313.538	2	76130.3	$35137_{3/2}-111268^{\circ}_{3/2}$	1276.937	1	78312.4	
1313.376	5*h*	76139.6		1276.817	2*h*	78319.8	
1312.336	7	76199.0	$39732_{11/2}-115933^{\circ}_{11/2}$	1276.612	2*h*	78332.3	
1310.972	1*h*	76279.3	$37011_{5/2}-113291^{\circ}_{7/2}$	1276.327	1	78349.8	$38694_{5/2}-117044^{\circ}_{7/2}$
1310.898	2*h*	76283.6		1275.701	1	78388.3	
1310.307	2	76318.0	$35024_{7/2}-111342^{\circ}_{7/2}$	1274.924	20	78436.0	
1310.001	1	76335.8		1273.361	5	78532.3	$35024_{7/2}-113556^{\circ}_{5/2}$
1309.831	2*h*	76345.7		1272.901	20	78560.7	$25244^{\circ}_{15/2}-103805_{13/2}$
1308.577	2	76418.9	$16135_{7/2}-92554^{\circ}_{5/2}$	1272.820	1	78565.7	$39120_{3/2}-117686^{\circ}_{3/2}$
1308.234	2	76438.9	$39870_{9/2}-116309^{\circ}_{11/2}$	1272.690	3	78573.7	$23091^{\circ}_{3/2}-101665_{5/2}$
1307.215	20*h*	76498.5		1271.934	10*h*	78620.4	
1306.420	1	76545.1	$37011_{5/2}-113556^{\circ}_{5/2}$	1271.829	1	78626.9	
1305.892	1	76576.0	$39732_{11/2}-116309^{\circ}_{11/2}$	1269.499	1	78771.2	$34520_{5/2}-113291^{\circ}_{7/2}$
1305.771	1	76583.1	$39870_{9/2}-116453^{\circ}_{9/2}$	1269.345	1	78780.8	$36640_{7/2}-115420^{\circ}_{7/2}$
1305.623	1	76591.8		1269.232	2	78787.8	$37011_{5/2}-115800^{\circ}_{5/2}$
1303.501	2	76716.5	$37197_{3/2}-113914^{\circ}_{5/2}$	1268.819	2	78813.4	
1302.961	3	76748.3	$34520_{5/2}-111268^{\circ}_{3/2}$	1268.084	1	78859.1	$36640_{7/2}-115499^{\circ}_{9/2}$
1302.884	3*h*	76752.8		1267.783	40	78877.8	$39732_{11/2}-118610^{\circ}_{13/2}$
1302.696	10	76763.9	$39725_{15/2}-116489^{\circ}_{17/2}$	1267.235	2*h*	78912.0	
1300.617	50	76886.6	$38785_{15/2}-115672^{\circ}_{15/2}$	1266.730	2*h*	78943.4	
1300.285	3	76906.2	$18241_{11/2}-95147^{\circ}_{9/2}$	1265.676	20	79009.2	$39870_{9/2}-118879^{\circ}_{11/2}$
1299.811	30*h*	76934.3		1265.347	5	79029.7	$36640_{7/2}-115670^{\circ}_{7/2}$
1299.407	10	76958.2	$36642_{13/2}-113600^{\circ}_{13/2}$				$36642_{13/2}-115672^{\circ}_{15/2}$
1299.193	2	76970.9	$38701_{13/2}-115672^{\circ}_{15/2}$	1264.221	10	79100.1	
1298.693	40	77000.5		1263.489	20	79145.9	$39732_{11/2}-118879^{\circ}_{11/2}$
1298.630	100	77004.2		1263.274	20	79159.4	$36640_{7/2}-115800^{\circ}_{5/2}$
1298.410	2	77017.3		1263.160	1	79166.5	
1298.139	10*h*	77033.4		1261.871	20	79247.4	$39024_{9/2}-118271^{\circ}_{11/2}$
1297.828	3	77051.8	$38448_{9/2}-115499^{\circ}_{9/2}$	1260.991	20	79302.7	
1295.473	30	77191.9	$36642_{13/2}-113833^{\circ}_{15/2}$	1259.747	4	79381.0	$36640_{7/2}-116021^{\circ}_{7/2}$
1294.860	2	77228.4		1258.859	4*h*	79437.0	

[a] For doubly-classified lines, the wavelength is entered only once.

TABLE X. *Observed spectral lines of* Pr III *in the vacuum ultra violet region*—Continued

λ_{vac} Å	Intensity	σ (cm^{-1})	Classification [a]	λ_{vac} Å	Intensity	σ (cm^{-1})	Classification [a]
1258.754	1	79443.6		1217.644	40	82125.8	
1258.700	2	79447.0	$24357^{\circ}_{11/2}-103805_{13/2}$	1217.473	3	82137.3	$30505_{11/2}-112643^{\circ}_{11/2}$
1257.936	1	79495.3	$35828_{9/2}-115324^{\circ}_{9/2}$	1217.169	4	82157.9	$29835_{9/2}-111993^{\circ}_{9/2}$
1257.835	10*h*	79501.7		1217.063	1	82165.0	
1256.362	20	79594.9	$12846_{9/2}-92441^{\circ}_{7/2}$	1215.996	2	82237.1	$36642_{13/2}-118879^{\circ}_{11/2}$
1255.468	1	79651.6	$38549_{1/2}-118201^{\circ}_{3/2}$	1214.562	1	82334.2	
1255.162	3	79671.0	$35828_{9/2}-115499^{\circ}_{9/2}$	1212.271	1	82489.8	$35828_{9/2}-118318^{\circ}_{7/2}$
1254.915	5	79686.7		1212.053	2	82504.6	
1252.937	7	79812.5	$36640_{7/2}-116453^{\circ}_{9/2}$	1211.998	1	82508.4	$39024_{9/2}-121532^{\circ}_{11/2}$
			$48401_{3/2}-128214^{\circ}_{3/2}$	1211.894	60	82515.5	
1250.337	20	79978.4		1211.111	3	82568.8	
1250.190	10	79987.8		1210.532	3	82608.3	
1249.025	3	80062.4	$23245^{\circ}_{5/2}-103308_{7/2}$	1210.158	4	82633.8	
1246.860	5*h*	80201.5		1210.078	20	82639.3	
1245.521	5	80287.7	$14859_{11/2}-95147^{\circ}_{9/2}$	1209.191	2	82699.9	
1244.669	2	80342.6	$37197_{3/2}-117540^{\circ}_{3/2}$	1208.938	2*h*	82717.2	
1242.667	1	80472.1		1208.755	2	82729.8	$27604_{9/2}-110333^{\circ}_{7/2}$
1241.027	5*h*	80578.4					$38701_{13/2}-121431^{\circ}_{13/2}$
1239.467	7	80679.8	$24886^{\circ}_{7/2}-105566_{9/2}$	1208.272	2	82762.8	$45805_{9/2}-128568^{\circ}_{9/2}$
1238.007	4	80775.0	$35024_{7/2}-115800^{\circ}_{5/2}$	1208.013	40*b l*	82780.6	
1237.976	2	80777.0		1205.675	2*h*	82941.1	
1236.596	1	80867.2		1205.511	20*h*	82952.4	
1235.607	20*h*	80931.9		1204.999	20*b l*	82987.6	
1235.369	1	80947.5		1204.511	4*h*	83021.2	
1234.649	1	80994.7	$36652_{5/2}-117647^{\circ}_{7/2}$	1204.078	50	83051.1	$35828_{9/2}-118879^{\circ}_{11/2}$
1234.534	3	81002.2		1204.000	4	83056.5	$35024_{7/2}-118081^{\circ}_{9/2}$
1234.351	1	81014.2		1203.946	2*h*	83060.2	
1234.150	3	81027.4		1203.448	2	83094.6	$30505_{11/2}-113600^{\circ}_{13/2}$
1233.869	3	81045.9	$29835_{9/2}-110881^{\circ}_{11/2}$	1203.266	1	83107.1	
			$36640_{7/2}-117686^{\circ}_{5/2}$	1203.106	10*h*	83118.2	
1233.573	1	81065.3	$29267_{5/2}-110333^{\circ}_{7/2}$	1203.054	2*h*	83121.8	
1233.242	1	81087.1	$29835_{9/2}-110922^{\circ}_{9/2}$	1202.997	1	83125.7	
1231.958	1	81171.6		1202.889	1	83133.2	
1229.989	3*h*	81301.5		1202.515	2	83159.0	
1229.728	20	81318.8		1202.463	5*b l*	83162.6	
1228.610	10*c l*	81392.8	$39725_{15/2}-121119^{\circ}_{15/2}$	1202.389	4	83167.8	$25391^{\circ}_{13/2}-108559_{11/2}$
1228.067	2	81428.8	$35024_{7/2}-116453^{\circ}_{9/2}$	1201.999	1	83194.8	$27138_{7/2}-110333^{\circ}_{7/2}$
1224.015	5	81698.3	$39732_{11/2}-121431^{\circ}_{13/2}$	1200.879	1	83272.3	$28720_{9/2}-111993^{\circ}_{9/2}$
1223.251	1	81749.4		1200.565	3	83294.1	$35024_{7/2}-118318^{\circ}_{7/2}$
1223.055	1	81762.5		1200.254	5	83315.7	
1222.497	10	81799.8	$39732_{11/2}-121532^{\circ}_{11/2}$	1200.203	5*b l*	83319.2	
1222.214	2	81818.7	$35828_{9/2}-117647^{\circ}_{7/2}$	1200.140	8	83323.6	$29835_{9/2}-113158^{\circ}_{9/2}$
1222.173	1	81821.5		1200.067	5*h*	83328.7	
1220.398	1	81940.5	$36670_{11/2}-118610^{\circ}_{13/2}$	1198.482	2*h*	83438.9	
1220.279	4	81948.5		1198.399	40	83444.7	$35024_{7/2}-118468^{\circ}_{9/2}$
1219.975	2	81968.9	$36642_{13/2}-118610^{\circ}_{13/2}$	1197.869	3	83481.6	
1219.500	1	82000.8	$29267_{5/2}-111268^{\circ}_{3/2}$	1197.651	2	83496.8	
1219.208	20	82020.5	$35024_{7/2}-117044^{\circ}_{7/2}$	1197.589	50	83501.1	$27380_{11/2}-110881^{\circ}_{11/2}$
1218.533	2	82065.9		1197.505	30	83507.0	$29263_{13/2}-112769^{\circ}_{13/2}$
1218.403	4	82074.6	$29267_{5/2}-111342^{\circ}_{7/2}$	1196.999	1	83542.3	$27380_{11/2}-110922^{\circ}_{9/2}$

[a] For doubly-classified lines, the wavelength is entered only once.

TABLE X. *Observed spectral lines of* Pr III *in the vacuum ultra violet region*—Continued

λ_{vac} Å	Intensity	σ (cm^{-1})	Classification[a]	λ_{vac} Å	Intensity	σ (cm^{-1})	Classification[a]
1196.893	10	83549.7	$44903\ _{5/2} - 128453^{\circ}{}_{7/2}$	1161.532	7	86093.2	$24788\ _{9/2} - 110881^{\circ}{}_{11/2}$
1196.513	1	83576.2		1161.460	8	86098.5	$29835\ _{9/2} - 115933^{\circ}{}_{11/2}$
1195.692	4	83633.6	$29263\ _{13/2} - 112896^{\circ}{}_{15/2}$	1160.892	2	86140.7	$29263\ _{13/2} - 115403^{\circ}{}_{11/2}$
1194.310	20	83730.4	$27380\ _{11/2} - 111110^{\circ}{}_{13/2}$	1160.821	3	86145.9	$29263\ _{13/2} - 115408^{\circ}{}_{13/2}$
1192.794	3	83836.8		1160.717	10	86153.6	$27138\ _{7/2} - 113291^{\circ}{}_{7/2}$
1192.472	1	83859.4		1160.409	4	86176.5	$27604\ _{9/2} - 113780^{\circ}{}_{9/2}$
1192.047	15	83889.3	$44679\ _{7/2} - 128568^{\circ}{}_{9/2}$	1159.818	20	86220.4	$27380\ _{11/2} - 113600^{\circ}{}_{13/2}$
1191.806	100	83906.3		1159.497	10	86244.3	
1190.132	10	84024.3	$29267\ _{5/2} - 113291^{\circ}{}_{7/2}$	1158.871	1	86290.9	
1190.043	100	84030.6		1158.222	5*h*	86339.2	
1189.183	20	84091.3		1157.964	2	86358.5	$35024\ _{7/2} - 121382^{\circ}{}_{9/2}$
1188.622	3	84131.0		1157.912	40	86362.3	
1187.589	15	84204.2	$27138\ _{7/2} - 111342^{\circ}{}_{7/2}$	1157.279	20	86409.6	$29263\ _{13/2} - 115672^{\circ}{}_{15/2}$
1187.470	4	84212.6		1156.410	15	86474.5	$29835\ _{9/2} - 116309^{\circ}{}_{11/2}$
1187.418	1	84216.3		1155.871	3	86514.8	
1187.176	2	84233.5		1155.747	40	86524.1	
1185.662	1	84341.1		1155.635	2	86532.5	$29267\ _{5/2} - 115800^{\circ}{}_{5/2}$
1185.135	2	84378.6		1154.705	1	86602.2	
1184.806	1	84402.0		1154.526	1	86615.6	
1183.796	1	84474.0		1154.091	1	86648.3	
1183.751	1	84477.2	$36642\ _{13/2} - 121119^{\circ}{}_{15/2}$	1153.796	5	86670.4	$29263\ _{13/2} - 115933^{\circ}{}_{11/2}$
1183.029	1	84528.8		1152.347	10	86779.4	$28720\ _{9/2} - 115499^{\circ}{}_{9/2}$
1182.794	20	84545.6	$31254\ _{7/2} - 115800^{\circ}{}_{5/2}$	1151.922	2	86811.4	
1182.655	15	84555.5		1151.863	3	86815.9	
1182.425	6*h*	84572.0		1151.718	5	86826.8	$31254\ _{7/2} - 118081^{\circ}{}_{9/2}$
1182.002	3*h*	84602.2		1151.530	10	86841.0	
1181.852	2	84612.	$27380\ _{11/2} - 111993^{\circ}{}_{9/2}$	1151.474	10	86845.2	$26446\ _{7/2} - 113291^{\circ}{}_{7/2}$
1181.804	1	84616.4		1150.956	2	86884.3	$14187^{\circ}{}_{5/2} - 101071\ _{5/2}$
1180.016	80	84744.6		1150.518	20	86917.4	$25979\ _{15/2} - 112896^{\circ}{}_{15/2}$
1179.786	4	84761.1		1149.956	30	86959.8	$24309\ _{3/2} - 111268^{\circ}{}_{3/2}$
1179.739	4	84764.5		1149.740	20	86976.2	$29263\ _{13/2} - 116238^{\circ}{}_{15/2}$
1178.552	3	84849.9		1149.180	5	87018.6	$24250\ _{3/2} - 111268^{\circ}{}_{3/2}$
1178.140	40	84879.6		1148.979	10	87033.8	$24461\ _{5/2} - 111494^{\circ}{}_{5/2}$
1178.012	5	84888.8	$28936\ _{3/2} - 113825^{\circ}{}_{3/2}$	1148.836	100	87044.6	
1177.911	5*c l*	84896.1	$26446\ _{7/2} - 111342^{\circ}{}_{7/2}$	1148.493	20*h*	87070.6	
1177.886	20*c l*	84897.9	$30505\ _{11/2} - 115403^{\circ}{}_{11/2}$	1148.136	5	87097.7	
1176.548	5	84994.4	$30505\ _{11/2} - 115499^{\circ}{}_{9/2}$	1146.717	1	87205.5	$24788\ _{9/2} - 111993^{\circ}{}_{9/2}$
1175.638	10	85060.2	$28720\ _{9/2} - 113780^{\circ}{}_{9/2}$	1146.659	1	87209.9	$29835\ _{9/2} - 117044^{\circ}{}_{7/2}$
1175.458	1	85073.2		1146.600	1	87214.4	$31254\ _{7/2} - 118468^{\circ}{}_{9/2}$
1175.410	1	85076.7		1146.346	4	87233.7	$23647\ _{13/2} - 110881^{\circ}{}_{11/2}$
1175.191	10	85092.6		1146.060	1	87255.5	$16089^{\circ}{}_{13/2} - 103344\ _{11/2}$
1172.829	30	85263.9		1145.869	4	87270.0	$30505\ _{11/2} - 117775^{\circ}{}_{13/2}$
1171.087	4	85390.8		1145.456	10	87301.5	$28720\ _{9/2} - 116021^{\circ}{}_{7/2}$
1170.564	10	85428.9		1145.216	1	87319.8	
1169.104	10	85535.6		1144.726	10	87357.2	$25934\ _{5/2} - 113291^{\circ}{}_{7/2}$
1166.804	10	85704.2	$35828\ _{9/2} - 121532^{\circ}{}_{11/2}$	1144.009	1	87411.9	
1165.446	3	85804.1	$30505\ _{11/2} - 116309^{\circ}{}_{11/2}$	1143.937	4	87417.4	$27380\ _{11/2} - 114797^{\circ}{}_{13/2}$
1164.659	1	85862.0	$24470\ _{7/2} - 110333^{\circ}{}_{7/2}$	1143.836	2	87425.1	
1163.805	4	85925.0		1143.342	50	87462.9	$23647\ _{13/2} - 111110^{\circ}{}_{13/2}$
1163.324	3*b l*	85960.6		1143.244	1	87470.4	

[a] For doubly-classified lines, the wavelength is entered only once.

TABLE X. *Observed spectral lines of* Pr III *in the vacuum ultra violet region*—Continued

λ_{vac} Å	Intensity	σ (cm^{-1})	Classification [a]	λ_{vac} Å	Intensity	σ (cm^{-1})	Classification [a]
1143.020	2	87487.5	$29835\ _{9/2} - 117323^{\circ}{}_{11/2}$	1130.153	3	88483.6	
1142.900	20	87496.7		1129.886	3	88504.5	$25409\ _{7/2} - 113914^{\circ}{}_{5/2}$
1142.788	10	87505.3	$26095\ _{11/2} - 113600^{\circ}{}_{13/2}$	1129.785	10	88512.4	$29263\ _{13/2} - 117775^{\circ}{}_{13/2}$
1142.690	20	87512.8		1129.054	1	88569.7	$27452\ _{5/2} - 116021^{\circ}{}_{7/2}$
1142.012	20	87564.8		1128.731	1	88595.1	$22747\ _{9/2} - 111342^{\circ}{}_{7/2}$
1141.868	2	87575.8	$30505\ _{11/2} - 118081^{\circ}{}_{9/2}$	1127.367	40	88702.3	$26095\ _{11/2} - 114797^{\circ}{}_{13/2}$
1141.795	20	87581.4		1127.107	4	88722.7	$21611\ _{5/2} - 110333^{\circ}{}_{7/2}$
1141.697	40	87588.9	$28720\ _{9/2} - 116309^{\circ}{}_{11/2}$	1127.030	2	88728.8	$39485\ _{1/2} - 128214^{\circ}{}_{3/2}$
1141.465	4	87606.7		1126.802	5	88746.7	$25033\ _{9/2} - 113780^{\circ}{}_{9/2}$
1141.419	1	87610.2		1126.623	2	88760.8	
1141.262	3	87622.3	$25934\ _{5/2} - 113556^{\circ}{}_{5/2}$	1126.282	3	88787.7	
1141.157	2	87630.4		1126.128	300*h*	88799.8	$29263\ _{13/2} - 118063^{\circ}{}_{15/2}$
1140.413	200	87687.5	$23647\ _{13/2} - 111335^{\circ}{}_{15/2}$	1125.935	4	88815.1	$22527\ _{7/2} - 111342^{\circ}{}_{7/2}$
1140.174	30	87705.9	$23175\ _{13/2} - 110881^{\circ}{}_{11/2}$	1125.895	5	88818.2	$25979\ _{15/2} - 114797^{\circ}{}_{13/2}$
1139.821	10	87733.1	$28720\ _{9/2} - 116453^{\circ}{}_{9/2}$	1125.725	20	88831.6	
1139.688	10	87743.3		1125.596	20	88841.8	$22080\ _{7/2} - 110922^{\circ}{}_{9/2}$
1139.245	1	87777.4	$29267\ _{5/2} - 117044^{\circ}{}_{7/2}$	1125.442	5	88854.0	$28720\ _{9/2} - 117574^{\circ}{}_{11/2}$
1139.090	3	87789.4		1125.355	1	88860.8	
1138.958	3	87799.6	$27604\ _{9/2} - 115403^{\circ}{}_{11/2}$	1124.668	30	88915.1	$21418\ _{5/2} - 110333^{\circ}{}_{7/2}$
1138.822	2	87810.0	$23532\ _{5/2} - 111342^{\circ}{}_{7/2}$	1124.366	1	88939.0	
1138.712	80	87818.5		1124.014	1	88966.9	$22527\ _{7/2} - 111494^{\circ}{}_{5/2}$
1138.231	2	87855.6	$24788\ _{9/2} - 112643^{\circ}{}_{11/2}$	1123.920	15	88974.3	$26446\ _{7/2} - 115420^{\circ}{}_{7/2}$
1137.886	30	87882.3	$25409\ _{7/2} - 113291^{\circ}{}_{7/2}$	1123.708	1	88991.1	$22277\ _{3/2} - 111268^{\circ}{}_{3/2}$
1137.809	50	87888.2		1123.647	3	88995.9	
1137.714	100	87895.6	$27604\ _{9/2} - 115499^{\circ}{}_{9/2}$	1123.103	2	89039.0	$21294\ _{7/2} - 110333^{\circ}{}_{7/2}$
1137.197	20	87935.5	$23175\ _{13/2} - 111110^{\circ}{}_{13/2}$	1123.041	1	89043.9	$29835\ _{9/2} - 118879^{\circ}{}_{11/2}$
1136.852	3	87962.2	$23532\ _{5/2} - 111494^{\circ}{}_{5/2}$	1122.803	3	89062.8	
1136.709	50	87973.3		1122.386	7	89095.9	$24461\ _{5/2} - 113556^{\circ}{}_{5/2}$
1136.628	8	87979.5	$25934\ _{5/2} - 113914^{\circ}{}_{5/2}$	1122.005	40	89126.2	
1136.551	1	87985.5	$29263\ _{13/2} - 117248^{\circ}{}_{13/2}$	1121.452	3	89170.1	
1136.484	4	87990.7	$17642^{\circ}{}_{15/2} - 105632\ _{13/2}$	1121.115	5	89196.9	
1135.927	20	88033.8		1120.707	3	89229.4	$26095\ _{11/2} - 115324^{\circ}{}_{9/2}$
1135.835	1	88041.0	$17409^{\circ}{}_{11/2} - 105450\ _{11/2}$	1120.577	2	89239.7	
1135.654	1	88055.0		1120.463	1	89248.8	$23647\ _{13/2} - 112896^{\circ}{}_{15/2}$
1135.268	10	88084.9		1120.300	4	89261.8	$22080\ _{7/2} - 111342^{\circ}{}_{7/2}$
1135.004	300	88105.4	$30505\ _{11/2} - 118610^{\circ}{}_{13/2}$	1120.257	1	89265.2	$28936\ _{3/2} - 118201^{\circ}{}_{3/2}$
1134.751	8	88125.1	$25033\ _{9/2} - 113158^{\circ}{}_{9/2}$	1119.698	2	89309.8	$24470\ _{7/2} - 113780^{\circ}{}_{9/2}$
1134.462	4	88147.5	$25409\ _{7/2} - 113556^{\circ}{}_{5/2}$	1119.636	30	89314.7	$23844\ _{9/2} - 113158^{\circ}{}_{9/2}$
1134.298	50	88160.2	$23175\ _{13/2} - 111335^{\circ}{}_{15/2}$				$27138\ _{7/2} - 116453^{\circ}{}_{9/2}$
1133.483	30	88223.6		1119.555	1	89321.2	
1133.272	20	88240.1		1119.470	10	89328.0	$23442\ _{11/2} - 112769^{\circ}{}_{13/2}$
1132.851	40	88272.9	$29267\ _{5/2} - 117540^{\circ}{}_{3/2}$	1119.241	40	89346.3	$21535\ _{9/2} - 110881^{\circ}{}_{11/2}$
1131.973	1	88341.3	$23651\ _{7/2} - 111993^{\circ}{}_{9/2}$	1119.153	40	89353.3	$26446\ _{7/2} - 115800^{\circ}{}_{5/2}$
1131.719	2	88361.2	$27138\ _{7/2} - 115499^{\circ}{}_{9/2}$	1119.054	100*h*	89361.2	
1131.558	10	88373.7	$30505\ _{11/2} - 118879^{\circ}{}_{11/2}$	1118.723	4	89387.6	$21535\ _{9/2} - 110922^{\circ}{}_{9/2}$
1131.283	8	88395.2	$22527\ _{7/2} - 110922^{\circ}{}_{9/2}$	1118.508	30	89404.8	$26095\ _{11/2} - 115499^{\circ}{}_{9/2}$
1130.988	15	88418.3	$29267\ _{5/2} - 117686^{\circ}{}_{5/2}$	1118.395	15	89413.8	$22080\ _{7/2} - 111494^{\circ}{}_{5/2}$
1130.753	2	88436.6	$29835\ _{9/2} - 118271^{\circ}{}_{11/2}$	1118.027	8	89443.3	$24470\ _{7/2} - 113914^{\circ}{}_{5/2}$
1130.654	1	88444.4	$23050\ _{3/2} - 111494^{\circ}{}_{5/2}$	1117.977	20	89447.3	$23844\ _{9/2} - 113291^{\circ}{}_{7/2}$
1130.363	3	88467.2		1117.904	5	89453.1	$24461\ _{5/2} - 113914^{\circ}{}_{5/2}$

[a] For doubly-classified lines, the wavelength is entered only once.

TABLE X. *Observed spectral lines of* Pr III *in the vacuum ultra violet region*—Continued

λ_{vac} Å	Intensity	σ (cm^{-1})	Classification[a]	λ_{vac} Å	Intensity	σ (cm^{-1})	Classification[a]
1117.803	10	89461.2		1107.998	40	90252.9	
1117.500	6	89485.5	$20848\ _{5/2} - 110333^{\circ}{}_{7/2}$	1107.911	80	90260.0	$25979\ _{15/2} - 116238^{\circ}{}_{15/2}$
			$25934\ _{5/2} - 115420^{\circ}{}_{7/2}$				$25409\ _{7/2} - 115670^{\circ}{}_{7/2}$
1117.230	3	89507.1	$23651\ _{7/2} - 113158^{\circ}{}_{9/2}$	1107.881	20 *c l*	90262.4	$23651\ _{7/2} - 113914^{\circ}{}_{5/2}$
1116.681	30	89551.1	$28720\ _{9/2} - 118271^{\circ}{}_{11/2}$	1107.536	100	90290.5	$25033\ _{9/2} - 115324^{\circ}{}_{9/2}$
1116.516	3	89564.3		1107.096	20	90326.4	
1116.382	30	89575.1	$24250\ _{3/2} - 113825^{\circ}{}_{3/2}$	1106.948	2	90338.5	$23442\ _{11/2} - 113780^{\circ}{}_{9/2}$
			$26446\ _{7/2} - 116021^{\circ}{}_{7/2}$	1106.755	3	90354.2	
1116.264	3	89584.5		1106.567	80	90369.6	$25033\ _{9/2} - 115403^{\circ}{}_{11/2}$
1116.139	50	89594.6	$23175\ _{13/2} - 112769^{\circ}{}_{13/2}$	1106.423	20	90381.4	$23532\ _{5/2} - 113914^{\circ}{}_{5/2}$
1115.725	15	89627.8	$21294\ _{7/2} - 110922^{\circ}{}_{9/2}$	1106.341	10 *c l*	90388.0	
1115.571	30	89640.2	$23651\ _{7/2} - 113291^{\circ}{}_{7/2}$	1106.311	30	90390.5	$25409\ _{7/2} - 115800^{\circ}{}_{5/2}$
1115.429	10	89651.6		1106.252	3	90395.3	$27380\ _{11/2} - 117775^{\circ}{}_{13/2}$
1115.353	1	89657.7	$21611\ _{5/2} - 111268^{\circ}{}_{3/2}$	1106.060	4	90411.0	$22747\ _{9/2} - 113158^{\circ}{}_{9/2}$
1114.912	60	89693.2	$25979\ _{15/2} - 115672^{\circ}{}_{15/2}$	1105.962	200	90419.0	
1114.581	30	89719.8		1105.754	6	90436.0	
1114.436	1	89731.5	$21611\ _{5/2} - 111342^{\circ}{}_{7/2}$	1105.492	2	90457.5	$21535\ _{9/2} - 111993^{\circ}{}_{9/2}$
1114.228	20	89748.2	$28720\ _{9/2} - 118468^{\circ}{}_{9/2}$	1105.386	80	90466.1	$25033\ _{9/2} - 115499^{\circ}{}_{9/2}$
1113.753	10	89786.5	$23844\ _{9/2} - 113630^{\circ}{}_{7/2}$	1105.214	20	90480.2	
1113.489	10	89807.8	$21535\ _{9/2} - 111342^{\circ}{}_{7/2}$	1104.843	2000	90510.6	$25979\ _{15/2} - 116489^{\circ}{}_{17/2}$
1112.965	10	89850.1	$21418\ _{5/2} - 111268^{\circ}{}_{3/2}$	1104.721	10	90520.6	
1112.582	10	89881.0		1104.525	40	90536.7	$24788\ _{9/2} - 115324^{\circ}{}_{9/2}$
1112.549	5	89883.7	$21611\ _{5/2} - 111494^{\circ}{}_{5/2}$	1104.389	4	90547.8	$27138\ _{7/2} - 117686^{\circ}{}_{5/2}$
1112.400	1	89895.7	$22747\ _{9/2} - 112643^{\circ}{}_{11/2}$	1104.173	2	90565.5	$20315\ _{9/2} - 110881^{\circ}{}_{11/2}$
1112.268	30	89906.4	$27138\ _{7/2} - 117044^{\circ}{}_{7/2}$	1103.780	20	90597.8	$26446\ _{7/2} - 117044^{\circ}{}_{7/2}$
1112.162	10	89915.0	$25409\ _{7/2} - 115324^{\circ}{}_{9/2}$	1103.660	40	90607.6	
1112.050	5	89924.0	$21418\ _{5/2} - 111342^{\circ}{}_{7/2}$	1103.605	10	90612.1	$25409\ _{7/2} - 116021^{\circ}{}_{7/2}$
1111.902	10	89936.0	$23844\ _{9/2} - 113780^{\circ}{}_{9/2}$	1103.553	20 *h*	90616.4	
1111.768	40	89946.8		1103.354	5	90632.7	$24788\ _{9/2} - 115420^{\circ}{}_{7/2}$
1111.694	100	89952.8	$23647\ _{13/2} - 113600^{\circ}{}_{13/2}$	1103.185	8	90646.6	$20848\ _{5/2} - 111494^{\circ}{}_{5/2}$
1111.539	20	89965.4		1103.150	15	90649.5	$37919\ _{7/2} - 128568^{\circ}{}_{9/2}$
1111.475	10	89970.5	$27604\ _{9/2} - 117574^{\circ}{}_{11/2}$	1103.035	400	90659.0	$23175\ _{13/2} - 113833^{\circ}{}_{15/2}$
1111.373	3	89978.8	$23651\ _{7/2} - 113630^{\circ}{}_{7/2}$	1102.938	1	90666.9	$27604\ _{9/2} - 118271^{\circ}{}_{11/2}$
1111.174	50	89994.9	$28885\ _{9/2} - 118879^{\circ}{}_{11/2}$	1102.556	20	90698.3	$21294\ _{7/2} - 111993^{\circ}{}_{9/2}$
1111.117	1	89999.5		1102.392	200	90711.8	$24788\ _{9/2} - 115499^{\circ}{}_{9/2}$
1111.035	1	90006.2	$26446\ _{7/2} - 116453^{\circ}{}_{9/2}$	1101.939	20	90749.1	$27452\ _{5/2} - 118201^{\circ}{}_{3/2}$
1110.898	1	90017.3	$20315\ _{9/2} - 110333^{\circ}{}_{7/2}$	1101.757	100	90764.1	$22527\ _{7/2} - 113291^{\circ}{}_{7/2}$
1110.656	1	90036.9		1101.660	1	90772.1	
1110.520	200	90047.9	$21294\ _{7/2} - 111342^{\circ}{}_{7/2}$	1101.542	1	90781.8	
1110.172	30	90076.1	$21418\ _{5/2} - 111494^{\circ}{}_{5/2}$	1100.673	40	90853.5	$24470\ _{7/2} - 115324^{\circ}{}_{9/2}$
1110.082	1	90083.4		1100.546	1	90864.0	$23050\ _{3/2} - 113914^{\circ}{}_{5/2}$
1109.801	5	90106.2					$27604\ _{9/2} - 118468^{\circ}{}_{9/2}$
1109.523	15	90128.8	$23651\ _{7/2} - 113780^{\circ}{}_{9/2}$	1100.515	2	90866.6	$27452\ _{5/2} - 118318^{\circ}{}_{7/2}$
1109.156	200	90158.6	$28720\ _{9/2} - 118879^{\circ}{}_{11/2}$	1100.389	4	90877.0	$30505\ _{11/2} - 121382^{\circ}{}_{9/2}$
1109.011	20	90170.4		1099.894	4	90917.8	
1108.879	10	90181.2		1099.803	200	90925.4	$30505\ _{11/2} - 121431^{\circ}{}_{13/2}$
1108.817	500	90186.2	$23647\ _{13/2} - 113833^{\circ}{}_{15/2}$	1099.596	4	90942.5	$27138\ _{7/2} - 118081^{\circ}{}_{9/2}$
1108.709	20	90195.0	$27452\ _{5/2} - 117647^{\circ}{}_{7/2}$	1099.505	20	90950.0	$24470\ _{7/2} - 115420^{\circ}{}_{7/2}$
1108.648	3	90200.0	$21294\ _{7/2} - 111494^{\circ}{}_{5/2}$	1099.389	7	90959.6	$24461\ _{5/2} - 115420^{\circ}{}_{7/2}$
1108.115	6	90243.3		1099.045	40	90988.1	$25033\ _{9/2} - 116021^{\circ}{}_{7/2}$

[a] For doubly-classified lines, the wavelength is entered only once.

TABLE X. *Observed spectral lines of* Pr III *in the vacuum ultra violet region* — Continued

λ_{vac} Å	Intensity	σ (cm^{-1})	Classification [a]	λ_{vac} Å	Intensity	σ (cm^{-1})	Classification [a]
1098.981	3	90993.4		1091.293	2	91634.4	$25409\ ^{7/2} - 117044\ ^{\circ}{}_{7/2}$
1098.735	1	91013.8	$21755\ ^{11/2} - 112769\ ^{\circ}{}_{13/2}$				$26446\ ^{7/2} - 118081\ ^{\circ}{}_{9/2}$
1098.573	40	91027.2	$20315\ ^{9/2} - 111342\ ^{\circ}{}_{7/2}$	1091.097	1	91650.9	
			$30505\ ^{11/2} - 121532\ ^{\circ}{}_{11/2}$	1091.047	2	91655.1	$23844\ ^{9/2} - 115499\ ^{\circ}{}_{9/2}$
1098.506	4	91032.7	$22747\ ^{9/2} - 113780\ ^{\circ}{}_{9/2}$	1090.876	2	91669.4	
1098.296	40	91050.1	$19872\ ^{7/2} - 110922\ ^{\circ}{}_{9/2}$	1090.839	2	91672.6	$23651\ ^{7/2} - 115324\ ^{\circ}{}_{9/2}$
1098.243	20	91054.5		1090.739	5	91681.0	$21611\ ^{5/2} - 113291\ ^{\circ}{}_{7/2}$
1098.164	2	91061.1		1090.626	50	91690.5	
1097.967	1	91077.4	$22080\ ^{7/2} - 113158\ ^{\circ}{}_{9/2}$	1090.536	200	91698.0	$29835\ ^{9/2} - 121532\ ^{\circ}{}_{11/2}$
1097.595	100	91108.3	$20160\ ^{3/2} - 111268\ ^{\circ}{}_{3/2}$	1090.366	10	91712.3	$25934\ ^{5/2} - 117647\ ^{\circ}{}_{7/2}$
1097.148	50	91145.4	$24788\ ^{9/2} - 115933\ ^{\circ}{}_{11/2}$				$36640\ ^{7/2} - 128352\ ^{\circ}{}_{9/2}$
1096.955	1	91161.4		1090.006	15	91742.6	
1096.731	20	91180.1	$19700\ ^{11/2} - 110881\ ^{\circ}{}_{11/2}$	1089.921	1	91749.8	$19360\ ^{13/2} - 111110\ ^{\circ}{}_{13/2}$
			$27138\ ^{7/2} - 118318\ ^{\circ}{}_{7/2}$	1089.844	4	91756.2	$21535\ ^{9/2} - 113291\ ^{\circ}{}_{7/2}$
1096.367	10*h*	91210.3	$22080\ ^{7/2} - 113291\ ^{\circ}{}_{7/2}$				$23647\ ^{13/2} - 115403\ ^{\circ}{}_{11/2}$
1096.121	100	91230.8	$27380\ ^{11/2} - 118610\ ^{\circ}{}_{13/2}$	1089.571	20	91779.2	
1096.080	50*b l*	91234.2	$24788\ ^{9/2} - 116021\ ^{\circ}{}_{7/2}$	1089.464	15	91788.2	
1095.856	30	91252.9	$22527\ ^{7/2} - 113780\ ^{\circ}{}_{9/2}$	1089.312	8	91801.1	$19308\ ^{11/2} - 111110\ ^{\circ}{}_{13/2}$
1095.766	100	91260.4	$29835\ ^{9/2} - 121095\ ^{\circ}{}_{11/2}$				$36652\ ^{5/2} - 128453\ ^{\circ}{}_{7/2}$
1095.587	60	91275.3	$25033\ ^{9/2} - 116309\ ^{\circ}{}_{11/2}$	1089.167	1	91813.3	$36640\ ^{7/2} - 128453\ ^{\circ}{}_{7/2}$
			$27604\ ^{9/2} - 118879\ ^{\circ}{}_{11/2}$	1088.933	30	91833.0	$22080\ ^{7/2} - 113914\ ^{\circ}{}_{5/2}$
1095.513	30	91281.4		1088.879	3	91837.6	
1095.403	15	91290.6		1088.659	500	91856.1	$29263\ ^{13/2} - 121119\ ^{\circ}{}_{15/2}$
1094.928	80	91330.2	$27138\ ^{7/2} - 118468\ ^{\circ}{}_{9/2}$	1088.572	20	91863.5	$21294\ ^{7/2} - 113158\ ^{\circ}{}_{9/2}$
1094.878	30	91334.4	$20160\ ^{3/2} - 111494\ ^{\circ}{}_{5/2}$	1088.353	10	91881.9	$23442\ ^{11/2} - 115324\ ^{\circ}{}_{9/2}$
1094.832	1	91338.2	$24461\ ^{5/2} - 115800\ ^{\circ}{}_{5/2}$	1088.284	10	91887.8	$23532\ ^{5/2} - 115420\ ^{\circ}{}_{7/2}$
1094.767	15	91343.6	$18990\ ^{7/2} - 110333\ ^{\circ}{}_{7/2}$	1088.125	70	91901.2	
1094.637	1	91354.5	$23442\ ^{11/2} - 114797\ ^{\circ}{}_{13/2}$	1087.804	100	91928.3	$36640\ ^{7/2} - 128568\ ^{\circ}{}_{9/2}$
1094.486	30	91367.1		1087.601	4	91945.5	$21611\ ^{5/2} - 113556\ ^{\circ}{}_{5/2}$
1094.255	80	91386.4	$22527\ ^{7/2} - 113914\ ^{\circ}{}_{5/2}$	1087.563	1	91948.7	
1094.058	3	91402.8	$21755\ ^{11/2} - 113158\ ^{\circ}{}_{9/2}$	1087.465	2	91957.0	
1093.870	10	91418.5		1087.418	2	91961.0	$23442\ ^{11/2} - 115403\ ^{\circ}{}_{11/2}$
1093.601	1	91441.0	$37011\ ^{5/2} - 128453\ ^{\circ}{}_{7/2}$	1087.362	1	91965.7	$23442\ ^{11/2} - 115408\ ^{\circ}{}_{13/2}$
1093.521	80	91447.7		1087.252	4	91974.0	$19360\ ^{13/2} - 111335\ ^{\circ}{}_{15/2}$
1093.253	80	91470.1	$19872\ ^{7/2} - 111342\ ^{\circ}{}_{7/2}$	1087.164	4	91982.4	$24470\ ^{7/2} - 116453\ ^{\circ}{}_{9/2}$
1093.185	60	91475.8	$22080\ ^{7/2} - 113556\ ^{\circ}{}_{5/2}$	1087.063	1	91991.0	
1092.910	20	91498.8	$27380\ ^{11/2} - 118879\ ^{\circ}{}_{11/2}$	1086.993	5	91996.9	$21294\ ^{7/2} - 113291\ ^{\circ}{}_{7/2}$
1092.529	2	91530.8	$21238\ ^{13/2} - 112769\ ^{\circ}{}_{13/2}$	1086.700	40	92021.7	$26446\ ^{7/2} - 118468\ ^{\circ}{}_{9/2}$
			$36683\ ^{1/2} - 128214\ ^{\circ}{}_{3/2}$	1086.598	10	92030.4	
1092.481	6	91534.8		1086.538	1	92035.4	
1092.325	20*c l*	91547.8	$22277\ ^{3/2} - 113825\ ^{\circ}{}_{3/2}$	1086.388	2	92048.1	
			$29835\ ^{9/2} - 121382\ ^{\circ}{}_{9/2}$	1086.321	3	92053.8	$18241\ ^{11/2} - 110295\ ^{\circ}{}_{11/2}$
1092.301	20*c l*	91549.9	$22080\ ^{7/2} - 113630\ ^{\circ}{}_{7/2}$	1086.280	2	92057.3	$23442\ ^{11/2} - 115499\ ^{\circ}{}_{9/2}$
			$24250\ ^{3/2} - 115800\ ^{\circ}{}_{5/2}$	1085.915	40	92088.2	$23844\ ^{9/2} - 115933\ ^{\circ}{}_{11/2}$
1092.032	2	91572.4	$19308\ ^{11/2} - 110881\ ^{\circ}{}_{11/2}$	1085.828	20	92095.6	$21535\ ^{9/2} - 113630\ ^{\circ}{}_{7/2}$
1091.983	3	91576.5	$23844\ ^{9/2} - 115420\ ^{\circ}{}_{7/2}$	1085.531	20	92120.8	$19872\ ^{7/2} - 111993\ ^{\circ}{}_{9/2}$
1091.676	1	91602.3		1085.435	1	92129.0	$21535\ ^{9/2} - 113664\ ^{\circ}{}_{11/2}$
1091.555	30	91612.4		1085.380	1	92133.6	
1091.477	70	91619.0		1085.283	2	92141.9	
1091.430	30*h*	91622.9		1085.236	10	92145.8	

[a] For doubly-classified lines, the wavelength is entered only once.

TABLE X. *Observed spectral lines of* Pr III *in the vacuum ultra violet region*—Continued

λ_{vac} Å	Intensity	σ (cm^{-1})	Classification [a]	λ_{vac} Å	Intensity	σ (cm^{-1})	Classification [a]
1085.112	8	92156.4		1079.013	10	92677.3	$21148\ _{3/2}-113825^{\circ}{}_{3/2}$
1084.976	15	92167.9	$29263\ _{13/2}-121431^{\circ}{}_{13/2}$	1078.672	1	92706.6	$17627\ _{9/2}-110333^{\circ}{}_{7/2}$
1084.873	10	92176.7	$23844\ _{9/2}-116021^{\circ}{}_{7/2}$	1078.516	2	92720.0	
			$26095\ _{11/2}-118271^{\circ}{}_{11/2}$	1077.972	2	92766.8	
1084.417	500	92215.4	$41026\ _{17/2}-133242^{\circ}{}_{19/2}$	1077.851	1	92777.2	
1084.262	8 *b l*	92228.6	$23175\ _{13/2}-115403^{\circ}{}_{11/2}$	1077.782	40	92783.1	
1084.204	7	92233.6	$23175\ _{13/2}-115408^{\circ}{}_{13/2}$	1077.742	4	92786.6	$24788\ _{9/2}-117574^{\circ}{}_{11/2}$
1084.157	20	92237.6	$25409\ _{7/2}-117647^{\circ}{}_{7/2}$	1077.623	2	92796.8	$22527\ _{7/2}-115324^{\circ}{}_{9/2}$
1084.071	1	92244.9	$21535\ _{9/2}-113780^{\circ}{}_{9/2}$	1077.571	30	92801.3	$23651\ _{7/2}-116453^{\circ}{}_{9/2}$
1083.936	20	92256.4	$24470\ _{7/2}-116727^{\circ}{}_{5/2}$	1077.451	10	92811.6	$28720\ _{9/2}-121532^{\circ}{}_{11/2}$
			$24788\ _{9/2}-117044^{\circ}{}_{7/2}$	1077.382	20	92817.6	$18063\ _{9/2}-110881^{\circ}{}_{11/2}$
1083.876	40	92261.5	$21294\ _{7/2}-113556^{\circ}{}_{5/2}$	1076.902	40	92856.0	$18063\ _{9/2}-110922^{\circ}{}_{9/2}$
1083.815	10	92266.7	$23532\ _{5/2}-115800^{\circ}{}_{5/2}$				$24788\ _{9/2}-117647^{\circ}{}_{7/2}$
			$25934\ _{5/2}-118201^{\circ}{}_{3/2}$	1076.831	3	92865.1	
1083.747	20	92272.4		1076.790	10	92868.6	$18241\ _{11/2}-111110^{\circ}{}_{13/2}$
1083.697	2	92276.7	$25409\ _{7/2}-117686^{\circ}{}_{5/2}$	1076.708	2	92875.7	
1083.548	5	92289.4	$18241\ _{11/2}-110530^{\circ}{}_{13/2}$	1076.325	30	92908.7	$25409\ _{7/2}-118318^{\circ}{}_{7/2}$
			$25033\ _{9/2}-117323^{\circ}{}_{11/2}$	1076.137	5	92925.0	
1083.393	10	92302.6	$21611\ _{5/2}-113914^{\circ}{}_{5/2}$	1075.961	100	92940.2	
1083.348	20	92306.4		1075.707	2	92962.1	
1083.285	1	92311.8		1075.586	10 *c l*	92972.6	$22527\ _{7/2}-115499^{\circ}{}_{9/2}$
1083.001	10	92336.0	$21294\ _{7/2}-113630^{\circ}{}_{7/2}$	1075.565	50 *c l*	92974.4	
1082.881	40	92346.2	$41026\ _{17/2}-133373^{\circ}{}_{17/2}$	1075.532	10 *c l*	92977.2	$20848\ _{5/2}-113825^{\circ}{}_{3/2}$
1082.824	8	92351.1		1075.448	1	92984.5	
1082.704	50	92361.4	$21238\ _{13/2}-113600^{\circ}{}_{13/2}$	1075.147	1	93010.5	$23442\ _{11/2}-116453^{\circ}{}_{9/2}$
1082.445	8	92383.4	$25934\ _{5/2}-118318^{\circ}{}_{7/2}$	1074.855	100	93035.8	
1082.091	20	92413.7	$18921\ _{15/2}-111335^{\circ}{}_{15/2}$	1074.726	5	93047.0	$25033\ _{9/2}-118081^{\circ}{}_{9/2}$
1082.045	10	92417.6	$24309\ _{3/2}-116727^{\circ}{}_{5/2}$	1074.669	40	93051.9	
1081.807	3	92437.9		1074.590	7	93058.8	$25409\ _{7/2}-118468^{\circ}{}_{9/2}$
1081.746	10	92443.1	$20848\ _{5/2}-113291^{\circ}{}_{7/2}$	1074.515	100	93065.2	$20848\ _{5/2}-113914^{\circ}{}_{5/2}$
1081.574	3	92457.8		1074.474	5	93068.8	$19700\ _{11/2}-112769^{\circ}{}_{13/2}$
1081.356	20	92476.5	$24250\ _{3/2}-116727^{\circ}{}_{5/2}$	1074.353	7	93079.3	$24461\ _{5/2}-117540^{\circ}{}_{3/2}$
1081.252	5	92485.4	$21294\ _{7/2}-113780^{\circ}{}_{9/2}$	1074.171	5	93095.0	
1081.210	5	92489.0	$23532\ _{5/2}-116021^{\circ}{}_{7/2}$	1074.041	5	93106.3	
1080.898	100	92515.7	$26095\ _{11/2}-118610^{\circ}{}_{13/2}$	1073.901	200	93118.4	$27380\ _{11/2}-120498^{\circ}{}_{13/2}$
1080.797	6	92524.3	$35828\ _{9/2}-128352^{\circ}{}_{9/2}$	1073.801	1	93127.1	
1080.553	2	92545.2		1073.661	100	93139.3	
1080.459	300	92553.3	$35828\ _{9/2}-128381^{\circ}{}_{11/2}$	1073.340	20	93167.1	
1080.187	50	92576.6	$22747\ _{9/2}-115324^{\circ}{}_{9/2}$	1073.308	3	93169.9	
1080.110	20	92583.2	$24461\ _{5/2}-117044^{\circ}{}_{7/2}$	1073.126	200	93185.7	$22747\ _{9/2}-115933^{\circ}{}_{11/2}$
1080.019	2	92591.0		1072.600	30	93231.4	$24309\ _{3/2}-117540^{\circ}{}_{3/2}$
1079.947	3	92597.1		1072.529	100	93237.6	$25033\ _{9/2}-118271^{\circ}{}_{11/2}$
1079.921	10	92599.4		1072.466	20	93243.0	$22080\ _{7/2}-115324^{\circ}{}_{9/2}$
1079.727	10	92616.0		1072.425	5	93246.6	$19649\ _{17/2}-112896^{\circ}{}_{15/2}$
1079.698	10	92618.5		1072.342	20	93253.8	$17627\ _{9/2}-110881^{\circ}{}_{11/2}$
1079.452	100	92639.6	$18241\ _{11/2}-110881^{\circ}{}_{11/2}$	1072.237	8	93263.0	
1079.268	60	92655.4	$22747\ _{9/2}-115403^{\circ}{}_{11/2}$	1072.108	50 *c l*	93274.2	$22747\ _{9/2}-116021^{\circ}{}_{7/2}$
1079.204	1	92660.9	$23647\ _{13/2}-116309^{\circ}{}_{11/2}$	1072.076	10 *c l*	93277.0	$35291\ _{9/2}-128568^{\circ}{}_{9/2}$
1079.078	50 *c l*	92671.7	$25409\ _{7/2}-118081^{\circ}{}_{9/2}$	1072.009	100	93282.8	
1079.058	50 *c l*	92673.4	$22747\ _{9/2}-115420^{\circ}{}_{7/2}$	1071.968	10	93286.4	$19872\ _{7/2}-113158^{\circ}{}_{9/2}$

[a] For doubly-classified lines, the wavelength is entered only once.

TABLE X. *Observed spectral lines of* Pr III *in the vacuum ultra violet region* – Continued

λ_{vac} Å	Intensity	σ (cm^{-1})	Classification [a]	λ_{vac} Å	Intensity	σ (cm^{-1})	Classification [a]
1071.865	200	93295.3	$17627\ _{9/2} - 110922^{\circ}{}_{9/2}$	1065.331	40	93867.5	$21535\ _{9/2} - 115403^{\circ}{}_{11/2}$
1071.487	100	93328.2	$35024\ _{7/2} - 128352^{\circ}{}_{9/2}$	1065.224	2	93877.0	
1071.422	300	93333.9	$19308\ _{11/2} - 112643^{\circ}{}_{11/2}$	1065.128	20	93885.4	$21535\ _{9/2} - 115420^{\circ}{}_{7/2}$
1071.334	50	93341.6		1064.971	40	93899.3	$19700\ _{11/2} - 113600^{\circ}{}_{13/2}$
1071.213	100	93352.1		1064.874	10	93907.8	$19872\ _{7/2} - 113780^{\circ}{}_{9/2}$
1070.750	3	93392.5	$23651\ _{7/2} - 117044^{\circ}{}_{7/2}$	1064.795	50	93914.8	
1070.617	7	93404.1		1064.640	20 *c l*	93928.5	$27604\ _{9/2} - 121532^{\circ}{}_{11/2}$
1070.554	80	93409.6	$19360\ _{13/2} - 112769^{\circ}{}_{13/2}$	1064.585	100	93933.3	$34520\ _{5/2} - 128453^{\circ}{}_{7/2}$
1070.461	60	93417.7	$17113\ _{13/2} - 110530^{\circ}{}_{13/2}$	1064.499	40	93940.9	$22080\ _{7/2} - 116021^{\circ}{}_{7/2}$
1070.336	10	93428.6	$35024\ _{7/2} - 28453^{\circ}{}_{7/2}$	1064.390	100	93950.5	$24250\ _{3/2} - 118201^{\circ}{}_{3/2}$
1070.246	100	93436.5		1064.289	50	93959.4	
1069.881	500	93468.3	$39725\ _{15/2} - 133194^{\circ}{}_{17/2}$	1064.127	10 *c l*	93973.7	
1069.768	20	93478.2	$23844\ _{9/2} - 117323^{\circ}{}_{11/2}$	1064.102	5 *c l*	93976.0	
1069.710	40	93483.3	$24788\ _{9/2} - 118271^{\circ}{}_{11/2}$	1063.926	20	93991.5	
1069.622	100	93491.0	$27604\ _{9/2} - 121095^{\circ}{}_{11/2}$	1063.858	60	93997.5	$17113\ _{13/2} - 111110^{\circ}{}_{13/2}$
							$24470\ _{7/2} - 118468^{\circ}{}_{9/2}$
1069.520	1	93499.9					
1069.385	60	93511.7	$23532\ _{5/2} - 117044^{\circ}{}_{7/2}$	1063.746	10	94007.4	$23532\ _{5/2} - 117540^{\circ}{}_{3/2}$
1069.265	5	93522.2	$22277\ _{3/2} - 115800^{\circ}{}_{5/2}$	1063.653	20	94015.6	$34198\ _{1/2} - 128214^{\circ}{}_{3/2}$
1069.108	20	93535.9	$19360\ _{13/2} - 112896^{\circ}{}_{15/2}$	1063.362	20	94041.4	$19872\ _{7/2} - 113914^{\circ}{}_{5/2}$
1068.852	500 *c l*	93558.3	$21238\ _{13/2} - 114797^{\circ}{}_{13/2}$	1063.255	100	94050.8	$27380\ _{11/2} - 121431^{\circ}{}_{13/2}$
1068.820	5 *c l*	93561.1	$22747\ _{9/2} - 116309^{\circ}{}_{11/2}$	1063.163	70	94059.0	$21611\ _{5/2} - 115670^{\circ}{}_{7/2}$
1068.761	10 *h*	93566.3		1063.104	50	94064.2	
1068.641	80	93576.8		1062.911	10	94081.2	
1068.397	200	93598.2		1062.819	5	94089.4	
1068.270	2	93609.3		1062.673	100	94102.3	$18921\ _{15/2} - 113023^{\circ}{}_{17/2}$
1068.014	10	93631.7		1062.392	50 *c l*	94127.2	$23647\ _{13/2} - 117775^{\circ}{}_{13/2}$
1067.950	300	93637.3		1062.356	50 *c l*	94130.4	
1067.910	5 *c l*	93640.8		1062.095	80	94153.5	$23532\ _{5/2} - 117686^{\circ}{}_{5/2}$
1067.848	10 *h*	93646.3		1061.975	40	94164.2	$21238\ _{13/2} - 115403^{\circ}{}_{11/2}$
1067.779	20	93652.3	$21755\ _{11/2} - 115408^{\circ}{}_{13/2}$	1061.909	20 *c l*	94170.0	$21238\ _{13/2} - 115408^{\circ}{}_{13/2}$
1067.503	50	93676.6	$23050\ _{3/2} - 116727^{\circ}{}_{5/2}$	1061.887	10 *c l*	94172.0	
1067.416	40	93684.2	$19872\ _{7/2} - 113556^{\circ}{}_{5/2}$	1061.830	4	94177.0	$21755\ _{11/2} - 115933^{\circ}{}_{11/2}$
1067.167	10	93706.0	$22747\ _{9/2} - 116453^{\circ}{}_{9/2}$	1061.695	10	94189.0	$21611\ _{5/2} - 115800^{\circ}{}_{5/2}$
1067.117	200	93710.4		1061.599	500	94197.5	$16135\ _{7/2} - 110333^{\circ}{}_{7/2}$
1067.068	20	93714.7	$27380\ _{11/2} - 121095^{\circ}{}_{11/2}$	1061.519	5	94204.6	$21294\ _{7/2} - 115499^{\circ}{}_{9/2}$
1067.000	10	93720.7		1061.328	200	94221.6	$17113\ _{13/2} - 111335^{\circ}{}_{15/2}$
1066.896	200	93729.8	$23844\ _{9/2} - 117574^{\circ}{}_{11/2}$	1061.162	30 *c l*	94236.3	$23844\ _{9/2} - 118081^{\circ}{}_{9/2}$
1066.570	20	93758.5	$19872\ _{7/2} - 113630^{\circ}{}_{7/2}$	1061.120	30 *c l*	94240.0	$19360\ _{13/2} - 113600^{\circ}{}_{13/2}$
1066.520	2	93762.9		1061.072	5 *c l*	94244.3	$27138\ _{7/2} - 121382^{\circ}{}_{9/2}$
1066.465	3	93767.7	$17113\ _{13/2} - 110881^{\circ}{}_{11/2}$	1061.051	5 *c l*	94246.2	
1066.345	100	93778.3	$27604\ _{9/2} - 121382^{\circ}{}_{9/2}$	1060.993	100	94251.3	$21418\ _{5/2} - 115670^{\circ}{}_{7/2}$
1066.223	20	93789.0	$21535\ _{9/2} - 115324^{\circ}{}_{9/2}$	1060.857	100	94263.4	
1066.177	3	93793.0		1060.734	20	94274.3	
1066.089	20 *c l*	93800.8	$17534\ _{15/2} - 111335^{\circ}{}_{15/2}$	1060.546	200	94291.0	$19308\ _{11/2} - 113600^{\circ}{}_{13/2}$
1066.034	500	93805.6	$23442\ _{11/2} - 117248^{\circ}{}_{13/2}$	1060.486	10	94296.4	$22747\ _{9/2} - 117044^{\circ}{}_{7/2}$
1065.791	30	93827.0		1060.250	30	94317.4	
1065.625	10	93841.6		1060.160	40	94325.4	
1065.586	10	93845.1	$25033\ _{9/2} - 118879^{\circ}{}_{11/2}$	1060.077	20	94332.8	$23442\ _{11/2} - 117775^{\circ}{}_{13/2}$
1065.524	80	93850.5		1059.926	10	94346.2	
1065.464	20	93855.8		1059.822	20	94355.5	$19308\ _{11/2} - 113664^{\circ}{}_{11/2}$

[a] For doubly-classified lines, the wavelength is entered only once.

TABLE X. *Observed spectral lines of* Pr III *in the vacuum ultra violet region* — Continued

λ_{vac} Å	Intensity	σ (cm^{-1})	Classification [a]	λ_{vac} Å	Intensity	σ (cm^{-1})	Classification [a]
1059.714	10	94365.1		1053.177	1	94950.8	
1059.631	100 *c l*	94372.5	$22080\ _{7/2} - 116453^{\circ}_{9/2}$	1053.105	1	94957.3	
1059.587	100 *c l*	94376.4		1053.021	100	94964.9	
1059.410	50	94392.2		1052.860	100 *c l*	94979.4	
1059.281	400 *c l*	94403.7	$26095\ _{11/2} - 120498^{\circ}_{13/2}$	1052.815	40	94983.4	
1059.250	100 *c l*	94406.4	$16516\ _{7/2} - 110922^{\circ}_{9/2}$	1052.633	1000	94999.9	$21238\ _{13/2} - 116238^{\circ}_{15/2}$
1059.157	200	94414.7		1052.571	100	95005.5	$15525\ _{11/2} - 110530^{\circ}_{13/2}$
1059.022	60	94426.8	$23844\ _{9/2} - 118271^{\circ}_{11/2}$	1052.456	3	95015.8	$17627\ _{9/2} - 112643^{\circ}_{11/2}$
1058.948	10	94433.3	$21238\ _{13/2} - 115672^{\circ}_{15/2}$	1052.262	3	95033.4	
1058.769	60	94449.3	$22277\ _{3/2} - 116727^{\circ}_{5/2}$	1052.202	5 *c l*	95038.8	
1058.510	100	94472.4		1052.133	5 *c l*	95045.0	
1058.393	3	94482.9		1051.929	30	95063.4	
1058.348	3	94486.9	$21535\ _{9/2} - 116021^{\circ}_{7/2}$	1051.851	5	95070.5	$21238\ _{13/2} - 116309^{\circ}_{11/2}$
1058.150	4	94504.6	$21294\ _{7/2} - 115800^{\circ}_{5/2}$	1051.792	200	95075.8	$19649\ _{17/2} - 114725^{\circ}_{17/2}$
1058.018	20	94516.4	$22527\ _{7/2} - 117044^{\circ}_{7/2}$	1051.732	40	95081.2	
1057.903	5 *c l*	94526.6		1051.568	200	95096.1	$19700\ _{11/2} - 114797^{\circ}_{13/2}$
1057.885	10 *c l*	94528.2	$18241\ _{11/2} - 112769^{\circ}_{13/2}$	1051.423	30	95109.2	
1057.783	100	94537.3		1051.347	5	95116.1	$21611\ _{5/2} - 116727^{\circ}_{5/2}$
1057.721	100	94542.9		1051.313	20	95119.2	$22527\ _{7/2} - 117647^{\circ}_{7/2}$
1057.490	10 *c l*	94563.5		1051.093	10	95139.1	
1057.456	20	94566.6	$18990\ _{7/2} - 113556^{\circ}_{5/2}$	1050.961	5	95151.0	$23050\ _{3/2} - 118201^{\circ}_{3/2}$
			$38785\ _{15/2} - 133352^{\circ}_{15/2}$	1050.881	10	95158.2	$21294\ _{7/2} - 116453^{\circ}_{9/2}$
1057.310	400	94579.6	$18063\ _{9/2} - 112643^{\circ}_{11/2}$				$22527\ _{7/2} - 117686^{\circ}_{5/2}$
1057.228	200	94587.0	$38785\ _{15/2} - 133373^{\circ}_{17/2}$	1050.770	1	95168.3	$23442\ _{11/2} - 118610^{\circ}_{13/2}$
1057.080	40	94600.2	$23175\ _{13/2} - 117775^{\circ}_{13/2}$	1050.652	7	95179.0	
1056.815	10	94623.9	$23647\ _{13/2} - 118271^{\circ}_{11/2}$	1050.595	3	95184.2	$20315\ _{9/2} - 115499^{\circ}_{9/2}$
			$23844\ _{9/2} - 118468^{\circ}_{9/2}$	1050.433	20	95198.8	
1056.619	8	94641.5		1050.323	100	95208.8	
1056.518	100	94650.5	$38701\ _{13/2} - 133352^{\circ}_{15/2}$	1050.107	70	95228.4	$18063\ _{9/2} - 113291^{\circ}_{7/2}$
1056.314	20	94668.8	$23532\ _{5/2} - 118201^{\circ}_{3/2}$	1050.056	20	95233.0	
1056.211	50	94678.0		1049.914	1	95245.9	
1056.030	80	94694.3	$21238\ _{13/2} - 115933^{\circ}_{11/2}$	1049.546	20	95279.3	
1055.857	20	94709.8		1049.456	100	95287.5	$15045\ _{5/2} - 110333^{\circ}_{7/2}$
1055.668	20	94726.8	$21294\ _{7/2} - 116021^{\circ}_{7/2}$				$26095\ _{11/2} - 121382^{\circ}_{9/2}$
1055.297	20	94760.0		1049.228	20	95308.2	$21418\ _{5/2} - 116727^{\circ}_{5/2}$
1055.143	300	94773.9	$21535\ _{9/2} - 116309^{\circ}_{11/2}$	1049.086	2000	95321.1	$19649\ _{17/2} - 114970^{\circ}_{19/2}$
1055.072	30	94780.3		1048.951	5	95333.3	$22747\ _{9/2} - 118081^{\circ}_{9/2}$
1054.613	50	94821.5	$20848\ _{5/2} - 115670^{\circ}_{7/2}$	1048.923	15	95335.9	$26095\ _{11/2} - 121431^{\circ}_{13/2}$
1054.558	50 *c l*	94826.5	$16516\ _{7/2} - 111342^{\circ}_{7/2}$	1048.703	100 *c l*	95355.9	$15525\ _{11/2} - 110881^{\circ}_{11/2}$
1054.525	80 *c l*	94829.4	$23442\ _{11/2} - 118271^{\circ}_{11/2}$	1048.672	20 *c l*	95358.7	$16135\ _{7/2} - 111494^{\circ}_{5/2}$
							$18241\ _{11/2} - 113600^{\circ}_{13/2}$
1054.441	60	94837.0					
1054.388	5	94841.7		1048.643	200 *c l*	95361.3	$17534\ _{15/2} - 112896^{\circ}_{15/2}$
1054.263	7	94853.0		1048.413	3	95382.2	
1053.876	400	94887.8	$23175\ _{13/2} - 118063^{\circ}_{15/2}$	1048.318	4	95390.9	
1053.584	6	94914.1		1048.255	40	95396.6	$15525\ _{11/2} - 110922^{\circ}_{9/2}$
1053.542	3	94917.9	$18241\ _{11/2} - 113158^{\circ}_{9/2}$	1048.122	7	95408.7	$22277\ _{3/2} - 117686^{\circ}_{5/2}$
			$21535\ _{9/2} - 116453^{\circ}_{9/2}$	1047.966	3	95422.9	$18241\ _{11/2} - 113664^{\circ}_{11/2}$
1053.412	1	94929.6		1047.924	8	95426.8	$15454\ _{13/2} - 110881^{\circ}_{11/2}$
1053.344	40	94935.8	$26446\ _{7/2} - 121382^{\circ}_{9/2}$	1047.811	100	95437.1	$19360\ _{13/2} - 114797^{\circ}_{13/2}$
1053.260	2	94943.3					$23442\ _{11/2} - 118879^{\circ}_{11/2}$

[a] For doubly-classified lines, the wavelength is entered only once.

TABLE X. *Observed spectral lines of* Pr III *in the vacuum ultra violet region* — Continued

λ_{vac} Å	Intensity	σ (cm^{-1})	Classification [a]	λ_{vac} Å	Intensity	σ (cm^{-1})	Classification [a]
1047.752	1	95442.4		1041.872	100	95981.1	
1047.625	10	95454.0		1041.740	100	95993.2	$20315\ _{9/2} - 116309^{\circ}{}_{11/2}$
1047.375	10 *c l*	95476.8	$16516\ _{7/2} - 111993^{\circ}{}_{9/2}$	1041.625	100	96003.8	$17627\ _{9/2} - 113630^{\circ}{}_{7/2}$
1047.352	10 *c l*	95478.9		1041.563	20	96009.6	$21238\ _{13/2} - 117248^{\circ}{}_{13/2}$
1047.244	3000	95488.7	$17534\ _{15/2} - 113023^{\circ}{}_{17/2}$	1041.459	400	96019.1	$21755\ _{11/2} - 117775^{\circ}{}_{13/2}$
1047.105	3	95501.4		1041.260	200	96037.5	$17627\ _{9/2} - 113664^{\circ}{}_{11/2}$
1047.048	1	95506.6		1041.205	20	96042.6	$19360\ _{13/2} - 115403^{\circ}{}_{11/2}$
1046.941	3	95516.4		1041.145	100	96048.1	$19360\ _{13/2} - 115408^{\circ}{}_{13/2}$
1046.779	300	95531.1		1041.002	60	96061.3	$25033\ _{9/2} - 121095^{\circ}{}_{11/2}$
1046.700	20	95538.4		1040.849	10	96075.4	$21611\ _{5/2} - 117686^{\circ}{}_{5/2}$
1046.594	1	95548.0	$19872\ _{7/2} - 115420^{\circ}{}_{7/2}$	1040.646	50	96094.2	$19308\ _{11/2} - 115403^{\circ}{}_{11/2}$
1046.543	1	95552.7		1040.591	100	96099.2	$19308\ _{11/2} - 115408^{\circ}{}_{13/2}$
1046.195	500	95584.5	$15525\ _{11/2} - 111110^{\circ}{}_{13/2}$	1040.437	6	96113.5	
1046.113	10	95592.0		1040.387	3	96118.1	
1046.014	30	95601.0	$18063\ _{9/2} - 113664^{\circ}{}_{11/2}$	1040.247	20	96131.0	$22747\ _{9/2} - 118879^{\circ}{}_{11/2}$
1045.900	10	95611.4		1040.180	100	96137.2	$20315\ _{9/2} - 116453^{\circ}{}_{9/2}$
1045.858	100	95615.3		1040.139	50	96141.0	
1045.765	5	95623.8	$19700\ _{11/2} - 115324^{\circ}{}_{9/2}$	1040.082	5	96146.3	
1045.707	20	95629.1		1040.051	5	96149.1	$19872\ _{7/2} - 116021^{\circ}{}_{7/2}$
1045.511	10 *b l*	95647.0		1039.943	10	96159.1	
1045.447	20 *c l*	95659.9		1039.778	50	96174.4	
1045.411	300 *c l*	95656.2	$15454\ _{13/2} - 111110^{\circ}{}_{13/2}$	1039.380	10	96211.2	
1045.248	8	95671.1	$14859\ _{11/2} - 110530^{\circ}{}_{13/2}$	1039.253	60 *c l*	96223.0	$15045\ _{5/2} - 111268^{\circ}{}_{3/2}$
1045.181	1	95677.2		1039.200	50 *c l*	96227.9	$21418\ _{5/2} - 117647^{\circ}{}_{7/2}$
1045.049	1	95689.3		1039.156	100 *c l*	96231.9	$19700\ _{11/2} - 115933^{\circ}{}_{11/2}$
1044.993	4	95694.4		1039.033	5	96243.3	
1044.909	30	95702.1	$18211\ _{5/2} - 113914^{\circ}{}_{5/2}$	1038.962	10	96249.9	$14859\ _{11/2} - 111110^{\circ}{}_{13/2}$
			$19700\ _{11/2} - 115403^{\circ}{}_{11/2}$	1038.773	3	96267.4	$21418\ _{5/2} - 117686^{\circ}{}_{5/2}$
1044.851	10	95707.4	$19700\ _{11/2} - 115408^{\circ}{}_{13/2}$	1038.451	10	96297.3	$15045\ _{5/2} - 111342^{\circ}{}_{7/2}$
1044.608	30	95729.7		1038.356	7	96306.1	
1044.239	50	95763.5		1038.293	1000	96311.9	$19360\ _{13/2} - 115672^{\circ}{}_{15/2}$
1044.203	50	95766.8		1038.186	400	96321.8	$14558\ _{9/2} - 110881^{\circ}{}_{11/2}$
1044.117	3	95774.7	$14558\ _{9/2} - 110333^{\circ}{}_{7/2}$	1038.066	40	96333.0	
1044.029	500	95782.8	$17113\ _{13/2} - 112896^{\circ}{}_{15/2}$	1037.862	5	96351.9	$21294\ _{7/2} - 117647^{\circ}{}_{7/2}$
1043.970	3	95788.2	$21535\ _{9/2} - 117323^{\circ}{}_{11/2}$	1037.738	50 *c l*	96363.4	$14558\ _{9/2} - 110922^{\circ}{}_{9/2}$
1043.853	50	95798.9	$19700\ _{11/2} - 115499^{\circ}{}_{9/2}$	1037.703	50 *c l*	96366.7	
1043.797	500	95804.1	$18921\ _{15/2} - 114725^{\circ}{}_{17/2}$	1037.584	20	96377.7	
1043.639	10	95818.6	$21755\ _{11/2} - 117574^{\circ}{}_{11/2}$	1037.479	5	96387.5	$22080\ _{7/2} - 118468^{\circ}{}_{9/2}$
1043.501	50	95831.2		1037.432	2	96391.9	$21148\ _{3/2} - 117540^{\circ}{}_{3/2}$
1043.294	5	95850.2					$21294\ _{7/2} - 117686^{\circ}{}_{5/2}$
1043.223	200	95856.8	$16135\ _{7/2} - 111993^{\circ}{}_{9/2}$	1037.390	30	96395.8	
1043.110	10	95867.2		1037.232	10	96410.4	$31803\ _{1/2} - 128214^{\circ}{}_{3/2}$
1042.964	1000	95880.6	$15454\ _{13/2} - 111335^{\circ}{}_{15/2}$	1036.823	15	96448.5	
1042.819	10	95893.9		1036.749	5	96455.4	
1042.651	7	95909.4		1036.623	10	96467.1	$15525\ _{11/2} - 111993^{\circ}{}_{9/2}$
1042.478	100	95925.3	$32288\ _{3/2} - 128214^{\circ}{}_{3/2}$	1036.410	60	96486.9	$17113\ _{13/2} - 113600^{\circ}{}_{13/2}$
1042.306	2	95941.1	$22527\ _{7/2} - 118468^{\circ}{}_{9/2}$				$18921\ _{15/2} - 115408^{\circ}{}_{13/2}$
1042.250	20	95946.3		1036.174	40 *c l*	96508.9	
1042.031	3	95966.4		1036.151	40 *c l*	96511.0	
1041.963	60	95972.7	$25409\ _{7/2} - 121382^{\circ}{}_{9/2}$	1035.765	8 *b l*	96547.0	

[a] For doubly-classified lines, the wavelength is entered only once.

TABLE X. *Observed spectral lines of* Pr III *in the vacuum ultra violet region* — Continued

λ_{vac} Å	Intensity	σ (cm^{-1})	Classification [a]	λ_{vac} Å	Intensity	σ (cm^{-1})	Classification [a]
1035.675	30	96555.4	$18241\ _{11/2}-114797^{\circ}{}_{13/2}$	1029.711	200	97114.6	$16516\ _{7/2}-113630^{\circ}{}_{7/2}$
1035.554	10	96566.7	$20160\ _{3/2}-116727^{\circ}{}_{5/2}$	1029.631	50	97122.2	
1035.386	20	96582.3		1029.393	5	97144.6	$19308\ _{11/2}-116453^{\circ}{}_{9/2}$
1035.312	10	96589.2	$19649\ _{17/2}-116238^{\circ}{}_{15/2}$	1029.284	10*h*	97154.9	
1035.260	10	96594.1	$24788\ _{9/2}-121382^{\circ}{}_{9/2}$	1029.212	100	97161.7	$18241\ _{11/2}-115403^{\circ}{}_{11/2}$
1035.111	50	96607.0	$19700\ _{11/2}-116309^{\circ}{}_{11/2}$	1029.158	30	97166.8	$18241\ _{11/2}-115408^{\circ}{}_{13/2}$
1035.063	2	96612.5		1029.032	2000	97178.7	$13352\ _{11/2}-110530^{\circ}{}_{13/2}$
1034.937	3	96624.2	$19308\ _{11/2}-115933^{\circ}{}_{11/2}$	1028.901	100	97191.1	$17534\ _{15/2}-114725^{\circ}{}_{17/2}$
1034.826	5	96634.6		1028.711	8*h*	97209.0	$18211\ _{5/2}-115420^{\circ}{}_{7/2}$
1034.804	30	96636.6		1028.277	10	97250.1	
1034.338	100	96680.2	$18990\ _{7/2}-115670^{\circ}{}_{7/2}$	1028.164	20 *c l*	97260.8	$18063\ _{9/2}-115324^{\circ}{}_{9/2}$
1034.114	7	96701.1		1028.029	2	97273.5	
1034.045	20 *c l*	96707.6	$21611\ _{5/2}-118318^{\circ}{}_{7/2}$	1027.569	100 *b l*	97317.1	$18921\ _{15/2}-116238^{\circ}{}_{15/2}$
1034.012	10 *c l*	96710.7		1027.488	10*h*	97324.7	
1033.827	10	96728.0		1027.226	40	97349.6	
1033.787	5	96731.7		1027.146	3	97357.1	$18063\ _{9/2}-115420^{\circ}{}_{7/2}$
1033.738	20	96736.3	$21535\ _{9/2}-118271^{\circ}{}_{11/2}$	1026.922	2	97378.4	
1033.680	20	96741.7		1026.706	1	97398.9	
1033.652	10	96744.4	$24788\ _{9/2}-121532^{\circ}{}_{11/2}$	1026.477	20	97420.6	$16135\ _{7/2}-113556^{\circ}{}_{5/2}$
1033.582	100	96750.9	$18921\ _{15/2}-115672^{\circ}{}_{15/2}$	1026.415	1	97426.5	
1033.424	5	96765.7		1026.333	2	97434.3	$14558\ _{9/2}-111993^{\circ}{}_{9/2}$
1033.329	30	96774.6		1026.251	100	97442.0	$15454\ _{13/2}-112896^{\circ}{}_{15/2}$
1033.238	50 *c l*	96783.1	$21535\ _{9/2}-118318^{\circ}{}_{7/2}$	1026.183	500	97448.5	$12846\ _{9/2}-110295^{\circ}{}_{11/2}$
1033.207	20 *c l*	96786.0	$21294\ _{7/2}-118081^{\circ}{}_{9/2}$	1026.030	100 *c l*	97463.0	$18990\ _{7/2}-116453^{\circ}{}_{9/2}$
1033.070	15	96798.9	$20848\ _{5/2}-117647^{\circ}{}_{7/2}$	1025.999	10 *c l*	97466.0	
1032.977	2	96807.6		1025.945	4	97471.1	$23647\ _{13/2}-121119^{\circ}{}_{15/2}$
1032.798	70	96824.4	$21238\ _{13/2}-118063^{\circ}{}_{15/2}$	1025.694	40*h*	97495.0	$16135\ _{7/2}-113630^{\circ}{}_{7/2}$
1032.496	2	96852.7		1025.243	10	97537.8	$23844\ _{9/2}-121382^{\circ}{}_{9/2}$
1032.450	200	96857.0		1025.144	50	97547.3	$19700\ _{11/2}-117248^{\circ}{}_{13/2}$
1032.299	10	96871.2		1024.944	10*h*	97566.3	
1032.221	7	96878.5	$19360\ _{13/2}-116238^{\circ}{}_{15/2}$	1024.711	10*h*	97588.5	$18211\ _{5/2}-115800^{\circ}{}_{5/2}$
1032.147	2	96885.4		1024.358	8	97622.1	$19700\ _{11/2}-117323^{\circ}{}_{11/2}$
1032.083	400	96891.4		1024.308	1	97626.9	
1031.870	10	96911.4	$24470\ _{7/2}-121382^{\circ}{}_{9/2}$	1024.210	5	97636.2	
1031.635	20	96933.5	$21535\ _{9/2}-118468^{\circ}{}_{9/2}$	1024.123	1	97644.5	$16135\ _{7/2}-113780^{\circ}{}_{9/2}$
1031.536	300	96942.8	$13352\ _{11/2}-110295^{\circ}{}_{11/2}$	1024.036	10	97652.8	$23442\ _{11/2}-121095^{\circ}{}_{11/2}$
1031.435	5	96952.3		1023.976	20	97658.5	
1031.360	3	96959.4		1023.670	5 *c l*	97687.7	$23844\ _{9/2}-121532^{\circ}{}_{11/2}$
1031.297	2	96965.3		1023.573	30	97697.0	$17627\ _{9/2}-115324^{\circ}{}_{9/2}$
1031.171	20	96977.1		1023.268	100	97726.1	
1030.944	5	96998.5		1023.223	10	97730.4	$23651\ _{7/2}-121382^{\circ}{}_{9/2}$
1030.851	300	97007.2	$20315\ _{9/2}-117323^{\circ}{}_{11/2}$	1022.935	200	97757.9	$13352\ _{11/2}-111110^{\circ}{}_{13/2}$
1030.687	50	97022.7	$16135\ _{7/2}-113158^{\circ}{}_{9/2}$	1022.900	10 *c l*	97761.3	
1030.600	5	97030.8		1022.756	50	97775.0	$19872\ _{7/2}-117647^{\circ}{}_{7/2}$
1030.500	20	97040.3	$16516\ _{7/2}-113556^{\circ}{}_{5/2}$	1022.560	2	97793.8	$17627\ _{9/2}-115420^{\circ}{}_{7/2}$
1030.329	20	97056.4	$23442\ _{11/2}-120498^{\circ}{}_{13/2}$	1022.395	2	97809.6	$18211\ _{5/2}-116021^{\circ}{}_{7/2}$
1030.193	40	97069.2		1022.301	4	97818.5	
1030.125	3	97075.6		1022.146	4	97833.4	
1030.047	20	97082.9	$18241\ _{11/2}-115324^{\circ}{}_{9/2}$	1022.077	4	97840.0	
1029.785	20	97107.6		1021.865	5*h*	97860.3	

[a] For doubly-classified lines, the wavelength is entered only once.

TABLE X. *Observed spectral lines of* Pr III *in the vacuum ultra violet region* — Continued

λ_{vac} Å	Intensity	σ (cm^{-1})	Classification [a]	λ_{vac} Å	Intensity	σ (cm^{-1})	Classification [a]
1021.764	1	97867.0	$18063\ _{9/2} - 115933^{\circ}{}_{11/2}$	1013.841	4	98634.8	$22747\ _{9/2} - 121382^{\circ}{}_{9/2}$
1021.726	30	97873.6	$17534\ _{15/2} - 115408^{\circ}{}_{13/2}$	1013.780	30	98640.7	$13352\ _{11/2} - 111993^{\circ}{}_{9/2}$
			$19700\ _{11/2} - 117574^{\circ}{}_{11/2}$	1013.462	100	98671.7	
1021.664	7	97879.5		1013.354	5	98682.2	$17627\ _{9/2} - 116309^{\circ}{}_{11/2}$
1021.578	15	97887.8	$19360\ _{13/2} - 117248^{\circ}{}_{13/2}$	1013.142	80	98702.8	$19360\ _{13/2} - 118063^{\circ}{}_{15/2}$
1021.352	1000	97909.4	$14859\ _{11/2} - 112769^{\circ}{}_{13/2}$	1012.832	5	98733.1	$14558\ _{9/2} - 113291^{\circ}{}_{7/2}$
1021.150	20	97928.8					$29835\ _{9/2} - 128568^{\circ}{}_{9/2}$
1021.039	7	97939.4	$19308\ _{11/2} - 117248^{\circ}{}_{13/2}$	1012.760	1	98740.1	$14859\ _{11/2} - 113600^{\circ}{}_{13/2}$
1020.990	50	97944.2	$23175\ _{13/2} - 121119^{\circ}{}_{15/2}$	1012.300	2	98784.9	$22747\ _{9/2} - 121532^{\circ}{}_{11/2}$
1020.609	10	97980.7		1012.101	400	98804.4	$14859\ _{11/2} - 113664^{\circ}{}_{11/2}$
1020.252	5	98015.0		1011.809	50	98832.9	$18211\ _{5/2} - 117044^{\circ}{}_{7/2}$
1020.189	5	98021.0		1011.307	10	98881.9	
1020.052	40	98034.2	$12846\ _{9/2} - 110881^{\circ}{}_{11/2}$	1011.012	60	98910.8	
1019.982	2	98040.9	$20160\ _{3/2} - 118201^{\circ}{}_{3/2}$	1010.914	10	98920.4	$14859\ _{11/2} - 113780^{\circ}{}_{9/2}$
1019.890	10	98049.8		1010.560	50	98955.0	$17534\ _{15/2} - 116489^{\circ}{}_{17/2}$
1019.699	1	98068.2	$18241\ _{11/2} - 116309^{\circ}{}_{11/2}$	1010.282	20	98982.3	
1019.631	60	98074.7	$15525\ _{11/2} - 113600^{\circ}{}_{13/2}$	1010.153	20	98994.9	
			$19700\ _{11/2} - 117775^{\circ}{}_{13/2}$	1010.034	20	99006.6	$18241\ _{11/2} - 117248^{\circ}{}_{13/2}$
1019.534	60	98084.0	$14558\ _{9/2} - 112643^{\circ}{}_{11/2}$	1009.750	1	99034.4	
1019.474	1	98089.8	$23442\ _{11/2} - 121532^{\circ}{}_{11/2}$	1009.570	1	99052.1	
1019.311	100	98105.5		1009.029	1	99105.2	$14558\ _{9/2} - 113664^{\circ}{}_{11/2}$
1019.207	2	98115.5		1008.938	1	99114.1	
1018.968	200	98138.5	$15525\ _{11/2} - 113664^{\circ}{}_{11/2}$	1008.742	15	99133.4	
1018.890	3	98146.0	$15454\ _{13/2} - 113600^{\circ}{}_{13/2}$	1008.612	500	99146.2	$12846\ _{9/2} - 111993^{\circ}{}_{9/2}$
1018.544	1	98179.4		1008.536	3	99153.6	$16516\ _{7/2} - 115670^{\circ}{}_{7/2}$
1018.373	5	98195.8		1008.285	2	99178.3	$19700\ _{11/2} - 118879^{\circ}{}_{11/2}$
1018.242	100	98208.5	$19872\ _{7/2} - 118081^{\circ}{}_{9/2}$	1008.220	20 *h*	99184.7	
1017.853	2	98246.0	$15045\ _{5/2} - 113291^{\circ}{}_{7/2}$	1007.847	40	99221.4	$14558\ _{9/2} - 113780^{\circ}{}_{9/2}$
			$18063\ _{9/2} - 116309^{\circ}{}_{11/2}$	1007.459	40	99259.6	$18063\ _{9/2} - 117323^{\circ}{}_{11/2}$
1017.516	10	98278.6					$21238\ _{13/2} - 120498^{\circ}{}_{13/2}$
1017.396	5 *c l*	98290.1	$17113\ _{13/2} - 115403^{\circ}{}_{11/2}$	1007.392	1	99266.2	
1017.345	50 *c l*	98295.1	$17113\ _{13/2} - 115408^{\circ}{}_{13/2}$	1007.336	7	99271.7	$15525\ _{11/2} - 114797^{\circ}{}_{13/2}$
1017.310	20 *c l*	98298.4	$14859\ _{11/2} - 113158^{\circ}{}_{9/2}$	1007.088	1	99296.2	
1017.231	5	98306.1	$17627\ _{9/2} - 115933^{\circ}{}_{11/2}$	1006.829	3	99321.7	
1016.991	10	98329.3		1006.681	5	99336.3	
1016.714	5	98356.1		1006.383	3	99365.7	
1016.471	200	98379.6	$15454\ _{13/2} - 113833^{\circ}{}_{15/2}$	1006.221	3	99381.7	
1015.785	20	98446.0	$19872\ _{7/2} - 118318^{\circ}{}_{7/2}$	1005.857	10	99417.7	$13352\ _{11/2} - 112769^{\circ}{}_{13/2}$
1015.730	10	98451.4					$17627\ _{9/2} - 117044^{\circ}{}_{7/2}$
1015.699	2	98454.4		1005.676	5	99435.6	$18211\ _{5/2} - 117647^{\circ}{}_{7/2}$
1015.469	5	98476.7		1005.584	1	99444.7	
1015.340	1	98489.2		1005.280	3	99474.8	
1015.274	30	98495.6		1004.912	30	99511.2	
1015.170	8	98505.7		1004.533	2	99548.8	$1398^{\circ}{}_{11/2} - 100947\ _{9/2}$
1015.046	3	98517.7	$29835\ _{9/2} - 128352^{\circ}{}_{9/2}$	1004.259	1	99575.9	
1014.815	3	98540.1		1003.399	8	99661.2	
1014.750	10	98546.4	$29835\ _{9/2} - 128381^{\circ}{}_{11/2}$	1003.258	10	99675.2	
1014.622	30	98558.9	$17113\ _{13/2} - 115672^{\circ}{}_{15/2}$	1002.876	1	99713.2	
1014.231	10 *c l*	98596.9	$19872\ _{7/2} - 118468^{\circ}{}_{9/2}$	1002.724	1	99728.3	
1014.202	100	98599.7	$14558\ _{9/2} - 113158^{\circ}{}_{9/2}$	1002.035	20 *b l*	99796.9	

[a] For doubly-classified lines, the wavelength is entered only once.

TABLE X. *Observed spectral lines of* Pr III *in the vacuum ultra violet region*—Continued

λ_{vac} Å	Intensity	σ (cm^{-1})	Classification [a]	λ_{vac} Å	Intensity	σ (cm^{-1})	Classification [a]
1001.528	4	99847.4		979.694	2	102072.7	
1001.224	50 *c l*	99877.7		979.218	1	102122.3	$19308\ _{11/2}-121431^{\circ}{}_{13/2}$
1001.197	20 *c l*	99880.4					$26446\ _{7/2}-128568^{\circ}{}_{9/2}$
1000.630	80	99937.0	$14859\ _{11/2}-114797^{\circ}{}_{13/2}$	978.001	4	102249.4	$15525\ _{11/2}-117775^{\circ}{}_{13/2}$
			$16516\ _{7/2}-116453^{\circ}{}_{9/2}$	977.928	7	102257.0	$18241\ _{11/2}-120498^{\circ}{}_{13/2}$
1000.525	7	99947.5	$17627\ _{9/2}-117574^{\circ}{}_{11/2}$	976.676	10	102388.1	$14859\ _{11/2}-117248^{\circ}{}_{13/2}$
1000.351	3	99964.9		974.231	2	102645.1	
1000.023	5	99997.7	$21535\ _{9/2}-121532^{\circ}{}_{11/2}$	973.100	3	102764.4	$14558\ _{9/2}-117323^{\circ}{}_{11/2}$
999.499	30	100050.1		972.263	1	102852.8	
999.118	3	100088.3	$21294\ _{7/2}-121382^{\circ}{}_{9/2}$	972.148	2	102865.0	
			$2893^{\circ}{}_{13/2}-102981\ _{13/2}$	971.675	10	102915.1	$14859\ _{11/2}-117775^{\circ}{}_{13/2}$
998.931	10	100107.0	$18211\ _{5/2}-118318^{\circ}{}_{7/2}$	971.358	1	102948.6	
998.827	1	100117.4		970.727	5	103015.6	$14558\ _{9/2}-117574^{\circ}{}_{11/2}$
997.048	10	100296.1		970.065	10	103085.9	
996.885	1	100312.5	$12846\ _{9/2}-113158^{\circ}{}_{9/2}$	969.090	20	103189.6	$18241\ _{11/2}-121431^{\circ}{}_{13/2}$
			$13352\ _{11/2}-113664^{\circ}{}_{11/2}$	968.140	2	103290.8	$18241\ _{11/2}-121532^{\circ}{}_{11/2}$
996.425	5	100358.8		966.531	2	103462.8	$12846\ _{9/2}-116309^{\circ}{}_{11/2}$
996.321	10	100369.3	$18241\ _{11/2}-118610^{\circ}{}_{13/2}$	965.313	10	103593.3	$24788\ _{9/2}-128381^{\circ}{}_{11/2}$
995.957	2	100405.9	$18063\ _{9/2}-118468^{\circ}{}_{9/2}$	964.531	1	103677.3	
995.571	2	100444.9	$12846\ _{9/2}-113291^{\circ}{}_{7/2}$	963.849	10	103750.7	$14859\ _{11/2}-118610^{\circ}{}_{13/2}$
995.520	5*h*	100450.0		954.857	8	104727.7	$12846\ _{9/2}-117574^{\circ}{}_{11/2}$
995.377	3	100464.4	$14859\ _{11/2}-115324^{\circ}{}_{9/2}$	936.296	5	106803.8	
994.598	70	100543.1	$14859\ _{11/2}-115403^{\circ}{}_{11/2}$	935.046	3	106946.6	
994.545	6	100548.5	$14859\ _{11/2}-115408^{\circ}{}_{13/2}$	934.970	5	106955.3	
994.380	3	100565.2	$4453^{\circ}{}_{15/2}-105019\ _{13/2}$	934.074	2	107057.9	$21294\ _{7/2}-128352^{\circ}{}_{9/2}$
994.123	1	100591.2	$16135\ _{7/2}-116727^{\circ}{}_{5/2}$	932.196	3	107273.6	$21294\ _{7/2}-128568^{\circ}{}_{9/2}$
			$2893^{\circ}{}_{13/2}-103484\ _{15/2}$	931.153	40	107393.7	$25979\ _{15/2}-133373^{\circ}{}_{17/2}$
994.075	2	100596.0	$4453^{\circ}{}_{15/2}-105049\ _{15/2}$	920.003	1	108695.3	
993.795	100	100624.4	$15045\ _{5/2}-115670^{\circ}{}_{7/2}$	914.635	1	109333.2	
993.642	2	100639.9	$14859\ _{11/2}-115499^{\circ}{}_{9/2}$	913.825	60	109430.1	
993.600	1	100644.1	$17627\ _{9/2}-118271^{\circ}{}_{11/2}$	912.340	1	109608.3	
993.422	4	100662.2	$17113\ _{13/2}-117775^{\circ}{}_{13/2}$	909.894	4	109902.9	
992.169	5	100789.3	$0^{\circ}{}_{9/2}-100788\ _{7/2}$	907.103	1	110241.1	$18211\ _{5/2}-128453^{\circ}{}_{7/2}$
992.085	30	100797.8	$19700\ _{11/2}-120498^{\circ}{}_{13/2}$	904.386	2	110572.2	
990.750	5	100933.6	$12846\ _{9/2}-113780^{\circ}{}_{9/2}$	903.766	2	110648.1	
989.627	2	101048.2		902.999	3	110742.1	
989.381	20	101073.3	$14859\ _{11/2}-115933^{\circ}{}_{11/2}$	896.172	1	111585.7	
988.353	2	101178.4		894.647	3	111775.9	
988.001	60	101214.5	$27138\ _{7/2}-128352^{\circ}{}_{9/2}$	890.276	1	112324.7	
987.960	3	101218.7	$1398^{\circ}{}_{11/2}-102617\ _{11/2}$	889.296	2	112448.5	
987.344	4	101281.8		888.257	1	112580.0	
987.023	2	101314.8	$27138\ _{7/2}-128453^{\circ}{}_{7/2}$	887.360	4	112693.8	
985.880	2	101432.2	$1398^{\circ}{}_{11/2}-102830\ _{9/2}$	886.233	2	112837.1	
985.120	3	101510.5	$19872\ _{7/2}-121382^{\circ}{}_{9/2}$	885.575	2	112921.0	
983.927	3	101633.6		885.279	20	112958.7	
983.461	8	101681.7	$19700\ _{11/2}-121382^{\circ}{}_{9/2}$	884.158	40	113102.0	
982.796	4	101750.5	$14558\ _{9/2}-116309^{\circ}{}_{11/2}$	883.838	3	113142.9	
982.709	20	101759.5	$19360\ _{13/2}-121119^{\circ}{}_{15/2}$	882.990	3	113251.6	
982.340	1	101797.8	$15525\ _{11/2}-117323^{\circ}{}_{11/2}$	882.336	1	113335.5	
979.899	1	102051.3	$13352\ _{11/2}-115403^{\circ}{}_{11/2}$	881.591	3	113431.3	

[a] For doubly-classified lines, the wavelength is entered only once.

TABLE X. *Observed spectral lines of* Pr III *in the vacuum ultra violet region* – Continued

λ_{vac} Å	Intensity	σ (cm^{-1})	Classification [a]	λ_{vac} Å	Intensity	σ (cm^{-1})	Classification [a]
880.303	10	113597.2		856.826	1	116709.8	
879.840	2	113657.0		856.740	2*h*	116721.5	
879.441	10	113708.6	$14859\ _{11/2}-128568^{\circ}_{9/2}$	856.285	1	116783.5	
878.749	1	113798.1		856.192	20	116796.2	
878.215	10	113867.3		855.808	3	116848.6	
876.355	2	114109.0		855.718	20	116860.9	
876.305	1	114115.5		855.422	1	116901.4	
875.339	1	114241.4		855.038	1	116953.9	
874.680	2	114327.5		854.692	1	117001.2	
874.481	1	114353.5		854.254	1	117061.2	
874.173	1	114393.8		853.782	2	117125.9	
874.147	1	114397.2		853.413	10	117176.6	
874.051	1	114409.8		853.318	2	117189.6	
873.749	1	114449.3		853.229	4	117201.8	
872.569	1	114604.1		853.120	1	117216.8	
872.104	30	114665.2		853.054	1	117225.9	
871.932	1	114687.8		852.968	1	117237.7	
871.699	3	114718.5		851.867	2	117389.2	
871.069	2	114801.5		851.524	2	117436.5	
870.893	1	114824.7		851.438	3	117448.4	
869.598	1	114995.7		851.361	8	117459.0	
868.558	10	115133.4		851.301	200	117467.3	
868.490	1	115142.4		851.168	15	117485.6	
868.414	1	115152.4		850.903	5	117522.2	
866.285	4	115435.4		850.331	5	117601.3	
864.910	1	115619.0		850.156	10*b l*	117625.5	
864.582	1	115662.8		850.061	1	117638.6	
864.320	1	115697.9		850.011	1	117645.5	
863.941	8	115748.6		849.895	20	117661.6	
863.349	1	115828.0		849.803	20	117674.3	
863.131	3*h*	115857.3		848.718	1	117824.8	
862.823	2	115898.6		848.657	10	117833.2	
862.427	2	115951.8		848.440	1	117863.4	
862.227	1	115978.7		847.729	1	117962.2	
861.535	2	116071.9		847.474	3	117997.7	
861.498	1	116076.9		846.565	2	118124.4	
861.307	1	116102.6		846.209	2	118174.1	
860.721	2	116181.7		845.710	7	118243.8	
860.522	2	116208.5		845.231	10	118310.8	
860.313	3	116236.8		845.066	5	118334.0	
859.956	2	116285.0		844.788	3	118372.9	
859.730	3	116315.6		844.395	100	118428.0	
859.541	1	116341.2		843.998	2	118483.7	
859.299	1	116373.9		843.887	10	118499.3	
859.102	7	116400.6		843.542	40*b l*	118547.7	
857.723	8	116587.8		843.338	200	118576.4	
857.614	1	116602.6		843.312	10*c l*	118580.1	
857.348	5	116638.8		842.497	40	118694.8	
857.210	1	116657.5		842.384	1	118710.7	
857.091	1	116673.7		842.130	1	118746.5	

[a] For doubly-classified lines, the wavelength is entered only once.

TABLE X. *Observed spectral lines of* Pr III *in the vacuum ultra violet region*—Continued

λ_{vac} Å	Intensity	σ (cm^{-1})	Classification [a]	λ_{vac} Å	Intensity	σ (cm^{-1})	Classification [a]
841.990	3	118766.2		832.631	2	120101.2	
841.779	1	118796.0		832.164	1	120168.6	
841.628	20 *b l*	118817.3		832.013	1	120190.4	
841.426	8	118845.9		831.919	3	120204.0	
841.015	4	118903.9		831.846	10	120214.6	
840.890	30 *c l*	118921.6		831.266	200	120298.4	
840.871	10 *c l*	118924.3		831.136	1	120317.2	
840.459	6	118982.6		830.927	2	120347.5	
840.282	8	119007.7		830.386	1	120425.9	
840.057	60	119039.5		830.061	2	120473.1	
839.995	60	119048.3		829.325	3	120580.0	
839.619	1	119101.6		828.364	50	120719.9	
839.529	1	119114.4		828.169	1	120748.3	
839.474	2	119122.2		828.134	1	120753.4	
839.358	30 *h*	119138.7		827.345	1	120868.6	
838.933	30	119199.0		825.989	30	121067.0	
838.809	1	119216.6		825.404	7	121152.8	
837.712	2	119372.8		824.880	3	121229.8	
837.223	3	119442.5		824.542	1	121279.4	
836.744	8	119510.9		823.117	1	121489.4	
836.295	1	119575.0		822.725	2	121547.3	
835.843	15 *b l*	119639.7		822.467	15	121585.4	
834.617	1	119815.4		821.942	10	121663.1	
833.478	10	119979.2					
833.190	10	120020.6					

[a] For doubly-classified lines, the wavelength is entered only once.

(Paper 73A3–557)

JOURNAL OF RESEARCH of the National Bureau of Standards—A. Physics and Chemistry
Vol. 73A, No. 3, May–June 1969

Publications of the National Bureau of Standards*

Selected Abstracts

Ambler, E., Schooley, J. F., Colwell, J. H., Pfeiffer, E. R., Frederikse, H. R., Hosler, W. R., Thurber, W. R., **Transition temperatures and critical fields of Sr TiO_3 and mixed titanates,** *Proc. Xth Intern. Conf. Low Temperature Physics, Moscow, U.S.S.R., Aug. 31-Sept. 6, 1966, Vol.* **2B,** *Superconductivity, Paper S123, 142-148 (1968).*

The experimental investigation of the superconducting properties of the semiconducting systems $SrTiO_3$, $(Ba_xSr_{1-x})TiO_3$, and $(Ca_ySr_{1-y})TiO_3$ is reviewed. The studies of a.c. magnetic susceptibility, which yields transition temperature and penetration depth; of heat capacity, which yields the electronic density of states and transition temperature; and of magnetic moment, which yields first and second critical fields and transition temperature, are discussed briefly. Tables of experimental values of the parameters mentioned above are included.

Key words: $(Ba_xSr_{1-x})TiO_3$; $(Ca_ySr_{1-y})TiO_3$; critical fields; magnetic moment; semiconducting systems; penetration depth; superconducting; $SrTiO_3$; transition temperature.

Bekkedahl, N., **Crystallization of natural rubber,** *Rev. Gen.* Caoutchouc Plastiques **45,** No. 3, 341-6–463-9 *)1968).*

This review article presents a resume of the research work that has been done at the National Bureau of Standards during the past thirty-five years in the field of crystallization of polymeris materials, with special emphasis on natural rubber. It contains only information on results of research work that has already been published.

Key words: chain folding; contractility; crystallization; dilatometry; heat engine; melting; polymers; rubber; stark rubber.

Bennett, L. H., **Nuclear magnetism,** *Chapt. in Book, Magnetism and Magnetic Materials 1968 Digest, Ed. H. Chang and T. R. McGuire, Chapt. 14, pp. 201–221 (Academic Press Inc., New York, N. Y. 1968).*

This chapter reviews the 1967 literature that was devoted to the study of magnetism and magnetic materials taking advantage of the atomic nucleus as a probe. The bulk of the experimental papers utilize nuclear magnetic resonance (NMR or FNR) or recoilless -ray absorption, i.e., the Mössbauer effect (ME), as in previous years. Most of the NMR papers reviewed here are for ferromagnetic materials in the ordered state, for which we use the special abbreviation FNR. Other techniques for determining hyperfine (hf) magnetic fields (H_{hf}) include nuclear specific heat and perturbed angular correlation.

Key words: Magnetic materials; Mössbauer effect; nuclear magnetic resonance; nuclear magnetism; nuclear specific heat; perturbed angular correlation.

Brinckman, F. E., Gordon, G., **Energetic intermediates in inorganic synthesis: characterization of transport species in electric discharge,** *Proc. Inter. Symp. Decomposition of Organometallic Compounds to Refractory Ceramics, Metals, and Metal Alloys, Dayton, Ohio, Nov. 1967, pp. 29–46 (Univ. Dayton Press, Dayton, Ohio, Oct. 1968).*

Commercial processes involving energetic chemical transport and deposition reactions are poorly understood with respect to the identity and mechanistic behavior of their intermediates. Work is presented resulting from recent development of a facility for *in situ* sampling of electric discharge reactions by time-of-flight mass spectrometry. With use of single or mixed reactant gases to sustain a microwave discharge plasma, both homogeneous and heterogeneous reactions have been examined for synthetic potential under conditions of optimized energy input. A number or new compounds thereby have been identified with aid of computerized polyisotopic mass spectral analyses, but also by independent syntheses where known. Several important cases are presented with emphasis on oxyfluorides since both hetero- and homo-μ-oxy-metalloid products form. These systems include Si-O-Si, Si-O-B, B-O-B, Si-O-Ge, Ge-O-Ge, and Ge-O-B species for which some relative stability data can be derived. Extension of these findings to analogous carbon-containing materials (derived from organometals or organometalloids) is also discussed.

Key words: Electric discharge; reactive intermediates; transport species; oxyfluorides; silicon; boron, germanium; time-of-flight; mass spectrometry.

Carter, G. C., **The NBS Alloy Data Center,** *Mater. Res. Bull.* **3,** *919–922 (1968).*

A summary of the detailed description of the Alloy Data Center will be given in this letter.

Key words: Automated; alloys; bibliography; data; files; information; indexing computer programs; metals; physical properties; reference books (material).

Clark, A. F., **Low temperature thermal expansion of some metallic alloys,** *Cryogenics* **8,** *No. 5, 282–289 (Oct. 1968).*

The low temperature thermal expansion of several aluminum, nickel, copper, and iron base alloys was measured from liquid hydrogen temperature, 20K, to room temperature, 293K. Both the thermal contraction from room temperature $(L_{293}-L_T)/L_{293}$, and the thermal expansion coefficient, $\frac{1}{L_{293}}\frac{dL}{dT}$, are tabulated as a function of temperature. Comparison of similar alloys and alloy conditions led to the general conclusions that relatively large changes in composition are required to produce significant changes in the thermal expansion, thermal treatment or condition has little effect except when it produces a basic structure change, and the thermal expansion coefficient at room temperature is a good indicator of the total length change to a low temperature.

Key words: Alloys; aluminum; copper; expansivity; iron; metals; nickel; thermal expansion.

Davis, G. T., Eby, R. K., Martin, G. M., **Variations of the unit-cell dimensions of polyethylene: effect of crystallization conditions annealing, and deformation,** *J. Appl. Phys.* **39,** *No. 11, 4973–4981 (Oct. 1968).*

It is shown that the orthorhombic unit cell dimensions of a given polyethylene are not unique but depend upon physical and thermal history. For polymer crystallized from a 3/4 percent *p*-xylene solution, the values of *a* and *b* determined by the powder camera technique vary (up to 0.6%) systematically with crystallization temperature

(50 °C, 70 °C, 90 °C) and the temperature of annealing (up to 127 °C). For "undeformed" crystals, the changes with annealing appear to accompany the increase in crystal thickness and for deformed crystals, they occur over a wider range of temperatures—even below the crystallization temperature. The dimensions change within the first two minutes of annealing and appear to be independent of time thereafter. The only exception observed is a slow decrease of b with time upon annealing at 100 °C. Crystals grown from other solvents exhibit very nearly identical effects and the presence of solvents does not alter the cell dimensions at room temperature. Similar effects are observed for crystals grown from the melt by slow cooling, quenching in ice water, and quenching in a dry ice—acetone suspension. The main difference is that cold working does not appear to alter the effects of annealing. The mechanism of the effects cannot be safely assigned but changes in the fold surface probably play a role and a discussion relevant to this and other mechanisms is presented. Corresponding to the changes in cell dimension are changes in cell density which are, however, too small to account for the frequently reported discrepancy between crystal and unit cell density. The effects of cell variation must be considered in interpreting the variation of physical properties.

Key words: Annealing; crystallization; deformation; density; fold surface; melt; polyethylene; solvent; temperature; time; unit cell.

Douglas, T. B., King, E. G., **High-temperature drop calorimetry,** *Chapt. in Book, Experimental Thermodynamics, Ed. J. P. McCullough and D. W. Scott, Vol.* **I,** *Calorimetry of Non-reacting Systems, Chapt. 8, 293–331 (Butterworth and Co., London, England, 1968).*

The principles and techniques of the drop method of determining relative enthalpies of solids and liquids above room temperature are discussed in detail and critically, with particular attention to those features which lead to the most accurate results. Typical precise results are compared with those obtained using other calorimetric methods, and the advantages and disadvantages of the drop method are considered. While alternative accessories are referenced and discussed briefly, two important types of furnace (with and without a good thermal conductor) and two types of calorimeter (the "ice" and "copper-block") are treated in detail with respect to their design, construction, and operation with accuracy and convenience. Numerous sample and container problemas peculiar to high temperatures are considered. Finally, various aspects of treating the data are dealt with. These aspects include correcting to standard conditions, correcting for chemical impurities and irrelevant phase changes, smoothing and representing enthalpy values, derivation of other thermodynamic properties from enthalpies, and the evaluation and representation of simple expressions of precision and accuracy.

Key words: Calorimetric methods; calorimetry; drop calorimetry; thermodynamic properties.

Haller, W., Macedo, P. B., **The origin of phase connectivity in microheterogeneous glasses,** *Phys. Chem. Glasses* **9,** *No. 5, 153–155 (Oct. 1968).*

Recently published electron micrographic studies have shown that microheterogeneous glasses with interconnected phases can form from early stages which consist of randomly distributed isolated spheres. These observations lend support to the previously postulated Intersecting Growth Theory, and not to the Spinoidal Decomposition Theory. While a classic diffusion model predicts that the terminal growth rate at approaching surfaces of growing spheres becomes infinitely small due to diffusional depletion of the separating matrix, the experimental facts do not show any such limitations since the approaching growth fronts join rapidly. Various mechanisms are discussed by which a finite joining-rate can be achieved. A mechanism is suggested which is based upon the fact that the classic boundary concept of diffusion is not anymore applicable to bodies of small magnitudes and has to be replaced by the concept of a transitional fluctuating boundary. From ultrasonic and electron microscopic evidence it is estimated that the fluctuations in the investigated systems are of the order of 50Å.

It is furthermore shown that for systems having close to equal volume fraction the criterion for the terminal formation of an interconnected network or of isolated spheroids will be the nucleation density.

Key words: Glass; microheterogeneous glass; spinoidal decomposition theory; connectivity of microphases; intersecting growth theory; fluctuation theroy.

Heinrich, K. F. J., **Electron probe microanalysis: a review,** *Appl. Spectry.* **22,** *No. 5, part 1, 395–403 (Sept.–Oct. 1968).*

This review covers the development of electron probe microanalysis in the last ten years. After a brief description of the instrument, the following subjects are discussed: progress in instrumentation, progress in the theory of quantitative analysis, and the future development of microprobe analysis.

Key words: Analysis; spectrometry; x-rays; electron probe; microanalysis.

Heinrich, K. F. J., Yakowitz, H., **Quantitative electron probe microanalysis: fluorescence correction uncertainty,** *Mikrochim. Acta* **5,** *905–916 (1968).*

In order to evaluate the fluorescence correction uncertainty in electron probe microanalysis, effects of two general types were investigated. The effects of uncertainty in (1) microprobe operational variables, including x-ray emergence angle and operating voltage, and (2) errors in model input parameters, such as fluorescence yield factors and mass attenuation coefficients, were evaluated. The major conclusion of this study is, that even in cases requiring large fluorescence corrections, microprobe operation at high ($\geq 30°$) x-ray emergence angles, and at the lowest voltage compatible with a reasonable x-ray output is entirely satisfactory. This conclusion is reached by substituting into existing fluorescence correction models reasonable input parameter errors, x-ray emergency angles, and operating voltages. Results show that absolute compositional errors vary quite slowly with x-ray emergence angle and operating voltage. The chief source of error among input parameters is the fluorescence yield factor. The role of model selection as a source of potential error is also discussed.

Key words: Electron probe microanalysis; error analysis; fluorescence corrections; quantitative analysis; x-ray fluorescence.

Hicho, G. E., Meyerson, M. R., Geil, G. W., **Effect of slack-quenched structures on the tensil properties of AISI 5140 steel,** *(Proc. Intern. Conf. Strength of Metals and Alloys), Suppl. Trans. Japan Inst. Metals* **9,** *134–142 (1968).*

Slack-quenched structures in steels are generally believed to be detrimental even though adequate data on the tensile behavior of these structures are not available. Results are reported of an investigation on the tensile behavior of specimens of AISI 5140 steel slack-quenched to different hardness levels and tested in the conditions as (1) slack quenched and stress relieved at 275° F, (2) slack quenched and tempered at 400, 550, 700, 850, and 1000° F, and (3) slack quenched and tempered to selected hardness levels. The tempering of the slack-quenched specimens had a very beneficial effect on the yield behavior and ductility; tempering slack-quenched specimens to a reduction of R_c 5 to 7 in hardness generally produced a maximum increase in the yield strength. Moreover, the yield strength and reduction of area of the slack-quenched specimens tempered to a reduction of R_c 5 to 7 or more in hardness were nearly equal to those of fully-hardened specimens tempered to the same hardness level.

Key words: AISI 5140 steel; slack-quenched structures; heat treatment; tempering temperature; tensile strength; yield strength; reduction of area; hardness.

Hudson, R. P., Kaeser, R. S., **Magnetic temperature scale 0.002–5° K,** *Prox. Xth Intern. Conf. Low Temperature Physics, Moscow, U.S.S.R., Aug. 31–Sept. 6, 1966, Vol.* **1,** *Properties of Helium, Paper H4, 171–173 (1968).*

Our previous measurements of the heat capacity of cerous magnesium nitrate (CMN) as a function of susceptibility using gamma-ray heating have been superseded by new data obtained with a new single-crystal sphere following various improvements in apparatus and procedure. The entropy-susceptibility relation is the same

for all specimens and is thus independent of ellipsoid axial ratio; the indicated value of b (coefficient of T^{-2} for "high temperature" heat capacity) is 15 percent smaller than calculated by Cooke, Duffus, and Wolf. Combining the heat capacity and entropy data led to values of absolute temperature, which fall below 0.002° K for the lowest entropy obtained, viz. $S/R = 0.25$. In the region bebetween 0.02° K where both dipole-dipole and lattice specific heat are very small, an anomalous and apparently non-magnetic contribution to the heat capacity was detected. No explanation for this has been found, but its existence undoubtedly accounts for the apparently non-isentropic demagnetizations experienced for "starting conditions" H/T less than 0.37 oesteds deg^{-1}.

Key words: Cerous magnesium nitrate; temperature scale; magnetic thermometer; low temperatures; magnetic cooling; paramagnetic salt.

Jacox, M. E., Milligan, D. E., **Matrix isolation study of the vacuum-ultraviolet photolysis of trichlorosilane. The infrared spectrum of the free radical $SiCl_3$,** *J. Chem. Phys.* **49,** *No. 7, 3130–3135 (Oct. 1, 1968).*

In studies of the vacuum-ultraviolet photolysis of $HSiCl_3$ in argon and nitrogen matrices at 14° K, features appear near 470 and 582 cm^{-1} which may be identified with the two stretching fundamentals of $SiCl_3$. Evidence supporting primary photodecomposition by detachment of the H atom has been obtained in CO matrix experiments, in which HCO is a major product. The observed frequencies permit estimation of an angle of $72° \pm 5°$ between the threefold axis and each of the Si-Cl bonds. Force constants have also been estimated. The FG-matrix treatment is presented for the stretching modes of a nonplanar X_2YZ species with equal XYX and XYZ valence angles. The calculated frequency and intensity pattern for the mixed chlorine isotopic species is in excellent correspondence with the observed pattern, providing strong support for the identification and proposed vibrational assignment. Unstructured absorptions between 2900 and 3300 Å and between 2150 and 2450 Å are tentatively attributed to $SiCl_3$.

Key words: Force constants; free radical; infrared spectrum; matrix isolation; photolysis; $SiCl_3$; trichlorosilane; ultraviolet spectrum.

Kim, Y-K., Inokuti, M., Chamberlain, G. E., Mielczarek, S. R., **Minima of generalized oscillator strengths,** *Phys. Rev. Letters* **21,** *No. 16, 1146–1148 (Oct. 14, 1968).*

Frequent occurrence of zero or near-zero minima of the generalized oscillator strength is closely connected with the nodes of the radial wave functions for the states involved. Some general implications of the minima are discussed, and, as an example, experimental and theoretical results for a transition in Xe are presented.

Key words: Generalized oscillator strengths; xenon; absolute; cross section; electron; theory; experiment.

Klose, J. Z., **Atomic lifetime measurements with pulsed electron beams,** *(Proc. Beam-Foil Sprectroscopy Conf., Univ. Arizona, Tucson, Arizona, Nov. 20–22, 1967), Chapt. in Book, Beam-Foil Spectroscopy,* **II,** *285–304 (Gordon and Breach Publ., New York, N.Y., 1968).*

Following a short discussion of the general method of measuring atomic lifetimes using pulsed electron beams, four separate determinations of the mean lives of the ten $2p$ levels (Paschen notation) in Ne I are presented for comparison. These four sets of results from different experimental groups are found to be in general agreement. Mention is next made of the published lifetime measurements in Ar I ($2p$ levels) and Ar II without presentation of results. Finally, measurements of the pressure-dependent lifetime of the $3s_2$ laser level in Ne I are analyzed using the Holstein theory of the imprisonment of resonance radiation. The analysis yields information about transition probabilities from which are derived the $3s_2$ lifetimes for absence of imprisonment (28 ± 5 nsec) and complete imprisonment (52 ± 2 nsec) of the 600.04 Å ($3s_2 - {}^1S_0$) resonance radiation.

Key words: Atomic spectra; atomic lifetimes; helium; neon; argon; laser.

Laufer, A. H., McNesby, J. R., **Photolysis of methane at 1236-A: quantum yield of hydrogen formation,** *J. Chem. Phys.* **49,** *No. 5, 2272–2278 (Sept. 1, 1968).*

Pure CH_4 and CD_4 have been separately but simultaneously photolyzed at 1236Å by means of a split cell technique in order to obtain accurate relative quantum yields for the various codes of production of H_2 and D_2. The split cell technique has been used to obtain absolute quantum yields by comparison with the CO_2 actinometer. Molecular elimination yields for CD_4 and CH_4 (0.58) are found to be nearly equal while the H atom yield greatly exceeds the D atom yield. It is concluded from the results that a significant fraction of the atoms produced disappears by the association reaction $M + H + CH_3 \rightarrow CH_4 + M$. The effect of scavengers and inert gas have been studied and the absolute quantum yields measured by comparison with the CO_2 actinometer. The total quantum yield for H and H_2 formation is at least 1.29 and fragmentation of CH_2 or CH_3 formed in the primary process is suggested.

$$CH_3 \rightarrow H + CH_2$$
$$CH_2 \rightarrow H + CH$$

However, the lower limit for the quantum yield for D and D_2 formation is 0.76 and evidence for fragmentation of CD_2 or CD_3 is absent.

Key words: Methane; vacuum ultraviolet; quantum yields; isotope effect.

Macedo, P. B., Simmons, J. H., Haller, W., **Spectrum of relaxation times and fluctuation theory: ultrasonic studies on an alkali-borosilicate melt,** *Phys. Chem. Glasses* **9,** *No. 5, 156–164 (Oct. 1968)*

Ultrasonic relaxation measurements (3 to 23 MHz and 750 to 1200° C) were made using shear waves on a molten glass of 6.72% Na_2O, 25.31% B_2O_3 and 67.97% SiO_2 with a solubility temperature of 749° C. The spectrum of shear relaxation times was determined between 840 and 1200° C, where it was found to be highly dependent. A model was proposed which predicts the observed temperature dependence of the spectrum in terms of composition fluctuations. The model is based upon the concept that the activation energy of a molecule depends on the environment within a sphere of radius r_0 about the molecule. The value of $r_0 \sim 50$Å obtained from the supercritical composition fluctuations is of the same order as sizes of microheterogeneities directly observed with an electron microscope in single oxide glasses by other workers.

Key words: Ultrasonic relaxation; composition fluctuations; spectrum of relaxation times; alkali-borosilicate glass; immiscible alkali-borosilicate glass.

Manning, J. R., **Vacancy-wind effect in diffusion and deviations from thermodynamic equilibrium conditions,** *Can. J. Phys.* **46,** *No. 23, 2633–2643 (1968).*

The vacancy flow (or "wind") term which appears in kinetic treatments of the diffusion equations is discussed in terms of the vacancy concentrations which appear when a vacancy flow is distorted by an impurity. It is pointed out that this term arises from local distortions in the vacancy concentration profile and not from any overall deviation of the material from equilibrium vacancy concentrations. Thus, the thermodynamic treatment of Kirkaldy and Lane does not include the vacancy wind term. Several physical analogies help to describe the basic process.

The vacancy wind effect arises from motion of atoms other than the particular diffusing atom. In addition, motion of the diffusing atom itself can introduce distortions in the local vacancy distribution. For a slow-diffusing impurity, mobile-impurity effects are unimportant; but, for a fast-diffusing impurity, they become very important, both in their effect on the diffusion equations and in their effect on local vacancy distributions. Equations are given for the resulting deviations from equilibrium at sites neighboring on an impurity. The close relationship between mobile-impurity effects and the correlation factor is shown. For self-diffusion, mobile-

impurity and vacancy wind effects exactly cancel in their influence on vacancy distributions.

Key words: Diffusion; vacancy concentrations; vacancy flow; correlation factor; distortions of vacancy flux; deviations from thermodynamic equilibrium; vacancy wind.

Mazur, J., McIntyre, D., Wims, A. M., **Asymptotic behavior of the light-scattering function of coiled molecules,** *J. Chem. Phys.* **49,** *No. 7, 2896–2904 (Oct. 1, 1968).*

This paper discusses the asymptotic solution of the scattering function $P(\theta)$ for large x where x is proportional to the scattering angle, radius of gyration and the wave number. The theoretical model employed for the calculation of the $P(\theta)$ vs. x curves was presented in the preceding paper. The results are discussed with respect to the experimental data, after the results for $P(\theta)$ are corrected for various values of polydispersity.

A general analysis of the theoretical $P(\theta)$ vs. x curves is presented, and the effect of the shape of the chain-end distribution function on the asymptotic behavior of the light scattering function is discussed.

Key words: Chain-end distribution; excluded volume; light scattering; particle scattering factor; polydispersity.

Mendlowitz, H., **Calculated line strengths for the transitions between the configurations ($3d^3 + 3d^24s$) and $3d^24p$ in Ti II,** *Astrophys. J.* **154,** *1099–1110 (Dec. 1968).*

We have calculated the relative line strengths in Ti II for the transitions between the configurations ($3d^3 + 3d^24s$) and $3d^24p$. The strengths have been calculated in the intermediate coupling scheme while also taking into account the interaction between configurations. The relative magnitude and phase of the radial transition integrals (s-p) and (d-p) for the jumping electron in the LS coupling scheme have been obtained empirically from the data of King and that of Wobig by means of a least-squares fit to each set of data separately. From both sets of data we determined the relative phase to be -1, and the ratio of the magnitudes of the radial integral parameters obtained from King's data differed from that obtained from Wobig's data by 10%. We have normalized the strengths in our paper to the absolute strengths of a group of lines corresponding to the transitions of the $a^4P - z^4D^0$ multiplet given by Wobig. A comparison of the calculated and experimentally determined line strengths are made. An analysis of the data indicates that a number of the experimentally determined lines are obtained under optically thick conditions.

Key words: Calculated line strengths; configuration interaction; intermediate coupling; Ti II; $3d^3$, $3d^24s$, $3d^24p$ configurations.

Meyerson, M. R., Giles, P. M., Newfeld, P. F., **Dimensional stability of gage block materials,** *J. Mater.* **3,** *No. 4, 727–743 (1968).*

Gage blocks which are necessary for the production of dimensionally precise items may undergo a change of dimensions with time. These changes are often extensive enough to cause the gage block to lose its value as a standard of length. This paper describes the program carried out at the National Bureau of Standards, Institute of Materials Research over the past eight years which has been successful in producing gage blocks which exhibit dimensional changes of less than $\pm 2 \times 10^{-7}$ in./in./yr.

Studies have been made on the effect on long term dimensional stability of variation of thermal and mechanical processing procedures of gage blocks produced from four general categories of material. These four categories include (1) through hardened steels, (2) steels with hard cases and annealed cores, (3) steels with hard cases and partially hardened cores, and (4) ceramic and cermet materials.

Key words: Gage blocks; dimensional stability; through hardening steel; secondary hardening steel; precipitation hardening steel; ceramic; cermets; length standards; tempering.

Mielenz, K. D., Length measurement and laser wavelength stability, *ISA Trans.* **6,** *No. 4, 293–297 (1967).*

The application of gas lasers as light sources for interferometric length metrology, and the limitations imposed by variations of laser wavelengths, are discussed.

Key words: Coherence; interferometry; lasers; length measurement; length standards; wavelength stability.

Milligan, D. E., Jacox, M. E., **Matrix-isolation study of the vacuum-ultraviolet photolysis of dichlorosilane. The infrared spectrum of the free radical $SiCl_2$,** *J. Chem. Phys.* **49,** *No. 4, 1938–1942 (Aug. 15, 1968).*

In the studies of the vacuum-ultraviolet photolysis of SiH_2Cl_2 and of SiD_2Cl_2 suspended in an argon matrix at 14° K, new absorptions appear at 502 and at 513 cm^{-1} which may be assigned as the two stretching fundamentals of $SiCl_2$. A broad, unstructured absorption is also observed in the region of the ultraviolet spectrum in which features tentatively ascribed to $SiCl_2$ were observed in earlier gas-phase emission studies. The detailed assignment of the observed infrared features is considered, and values of the valence angle, the Si-Cl stretching force constant, and the stretching-interaction force constant are estimated, corresponding to the two possible assignments for the infrared absorptions.

Key words: Dichlorosilane; dichlorosilane-d_2; force constants: infrared spectrum; matrix isolation; photolysis; $SiCl_2$ free radical; ultraviolet spectrum.

Okabe, H., **Photodissociation of HN_3 in the vacuum-ultraviolet production and reactivity of electronically excited NH,** *J. Chem. Phys.* **49,** *No. 6, 2726–2733 (Sept. 15, 1968).*

Photodissociation processes of HN_3 yielding electronically excited species have been studied in the vacuum ultraviolet. The fluorescence originating from these species has been investigated in the spectral region from 1700Å to 6000Å. The predominant excited species are NH $c^1\Pi$, NH $A^3\Pi_i$ and probably N_2 $B^3\Pi_g$. The yield of the NH $c^1\Pi$ is produced mainly in $v = 0$ levels with only 7% in $v = 1$ levels both at the Kr and Xe lines. However, it is rotationally excited up to K = 18. Direct formation of the NH $A^3\Pi_i$, a spin forbidden process, appears to be minor. The pressure dependence of the ratio, NH $A^3\Pi_i$ to NH $c^1\Pi$, indicates that the NH $A^3\Pi_i$ may be formed largely by the reaction of electronically excited N_2, most probably N_2 $B^3\Pi_g$, with HN_3. The absorption coefficient of HN_3 has been measured in the vacuum ultraviolet region in order to examine its correlation with dissociation processes. It was concluded that the NH $c^1\Pi$ may be formed from predissociation of electronically excited HN_3 below 1450Å, while above 1450Å from direct dissociation. The NH $c^1\Pi$ is quenched almost in every collision with H_2, CO, O_2, and NO. It was found that the main quenching process by paramagnetic gases, O_2 and NO, is the conversion of the $c^1\Pi$ to the $A^3\Pi_i$. Other primary processes are discussed in conjunction with the present work.

Key words: Photodissociation; HN_3; vacuum ultraviolet; fluorescence; NH $c^1\Pi$; $A^3\Pi_i$; absorption spectrum; fluorescence quenching.

Shives, T. R., Bennett, J. A., **The effect of environment on the fatigue properties of selected engineering alloys,** *J. Mater.* **3,** *No. 3, 695–715 (1968).*

Rotating beam fatigue tests were conducted in controlled environments on specimens of free cutting brass, titanium alloy Ti-4Al-4Mn, magnesium alloy AZ61A, and AISI4340 steel. The fatigue strengths of all the alloys were lower in a moist atmosphere than in a dry one, although the difference was small for the brass specimens. The effect of oxygen on the fatigue behavior of the titanium alloy and a vacuum-melted 4340 steel was investigated by conducting tests both in air and in an inert gas; the influence of oxygen was found to depend on whether or not moisture was present. In many of the vacuum-melted steel specimens the fatigue crack started below the surface, and the performance of these individual specimens was related to the size of the inclusion at the origin of the crack. A coating of dodecyl alcohol had a beneficial effect on the two materials (magnesium alloy and steel) on which its influence was investigated.

An interesting tarnishing effect was observed on the fatigue portion of the magnesium alloy fracture surfaces.

Key words; Fatigue; engineering alloys; environment; humidity; oxygen; crack initiation.

Sugar, J., **Nuclear magnetic dipole moment of ^{165}Ho,** *J. Opt. Soc. Am.* **58,** *No. 11, 1519–1523 (Nov. 1968).*

The first energy interval of the $4f^{11}6s$ configuration of Ho II was recently found by N. Spector and J. Sugar to be 637.8 cm^{-1}. The hfs of four of the lines defining this interval have been measured with an HYPEAC spectrometer at a resolution of 600 000. Seven independent equations relating the splitting factors a_{6s}, a_{4f}, and b_{4f} to the measured hfs were derived. Known values of a_{4f} and b_{4f} from Ho I (deduced in an atomic beam magnetic resonance experiment) were inserted in these equations, giving $a_{6s}=0.4437$ cm^{-1} (corrected for core polarization) with a probable error of 0.0004 cm^{-1}. From a_{6s}, a value for the nuclear magnetic dipole moment $\mu_I=(3.94\pm0.05)\mu_N$ was derived (1 $\mu_N=5.05050\times10^{-27}$ JT^{-1}). The uncertainty in μ_I is the rms deviation due to uncertainties in a_{6s} and in $\Psi^2_{6s}(0)$, the value of the probability density of the 6s-electron at the nucleus.

Key words: Holmium, nuclear moment; hyperfine structure.

Tsai, D. H., Beckett, C. W., **Shock wave propagation in a two-dimensional crystqlline lattice** *(Proc. Intern. Union of Theoretical and Applied Mechanics: Intern. Symp. Behavior of Dense Media Under High Dynamic Pressure, Paris, France, Sept. 11–15, 1967), Chapt. in Book, The Behavior of Dense Media Under High Dynamic Pressure, pp. 99–108 (Gordon and Breach Publ., New York, N.Y., 1968).*

Lattice dynamics has been applied to the study of the propagation of a strong, one-dimensional shock wave in a two-dimensional face-centered cubic lattice. The shock was generated at the free surface of the lattice by impact, and propagated into the lattice in the longitudinal direction perpendicular to the free surface. The transverse motion of the lattice points allowed the shock wave to be scattered and the compressive energy to be distributed between the longitudinal and transverse degrees of freedom. In our calculation, a Morse type potential function between pairs of lattice points was employed, and the interactions were assumed to extend to the fourth-neighbors. The equations of motion of the lattice points were solved by an approximate numerical method, and from the solutions, the dynamical behavior of the shock wave, the vibrational energy, and the Grüneisen parameter in the shock compressed region were obtained. These results were compared with similar results for a one-dimensional lattice model.

Key words: Shock wave propagation; two-dimensional lattice dynamics; lattice stability; thermal oscillations; energy calculations; Grüneisen parameter.

Weiss, B-Z., Meyerson, M. R., **Localized microstructural changes and fatigue crack propagation,** *Trans. Met. Soc. AIME* **242** *2515–2518 (1968).*

Changes of plastic zone size during fatigue crack propagation in fully reversed cyclic bending at constant load amplitude for conditions of plain strain were investigated by two different techniques. It appears that the rate of fatigue crack propagation cannot be expressed as a continuous simple function of plastic zone size. This was related to the anisotropic conditions of plastic deformation in the plastic zone preceding the crack. A theoretical-mathematical evaluation was formulated for fatigue crack propagation during repeated cyclic bending under conditions of plane strain. The theory is based on an elastic model and the assumption that the plastic deformation at the tip of the propagating crack does not cause drastic redistribution of stresses in the stress field around the tip of the crack. It was found that fatigue crack propagation can be expressed as a function of stress intensity factor.
Experimental results are in good agreement with the presented theoretical evaluation.
The effect of localized (heterogenous) structural changes such as selective precipitation of carbides in austenitic steels, temper embrittlement in a low alloy steel, and partial martensitic transformation in a metastable austenitic steel have been investigated and are discussed.

Key words: Fatigue crack propagation; plastic deformation; temper embrittlement; carbide precipitation; plastic zone size; austenitic steels.

Wiese, W. L., **Dependence of atomic *f*-values on nuclear charge,** *(Proc. Conf. Beam-Foil Spectroscopy, University of Arizona, Tucson, Arizona, Nov. 20–22, 1967), Chapt. in Book, Beam Foil Spectroscopy, II, 386–406 (Gordon and Breach Publ., New York, N.Y., 1968).*

Conventional perturbation theory predicts a simple relationship between atomic oscillator strength and nuclear charge, which is rederived and discussed in some detail. By utilizing available *f*-value data for the lighter elements, it is then shown that this dependence is clearly evident in the numerical material supplied by theory as well as experiment. Several representative examples are given in graphical form and discussed.

Key words: Oscillator strength; systematic trend; nuclear charge; perturbation theory.

Wolfgang, R., Zare, R. N., Branscomb, L. M., **Chemical accelerators,** *Science* **162,** *818–822 (Nov. 15, 1968).*

This is a brief account of a conference on chemical accelerators held at the University of Colorado March 28–29, 1968, supported by the Advanced Research Projects Agency.

Key words: Chemical accelerators.

Yakowitz, H., Heinrich, K. F. J., **Inclusion identification by means of electron probe microanalysis,** *Metallography* **1,** *No. 1, 55–78* (1968).

Each stage in the analysis of inclusions by electron probe microanalysis is evaluated. These stages include experimental design and instrument operation, specimen preparation, element identification, element distribution mapping and quantitative data scanning. The use of signals other than x-rays for inclusion analysis is considered as well as the analysis of sub-micron inclusions. The approach taken assumes that microprobe analysis will be used in conjunction with careful optical microscopy and that quantitative microscopy may be used to classify the inclusions after microprobe analysis is carried out.

Key words: Electron probe microanalysis; inclusion analysis; microscopy; quantitative data scanning; concentration mapping; experiment design.

Other NBS Publications

J. Res. NBS 73B (Math. Sci.), No. 1 (Jan.–Mar. 1969), $.75 cents.

A table of integrals of the error functions. E. W. Ng and M. Geller.
Fourier coefficients of Mathieu functions in stable regions. H. Früchting.
A note on the *T*-transformation of Lubkin. W. D. Clark, H. L. Gray, and J. E. Adams.
The cylinder problem in thermoviscoelasticity. W. S. Edelstein.
Relations within sequences of congruential pseudo-random numbers. P. H. Verdier.
On the mean dimensions of restricted random walks. P. H. Verdier and E. A. DiMarzio.
The cube of every connected graph is 1-hamiltonian. G. Chartrand and S. F. Kapoor.
Minimum-length covering by intersecting intervals. W. A. Horn.

Anderson, G. B., Raybold, R. C., Studies of calibration procedures for load cells and proving rings as weighing devices, Tech. Note 436 (Jan. 1969), 30 cents.

Barnes, J. A., Tables of bias functions, B_1 and B_2, for variances based on finite samples of processes with power law spectral densities, Tech. Note 375 (Jan. 1969), 50 cents.

Boone, T. H., Skoda, L. F., Cullen, W. C., Laboratory-field comparisons of built-up roofing membranes, Tech. Note 473 (Dec. 1968), 25 cents.

Brief history and use of the English and metric systems of measurement with a chart of the modernized metric system, ⅛ the dimensions of actual chart (SP304), Spec. Publ. 304A (1968), 20 cents.

Bullis, W. M., Editor, Methods of measurement for semiconductor materials, process control, and devices, quarterly report July 1 to September 30, 1968, Tech. Note 472 (Dec. 1968), 50 cents.

Freeman, D. H., Editor, Separation and Purification Section: Summary of activities July 1967 to June 1968, Tech. Note 459 (Dec. 1968), 60 cents.

Gebbie, K. B., Thomas, R. N., Editors, Wolf-Rayet stars, Proc. Symp. held at Joint Institute for Laboratory Astrophysics, University of Colorado, Boulder, Colorado, June 10–14, 1968, Spec. Publ. 307 (Dec. 1968), $3.00.

Hermach, F. L., Dziuba, R. F., Precision measurement and calibration. Selected NBS papers on electricity-low frequency, Spec. Publ. 300, Vol. **3** (Dec. 1968), $4.50. (Supersedes in part Handbook 77, Vol. **I**).

Miles, B. M., Wiese, W. L., Critically evaluated transition probabilities for Ba I and II, Tech. Note 474 (Jan. 1969), 30 cents.

Shields, W. R., Editor, Analytical Mass Spectrometry Section: Summary of activities July 1967 to June 1968, Tech. Note 456 (Nov. 1968), 55 cents.

The modernized metric system, the International System of units (SI) and its relationship to U.S. customary units, illustrated color wall chart 45 x 29 inches, Spec. Publ. 304 (1968), 50 cents. (Supersedes Misc. Publ. 232).

White, H. S., Jr., Editor, General description of the Federal Information Processing Standards Register, Fed. Info. Process. Std. Pub. (FIPS) 0 (Nov. 1, 1968), 20 cents

White, H. S., Jr., Editor, Code for information interchange, Fed. Info. Process. Std. Pub. (FIPS) 1 (Nov. 1, 1968), 10 cents.

White, H. S., Jr., Editor, Perforated tape code for information interchange, Fed. Info. Process. Std. Pub. (FIPS) 2 (Nov. 1, 1968), 10 cents.

White, H. S., Jr., Editor, Recorded magnetic tape for information interchange (800 CPI, NRZI), Fed. Info. Process. Std. Pub. (FIPS) 3 (Nov. 1, 1968), 10 cents.

White, H. S., Jr., Editor, Calendar date, Fed. Info. Process. Std. Pub. (FIPS) 4 (Nov. 1, 1968), 20 cents.

White, H. S., Jr., Editor, States of the United States, Fed. Info. Process. Std. Pub. (FIPS) 5 (Nov. 1, 1968), 20 cents.

White, H. S., Jr., Editor, Counties of the States of the United States, Fed. Info. Process. Std. Pub. (FIPS) 6 (Nov. 1, 1968), 40 cents.

Youden, W. W., Computer literature bibliography. Volume **2**, 1964–1967, Spec. Publ. 309, (Dec. 1968), $5.00.

Beckett, C. W., Cezairliyan, A., High-speed thermodynamic measurements and related techniques, Chapt. in Book, Experimental Thermodynamics, Ed. J. P. McCullough and D. W. Scott, Vol. **I**, Calorimetry of Non-reacting Systems, Chapt. 14, 551–585 (Butterworth and Co., London, England, 1968).

Blanford, M. M., NBS–ARF apparel materials testing and evaluation project, Second Annual Conf. Apparel Research Foundation, Washington, D.C., Oct. 7–9, 1968, 4 pages (Apparel Research Foundation. Washington, D.C., 1968).

Case, W. E., Harrington, R. D., Hysteresis effects in the slope calibration method for magnetometers, Proc. IEEE **56**, No. 10, 1733–1734 (Oct. 1968).

Coriell, S. R., Jackson, J. L., Bounds on transport coefficients of two-phase materials, J. Appl. Phys. **39**, No. 4733–4736 (Sept. 1968).

Crumlish, J. D., Notes on U.S. Government information systems, Law Computer Technol. **1**, No. 11, 15–21 (Nov. 1968).

Davis, D. D., Braun, W., Intense vacuum ultraviolet atomic line sources, Appl. Opt. **7**, No. 10, 2071–2074 (Oct. 1968).

Diller, D. E., Refractive index of gaseous and liquid hydrogen, J. Chem. Phys. **49**, No. 7, 3096–3105 (Oct. 1, 1968).

Engen, G. F., A method of calibrating coaxial noise sources in terms of a waveguide standard, IEEE Trans. Microwave Theory Tech. **MTT–16**, No. 9, 636–639 (Sept. 1968).

Foster, B. E., Blaine, R. L., A comparison of ISO and ASTM tests for cement strength, Am. Soc. Testing Mater. Spec. Tech. Publ. 441, 33–60 (1968).

Halford, D., Wainwright, A. E., Barnes, J. A., Flicker noise of phase in RF amplifiers and frequency multipliers: characterization, cause, and cure, Proc. 22nd Annual Symp. Frequency Control, Atlantic City, New Jersey, Apr. 22–24, 1968, pp. 340–341 (Solid State and Frequency Control Division, Electronic Components Laboratory, U.S. Army Electronics Command, Fort Monmouth, New Jersey, Apr. 1968).

Koidan, W., Calibration of standard condenser microphones: coupler versus electrostatic actuator, J. Acoust. Soc. Am. **44**, No. 5, 1451–1453 (Nov. 1968).

McCamy, C. S., A half century of photographic standardization in the United States, Photo. Sci. Engr. **12**, No. 6, 308–312 (Nov.-Dec. 1968).

Mielenz, K. D., Gas lasers and conventional sources in interferometry, Chapt. in Book, Electron Beam and Laser Beam Technology, pp. 89–137 (Academic Press Inc., New York, N.Y., 1968).

Nimeroff, I., A survey of papers on degree of metamerism, Color Eng. **6**, No. 6, 44–46 (Nov.-Dec. 1968).

Thomas, A. M., Monte Carlo study of vacuum vane gauge design criteria, J. Vacuum Sci. Technol. **5**, No. 6, 187–193 (Nov.-Dec. 1968).

Wait, D. F., Thermal noise from a passive linear multiport, IEEE Trans. Microwave Theory Tech. **MTT–16**, No. 9, 687–691 (Sept. 1968).

Wait, D. F., Nemoto, T., Measurement of the noise temperature of a mismatched noise source, IEEE Trans. Microwave Theory Tech. **MTT–16**, No. 9, 670–675 (Sept. 1968).

Wolfe, W. C., Field study of floor coverings, Flooring **74**, No. 11, 52–58 (Nov. 1968).

**Publications for which a price is indicated are available by purchase from the Superintendent of Documents, U.S. Government Printing Office, Washington, D.C. 20402 (foreign postage, one-fourth additional). The NBS non-periodical series are also available from the Clearinghouse for Federal Scientific and Technical Information, Springfield, Va. 22151. Reprints from outside journals and the NBS Journal of Research may often be obtained directly from the authors.*

U.S. GOVERNMENT PRINTING OFFICE : 1969 OL – 335–761

OCT 68189
UNIVERSITY MICROFILMS INC
ATTN SERIALS SECTION
300 NORTH ZEEB RD
ANN ARBOR MICH 48106

UNITED STATES
GOVERNMENT PRINTING OFFICE
DIVISION OF PUBLIC DOCUMENTS
WASHINGTON, D.C. 20402

OFFICIAL BUSINESS

POSTAGE AND FEES PAID
U.S. GOVERNMENT PRINTING OFFICE

JOURNAL OF RESEARCH of the National Bureau of Standards
A. Physics and Chemistry

Vol. 73A, No. 3 May–June 1969

Contents

	Page
New even levels and classified lines in the first spectrum of tungsten (WI) C. H. Corliss.	277
The heat of combustion of beryllium in fluorine. K. L. Churney, and G. T. Armstrong.	281
Deuterium isotope effect on the dissociation of weak acids in water and deuterium oxide. R. A. Robinson, Maya Paabo, and Roger G. Bates.	299
Vortex motions in ideal Bose superfluid. Martin J. Cooper.	309
Franck-Condon factors for the ionization of H_2O and D_2O. R. Botter and H. M. Rosenstock.	313
Topological features of hot carrier induced anisotropic breakdown on silicon diode surfaces. George G. Harman.	321
The third spectrum of praseodymium (PrIII) in the vacuum ultraviolet. Jack Sugar.	333
Publications of the National Bureau of Standards.	383

Library of Congress Catalog Card Number: 62-37039
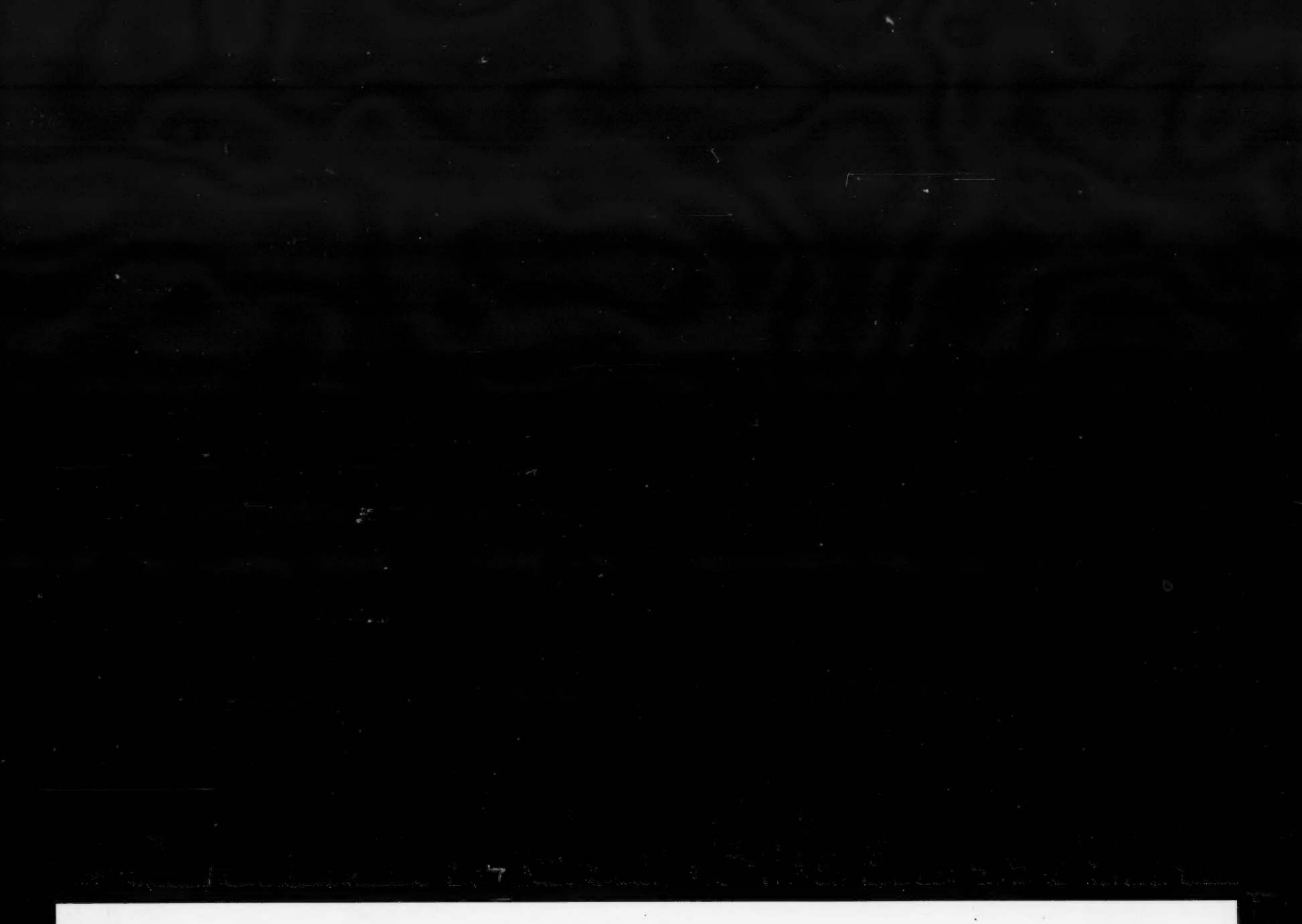
For sale by the Superintendent of Documents, U.S. Government Printing Office, Washington, D.C. 20402. Price single copy, this issue $1.50. Subscription price: $9.50 a year; $2.25 additional for foreign mailing.
UNITED STATES GOVERNMENT PRINTING OFFICE, WASHINGTON : 1969